

# Thermal-Hydraulic Analysis of an Experimental Reactor Cavity Cooling System with Air

---

## Reactor Concepts

Dr. Michael Corradini  
University of Wisconsin-Madison

In collaboration with:  
Texas A&M University  
University of Idaho

Steve Reeves, Federal POC  
Mitchel Farmer, Technical POC

**Thermal-Hydraulic Analysis of an Experimental  
Reactor Cavity Cooling System with Air  
NEUP Final Report Part I: Experiments**

---

**PART I: Experiments**

**M. Corradini (UW PI), M.Anderson, M.Muci**

Department of Engineering Physics, UW-Madison

[Corradini@engr.wisc.edu](mailto:Corradini@engr.wisc.edu)

**PART II: Separate Effects Tests and Modeling**

**Y.Hassan\*, A.Dominguez\*, A.Tokuhiro\*\*, K.Hamman\*\***

\*Texas A&M University, \*\*University of Idaho

October 15, 2014

# Executive Summary

This experimental study investigates the thermal hydraulic behavior and the heat removal performance for a scaled Reactor Cavity Cooling System (RCCS) with air. A quarter-scale RCCS facility was designed and built based on a full-scale General Atomics (GA) RCCS design concept for the Modular High Temperature Gas Reactor (MHTGR). The GA RCCS is a passive cooling system that draws in air to use as the cooling fluid to remove heat radiated from the reactor pressure vessel to the air-cooled riser tubes and discharged the heated air into the atmosphere.

Scaling laws were used to preserve key aspects and to maintain similarity. The scaled air RCCS facility at UW-Madison is a quarter-scale reduced length experiment housing six riser ducts that represent a 9.5° sector slice of the full-scale GA air RCCS concept. Radiant heaters were used to simulate the heat radiation from the reactor pressure vessel. The maximum power that can be achieved with the radiant heaters is 40 kW with a peak heat flux of 25 kW per meter squared.

The quarter-scale RCCS was run under different heat loading cases and operated successfully. Instabilities were observed in some experiments in which one of the two exhaust ducts experienced a flow reversal for a period of time. The data and analysis presented show that the RCCS has promising potential to be a decay heat removal system during an accident scenario.

# Table of Contents

Executive Summary.....	i
Acknowledgements.....	<b>Error! Bookmark not defined.</b>
Introduction.....	1
1.1 Motivation.....	1
1.2 General Atomics MHTGR.....	2
1.3 Argonne National Lab NSTF.....	4
1.4 Research Purpose, Scope, and Objectives .....	6
Scaling of RCCS Facility Design .....	7
2.1 Integral (Top Down) Scaling .....	8
2.2 Bottom-Up Scaling .....	10
2.3 Power Scaling .....	11
Facility Overview .....	13
3.1 Design Considerations .....	17
3.1.1 Inlet Plenum.....	18
3.1.2 Riser Ducts.....	20
3.1.3 Heated Cavity .....	21
3.1.4 Outlet Plenum and Exhaust Ducts .....	27
3.1.5 Thermal Insulation.....	30
3.2 Instrumentation .....	31

3.2.1 Power Controllers .....	33
3.2.2 Temperature Measurements.....	34
3.2.3 Velocity Measurements .....	37
3.2.4 Weather Station .....	38
3.2.5 Measurement Uncertainty.....	40
Characterization of the Facility .....	42
4.1 Heat Source.....	42
4.2 Heat Losses.....	44
4.3 Flow Profile .....	47
4.4 Nominal Behavior.....	50
4.4.1 Forced Flow Testing at 19.82 kW .....	50
4.4.2 Forced Flow Testing at 37.97 kW .....	54
4.5 Repeatability .....	57
4.5.1 Forced Flow Testing at 19.82 kW .....	57
4.5.2 Forced Flow Testing at 37.97 kW .....	59
4.6 Propagation of Error .....	61
Steady State Performance .....	63
5.1 Constant Heat Flux Power Testing .....	63
5.1.1 Constant Heat Flux at 19.82 kW.....	64
5.1.2 Constant Heat Flux at 37.97 kW.....	67
5.2.1 Asymmetric Power at 9.91 kW.....	71

5.2.2 Asymmetric Power at 18.99 kW .....	75
5.3 Natural Circulation Repeatability .....	79
5.3.1 Constant Heat Flux at 19.82 kW .....	79
5.3.2 Constant Heat Flux at 37.97 kW .....	81
5.3.3 Asymmetric Power at 9.91 kW .....	83
5.3.4 Asymmetric Power at 18.99 kW .....	85
5.4 Flow Instabilities .....	88
5.4.1 Test 19 .....	88
5.4.2 Test 27 .....	91
Conclusion and Recommendations.....	93
6.1 Conclusion .....	93
6.2 Future Work.....	98
6.2.1 Exhaust Duct Modifications .....	98
6.2.2 Riser Duct Instrumentation.....	99
6.2.1 Upper Plenum Investigation .....	99
Bibliography .....	100
Appendix A: Facility Photographs .....	101
Appendix B: Engineering Drawings.....	113
Appendix C: Velocity Transducers in Risers .....	124
Appendix D: Heat Loss Calculation .....	126
Appendix E: Alternate Heat Loss Calculation.....	127

Appendix F: Flow Profiles.....	128
Appendix G: Time Variation of Inlet Piping Velocity Measurement .....	133
Appendix H: Forced Flow Tests 16 and 20.....	134
Appendix I: LabVIEW Screen Shot .....	139
Appendix J: Operational Manual.....	140

# List of Figures

Figure 1 – Reactor cavity cooling system conceptual schematic. ....	2
Figure 2 – Reactor cavity cooling system.....	3
Figure 3 – Cavity plane view of reactor vessel and RCCS.....	4
Figure 4 – NSTF facility.....	5
Figure 5 – Scaled representation of experiment. ....	7
Figure 6 - Silo and support structure in Stoughton, WI.....	13
Figure 7 – Simplified model of quarter – scale air RCCS (total height of 13 meters). ....	15
Figure 8 - UW-Madison quarter-scale RCCS.....	16
Figure 9 - Inlet plenum and piping. ....	19
Figure 10 - Interior of inlet plenum. ....	19
Figure 11 - Riser duct (x6) dimensions, inches. ....	20
Figure 12 – 2D ANSYS geometry for thermal simulations.....	22
Figure 13 – 2D ANSYS geometry for thermal simulations.....	23
Figure 14 – Convection at various cavity depths.....	24
Figure 15 – Dimensions of heated cavity in inches. ....	25
Figure 16 – Heated cavity after construction.....	26
Figure 17 – Close-up of heated cavity. ....	26
Figure 18 – Pressure drop through exhaust ducting.....	27
Figure 19 – Particle path lines in exhaust ducts (left), velocity vectors in outlet plenum (right). ....	28
Figure 20 – Outlet plenum and exhaust ducts.....	29

Figure 21 – Exhaust ducts on silo exterior.....	29
Figure 22 – Insulation on the two exhaust ducts.....	31
Figure 23 – RCCS schematic of instrumentation (TC: thermocouple, V: velocity transducer). .....	32
Figure 24 – Arrangement of heater zones.....	33
Figure 25 – Riser front surface thermocouple locations.....	35
Figure 26 – Riser cross section at thermocouple locations.....	36
Figure 27 – Heated cavity wall thermocouples (dimensions in inches). ....	36
Figure 28 – Velocity transducer in the inlet piping. ....	37
Figure 29 – Velocity transducers in the six riser ducts.....	38
Figure 30 – Weather station mounted on silo. ....	39
Figure 31 – Weather station orientation.....	39
Figure 32 - Riser front surface temperatures for Test 15.....	43
Figure 33 - Riser front surface temperatures for Test 23.....	43
Figure 34 – 1-D heat loss schematic.....	45
Figure 35 - Heat losses in heated cavity. ....	45
Figure 36 – Inlet duct centerline .....	48
Figure 37 - Inlet duct velocity profile for Test 14. ....	49
Figure 38 - Inlet duct velocity profile for Test 16. ....	49
Figure 39 - Inlet/outlet duct air temperatures for Test 14 (Uncertainty: $\pm 0.7^{\circ}\text{C}$ ).....	51
Figure 40 - Heated cavity wall temperatures for Test 14 (Uncertainty: $\pm 0.7^{\circ}\text{C}$ ). ....	52
Figure 41 - Riser air temperatures for Test 14 (Uncertainty: $\pm 0.7^{\circ}\text{C}$ ).....	52
Figure 42 - Riser front surface temperatures for Test 14 (Uncertainty: $\pm 2.2^{\circ}\text{C}$ ). ....	53

Figure 43 - Riser 4 temperatures for Test 14 (Uncertainty: $\pm 2.2^{\circ}\text{C}$ for Front, Others $\pm 0.7^{\circ}\text{C}$ ). .....	53
Figure 44 - Inlet/outlet duct air temperatures for Test 18 (Uncertainty: $\pm 0.7^{\circ}\text{C}$ ).....	55
Figure 45 - Heated cavity wall temperatures for Test 18 (Uncertainty: $\pm 0.7^{\circ}\text{C}$ ). ....	55
Figure 46 - Riser air temperatures for Test 18 (Uncertainty: $\pm 0.7^{\circ}\text{C}$ ).....	56
Figure 47 - Riser front surface temperatures for Test 18 (Uncertainty: $\pm 2.2^{\circ}\text{C}$ ). ....	56
Figure 48 - Riser 4 temperatures for Test 18 (Uncertainty: $\pm 2.2^{\circ}\text{C}$ for Front, Others $\pm 0.7^{\circ}\text{C}$ ). .....	57
Figure 49 – Differential duct air temperatures for Test 14 and Test 16. ....	58
Figure 50 – Average riser front surface temperatures for Test 14 and Test 16. ....	58
Figure 51 – Average riser air temperatures for Test 14 and Test 16. ....	59
Figure 52 – Differential duct air temperatures for Test 18 and Test 20. ....	60
Figure 53 – Average riser front surface temperatures for Test 18 and Test 20. ....	60
Figure 54 – Average riser air temperatures for Test 18 and Test 20. ....	61
Figure 55 - Inlet/outlet duct air temperatures for Test 17 (Uncertainty: $\pm 0.7^{\circ}\text{C}$ ).....	65
Figure 56 - Heated cavity wall temperatures for Test 17 (Uncertainty: $\pm 0.7^{\circ}\text{C}$ ). ....	65
Figure 57 - Riser front surface temperatures for Test 17 (Uncertainty: $\pm 2.2^{\circ}\text{C}$ ). ....	66
Figure 58 - Riser air temperatures for Test 17 (Uncertainty: $\pm 0.7^{\circ}\text{C}$ ).....	66
Figure 59 - Riser 4 temperatures for Test 17 (Uncertainty: $\pm 2.2^{\circ}\text{C}$ for Front, Others $\pm 0.7^{\circ}\text{C}$ ). .....	67
Figure 60 - Inlet/outlet duct air temperatures for Test 25 (Uncertainty: $\pm 0.7^{\circ}\text{C}$ ).....	68
Figure 61 - Heated cavity wall temperatures for Test 25 (Uncertainty: $\pm 0.7^{\circ}\text{C}$ ). ....	68

Figure 62 - Riser front surface temperatures for Test 25 (Uncertainty: $\pm 2.2^{\circ}\text{C}$ ). .....	69
Figure 63 - Riser air temperatures for Test 25 (Uncertainty: $\pm 0.7^{\circ}\text{C}$ ).....	69
Figure 64 - Riser 4 temperatures for Test 25 (Uncertainty: $\pm 2.2^{\circ}\text{C}$ for Front, Others $\pm 0.7^{\circ}\text{C}$ ). .....	70
Figure 65 – Asymmetric power schematic. ....	71
Figure 66 - Inlet/outlet duct air temperatures for Test 19 (Uncertainty: $\pm 0.7^{\circ}\text{C}$ ).....	72
Figure 67 - Heated cavity wall temperatures for Test 19 (Uncertainty: $\pm 0.7^{\circ}\text{C}$ ). ....	73
Figure 68 - Riser front surface temperatures for Test 19 (Uncertainty: $\pm 0.7^{\circ}\text{C}$ ). ....	73
Figure 69 - Riser air temperatures for Test 19 (Uncertainty: $\pm 0.7^{\circ}\text{C}$ ).....	74
Figure 70 - Riser 4 temperatures for Test 19 (Uncertainty: $\pm 2.2^{\circ}\text{C}$ for Front, Others $\pm 0.7^{\circ}\text{C}$ ). .....	74
Figure 71 - Inlet/outlet duct air temperatures for Test 29 (Uncertainty: $\pm 0.7^{\circ}\text{C}$ ).....	76
Figure 72 - Heated cavity wall temperatures for Test 29.....	76
Figure 73 - Riser front surface temperatures for Test 29 (Uncertainty: $\pm 0.7^{\circ}\text{C}$ ). ....	77
Figure 74 - Riser air temperatures for Test 29 (Uncertainty: $\pm 0.7^{\circ}\text{C}$ ).....	77
Figure 75 - Riser 4 temperatures for Test 29 (Uncertainty: $\pm 2.2^{\circ}\text{C}$ for Front, Others $\pm 0.7^{\circ}\text{C}$ ). .....	78
Figure 76 – Outlet duct air temperatures for Test 15 and Test 17. ....	80
Figure 77 – Average riser front surface temperatures for Test 15 and Test 17. ....	80
Figure 78 – Average riser air temperatures for Test 15 and Test 17. ....	81
Figure 79 – Outlet duct air temperatures for Test 23 and Test 25. ....	82
Figure 80 – Average riser front surface temperatures for Test 23 and Test 25. ....	82

Figure 81 – Average riser air temperatures for Test 23 and Test 25. ....	83
Figure 82 – Outlet duct air temperatures for Test 19 and Test 21. ....	84
Figure 83 – Average riser front surface temperatures for Test 19 and Test 21. ....	84
Figure 84 – Average riser air temperatures for Test 19 and Test 21. ....	85
Figure 85 – Outlet duct air temperatures for Test 27 and Test 29. ....	86
Figure 86 – Average riser front surface temperatures for Test 27 and Test 29. ....	86
Figure 87 – Average riser air temperatures for Test 27 and Test 29. ....	87
Figure 88 – Inlet and outlet duct air temperatures for Test 19.....	89
Figure 89 – Outside wind speed and direction for Test 19. ....	90
Figure 90 – Outside temperature and barometric pressure for Test 19.....	90
Figure 91 – Inlet and outlet duct air temperatures for Test 27.....	91
Figure 92 – Outside wind speed and direction for Test 27. ....	92
Figure 93 – Outside temperature and barometric pressure for Test 27.....	92
Figure 94 – Integral power vs. mass flow rate.....	95
Figure 95 – Peak heat flux vs. mass flow rate (Areas: 18,987 cm <sup>2</sup> for Const. Heat Flux, 9,493.5 cm <sup>2</sup> for Asymmetric).....	96
Figure 96 – Integral power vs. system differential temperature. ....	96
Figure 97 – Peak heat flux vs. system differential temperature (Areas: 18,987 cm <sup>2</sup> for Const. Heat Flux, 9,493.5 cm <sup>2</sup> for Asymmetric).....	97
Figure 98 – Integral power vs. number of flow reversals. ....	97
Figure 99 – Support structure being lifted into silo. ....	101
Figure 100 – Support structure lowered into silo.....	101
Figure 101 – Outlet plenum without insulation panels. ....	102

Figure 102 – Inlet Plenum and heated cavity without insulation panels. ....	102
Figure 103 – Heater frames.....	103
Figure 104 – Assembled heater module.....	103
Figure 105 – Heater module exterior. ....	104
Figure 106 – Insulation inside heated cavity. ....	104
Figure 107 – Finished riser ducts (Riser 4 missing in photo). ....	105
Figure 108 – Painted riser ducts inserted into cavity.....	105
Figure 109 – Riser ducts inside heated cavity. ....	106
Figure 110 – Heater modules installed. ....	106
Figure 111 – Completed inlet plenum. ....	107
Figure 112 – Inlet duct piping.....	107
Figure 113 – Initial exhaust duct installation.....	108
Figure 114 – Exhaust duct installation inside silo. ....	108
Figure 115 – Outlet plenum insulation. ....	109
Figure 116 – Exhaust ducts insulation. ....	109
Figure 117 – Exhaust ducts outside silo. ....	110
Figure 118 – Close-up of exhaust ducts.....	110
Figure 119 – Electrical box housing data acquisition and controllers.....	111
Figure 120 – Data acquisition and controllers. ....	111
Figure 121 – Transformer outside silo.....	112
Figure 122 – Electrical line from Stoughton facility to silo. ....	112
Figure 123 – Overall dimensions for quarter-scale air RCCS (in inches). ....	113
Figure 124 – Side view dimensions of inlet duct (in inches).....	114

Figure 125 – Top view dimensions of inlet duct (in inches). .....	114
Figure 126 – Side view dimensions of exhaust duct (in inches).....	115
Figure 127 – Top view dimensions of exhaust duct (in inches). .....	115
Figure 128 – Nominal riser duct dimensions (in inches).....	116
Figure 129 – Riser duct cross section (in inches). .....	116
Figure 130 – Heated cavity dimensions (in inches).....	117
Figure 131 – As-built cross sectional area of inlet plenum (in inches). .....	118
Figure 132 – As-built dimensions for inlet plenum (front view; in inches). .....	119
Figure 133 – As-built dimensions for inlet plenum (side view; in inches).....	120
Figure 134 – As-built cross sectional area of outlet plenum (in inches). .....	121
Figure 135 – As-built dimensions for outlet plenum (front view; in inches). .....	122
Figure 136 – As-built dimensions for outlet plenum (side view; in inches).....	123
Figure 137 – Inlet pipe velocity vs. time for Test 23.....	124
Figure 138 – Riser duct velocity vs. time for Test 23.....	125
Figure 139 - Inlet duct velocity profile for Test 15. ....	128
Figure 140 - Inlet duct velocity profile for Test 17. ....	128
Figure 141 - Inlet duct velocity profile for Test 18. ....	129
Figure 142 - Inlet duct velocity profile for Test 19. ....	129
Figure 143 - Inlet duct velocity profile for Test 20. ....	130
Figure 144 - Inlet duct velocity profile for Test 21. ....	130
Figure 145 - Inlet duct velocity profile for Test 23. ....	131
Figure 146 - Inlet duct velocity profile for Test 25. ....	131
Figure 147 - Inlet duct velocity profile for Test 27. ....	132

Figure 148 - Inlet duct velocity profile for Test 29. ....	132
Figure 149 - Inlet/outlet duct air temperatures for Test 16 (Uncertainty: $\pm 0.7^{\circ}\text{C}$ ).....	134
Figure 150 - Heated cavity wall temperatures for Test 16 (Uncertainty: $\pm 0.7^{\circ}\text{C}$ ). ....	134
Figure 151 - Riser front surface temperatures for Test 16 (Uncertainty: $\pm 2.2^{\circ}\text{C}$ ). ....	135
Figure 152 - Riser air temperatures for Test 16 (Uncertainty: $\pm 0.7^{\circ}\text{C}$ ).....	135
Figure 153 - Riser 4 temperatures for Test 16 (Uncertainty: $\pm 2.2^{\circ}\text{C}$ for Front, Others $\pm 0.7^{\circ}\text{C}$ ). .....	136
Figure 154 - Inlet/outlet duct air temperatures for Test 20 (Uncertainty: $\pm 0.7^{\circ}\text{C}$ ).....	136
Figure 155 - Heated cavity wall temperatures for Test 20 (Uncertainty: $\pm 0.7^{\circ}\text{C}$ ). ....	137
Figure 156 - Riser front surface temperatures for Test 20 (Uncertainty: $\pm 2.2^{\circ}\text{C}$ ). ....	137
Figure 157 - Riser air temperatures for Test 20 (Uncertainty: $\pm 0.7^{\circ}\text{C}$ ).....	138
Figure 158 - Riser 4 temperatures for Test 20 (Uncertainty: $\pm 2.2^{\circ}\text{C}$ for Front, Others $\pm 0.7^{\circ}\text{C}$ ). .....	138

# List of Tables

Table 1 - Key dimensions. ....	8
Table 2 - Scaling correlations. ....	10
Table 3 - Power scaling requirements.....	12
Table 4-Insulation material properties.....	30
Table 5-cRio modules. ....	31
Table 6-Measurement device and associated uncertainties. ....	40
Table 7-Measurement device and associated uncertainties. ....	41
Table 8 – Heater Temperatures.....	44
Table 9 - Heat loss calculations for tests. ....	46
Table 10 - Test 14 parameters.....	50
Table 11 - Test 18 parameters.....	54
Table 12 - Test 14 and 16 parameters.....	58
Table 13 - Test 18 and 20 parameters.....	59
Table 14 – Error propagation.....	62
Table 15 – Natural circulation test matrix. ....	63
Table 16 – Test 17 parameters.....	64
Table 17 – Test 25 parameters.....	67
Table 18 - Test 19 parameters.....	72
Table 19 – Test 29 parameters.....	75
Table 20 – Observed flow instabilities. ....	79
Table 21 - Test 15 and 17 parameters.....	80

Table 22 - Test 23 and 25 parameters. ....	81
Table 23 - Test 19 and 21 parameters. ....	83
Table 24 - Test 27 and 29 parameters. ....	85
Table 25 – Scaled RCCS experimental results. ....	94
Table 26 – Average velocities for Test 23. ....	124
Table 27 – Mass flow rates for Test 23. ....	125
Table 28 – Parasitic heat losses for Test 18. ....	126
Table 29 – Parasitic heat losses for new calculation method. ....	127
Table 30 – Velocity at normalized inlet duct diameter. ....	133

# Chapter 1

## Introduction

### 1.1 Motivation

An emphasis has been placed on passive heat removal systems for long term removal of decay heat in the next generation of advanced nuclear reactors (Pope, 2009). Passive cooling systems rely on fundamental physics in nature to remove heat from the system and do not employ fans, compressors, fans, or other active components that require AC electrical power. In the event of an accident scenario, minimal human intervention is needed to ensure proper cooling for heat removal to an ultimate heat sink. In particular, we focus on the Reactor Cavity Cooling System (RCCS) designed by General Atomics (GA) for the Modular High Temperature Gas Reactor (MHTGR). The RCCS draws in air to use as the cooling fluid to remove heat radiated from the reactor pressure vessel to the air-cooled riser tubes and discharges the heated air into the atmosphere (HTGR-86-024). The atmosphere serves as the ultimate heat sink. Fundamentally, the RCCS is an open natural circulation air loop as seen in Figure 1. The RCCS offers a clear advantage compared to forced cooling systems in that it does not require electrical power and can in theory operate indefinitely in an accident scenario. Before the RCCS can be seriously considered, the thermal hydraulic behavior needs to be better understood. It is critical to determine the stability and heat removal performance of the RCCS.

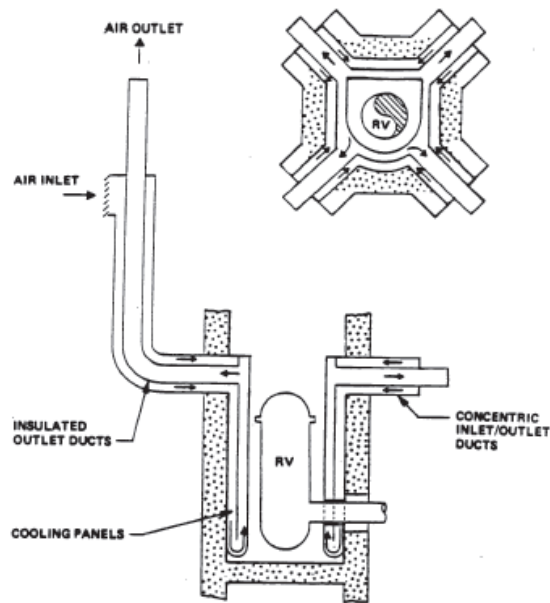
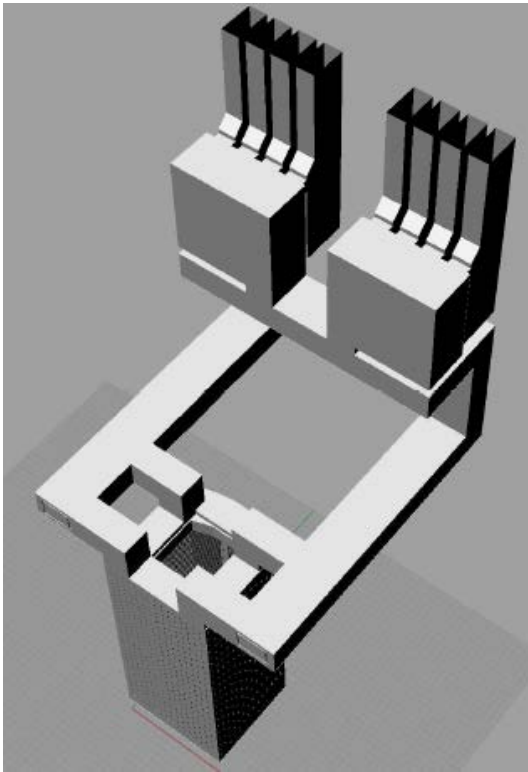


Figure 1 – Reactor cavity cooling system conceptual schematic.

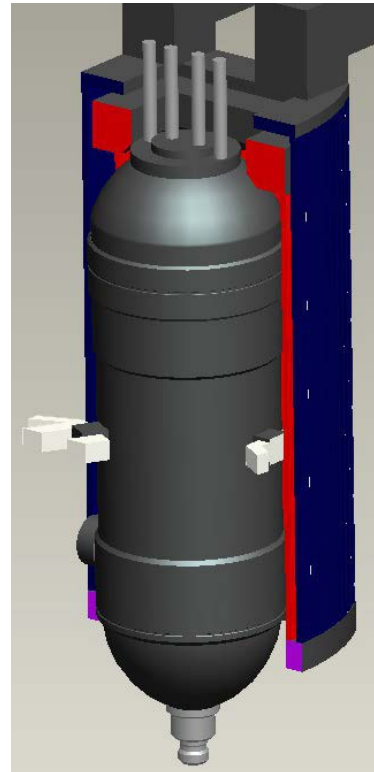
## 1.2 General Atomics MHTGR

The GA MHTGR is a modular reactor design with a capacity of 450 MWt per module. It has a primary helium coolant loop. The RCCS is a secondary cooling loop in which 227 rectangular ducts (5 cm by 24 cm) line the concrete containment around the reactor pressure vessel (HTGR-86-024). The spacing between the rectangular ducts is 5 cm. The rectangular ducts are connected to two sets of four chimneys as seen in Figure 2. In each of the two sets, there are two alternating groups of a hot outlet chimney and a cold inlet chimney. This redundancy is place to ensure that no one failure can compromise the system. Figure 3 shows a cavity drawing of the reactor vessel and the RCCS. It should be noted that the RCCS concept can also be used in other high temperature reactors such as the sodium-cooled or molten salt cooled reactor designs.

The heat is radiated from the reactor pressure vessel wall to the RCCS. The RCCS must remove 700 kW during normal operation since the normal heat transport system removes over 99% of the reactor thermal output. In the event of an accident where forced cooling systems become inoperable, the RCCS is designed to remove the decay heat load ( $<1.5$  MW) during accident transients and the estimated peak vessel wall heat flux ( $10 \text{ kW/m}^2$ ).



*(a) Overall view of RCCS*



*(b) Cavity view of RPV and RCCS*

Figure 2 – Reactor cavity cooling system.

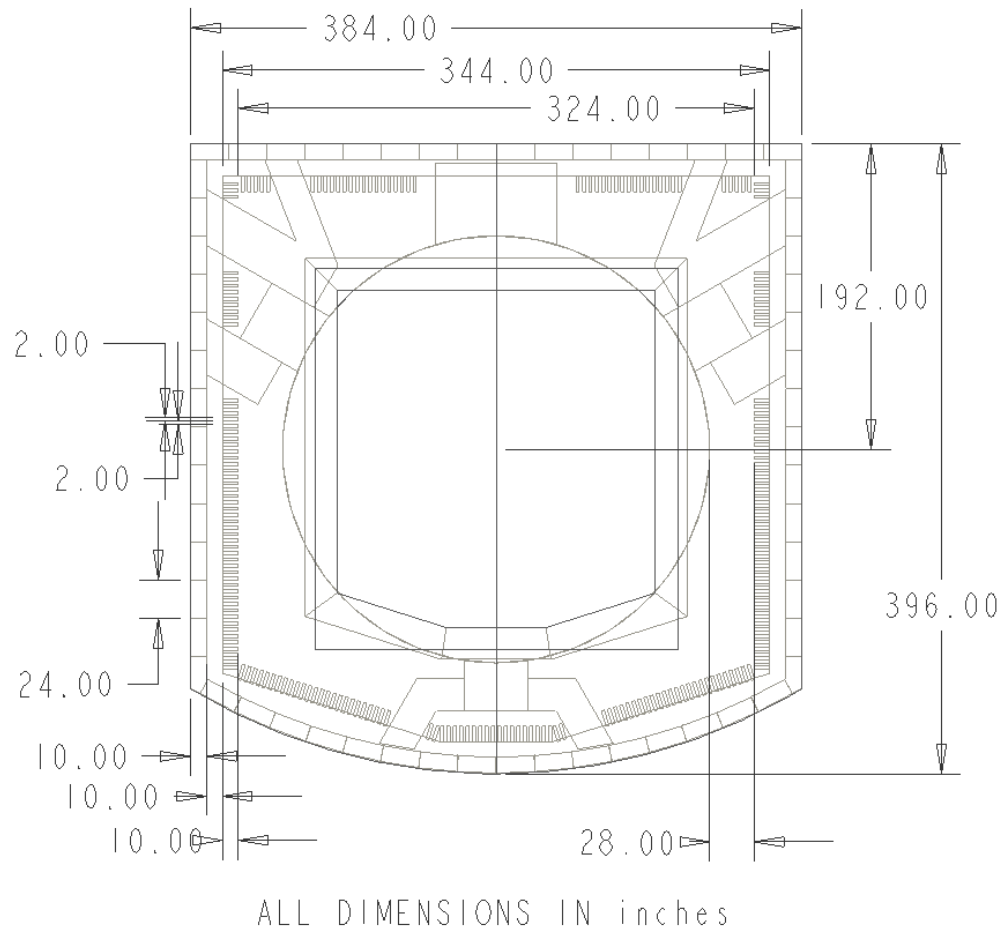


Figure 3 – Cavity plane view of reactor vessel and RCCS.

## 1.3 Argonne National Lab NSTF

The University of Wisconsin-Madison (UW-Madison) collaborated with Argonne National Laboratory (ANL). As part of the collaboration, UW-Madison performed experiments with a quarter-scale air cooled RCCS. ANL performed experiments with the Natural convection Shutdown heat removal Test Facility (NSTF) which is a half-scale air cooled RCCS that is also based on the General Atomics RCCS design concept (Lomperski, 2011). The overall objectives were to provide validation data for code development and to support RCCS design validation. The ANL NSTF facility has an overall facility height of 26 m with a heated test

section length of 6.7 m. Radiant heaters were used to radiate heat to twelve riser ducts inside the heated test section. The facility has a maximum input power of 220 kW.

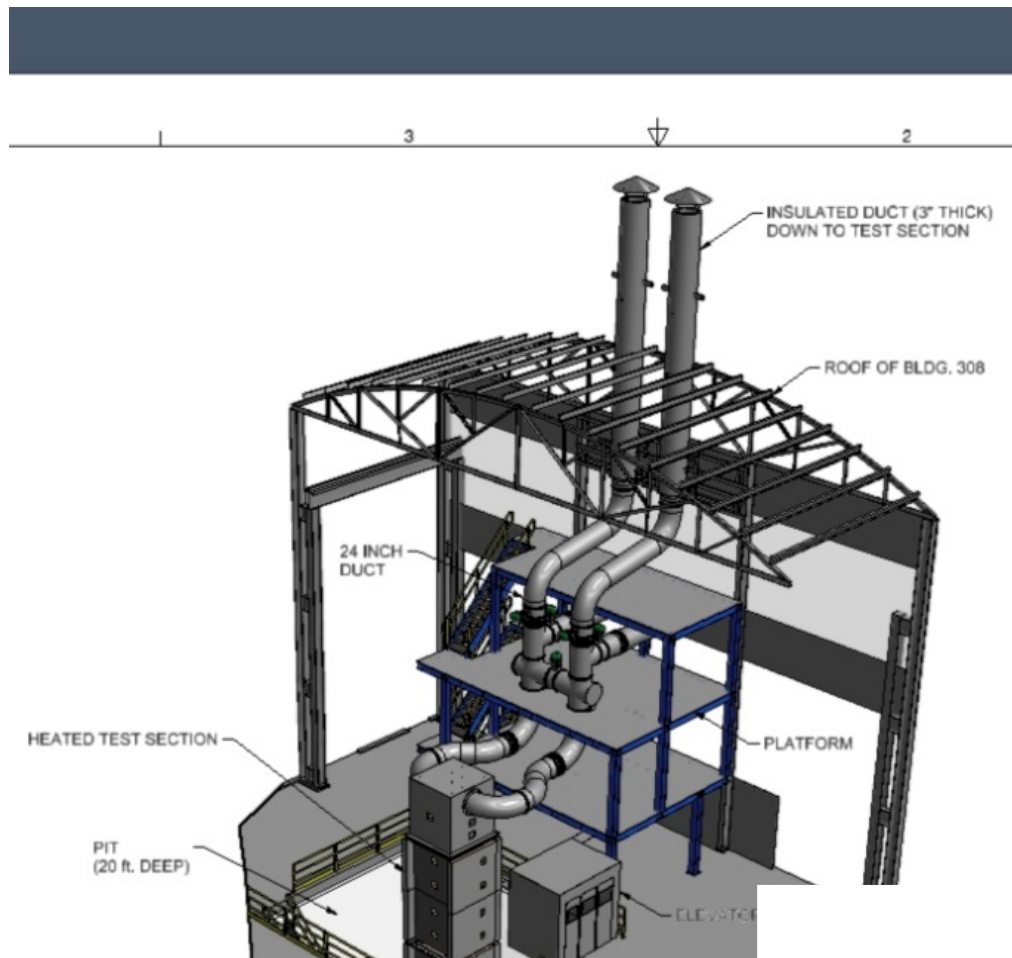


Figure 4 – NSTF facility.

## 1.4 Research Purpose, Scope, and Objectives

The scope of the research presented is to design, build, and obtain experimental data for a quarter-scale RCCS experiment. The purpose of this research is to better understand the thermal hydraulic behavior of the RCCS in order to advance design and development efforts.

Four objectives were established and listed below:

1. Use scaling laws and methods to study particular key phenomena and to maintain similarity among the full-scale GA RCCS concept and the quarter-scale air RCCS at UW-Madison.
2. Design and build a quarter-scale air RCCS that is flexible and accommodates a variety of tests in order to better understand the thermal hydraulic phenomena.
3. Characterize the scaled experiment and verify repeatability.
4. Evaluate the heat removal performance at steady-state conditions.

## Chapter 2

# Scaling of RCCS Facility Design

Building a full-scale test facility of the GA air RCCS to understand the behavior, performance, and stability is cost prohibitive. Scaling methods allow for the study of particular key phenomena that may occur at full-scale with a smaller scaled experiment. Scaling laws were used to preserve key aspects and to maintain similarity. An integral (top down) scaling approach was used (Tzanos, 2006). Using that scaling analysis, the scaled air RCCS facility at UW-Madison is a quarter-scale reduced length experiment housing six riser ducts that represent a  $9.5^\circ$  sector slice of the full-scale GA air RCCS concept. Table 1 presents the key dimensions for full-scale design concept and both the scaled facilities at ANL and UW-Madison. The integral scaling of system behavior and local phenomena has been performed by Argonne National Lab for their half-scale air RCCS facility, Natural convection Shutdown heat removal Test Facility (NSTF). The scaling analysis can be found in an earlier published report (Lomperski, 2011).

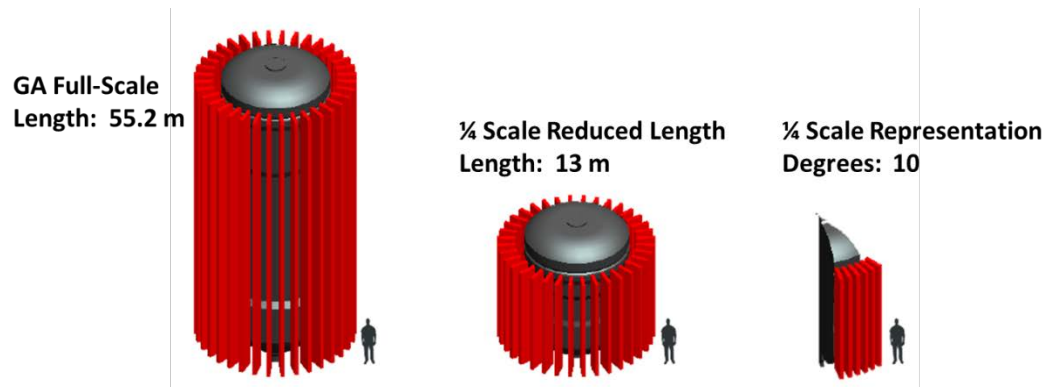


Figure 5 – Scaled representation of experiment.

Table 1 - Key dimensions.

Parameter	GA Scale	ANL ½ Scale	UW ¼ Scale
No. Riser Ducts	227	12	6
Total RCCS Height	55.2 meters	26.2 meters	13 meters
Heated Riser Section	11.3 meters	6.7 meters	2.8 meters

## 2.1 Integral (Top Down) Scaling

Integral scaling of a full-scale facility has been done before at UW-Madison. A quarter-scale water RCCS based on a GA RCCS hybrid concept was designed and built by Darius Lisowski. The facility was fundamentally a closed water natural circulation loop and measured 7.6 m in total height (Lisowski, 2011). It contained a 1,200 liter water storage tank and had 3 circular cooling tubes. Though the working fluid is different, both facilities were designed with similar heat removal requirements. Hence, there is some similarity in the overall scaling approach used for both facilities.

The integral scaling of the system behavior and phenomena was based on a reduced axial length scale ( $l_R$ ). The height of the scaled facility is one quarter of the full-scale GA design concept. Scaling in the radial direction is 1:1 thus preserving cross sectional areas. The riser duct dimensions and spacing are the same in both the quarter-scale facility and the full-scale GA design concept (Lomperski, 2011). Eq. 1 provides the similarity relationship between the quarter-scale facility (model) and the full-scale GA design concept (prototype).

$$\Psi_R = \frac{\Psi(model)}{\Psi(prototype)} = \frac{\Psi_m}{\Psi_p} \quad (1)$$

The heat transferred to the riser ducts in the RCCS from the reactor pressure vessel at time  $t$  can be approximated as

$$Q(t) = A_{conv} h_{cavity} (T_{RPV} - T_{riser}) + A_{rad} \epsilon \sigma (T_{RPV}^4 - T_{riser}^4) \quad (2)$$

The heat transferred to the air inside the riser ducts at steady state is

$$Q(o) = A_o U_o \rho_o C_p (T_{out} - T_{in}) \quad (3)$$

Eq. 3 can be rearranged to find the total temperature rise along the heated riser duct section

$$\Delta T_o = Q_o / A_o U_o \rho_o C_p \quad (4)$$

If constant thermal properties are assumed, the similarity relationship for Eq. 4 is

$$\Delta T_{oR} = Q_R / U_{oR} A_{oR} \quad (5)$$

If similar thermodynamic reference values are assumed, the similarity relationship for reference velocity can be calculated by

$$U_{oR} = \sqrt{l_R} \quad (6)$$

The similarity relationship for total power (Eq. 7) and heat flux (Eq. 9) can be derived from the relationship between power and heat flux.

$$Q_R = U_{oR} = \sqrt{l_R} \quad (7)$$

$$Q = q'' WL \quad (8)$$

$$q_R'' = 1 / \sqrt{l_R} \quad (9)$$

As previously mentioned, the scaling correlations were derived in similar fashion to the quarter-scale water RCCS work (Lisowski, 2011). The correlation parameters for the reference velocity ( $U$ ), time ratio ( $T_R^*$ ), temperature rise ( $\Delta T$ ), power ( $\dot{Q}$ ), and heat flux ( $q''$ ) can be seen in Table 2.

Table 2 - Scaling correlations.

Parameter	Similarity Relation	$\ell_R = 0.25$
Radial	-	1.0
$U_{oR}$	$\sqrt{\ell_R}$	0.5
$T_R^*$	$\sqrt{\ell_R}$	0.5
$\Delta T_{oR}$	1	1.0
$\dot{Q}_R$	$\sqrt{\ell_R}$	0.5
$q''_R$	$\frac{1}{\sqrt{\ell_R}}$	2.0

## 2.2 Bottom-Up Scaling

Thermo-fluid phenomena in the risers and the plenums were scaled with a bottom-up approach (Lomperski, 2011). A bottom-up approach preserves local phenomena and must be applied to specific regions. An emphasis was placed on the behavior of the heated air jet flow into the outlet plenum. It is crucial to ensure that proper mixing occurs inside of the outlet plenum to prevent the stratification of the flow. Stratification and recirculation in the natural convection flow could hamper heat removal performance. A focus was placed on the maximum ceiling height ( $X_m$ ) for jet penetration. The jet penetration of the heated air entering the outlet plenum from the riser ducts should influence thermal stratification and the potential for recirculation. The relationship in Eq. 10 developed by J.S. Turner was used (Turner, 1966). The characteristic length parameter ( $D_j$ ) was set to 1. Eq. 10 was then rearranged to Eq. 11.

$$\frac{X_m}{D_j} \propto F_j^{1/2} \quad (10)$$

$$X_m \propto D_j^{1/2} U_j \quad (11)$$

The equation can be written using the notation in Table 2.

$$X_{mR} = D_{jR}^{1/2} \ell_R^{1/2} \quad (12)$$

Using the notation from the scaling correlations,  $D_{jR} = 1$  and  $\ell_R = 0.25$ . The scaling factor ( $X_{mR}$ ) was then determined to be 0.5 so the height of the outlet plenum for the quarter-scale experiment will be scaled to 0.5 the height of the full-scale design concept. This also translates to 0.707 the height of the half-scale facility at ANL.

## 2.3 Power Scaling

The GA air RCCS design concept must remove 700kW<sub>t</sub> during normal operations. In the event of an accident where active cooling systems are incapacitated, the GA air RCCS must remove 1.5 MW<sub>t</sub> and also accommodate for peak wall heat flux values of 10 kW/m<sup>2</sup>. A design criterion of the RCCS states that the outlet should not be above 152°C when the inlet is at 22°C ( $\Delta T = 130^\circ\text{C}$ ). The full-scale GA RCCS prototype employs 227 riser ducts while the quarter-scale air RCCS model employs 6 riser ducts. Power scaling was derived to determine the power conditions necessary for operating the scaled experiment.

Scaling with similarity parameters was necessary to determine the power required for the quarter-scale facility to simulate the maximum decay heat load of 1.5 MW<sub>t</sub> for the full-scale GA RCCS. The power required for the quarter-scale air RCCS with six risers can be calculated by

$$\dot{Q}_m = \dot{Q}_p \sqrt{\ell_R} \cdot \frac{6 \text{ risers}}{227 \text{ risers}} \quad (13)$$

The heat flux required at the quarter-scale facility to model the peak heat flux at full-scale can be calculated by

$$q''_m = q''_p \frac{1}{\sqrt{\ell_R}} \quad (14)$$

The power required to provide the heat flux can be calculated by multiplying the peak heat flux by the area of the heat flux.

$$\dot{Q}_{m,flux} = q''_m \cdot A_m \quad (15)$$

Table 3 lists a summary of the scaled power requirements. The quarter-scale RCCS has 32 radiant heaters, which can output a maximum of 40 kW and provide a peak heat flux of 21 kW/m<sup>2</sup>.

Table 3 - Power scaling requirements.

<b>Criteria</b>	<b>GA RCCS</b>	<b>UW ¼ Scale</b>
Max. Decay Heat	1.5 MW	19.82 kW
Peak Heat Flux	10 kW/m <sup>2</sup>	20 kW/m <sup>2</sup>
Riser Duct Count	227	6

## Chapter 3

### Facility Overview

The air RCCS facility was built in the off-campus Thermal Hydraulics Laboratory in Stoughton, WI. The air RCCS facility was designed and built as a quarter-scale experiment of the full-scale GA MHTGR system with an objective to study its key thermal hydraulics behavior. An emphasis was placed to maintain similarity with the half-scale NSTF passive cooling system at Argonne National Laboratory (ANL). The air RCCS facility was placed in a support structure that was housed in a silo. The silo, support structure, and the crane used to lift the support structure into the silo can be seen in Figure 6.



*(a) Silo*



*(b) Support structure*



*(c) Crane*

Figure 6 - Silo and support structure in Stoughton, WI.

The quarter-scale air RCCS facility stands over 13 meters in height with 6 riser ducts that represent a 9.5° sector slice of the full-scale GA MHTGR RCCS design. The air RCCS facility consists of three important components: inlet plenum, heated cavity, and the outlet plenum/exhaust ducts. The inlet plenum is the entry point for air drawn from the environment by the air RCCS. Electrical resistance heaters inside the heated cavity simulate the reactor pressure vessel of the reactor and radiate heat to the six riser ducts. The outlet plenum provides a volume to allow mixing before the heated air returns to the outside environment via two exhaust ducts.

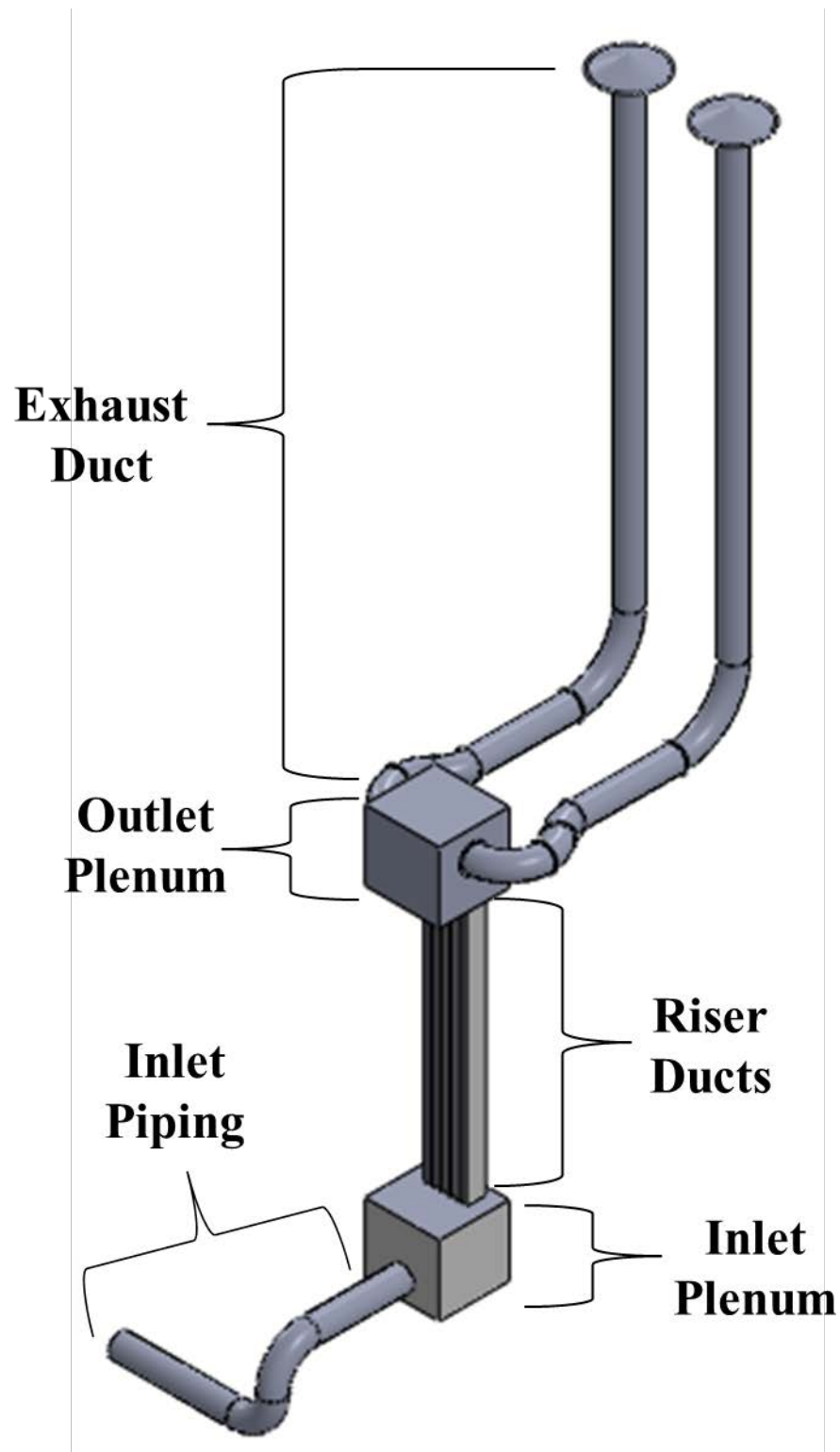


Figure 7 – Simplified model of quarter – scale air RCCS (total height of 13 meters).

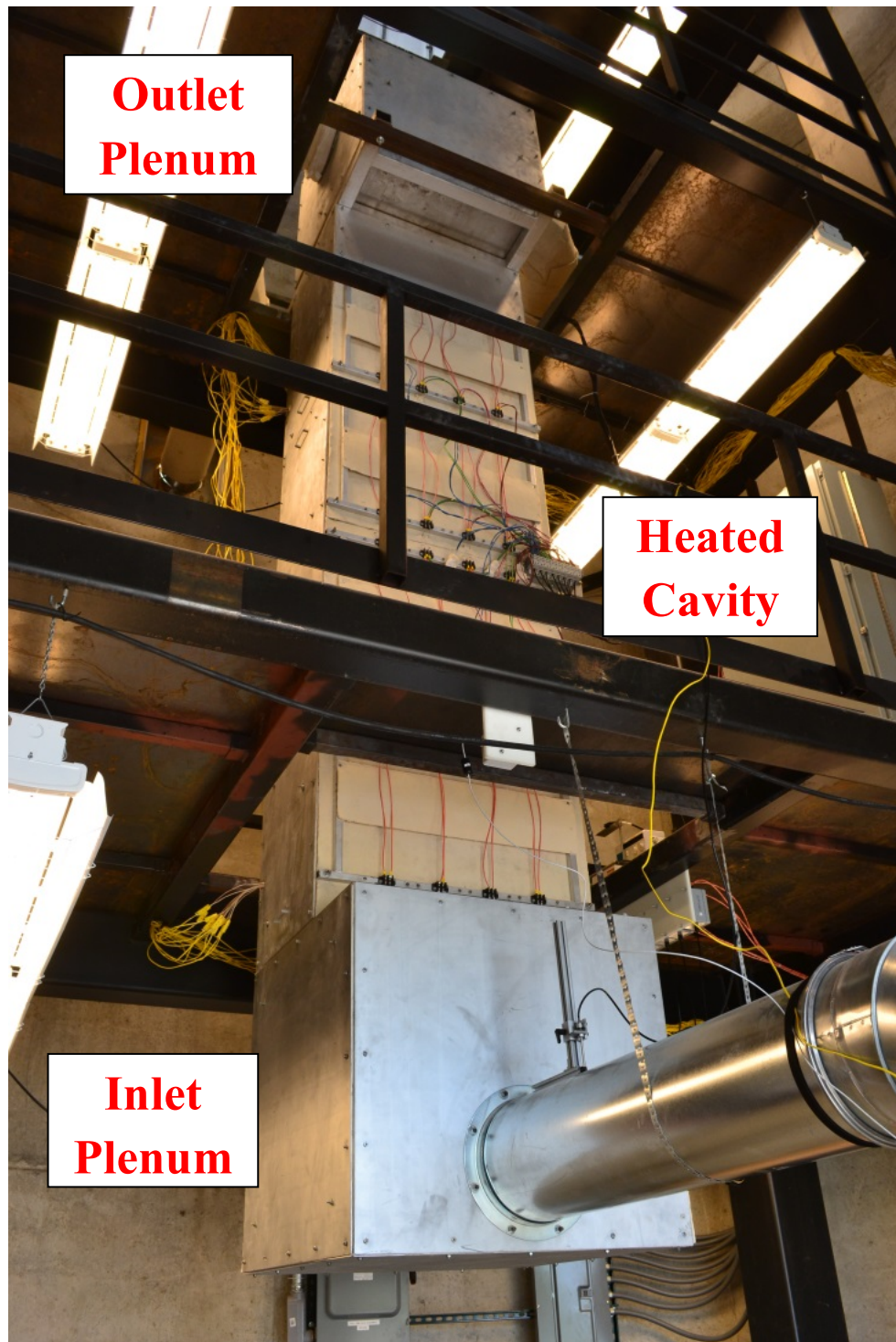


Figure 8 - UW-Madison quarter-scale RCCS.

## 3.1 Design Considerations

The key overall dimensions for the quarter-scale air RCCS facility at UW-Madison were derived through the scaling of the full-scale facility design. There were other design and construction considerations that were determined in order to complete the facility. The scaled air RCCS had to meet several goals in order to develop a facility that behave similarly to the GA MHTGR reactor cavity cooling system. The facility must be flexible and accommodate a variety of tests in order to better understand the thermal hydraulic phenomena. Key parameters have to be measured and recorded via instrumentation and data acquisition. Similarity must also be preserved with the half-scale passive cooling NSTF facility at ANL. Dr. Darius Lisowski, former Ph.D. student at the UW-Madison, performed a series of numerical simulations which was critical for the design of this facility. These simulations and other work critical to the air RCCS facility were published in the NURETH 15 Conference Proceedings and co-authored by Dr. Lisowski and Moses Muci (Lisowski, 2013).

### 3.1.1 Inlet Plenum

The design of the inlet plenum is based on the half-scale facility at ANL. The inlet plenum is an enclosure measuring 36" x 38" x 36". There is inlet piping which is 12 inches in diameter that directs the flow of air into the center of the inlet plenum. The inlet plenum provides a large volume in which the flow can decelerate and stabilize before entering the six riser ducts. An inline centrifugal duct fan with variable speed control can be placed before the inlet piping to allow for forced flow conditions as needed in particular experiments. This facilitates instrument calibration and provides a baseline characterization of the facility. Figure 9 shows the inlet plenum, the piping assembly, and the fan. Figure 10 shows the interior of the inlet plenum without panels to observe the portion of the six risers that penetrate 3.5 inches into the inlet plenum.



Figure 9 - Inlet plenum and piping.

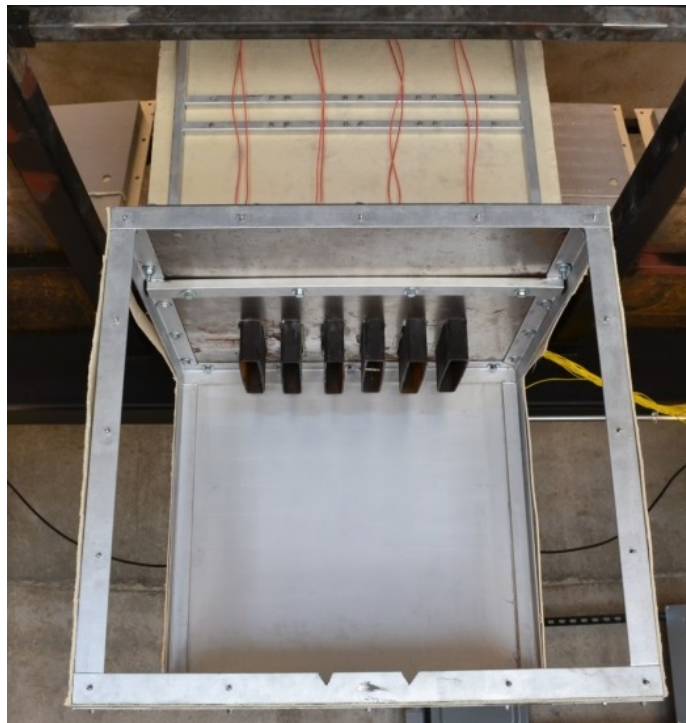


Figure 10 - Interior of inlet plenum.

### 3.1.2 Riser Ducts

The available space at UW-Madison limited the physical size of the facility. Due to the limitations it was not feasible to replicate the 12 riser ducts of the half-scale air RCCS at ANL. A reduced quarter-scale facility was decided upon which contained a total of six risers. The six riser ducts (rectangular ducts) in the quarter-scale facility have the same dimension and spacing as the full-scale GA MHTGR reactor cavity cooling system. The risers are 2 inches (width) by 10 inches (length) and 2 inches of spacing was placed in between risers. These dimensions and the total length of the risers (148 inches) can be seen in Figure 11. The six risers were coated with a black paint that is heat resistant to prevent rust formation.

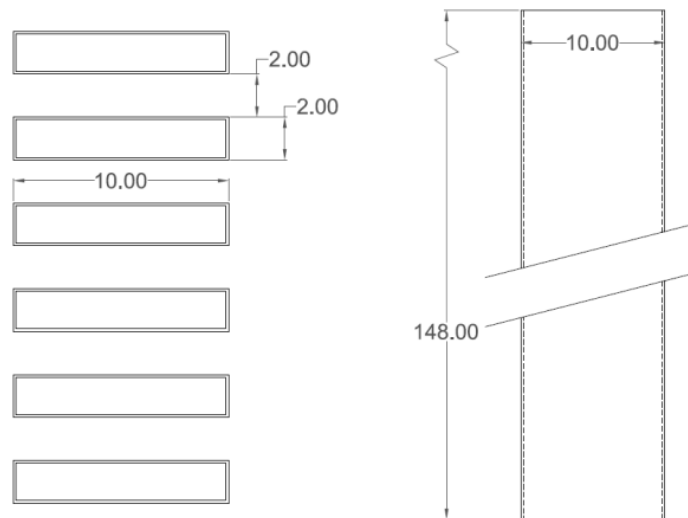


Figure 11 - Riser duct (x6) dimensions, inches.

### 3.1.3 Heated Cavity

The heated cavity is a critical component of the air RCCS facility. Its main function is to serve as a thermal enclosure for the heat transfer from the radiant heaters to the six riser ducts and to minimize heat losses to the outside environment. Natural convection cells develop inside the heated cavity much like they would in the reactor cavity of the GA MHTGR. Three specific design requirements were established for the heated cavity of the quarter-scale air RCCS facility:

- 1) Match or exceed the integral power and peak heat flux during prototypic accident scenarios with the ability to vary the heating profile
- 2) Ensure a minimum 2 to 1 heat flux skew during asymmetric heating
- 3) Prevent geometric influences that would hinder the formation of natural convection cells inside of the heated cavity.

An 8 by 4 array of radiant heaters were selected to simulate the reactor pressure vessel wall. Each heater can supply up to 1.25 kW and the maximum power that can be achieved with the thirty-two heaters is 40 kW with a peak heat flux of 25 kW per meter squared. The radiant heaters will be grouped into 4 independent vertical zones which allows for power shaping in the radial direction.

Numerical studies were necessary to ensure a design with a minimum 2 to 1 heat flux skew during asymmetric heating. An optimization study of the front of the cavity was published by Lisowski (Lisowski, 2013). This optimization was done with a steady-state thermal simulation in ANSYS which included the six riser ducts, the heated cavity enclosure

walls, and the radiant heaters as seen in Figure 5. Representative material properties and boundary conditions were chosen. The following criteria were imposed on the model: heat losses from the heated cavity to the outside environment, convection within the risers and the heated cavity, and radiation from the heaters.

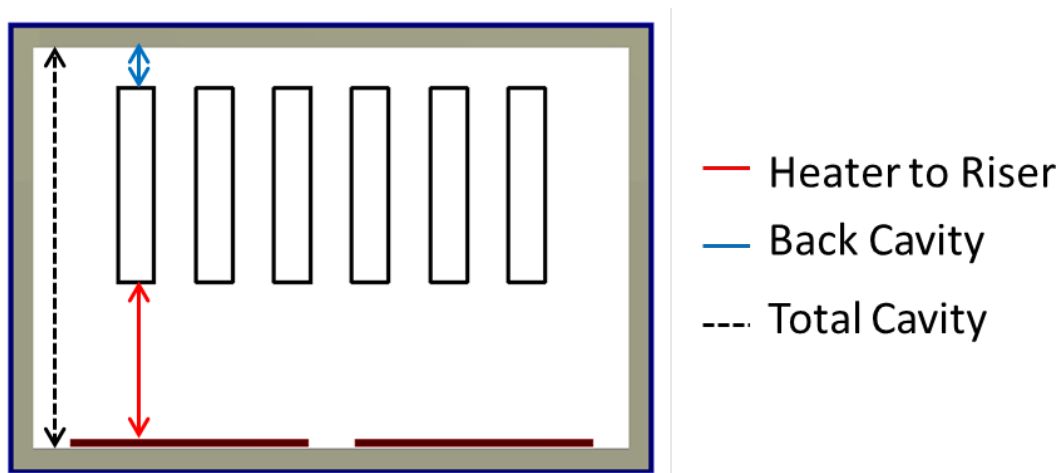


Figure 12 – 2D ANSYS geometry for thermal simulations.

Lisowski provided implicit definitions for the thermal boundary conditions and determined that buoyancy is relatively unimportant as determined by the Richardson number within the ducts. The Richardson number is a dimensionless number that calculates the ratio of potential energy to kinetic energy. The behavior inside of the risers was modelled as forced flow. The Dittus-Boelter model was used to determine the heat transfer coefficient within the riser ducts. At the inner walls of the riser ducts, a heat transfer coefficient of  $18 \text{ W/m}^2\text{-K}$  was imposed as well as a free stream temperature of  $109 \text{ }^\circ\text{C}$ . Along the outer walls of the riser ducts and the interior of the enclosure, a heat transfer coefficient of  $2.6 \text{ W/m}^2\text{-K}$  was imposed at a temperature of  $150 \text{ }^\circ\text{C}$ . Along the exterior of the enclosure, a heat transfer coefficient of  $3.4 \text{ W/m}^2\text{-K}$  was imposed at a temperature of  $22 \text{ }^\circ\text{C}$ . The heat flux imposed on the heater

surfaces was  $9.7 \text{ kW/m}^2$ , which is the prototypic decay heat load for the GA MHTGR. Two different heating scenarios were carried out in the simulation. One scenario was uniform heating in which each heater surfaces has the same equal heat flux imposed. The second scenario was asymmetric heating in which one heater surface receives double the heat flux while the other heater surface is turned off. Figure 13 shows the front and back face temperatures for the riser ducts. The simulations provided that the distance from the heaters to the front faces of the risers should be 18.64 cm (7.34 inches).

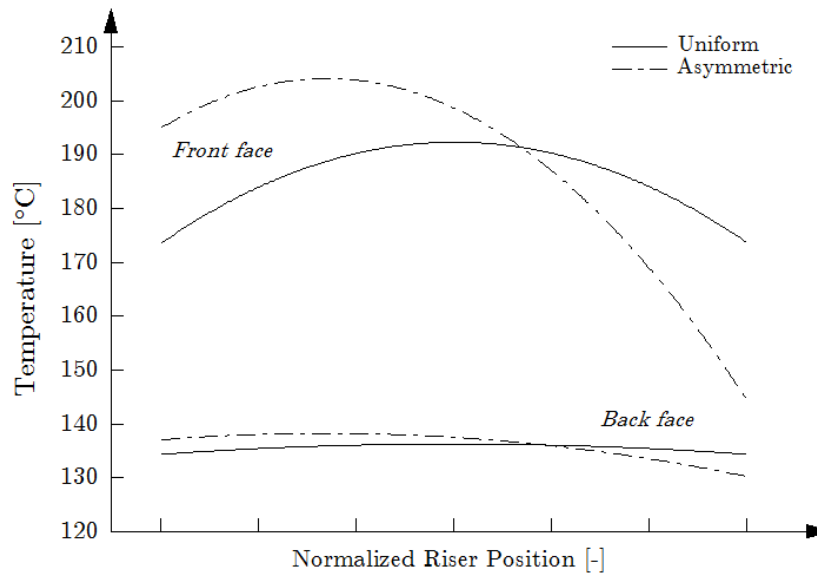


Figure 13 – 2D ANSYS geometry for thermal simulations.

After finding the dimension from heater to the riser ducts, it was necessary to calculate the distance between the riser ducts and the back wall of the heated cavity. In order to ensure that the geometry of the heated cavity will not impede natural convection cells, Lisowski performed an analysis that investigated the effects of convection over a range of cavity depths by using a Nusselt correlation. The results seen in Figure 14 determined that cavity depths shorter than 20 cm (7.87 inches) would result in a much lower heat transfer

coefficient. The heat transfer coefficient remains relatively constant around  $2.6 \text{ W/m}^2\text{-K}$  at cavity depths greater than 20 cm. Lisowski originally proposed a final cavity depth of 51.5 cm (20.25 inches) which resulted in a back cavity spacing of 7.12 cm (2.8 inches). This was proposed to reduce material costs and to minimize heat losses. The final cavity depth was changed to 49.02 cm (19.30 inches) to ease the construction of the heated cavity frame. This resulted in a back cavity spacing of 3.58 cm (1.41 inches).

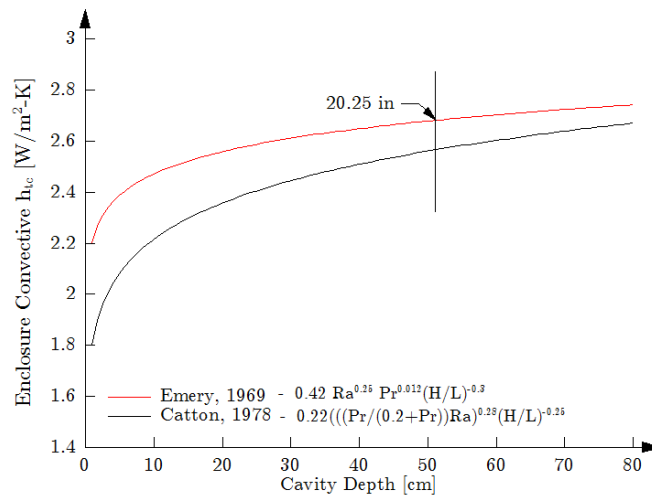


Figure 14 – Convection at various cavity depths.

The heated cavity after construction can be seen in Figure 2. The heated cavity is surrounded by thermal insulation on all sides to minimize heat losses to the environment. The heaters were arranged into four 4x2 heater array modules to ease fabrication and assembly. The heater modules were mounted on one end of the heated cavity with weld studs. A close-up photograph of the heated cavity can be seen in Figure 17.

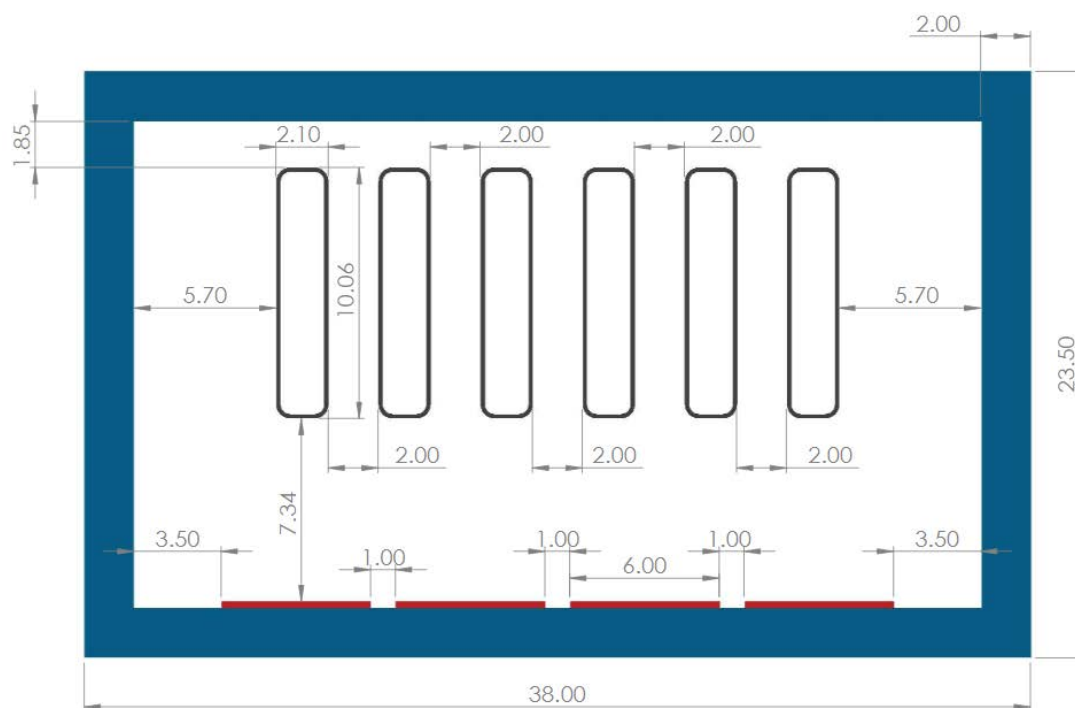


Figure 15 – Dimensions of heated cavity in inches.



*(a) Bottom and middle of heated cavity*



*(b) Top of heated cavity*

Figure 16 – Heated cavity after construction.



Figure 17 – Close-up of heated cavity.

### 3.1.4 Outlet Plenum and Exhaust Ducts

After air flows through the riser ducts inside the heated cavity, the air expands into the outlet plenum. The outlet plenum allows mixing to occur and is connected to two exhaust ducts which vent the heated air to the environment outside the silo. The dimensions for the outlet plenum were based off the aspect ratio for the half-scale air passive cooling NSTF facility at ANL. The dimensions of the outlet plenum box are 36" x 38" x 36". In order to ensure that the dimensions used for the outlet plenum and the exhaust ducts preserved expected flow patterns and did not impede natural circulations, Lisowski performed analytical calculations and CFD analysis (Lisowski, 2013). Results from pressure drop calculations can be seen in Figure 18. A 12" diameter pipe was chosen for the exhaust ducts due to availability and because that diameter provided a hydraulic diameter to minimize influence on the flow resistance within the riser ducts and outlet plenum. This behavior would then be similar to the NSTF facility. The exhaust duct piping dimensions were made such that it would exit the silo at two windows.

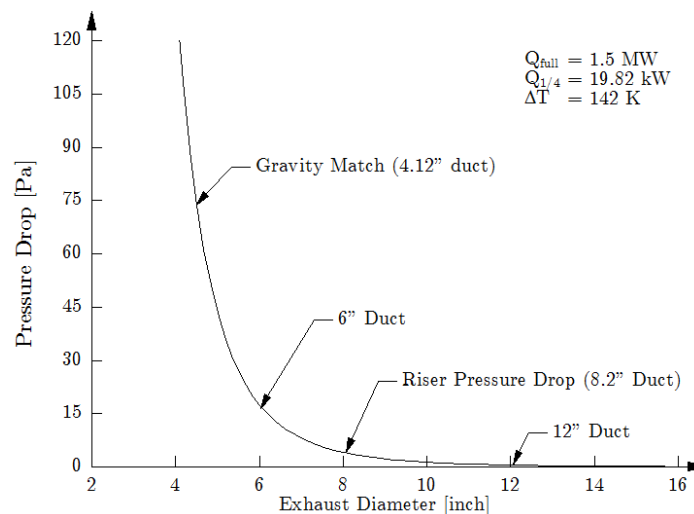


Figure 18 – Pressure drop through exhaust ducting.

Lisowski ran CFD simulations using 3D model in FLUENT. It was of special interest to observe the mixing behavior inside the upper plenum. After passing through the riser ducts, the air flow enters the outlet plenum at a nominal velocity of 2.3 meters per second. Figure 19 shows the particle path lines in the exhaust ducts and the velocity vector in the outlet plenum. The velocity vectors in the outlet plenum show that adequate mixing occurs before the air flows to the two exhaust ducts.

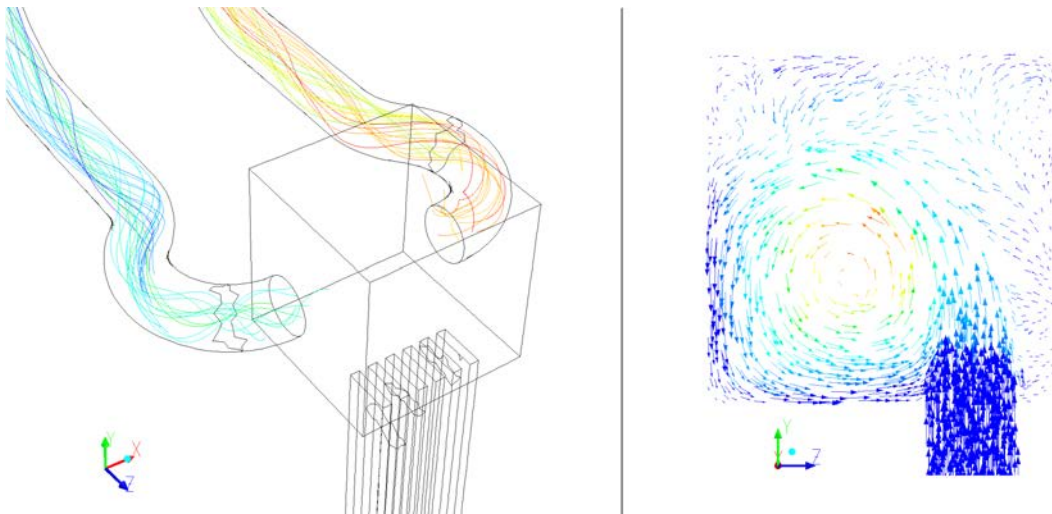


Figure 19 – Particle path lines in exhaust ducts (left), velocity vectors in outlet plenum (right).

The outlet plenum was constructed in similar fashion to the heated cavity (Figure 20). The outlet plenum interior is surrounded by thermal insulation on all sides to minimize heat losses to the environment. The material of the exhaust ducts obtained from KB Ducts is galvanized steel. The sections of the exhaust ducts were clamped together using silicone gaskets for ease of assembly. The exhaust duct piping inside of the silo was insulated with a layer of Pyrogel thermal insulation. The exhaust duct piping that was mounted on the exterior wall of the silo

was not insulated at this time and can be seen in Figure 21. Insulation can be added if so desired.

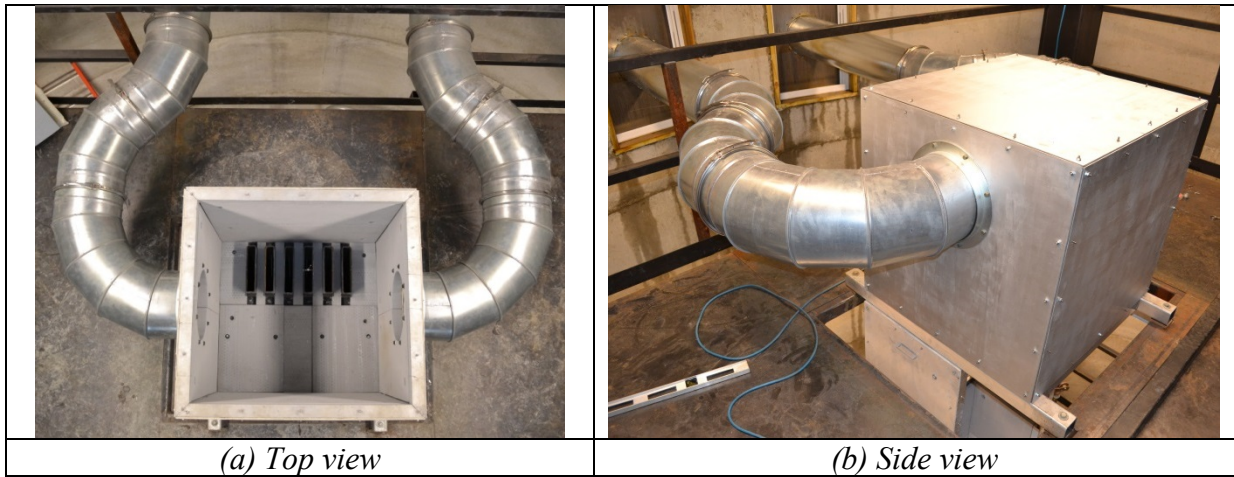


Figure 20 – Outlet plenum and exhaust ducts.



Figure 21 – Exhaust ducts on silo exterior.

### 3.1.5 Thermal Insulation

Thermal insulation is necessary in order to minimize heat loss from inside the heated cavity and the outlet plenum to the environment. Three insulation materials (Zircal-18, Pyrogel-XT, and Kaowool) are used in the heated cavity and the outlet plenum. Zircal-18 is a refractory board made from high temperature calcium silicate and the thickness used was 2 inches. Pyrogel-XT is an insulation blanket formed of silica aerogel and glass fibers. The thickness of the Pyrogel-XT used is 0.25 inches. Kaowool is a refractory ceramic fiber blanket and the thickness used is 1 inch. The properties of the three insulation materials can be seen below in Table 2.

Table 4-Insulation material properties.

<b>Zircal – 18 (2")</b>		<b>Pyrogel – XT (0.25")</b>		<b>Kaowool (1")</b>	
°C	W/m-K	°C	W/m-K	°C	W/m-K
200	0.07	200	0.028	260	0.06
400	0.09	400	0.046	538	0.12
600	0.10	600	0.089	816	0.21
Max: 1,100 °C		Max: 650 °C		Max: 1,093 °C	

The heated cavity and the outlet plenum are insulated with 2 inches of Zircal-18 with an exterior layer of 0.25 inches of Pyrogel-XT. Kaowool was used to fill gaps in between different Zircal-18 boards.

The exhaust ducts inside of the silo were insulated with a layer of 0.25 inch Pyrogel-XT. One inch thick Kaowool blanket was used to wrap around the clamps holding the exhaust duct sections together.



Figure 22 – Insulation on the two exhaust ducts.

## 3.2 Instrumentation

Instrumentation was placed in the air RCCS facility to control the heating zones and to record temperature and velocity measurements at certain locations to better understand the thermal hydraulic phenomena. The data acquisition device used was the National Instruments cRio 9024. The cRio 9024 is an embedded controller that runs LabVIEW Real-Time for device control and data logging. Six modules were fitted into the cRio 9024 and are listed in Table 5.

Table 5-cRio modules.

Model No.	Qty.	Signal Type	No. Channels	Measurement
NI 9264	1	Analog output (voltage)	16	Heater controller signal
NI 9205	1	Analog input (voltage)	16	Heater controller feedback, velocity, humidity
NI 9213	4	Thermocouple input	64	Temperature

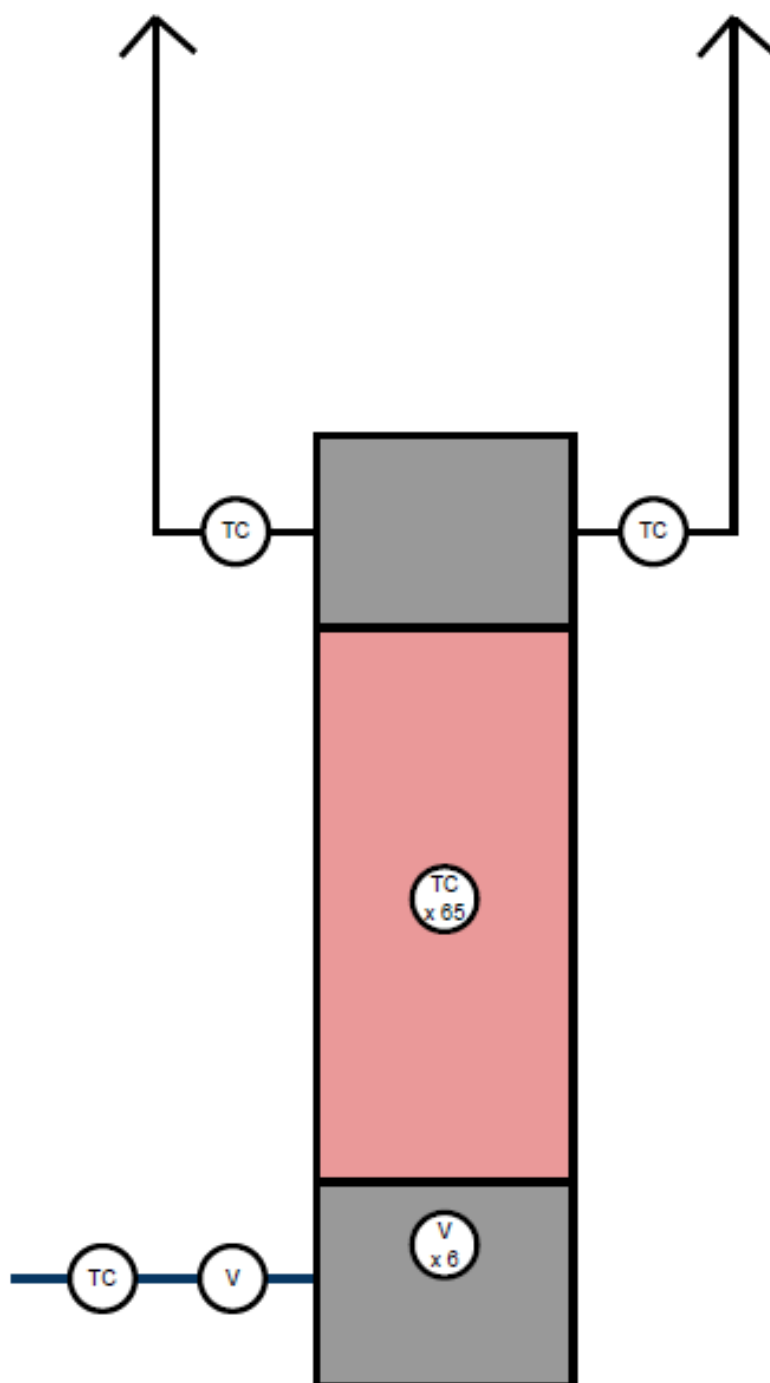


Figure 23 – RCCS schematic of instrumentation (TC: thermocouple, V: velocity transducer).

### 3.2.1 Power Controllers

Power controllers are needed to provide power for the electrical resistance heaters inside of the heated cavity. A total of thirty-two heaters can provide 40 kW (1.25 kW per heater). The heaters are arranged in four vertical heating zones to allow for different power shaping. Each of the four heating zones is controlled by a Eurotherm TE10P controller. The heater zones and the riser ducts are labeled in Figure 24. The TE10P operates on 208 V to provide power to each heating zone. The NI 9264 module inside of the NI cRio 9024 controller was used to send a 0 to 10 V signal to vary the power provided by the TE10P controller to the heating zone.

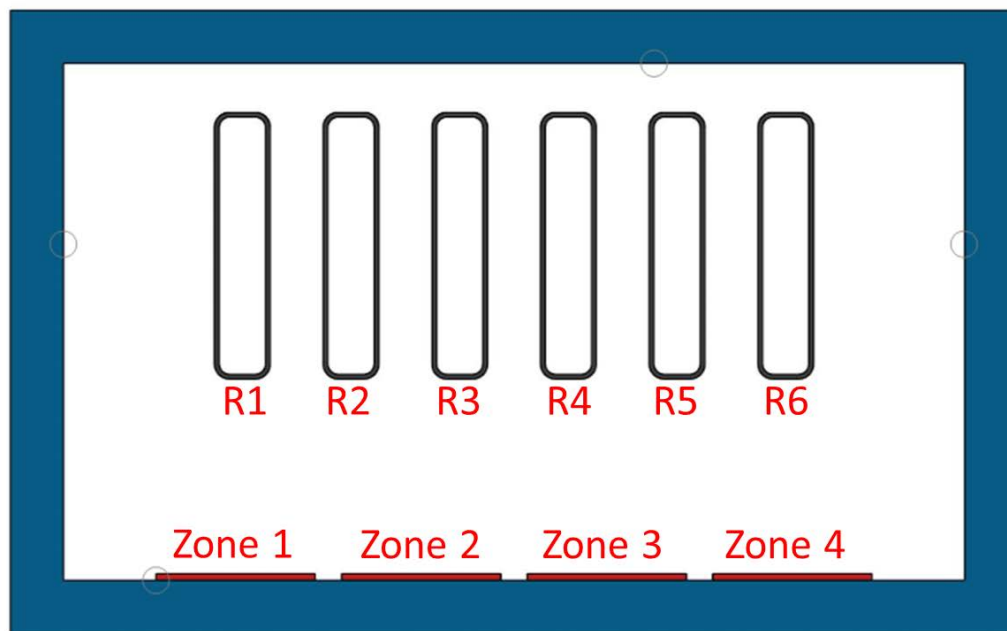


Figure 24 – Arrangement of heater zones.

### 3.2.2 Temperature Measurements

K-type thermocouples were placed throughout the air RCCS facility to measure local temperatures as one input to determine the heat removal performance of the facility. Omega 1/8" premade type-K thermocouple probes were used to measure the air temperature. In order to measure the surface temperature of the risers, a bulk spool of type-K thermocouple was used to weld the thermocouple wire to the metal surface. Out of the six risers, Riser 4 was more heavily instrumented. The vertical locations for the thermocouples welded on the front surface of the riser are shown in Figure 25. The cross section at these vertical thermocouple locations can be seen in Figure 26. A thermocouple was placed at the inlet ducting and a thermocouple was placed in each of the exhaust ducts before exiting the silo.

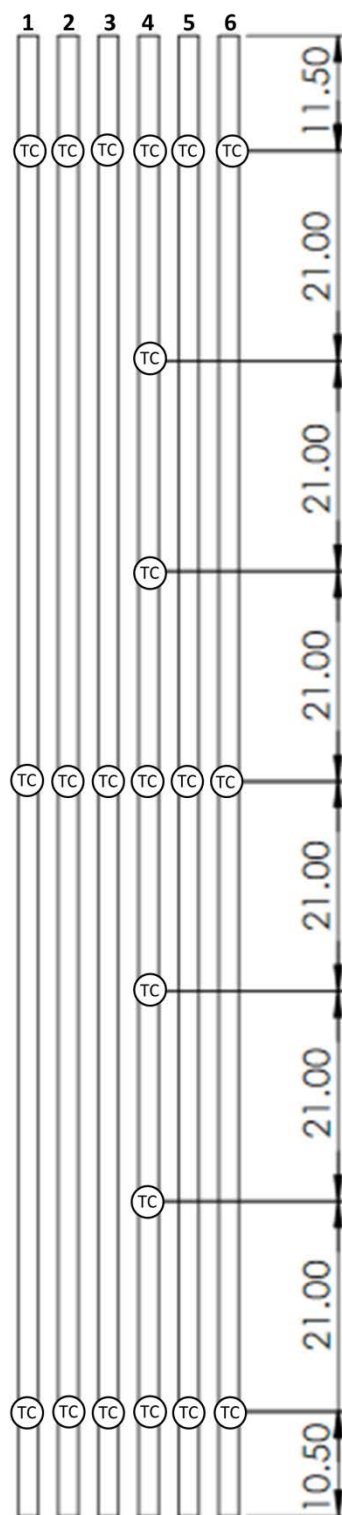
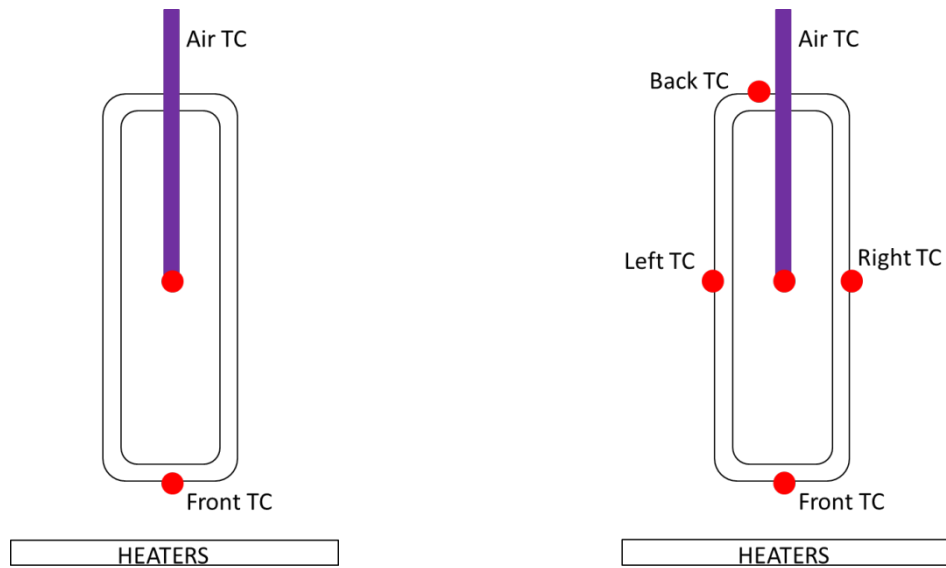


Figure 25 – Riser front surface thermocouple locations.



(a) Risers 1-3, 5-6 cross section

(b) Riser 4 cross section

Figure 26 – Riser cross section at thermocouple locations.

In addition to the thermocouples in the risers and exhaust ducts, 3 thermocouples were placed mid-plane of the heated section. The 3 thermocouples were attached to the Zircal insulation.

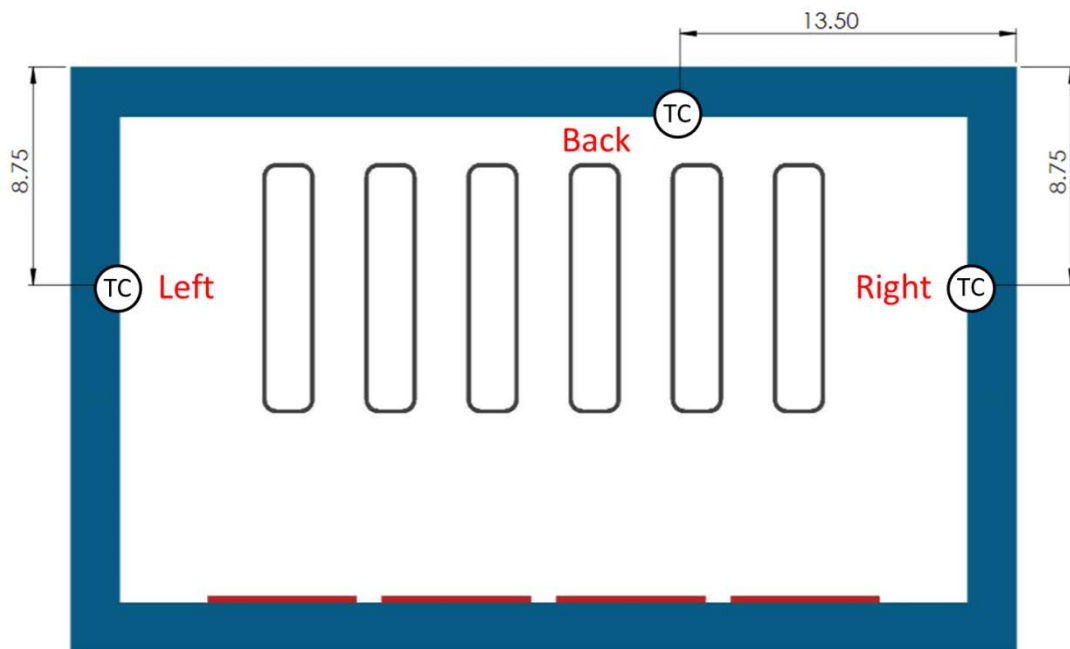


Figure 27 – Heated cavity wall thermocouples (dimensions in inches).

### 3.2.3 Velocity Measurements

In order to calculate the total air mass flow of the system, the velocity profile in the inlet piping is measured. A TSI 8455 air velocity transducer was installed with a probe length of 12". The velocity range of the TSI 8455 was 0.125 to 50 meters per second. A field selectable range of 0 to 10 meters per second was chosen along with a 0 to 10 V linear output range.



*(a) Velocity transducer in inlet piping*



*(b) View inside inlet plenum*

Figure 28 – Velocity transducer in the inlet piping.

TSI 8455 air velocity transducers were also placed in the middle of the flow cross section inside the inlet of the six risers. Due to the confined space, the transducers were placed 1.75" up from the bottom of the risers. This capability was used mostly for diagnostics to see if a riser was behaving differently from the other five. This is due to the short distance (1.75") between the entry of the risers and the velocity probes which do not allow the flow to fully

develop. Hence, the flow velocity vectors may not be perpendicular to the velocity probe. Due to the elevated temperatures, it was not possible to place the velocity probes further along the risers because of temperature limitations. Details on the velocity transducers placed at the entry of the riser ducts is discussed in Appendix C



Figure 29 – Velocity transducers in the six riser ducts.

### 3.2.4 Weather Station

The exhausts of the quarter-scale air RCCS facility are exposed to the outside environment. Hence, it is of interest to observe and record weather conditions during testing to better understand if the natural circulation flow in the facility is affected by adverse weather. A Vantage VUE weather station from Davis Instruments was mounted on the silo exterior as seen in Figure 30. The weather station can collect a wide variety of weather data including wind speed, wind direction, temperature, humidity, and rain fall.



(a) Silo exterior



(b) Weather station

Figure 30 – Weather station mounted on silo.

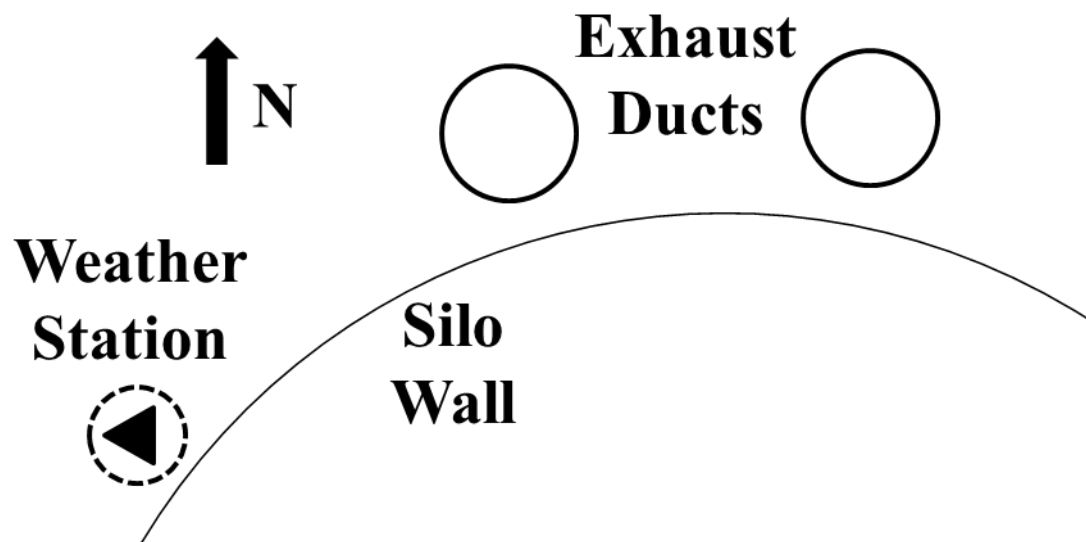


Figure 31 – Weather station orientation.

Several instrumentation is available onboard the weather station. Table 6 lists the devices available, their corresponding measurement range, and the measurement uncertainty.

Table 6-Measurement device and associated uncertainties.

<b>Sensor</b>	<b>Range</b>	<b>Uncertainty</b>
Temperature	-40-60 °C	$\pm 0.5^{\circ}\text{C}$
Wind speed	1/80 m/s	$\pm 0.05 \text{ m/s}$
Wind direction	0-360°	$\pm 3.0^{\circ}$
Barometric pressure	410-820 mmHg	$\pm 0.8 \text{ mmHg}$
Humidity	1-100 %	$\pm 0.03\%$
Rainfall	0-6553 mm	$\pm 0.04 \text{ mm}$

### 3.2.5 Measurement Uncertainty

The various devices previously described have specific ranges in which they can provide measurements and there is an uncertainty associated with that measurement. Table 3 list the uncertainties associated with the measurement devices.

K-type thermocouple 1/8" probes were placed in a circulating hot silicone bath to measure their deviation from a high-accuracy RTD. The thermocouple probes were connected to the same extension wires used during testing. The uncertainty was reduced from  $\pm 1.1^{\circ}\text{C}$  to  $\pm 0.7^{\circ}\text{C}$ . Thermocouples that were welded on the risers were purchased in a bulk spool and are accurate within  $\pm 2.2^{\circ}\text{C}$ .

The velocity sensors, TSI 8455, came with an NIST calibration certificate from the factory for each individual sensor. The manufacturer listed the uncertainty as  $\pm 2.0\%$  of the reading.

Table 7-Measurement device and associated uncertainties.

<b>Measurement</b>	<b>Type</b>	<b>Manufacturer</b>	<b>Range</b>	<b>Uncertainty</b>
Temperature	K, 1/8" probe	Omega	1250°C max	$\pm 0.7^{\circ}\text{C}$
Temperature	K, bulk spool	Omega	1250°C max	$\pm 2.2^{\circ}\text{C}$
Velocity	Ceramic sensor	TSI 8455	0.125-50 m/s	$\pm 2.0\%$
Rel. humidity	Transmitter	Omega HX93B	0-100%	$\pm 2.5\%$

## Chapter 4

### Characterization of the Facility

The quarter-scale air RCCS facility must be characterized due to the sensitivity of natural circulation loops. It is important to take into account the geometry, material selections, heat source, and instrumentation to estimate heat losses, propagation of error, and the overall energy balance. The following equation can be used to determine the heat removal performance of the RCCS:

$$\dot{Q}_{RCCS} = \dot{m}c_p\Delta T \quad (16)$$

A velocity profile at the inlet pipe duct can be measured and those point measurements can then be used to determine a total mass flow rate. Temperatures measured at the inlet piping and at the exhaust ducts were used to find the overall temperature difference ( $\Delta T$ ) for the overall system.

#### 4.1 Heat Source

Thirty-two radiant heaters are used in the heated cavity to simulate the reactor pressure vessel heating due to decay heat and radiate this heat to the air-cooled RCCS. The radiant heaters are configured in a four by eight array. The front surface temperature profile for all six risers shows that there is excellent uniformity across the test section during natural circulation tests. Figure 32 and Figure 33 show the riser front surface temperatures for two particular

experiments, Test 15 and Test 23, respectively as an illustration. The power provided to the heaters in Test 15 and Test 23 was 19.82 kW and 37.97 kW, respectively.

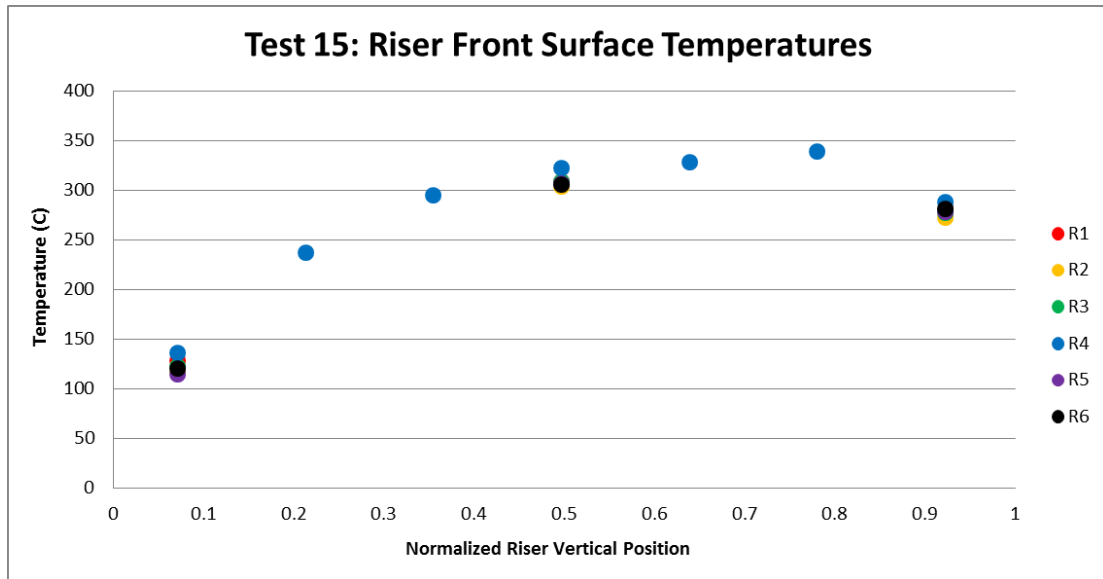


Figure 32 - Riser front surface temperatures for Test 15.

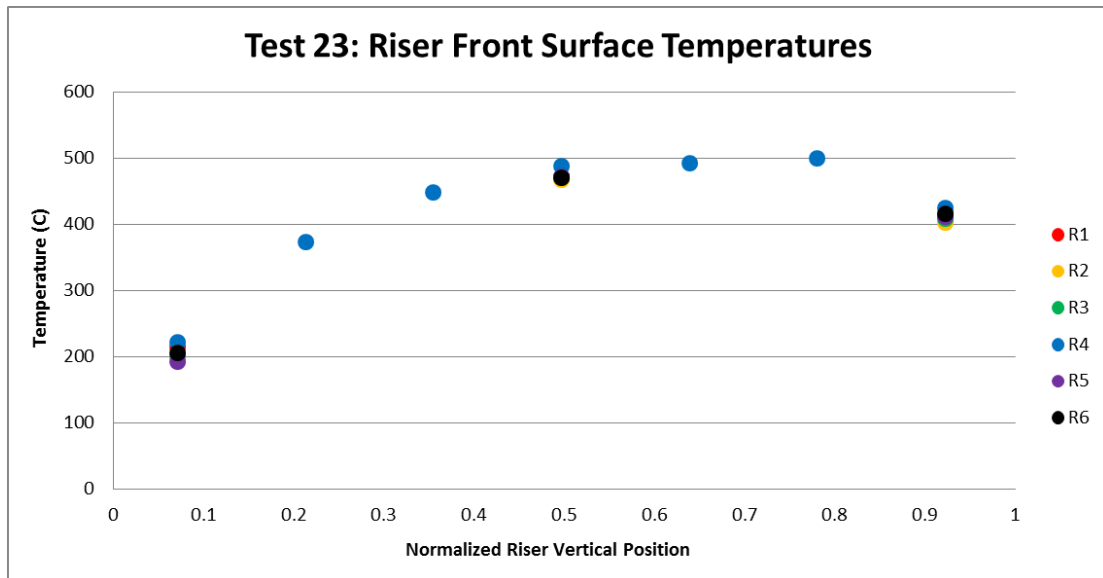


Figure 33 - Riser front surface temperatures for Test 23.

A k-type thermocouple was used inside the heated cavity to measure the radiant heater temperature. The thermocouple was placed on the back surface of the heater. There is a ceramic backing with a thickness of 0.125 inch. Taking measurements with thermocouple probes on the front surface where live wires are exposed could present electrical hazards. The ceramic backing provides minimal thermal resistance and at thermal equilibrium can be used to approximate the heater surface temperature as a lower bound to the actual temperature.

Table 8 – Heater Temperatures.

<b>Integral Power</b>	<b>Temperature</b>
19.82 kW	520.1 °C
37.97 kW	879.6 °C

## 4.2 Heat Losses

The heat losses for the air RCCS were estimated using hand-held measurements of exterior surface temperature and probe measurements of interior wall temperature coupled with fundamental heat transfer equations. Heat losses were calculated for the heated section, outlet plenum, and the exhaust duct piping inside of the silo. Exterior surface measurements were taken with an IR thermometer (point measurements) and k-type thermocouples for internal temperature measurements. Heat transfer by conduction can be used to model the heat loss through the heated cavity section walls. The rate of heat loss can be expressed by:

$$\dot{Q}_{loss} = kA(T_{probe} - T_{infrared})/d \quad (17)$$

where k is the thermal conductivity, d is the thickness, and A is the area in which the heat transfer occurs.

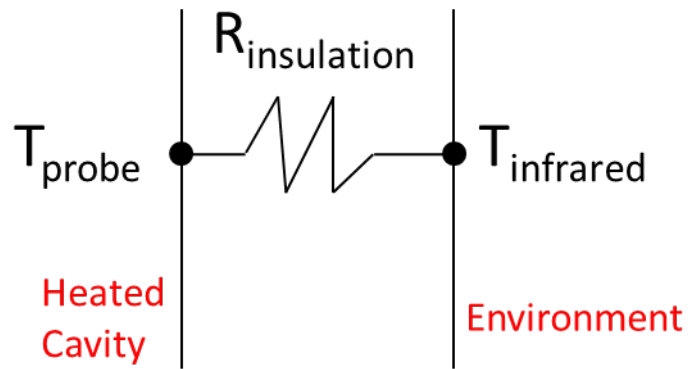


Figure 34 – 1-D heat loss schematic.

Figure 6 shows a cross-section of the heated cavity and shows the thermocouple probe locations along with the calculated heat loss on each side of the cavity. Exterior surface temperatures of the heated cavity were obtained with an infrared (IR) temperature gun. The heat losses were calculated in similar fashion for the outlet plenum box. However, due to the complexity of the flow and temperature profiles inside the outlet plenum, the average air exit temperature in the riser ducts was used as the internal temperature in lieu of thermocouple probe measurements.

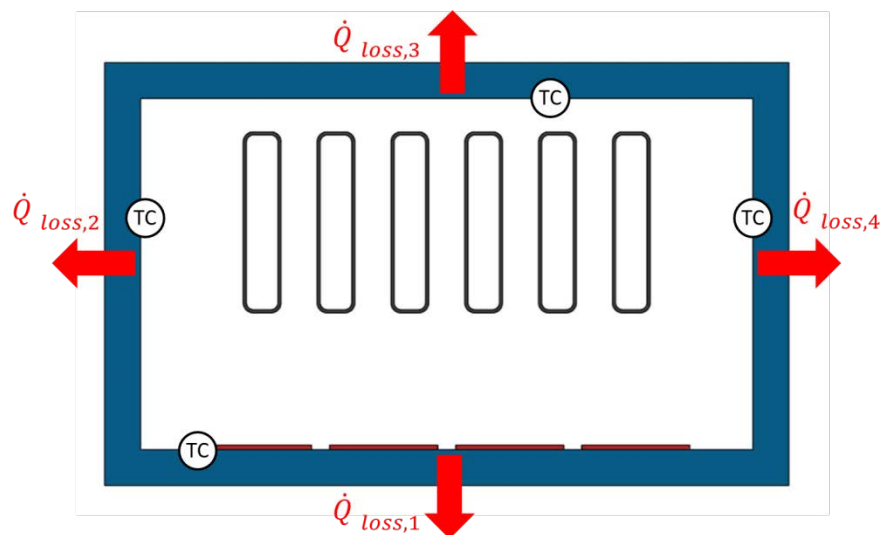


Figure 35 - Heat losses in heated cavity.

The heat loss in the exhaust ducts was only calculated for the piping inside of the silo. Thermocouple probes were placed in both exhaust ducts and were used as the internal temperature. Exterior surface temperatures of the insulation were taken with the IR gun. Table 9 lists the heat losses calculated for each test. Insulation thickness and thermal properties can be found in Table 4 (Section 3.2.5 Thermal Insulation). A detailed analysis can be found in Appendix D. An alternate method for calculating heat losses was also performed and can be found in Appendix E.

Table 9 - Heat loss calculations for tests.

Test	Case	Power (kW)	Heat Loss (kW)	Heat Loss (%)
14	Forced Flow	19.82	3.54	17.85
16			3.56	17.97
15	Constant Flux	19.82	4.66	23.51
17			4.67	23.55
19	Asymmetric	9.91	2.16	21.80
21			2.23	22.53
18	Forced Flow	37.97	6.39	16.83
20			6.42	16.92
23	Constant Flux	37.97	8.15	21.47
25			8.14	21.46
27	Asymmetric	18.99	4.13	21.79
29			4.29	22.60

## 4.3 Flow Profile

In order to quantify the thermal power (and thus energy balance) of the RCCS, it is necessary to translate the point velocity measurements into a total mass flow rate of the system. The characterization of the flow regime at the inlet duct (where the velocity probe is installed) is very important. The Reynolds number is the ratio of inertial forces to viscous forces and can be used to characterize whether the flow regime is laminar or turbulent. The internal flow in a circular pipe is classified as a developed turbulent flow when the Reynolds number is greater than or equal to 4,000 (Cengel, 2006). The range of the Reynolds number observed in the natural circulation experiments was 35,451 to 39,780 and hence the flow is turbulent.

$$Re = \frac{\rho V D_H}{\mu} \quad (18)$$

A velocity probe (TSI 8455) was placed at the inlet piping as discussed in Chapter 3 (Facility Overview). The mass flow rate at the inlet piping can be calculated by

$$\dot{m}_{total} = \rho_i V_i A_i \quad (19)$$

where  $\rho_i$  is the air density,  $V_i$  is the velocity, and  $A_i$  is the cross-sectional area. The velocity is calculated by recording the velocity along the center-line vertical position of the duct shown in Figure 36. The distances from the center at which the velocity was recorded along the centerline were 0, 1, 2, 3, 4, 5, 5.5 inches. The diameter of the inlet ducts is 12 inches. Two velocity profiles were obtained for Test 14 and Test 16 and can be seen in Figure 37 and Figure 38, respectively. Test 14 and Test 16 were carried out under forced flow conditions with an inline duct fan. The flow profiles for all other tests can be found in Appendix F. The

variation of the velocity measurements (at the inlet piping) with respect to time is presented in Appendix G.

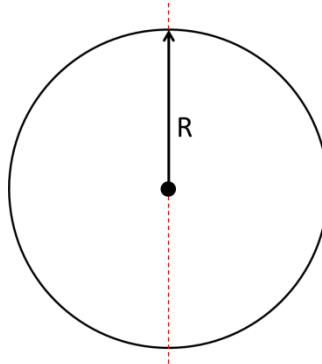


Figure 36 – Inlet duct centerline

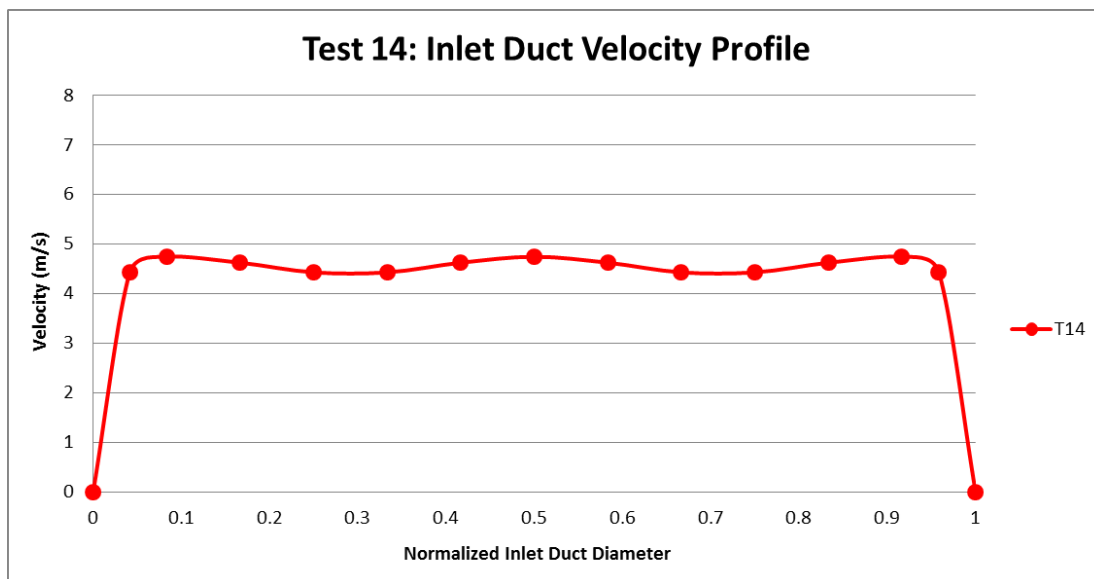


Figure 37 - Inlet duct velocity profile for Test 14.

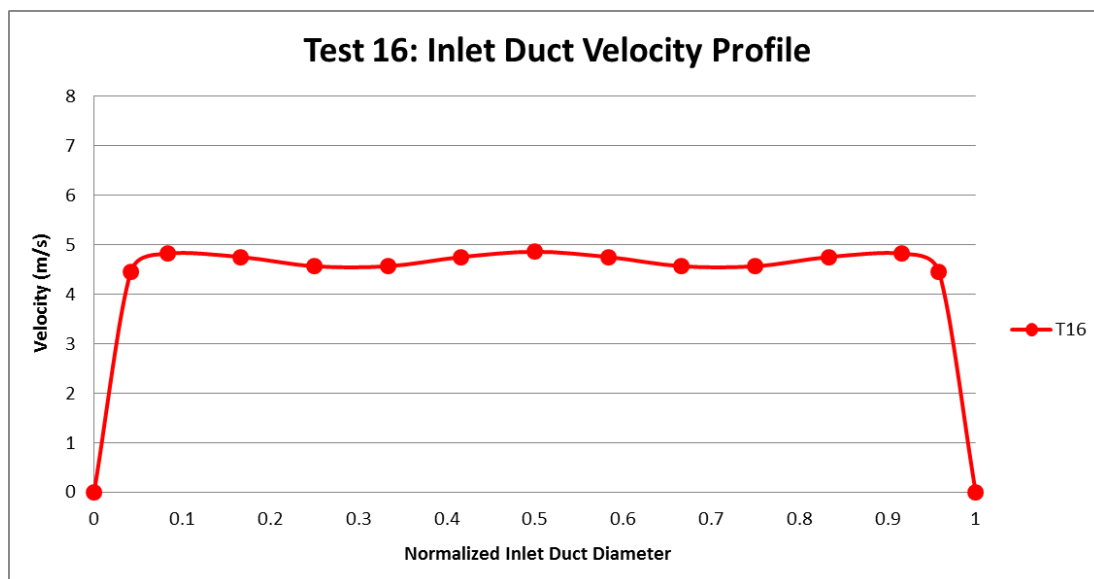


Figure 38 - Inlet duct velocity profile for Test 16.

## 4.4 Nominal Behavior

Four experiments were carried out under forced flow conditions to ensure that the air RCCS facility produces repeatable data. An inline duct fan was placed at the beginning of the inlet piping and set at 50 percent power. A total of 4 tests were run at two different powers; 19.82 kW and 37.93 kW. The power was equally distributed among the four heating zones.

### 4.4.1 Forced Flow Testing at 19.82 kW

Test 14 was run under forced flow conditions with a power input of 19.82 kW. The power delivered to the heaters was gradually increased with a ramp up time duration of 3 hours and 20 minutes. The experiment was run for 7 hours and thermal equilibrium was reached. The parameters calculated for Tests 14 are shown in Table 10.

Table 10 - Test 14 parameters.

Parameter	Test 14
$\Delta T$ ( $^{\circ}\text{C}$ )	41.50
$\dot{m}_{total}$ (kg/s)	0.38
$\dot{m}_{total}c_p\Delta T$ (kW)	15.76

The time history for the inlet and outlet duct temperatures for Test 14 can be seen in Figure 39. Throughout the duration of the tests, the temperatures in the heated cavity wall were observed and the time history for Test 14 can be seen in Figure 40. Thermocouples were placed in the six risers to observe the air temperatures. Time averaging of the thermocouple data was done between the fifth and seventh hour of the test when thermal equilibrium was achieved. The riser air temperatures at steady-state for Test 14 can be seen in Figure 41. Thermocouples were welded on the front surface of the riser ducts. The front surface

temperatures at steady-state for Test 14 can be seen in Figure 42. Riser 4 was heavily instrumented compared to the other risers. Additional thermocouples were welded on the left, back, and right sides of Riser 4. Riser 4 temperature trends can be seen in Figure 43.

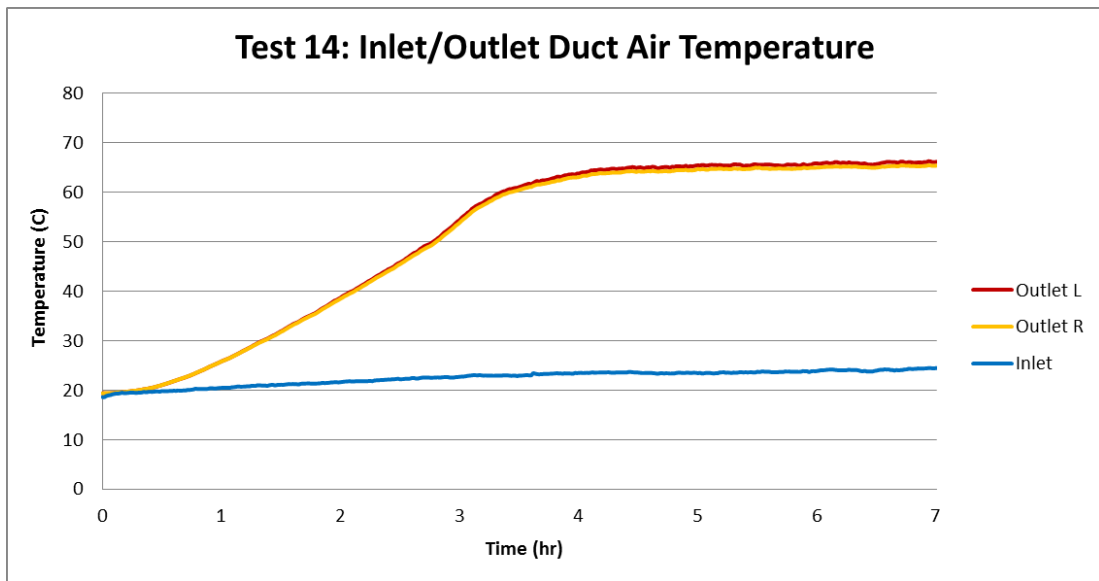


Figure 39 - Inlet/outlet duct air temperatures for Test 14 (Uncertainty:  $\pm 0.7^{\circ}\text{C}$ ).

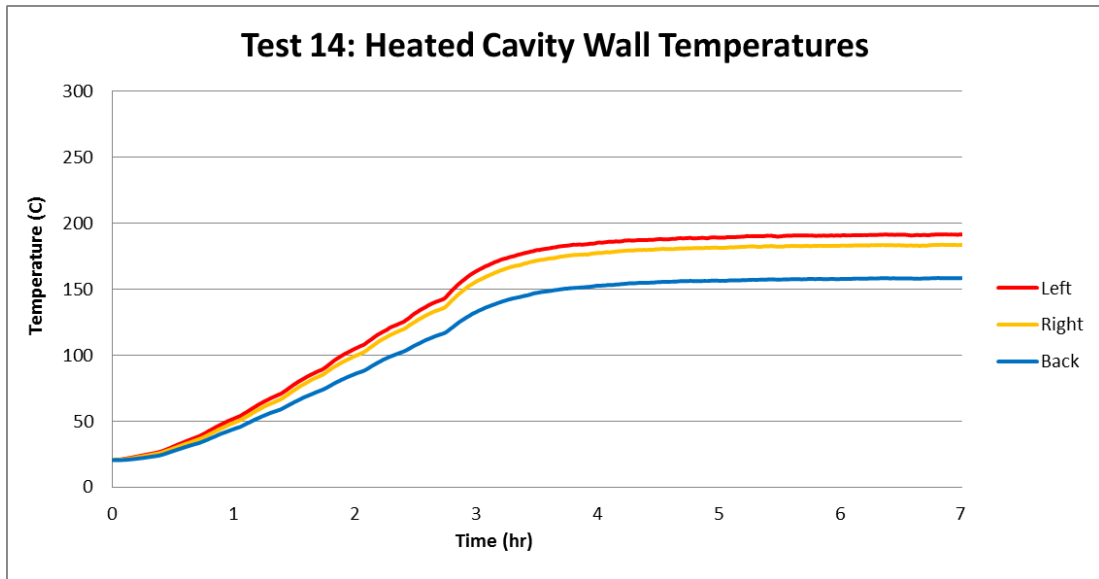


Figure 40 - Heated cavity wall temperatures for Test 14 (Uncertainty:  $\pm 0.7^{\circ}\text{C}$ ).

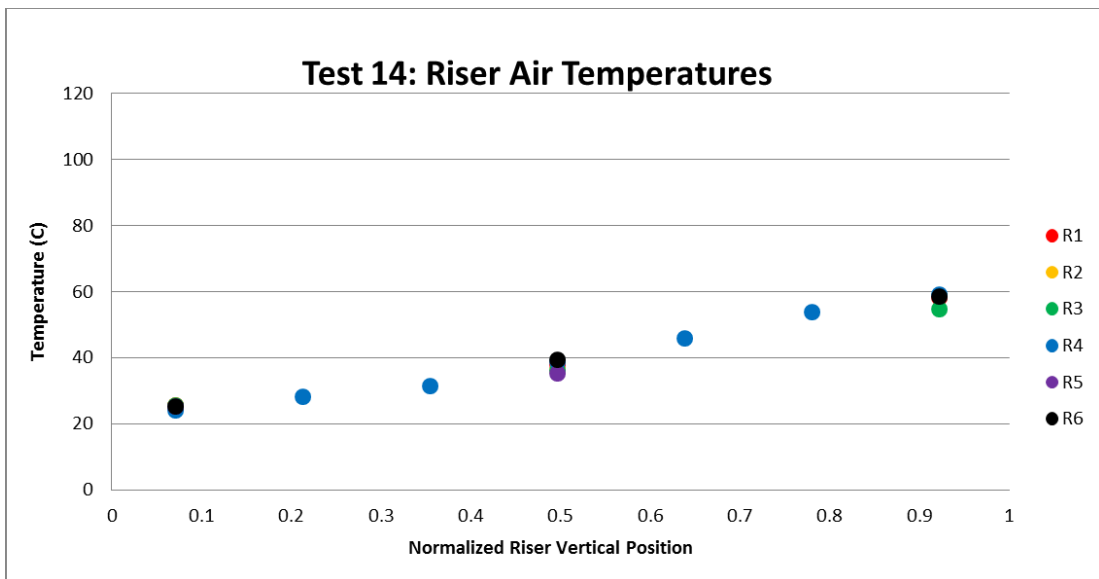


Figure 41 - Riser air temperatures for Test 14 (Uncertainty:  $\pm 0.7^{\circ}\text{C}$ ).

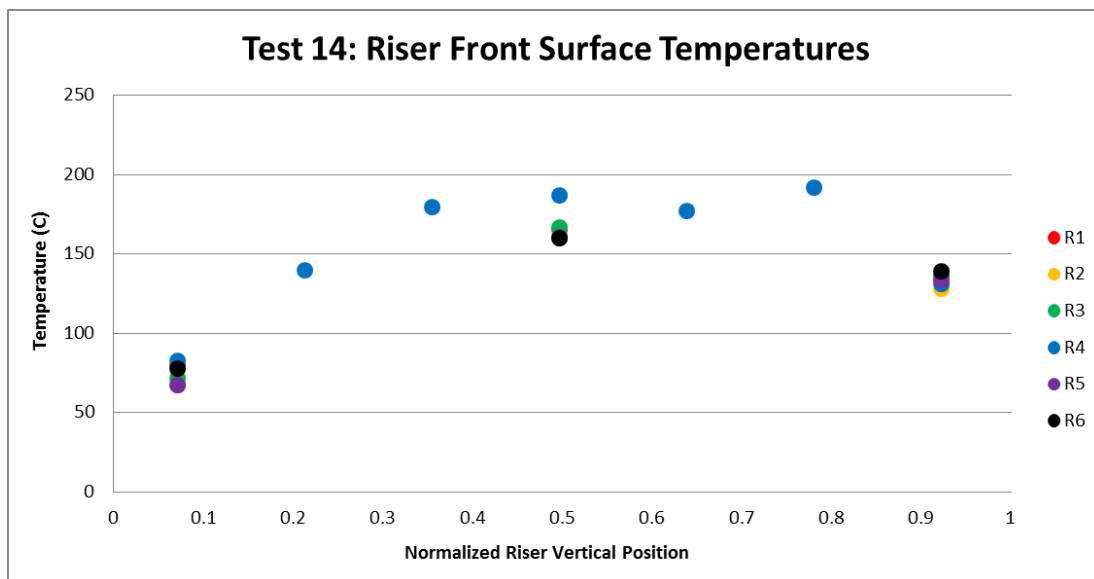


Figure 42 - Riser front surface temperatures for Test 14 (Uncertainty:  $\pm 2.2^{\circ}\text{C}$ ).

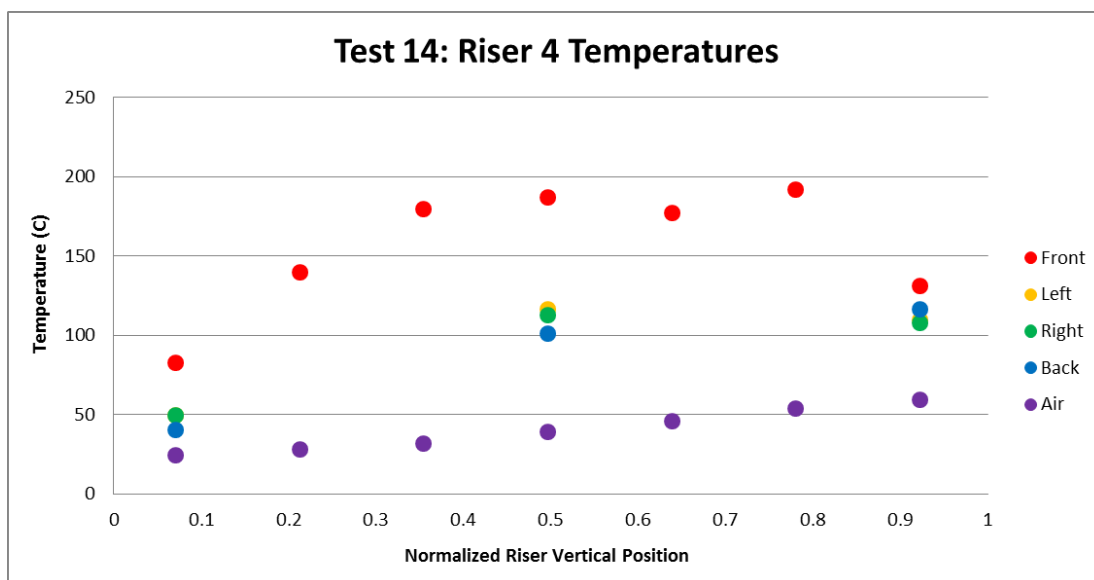


Figure 43 - Riser 4 temperatures for Test 14 (Uncertainty:  $\pm 2.2^{\circ}\text{C}$  for Front, Others  $\pm 0.7^{\circ}\text{C}$ ).

## 4.4.2 Forced Flow Testing at 37.97 kW

Test 18 was run under forced flow conditions with a power input of 37.82 kW. The power delivered to the heaters was gradually increased with a ramp up time duration of 3 hours and 20 minutes. The experiment was run for 8 hours and thermal equilibrium was reached. Parameters calculated for Test 18 are shown in Table 11.

Table 11 - Test 18 parameters.

Parameter	Test 18
$\Delta T$ ( $^{\circ}\text{C}$ )	76.12
$\dot{m}_{total}$ (kg/s)	0.38
$\dot{m}_{total}c_p\Delta T$ (kW)	29.35

The time history for the inlet and outlet duct temperatures for Test 18 can be seen in Figure 44. Throughout the duration of the tests, the temperatures in the heated cavity wall were observed and the time history for Test 18 can be seen in Figure 45. Thermocouples were placed in the six risers to observe the air temperatures. Time averaging of the thermocouple data was done between the fifth and seventh hour of the test when thermal equilibrium was achieved. The riser air temperatures at steady-state for Test 18 can be seen in Figure 46. Thermocouples were welded on the front surface of the riser ducts. The front surface temperatures at steady-state for Test 18 can be seen in Figure 47. Riser 4 was heavily instrumented compared to the other risers. Additional thermocouples were welded on the left, back, and right sides of Riser 4. Riser 4 temperature trends can be seen in Figure 48.

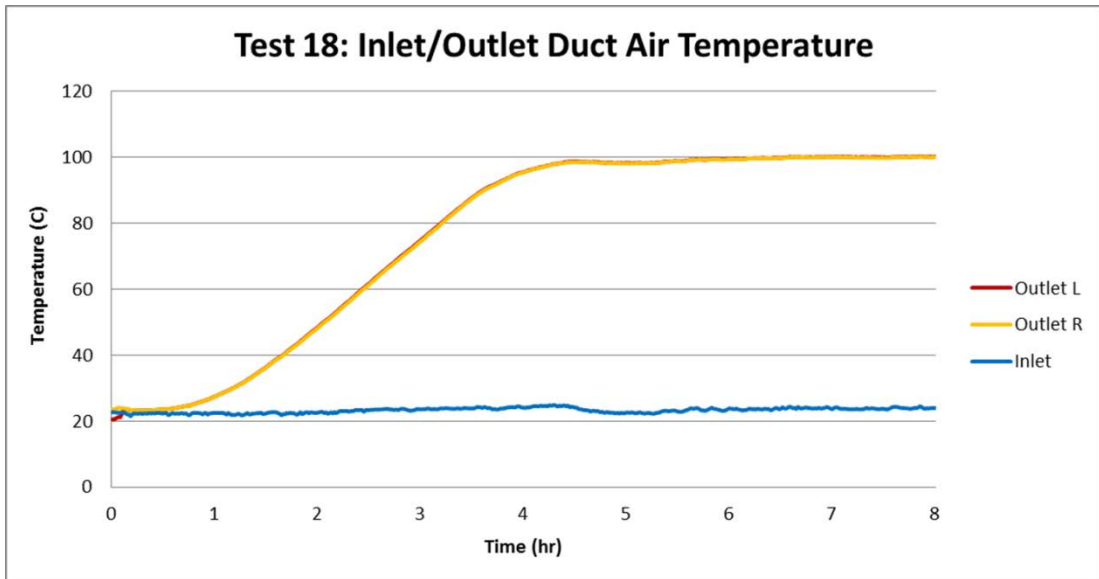


Figure 44 - Inlet/outlet duct air temperatures for Test 18 (Uncertainty:  $\pm 0.7^{\circ}\text{C}$ ).

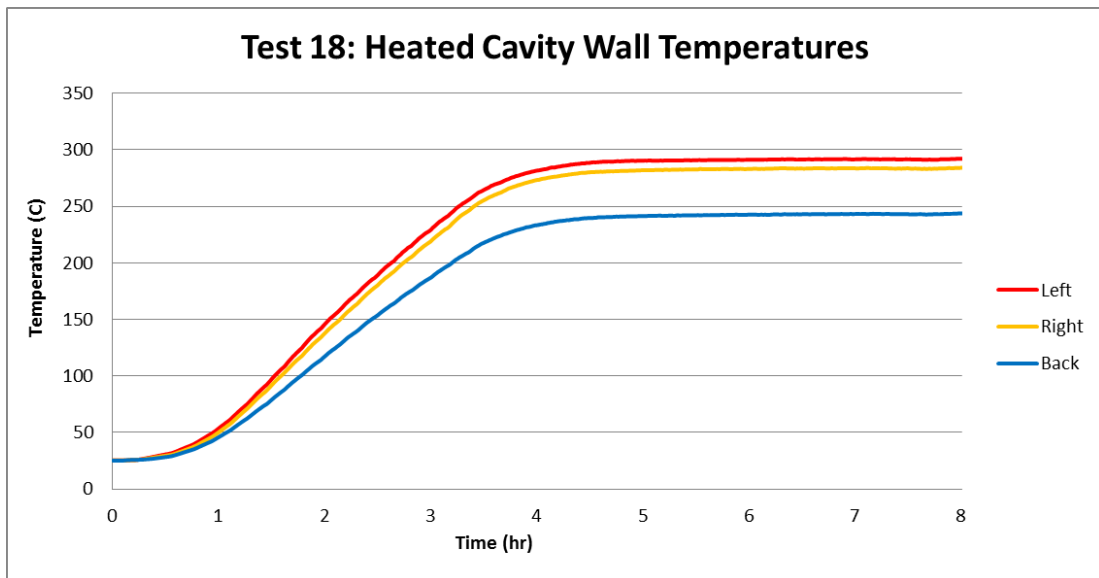


Figure 45 - Heated cavity wall temperatures for Test 18 (Uncertainty:  $\pm 0.7^{\circ}\text{C}$ ).

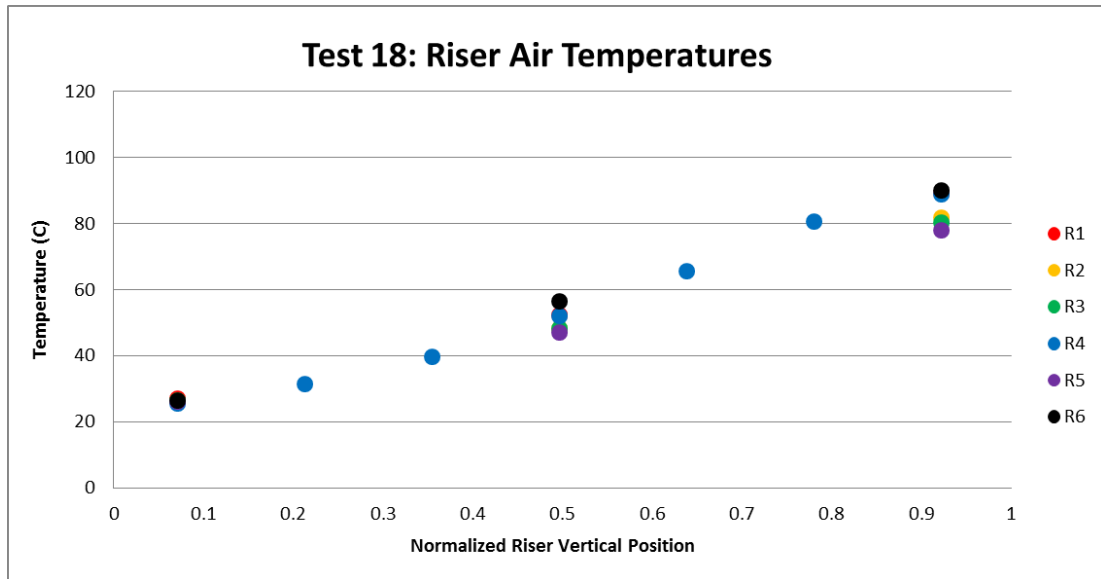


Figure 46 - Riser air temperatures for Test 18 (Uncertainty:  $\pm 0.7^{\circ}\text{C}$ ).

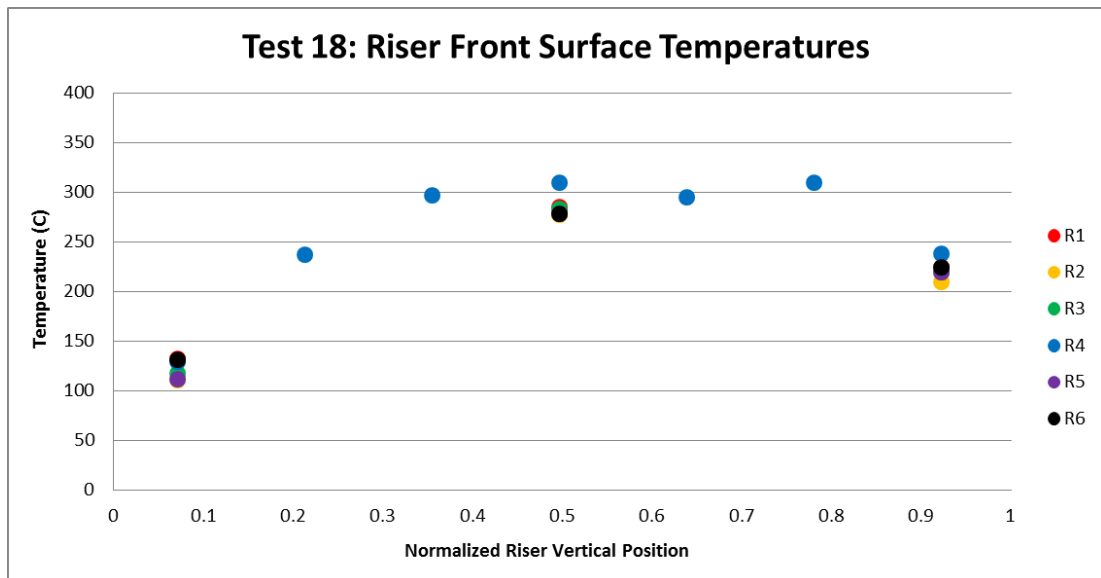


Figure 47 - Riser front surface temperatures for Test 18 (Uncertainty:  $\pm 2.2^{\circ}\text{C}$ ).

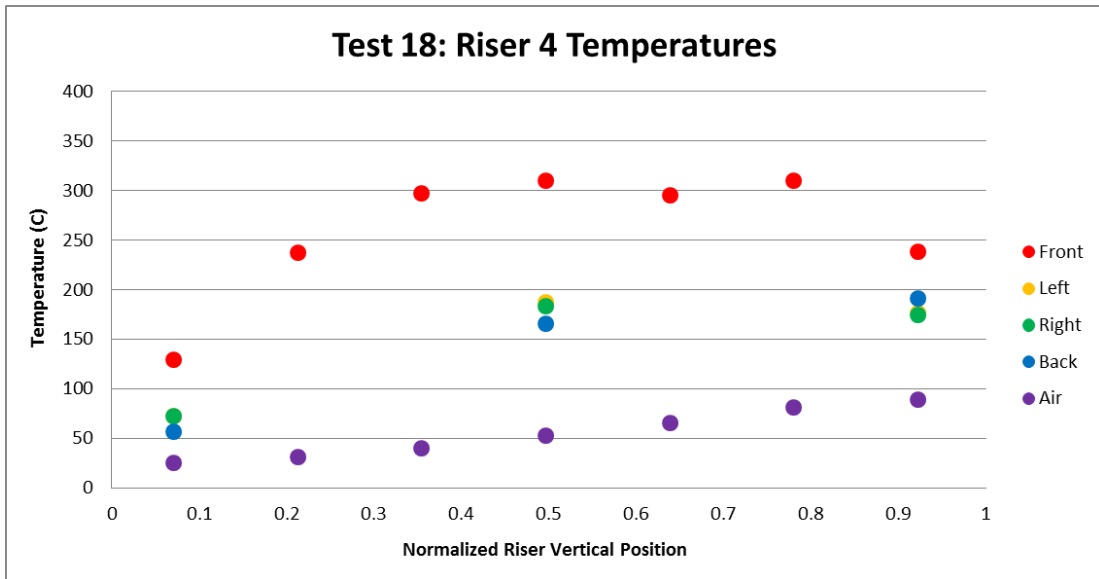


Figure 48 - Riser 4 temperatures for Test 18 (Uncertainty:  $\pm 2.2^{\circ}\text{C}$  for Front, Others  $\pm 0.7^{\circ}\text{C}$ ).

## 4.5 Repeatability

Two tests (Test 16 and Test 20) were run in addition to Test 14 and Test 18 at the respective power to ensure repeatability. Different parameters (temperature differential across the system, mass flow, and energy balance) were calculated as well as the deviation. The complete set of figures for Test 16 and Test 20 can be seen in Appendix E.

### 4.5.1 Forced Flow Testing at 19.82 kW

Tests 14 and 16 both produced very similar results. Table 12 lists parameters calculated for each test and their deviation. Figure 49 shows the  $\Delta T$  of the RCCS system for both tests with respect to time. The average riser front surface temperatures for Test 14 and Test 16 can be seen in Figure 50. Figure 51 shows the average riser air temperatures for both tests.

Table 12 - Test 14 and 16 parameters.

Parameter	Test 14	Test 16	Deviation
$\Delta T$ ( $^{\circ}\text{C}$ )	41.50	41.13	0.89 %
$\dot{m}_{total}$ (kg/s)	0.38	0.39	2.56 %
$\dot{m}_{total} c_p \Delta T$ (kW)	15.76	15.93	1.07 %

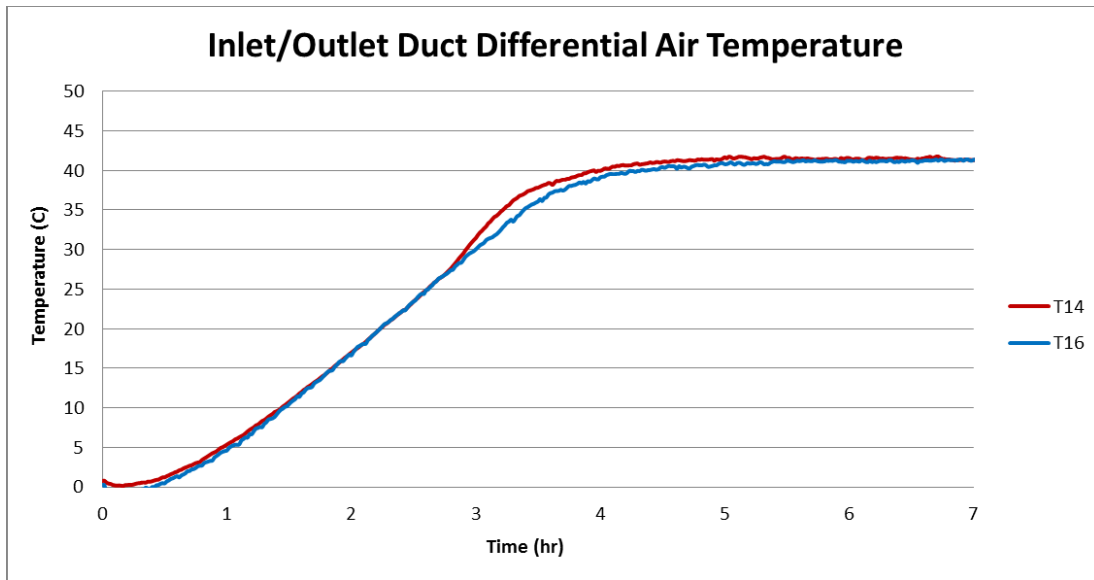


Figure 49 – Differential duct air temperatures for Test 14 and Test 16.

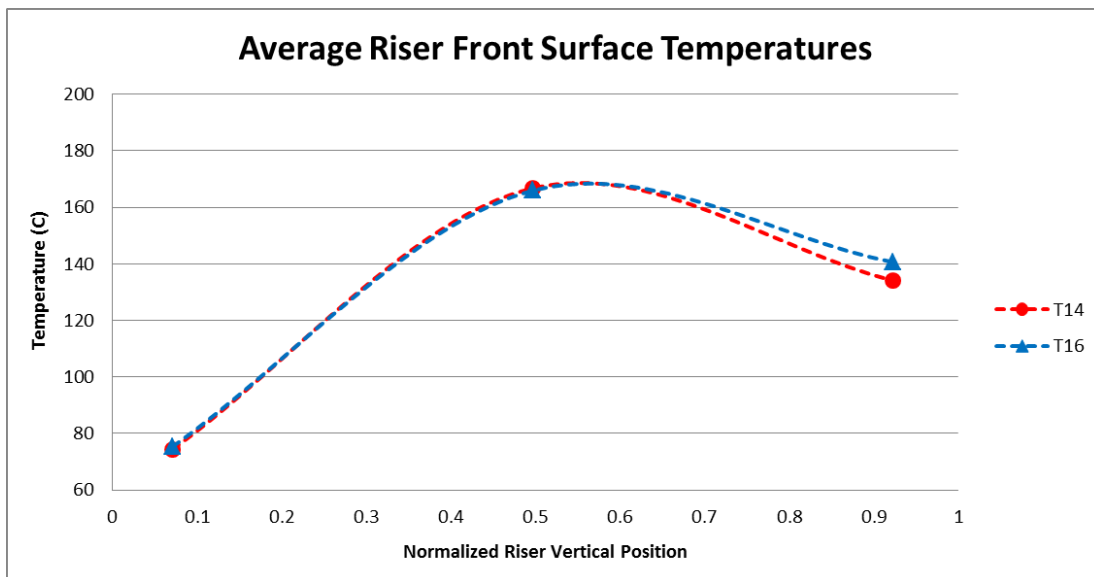


Figure 50 – Average riser front surface temperatures for Test 14 and Test 16.

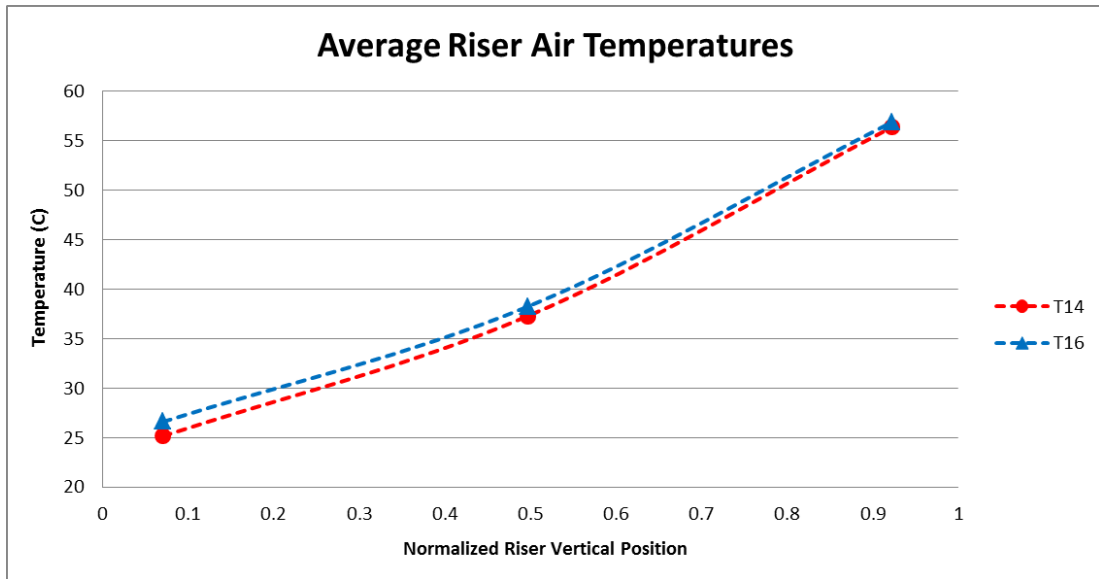


Figure 51 – Average riser air temperatures for Test 14 and Test 16.

## 4.5.2 Forced Flow Testing at 37.97 kW

Tests 18 and 20 both produced very similar results. Table 13 lists parameters calculated for each test and their deviation. Figure 49 shows the  $\Delta T$  of the RCCS system for both tests with respect to time. The average riser front surface temperatures for Test 18 and Test 20 can be seen in Figure 53. Figure 54 shows the average riser air temperatures for both tests.

Table 13 - Test 18 and 20 parameters.

Parameter	Test 18	Test 20	Deviation
$\Delta T$ ( $^{\circ}\text{C}$ )	76.12	75.08	1.37 %
$\dot{m}_{total}$ (kg/s)	0.38	0.39	2.56 %
$\dot{m}_{total}c_p\Delta T$ (kW)	29.35	29.38	0.10 %

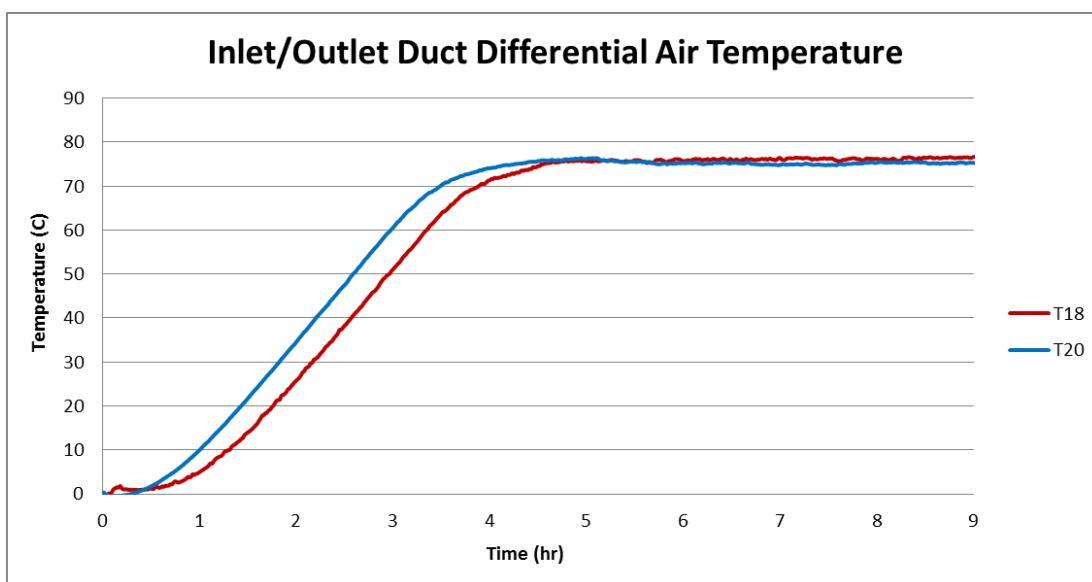


Figure 52 – Differential duct air temperatures for Test 18 and Test 20.

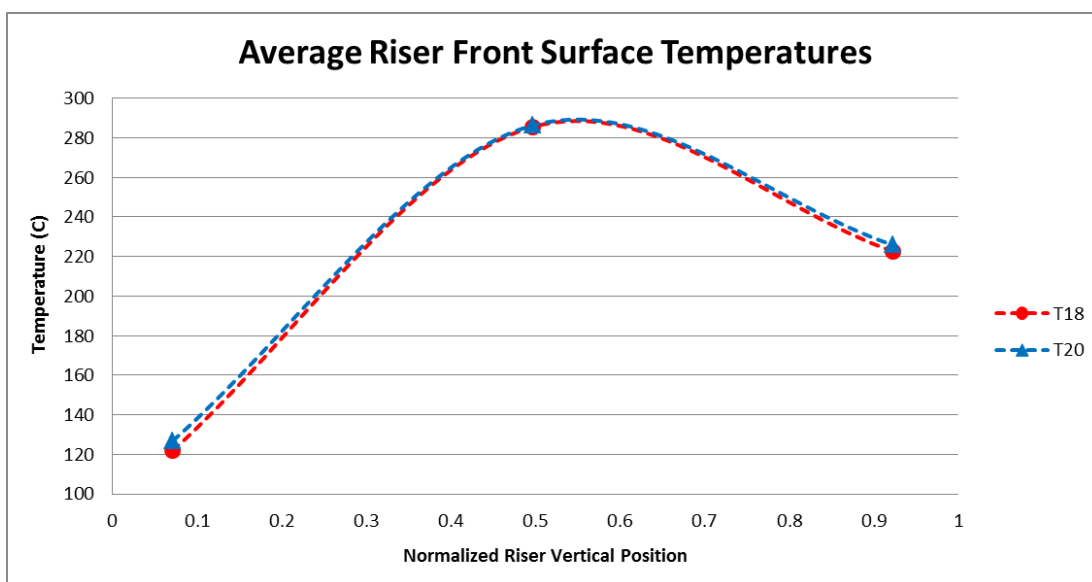


Figure 53 – Average riser front surface temperatures for Test 18 and Test 20.

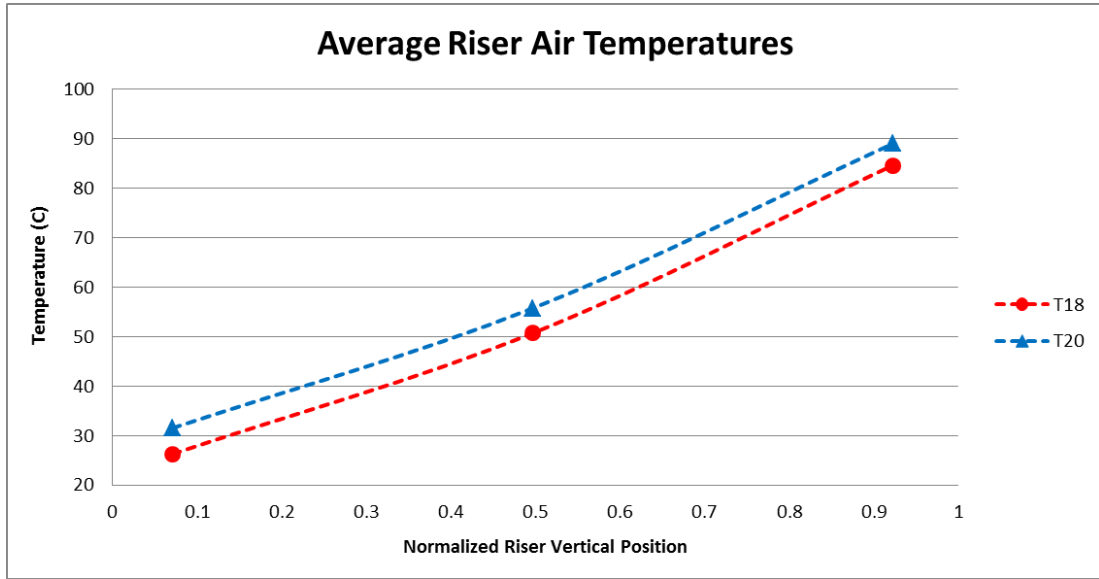


Figure 54 – Average riser air temperatures for Test 18 and Test 20.

## 4.6 Propagation of Error

There is error associated with measurement devices that is listed in manufacturer specification sheets (see Table 4 in section 3.3.5). The propagation of this error is accounted for in error analysis and uncertainty for calculations made with the data. Experimental data was used to calculate the heat removal of the RCCS as shown in Eq. 2.

$$\dot{Q}_{RCCS} = \dot{m}c_p(T_{exhaust}-T_{inlet}) \quad (20)$$

The equation can be expanded into Eq. 3.

$$\dot{Q}_{RCCS} = \rho V A c_p(T_{exhaust}-T_{inlet}) \quad (21)$$

The propagation of the error contributed by each variable can be found by calculating the partial derivative with respect to an individual variable.

Table 14 – Error propagation.

Variable	Error	Relative Error
Mass Flow	$\sigma_M = \sigma_{rel}V_m + \sigma_{abs}$	$\frac{\partial \dot{Q}}{\partial V_m} = \rho A c_p (T_{exhaust} - T_{inlet})$
Inlet Temperature	$\sigma_T = 0.7 \text{ } ^\circ\text{C}$	$\frac{\partial \dot{Q}}{\partial T_i} = \rho V_m A c_p$
Outlet Temperature	$\sigma_T = 0.7 \text{ } ^\circ\text{C}$	$\frac{\partial \dot{Q}}{\partial T_o} = \rho V_m A c_p$

The full uncertainty in the equation is expressed in Eq. 4.

$$\sigma_Q = \sqrt{\rho^2 A^2 c_p^2 [(T_{exhaust} - T_{inlet})^2 (\sigma_{rel}V_m + \sigma_{abs})^2 + 2V_m \sigma_T^2]} \quad (22)$$

The energy balance for Test 25 is 25.43 kW. Test 25 was a test operated at constant heat flux in which the power was distributed equally to all four heater zones. The uncertainty for this particular test is 25.43 kW  $\pm$  1.15 kW.

## Chapter 5

### Steady State Performance

The steady-state performance of the RCCS was investigated through natural circulation experiments where no inline duct fan was placed at the inlet piping. These experiments allowed the study of the thermal hydraulic behavior under different heat loads. Two different heat loads were utilized: constant heat flux power load and asymmetric power shaping. Table 9 presents the test matrix for the natural circulation tests. Repeatability of the natural circulations tests will be presented in Section 5.3.

Table 15 – Natural circulation test matrix.

Test	Case	Power (kW)	$\dot{m}_{total}$ (kg/s)	$\Delta T$ ( $^{\circ}\text{C}$ )	$\dot{m}_{total}c_p\Delta T$ (kW)
15	Constant Flux	19.82	0.16	90.28	14.39
17			0.15	90.38	13.90
19	Asymmetric	9.91	0.13	55.16	7.52
21			0.12	62.18	7.49
23	Constant Flux	37.97	0.18	141.63	25.60
25			0.18	141.71	25.43
27	Asymmetric	18.99	0.16	82.08	13.58
29			0.15	85.38	12.97

### 5.1 Constant Heat Flux Power Testing

The steady-state behavior at two varying power levels were investigated to observe the thermal hydraulic behavior and to calculate the heat removal performance of the air RCCS. A total of four tests were run at two power levels for the heaters (19.82 kW and 37.97 kW). The power input for the heaters was distributed equally into the four heating zones. During testing at both power levels, higher air temperatures were seen in Riser 4 compared to the other five

risers. In constant heat flux power conditions, it was expected that all risers would have similar air temperatures. As built drawings (in Appendix B) show that the inlet cross sectional area of Riser 4 is roughly 3.5% smaller than the other riser ducts. This variation in physical geometry could be playing a role in the higher temperatures observed.

### 5.1.1 Constant Heat Flux at 19.82 kW

Test 17 was run with a heater input of 19.82 kW that was equally distributed to the four heating zones. The power delivered to the heaters was gradually increased with a ramp up time duration of 3 hours and 20 minutes. The experiment was run for 10 hours and thermal equilibrium was reached. Table 10 lists the parameters calculated for Test 17. An additional test, Test 15, was run under similar conditions and is documented in Section 5.3.1.

Table 16 – Test 17 parameters.

Parameter	Test 17
$\Delta T$ ( $^{\circ}\text{C}$ )	90.38
$\dot{m}_{total}$ (kg/s)	0.15
$\dot{m}_{total}c_p\Delta T$ (kW)	13.90

The time history for the inlet and outlet duct temperatures for Test 17 can be seen in Figure 55. A sharp drop in temperature can be observed in the sixth hour of the test which is believed to be caused by a flow reversal in one of the exhaust ducts. After an hour, the desired flow pattern is restored without any human intervention.

The heated cavity wall temperatures can be seen in Figure 56. Time averaging was done between the eight and tenth hour to observe trends for all risers at thermal equilibrium. The front surface temperatures at steady-state for Test 17 can be seen in Figure 57. The riser air temperatures at steady-state can be seen in Figure 58. Riser 4 experienced higher air

temperatures compared to the five other risers. Riser 4 temperature trends can be seen in Figure 59.

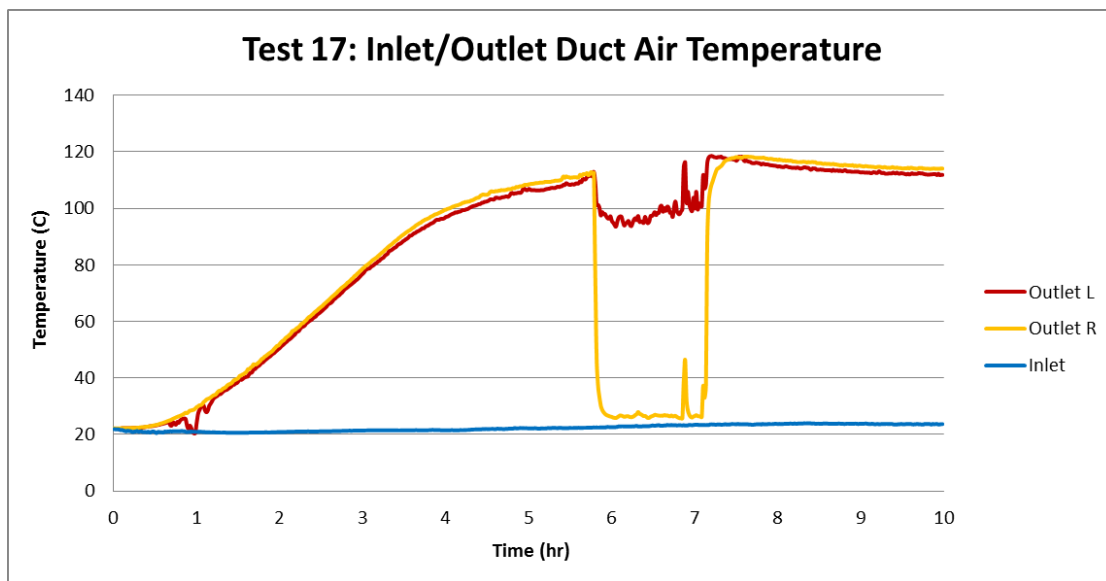


Figure 55 - Inlet/outlet duct air temperatures for Test 17 (Uncertainty:  $\pm 0.7^{\circ}\text{C}$ ).

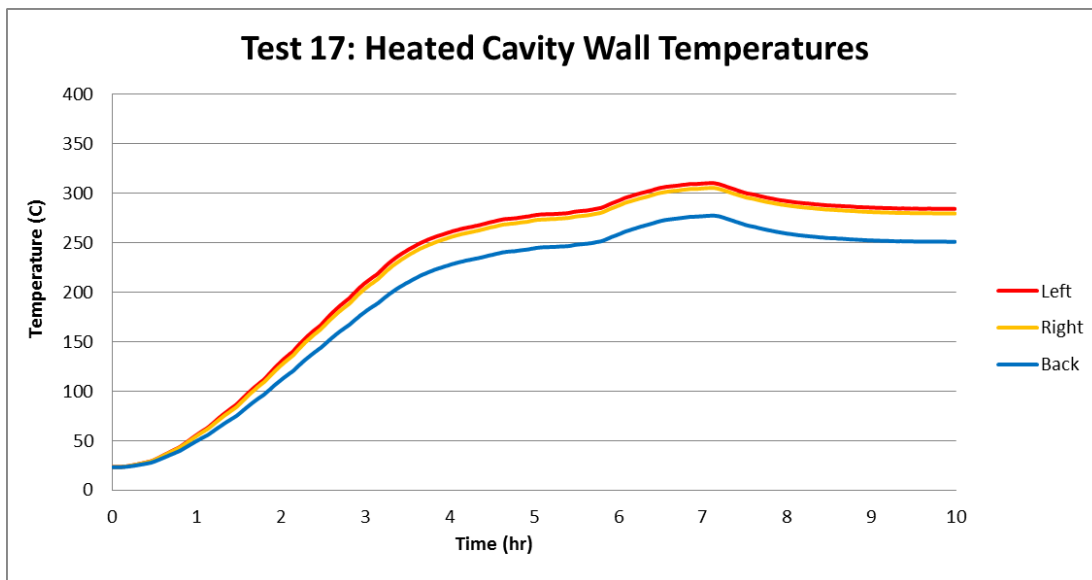


Figure 56 - Heated cavity wall temperatures for Test 17 (Uncertainty:  $\pm 0.7^{\circ}\text{C}$ ).

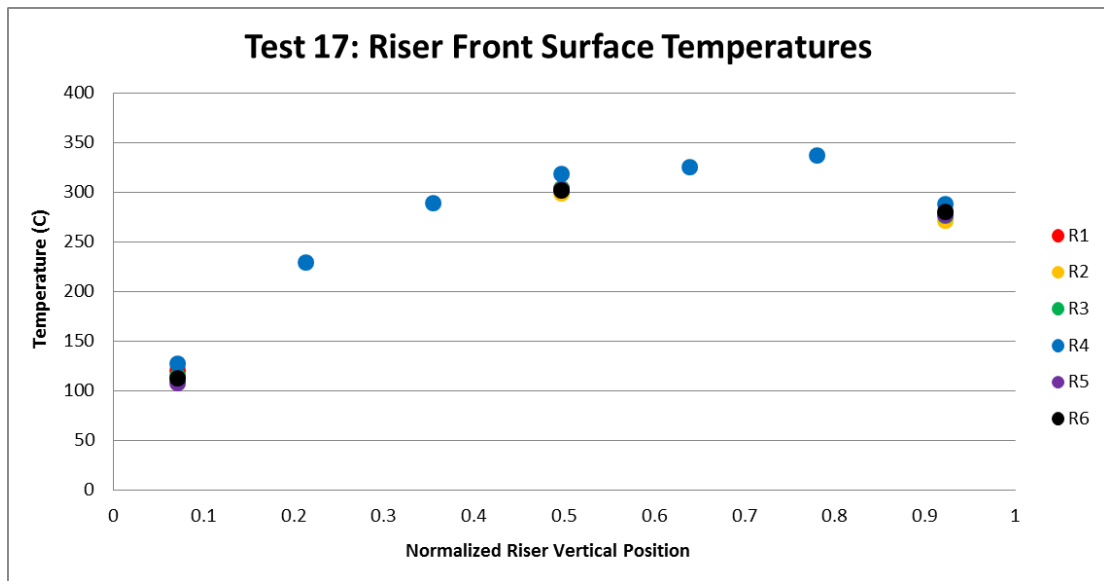


Figure 57 - Riser front surface temperatures for Test 17 (Uncertainty:  $\pm 2.2^{\circ}\text{C}$ ).

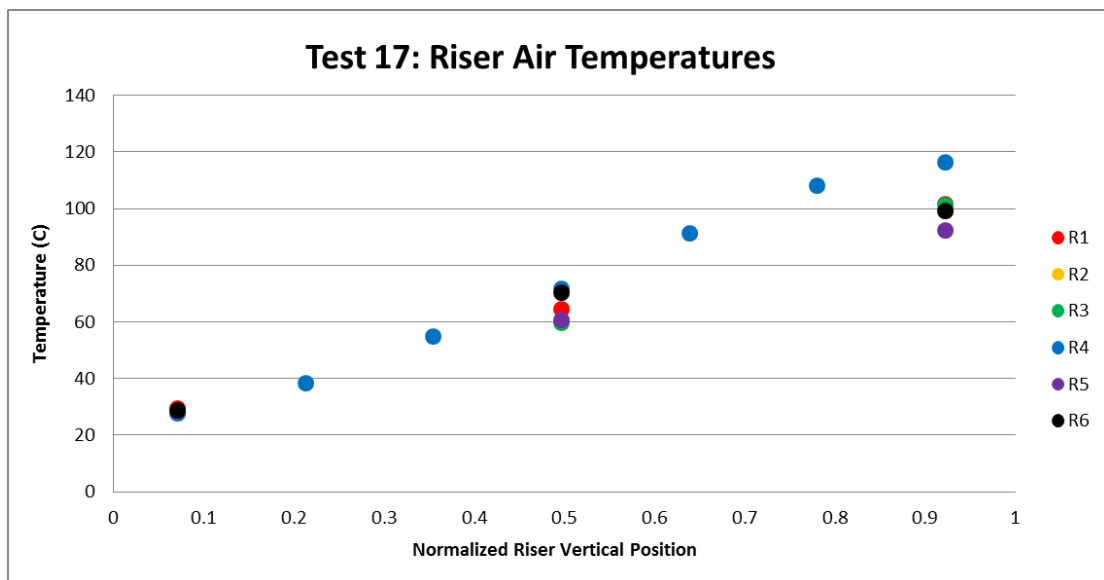


Figure 58 - Riser air temperatures for Test 17 (Uncertainty:  $\pm 0.7^{\circ}\text{C}$ ).

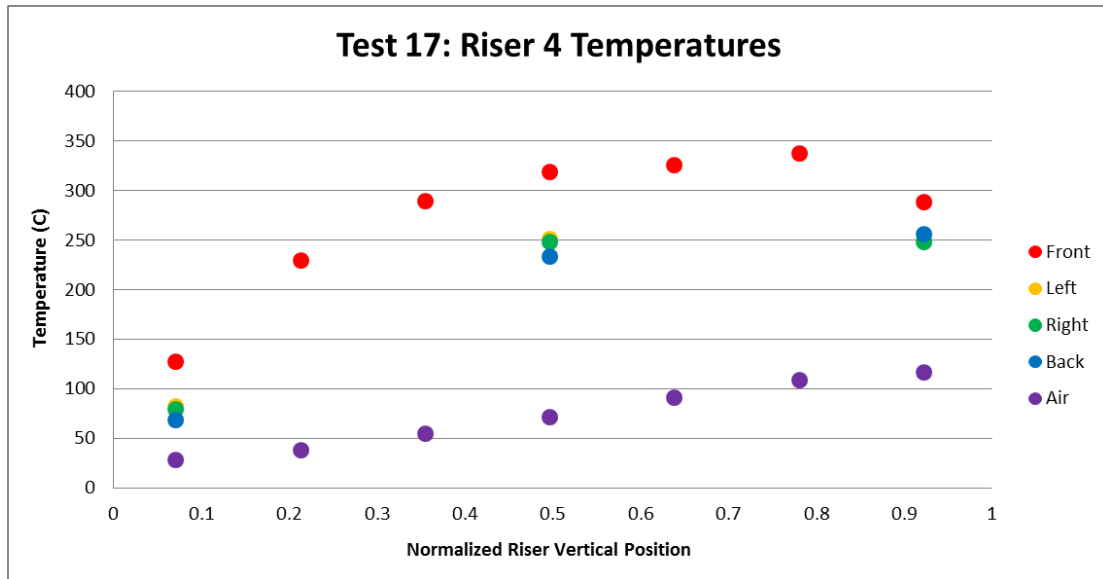


Figure 59 - Riser 4 temperatures for Test 17 (Uncertainty:  $\pm 2.2^{\circ}\text{C}$  for Front, Others  $\pm 0.7^{\circ}\text{C}$ ).

## 5.1.2 Constant Heat Flux at 37.97 kW

Test 25 was run with a heater input of 37.97 kW that was equally distributed to the four heating zones. The power delivered to the heaters was gradually increased with a ramp up time duration of 3 hours and 20 minutes. The experiment was run for 10 hours and thermal equilibrium was reached. Table 17 lists the parameters calculated for Test 25. An additional test, Test 23, was run under similar conditions and is documented in Section 5.3.2.

Table 17 – Test 25 parameters.

Parameter	Test 25
$\Delta T$ ( $^{\circ}\text{C}$ )	141.71
$\dot{m}_{total}$ (kg/s)	0.18
$\dot{m}_{total}c_p\Delta T$ (kW)	25.43

The time history for the inlet and outlet duct temperatures for Test 25 can be seen in Figure 60. The heated cavity wall temperatures can be seen in Figure 61. Time averaging was done between the eighth and tenth hour to observe trends for all risers at thermal equilibrium. The

front surface temperatures at steady-state for Test 25 can be seen in Figure 62. The riser air temperatures at steady-state can be seen in Figure 63. Riser 4 experienced higher air temperatures compared to the five other risers. Riser 4 temperature trends can be seen in Figure 64.

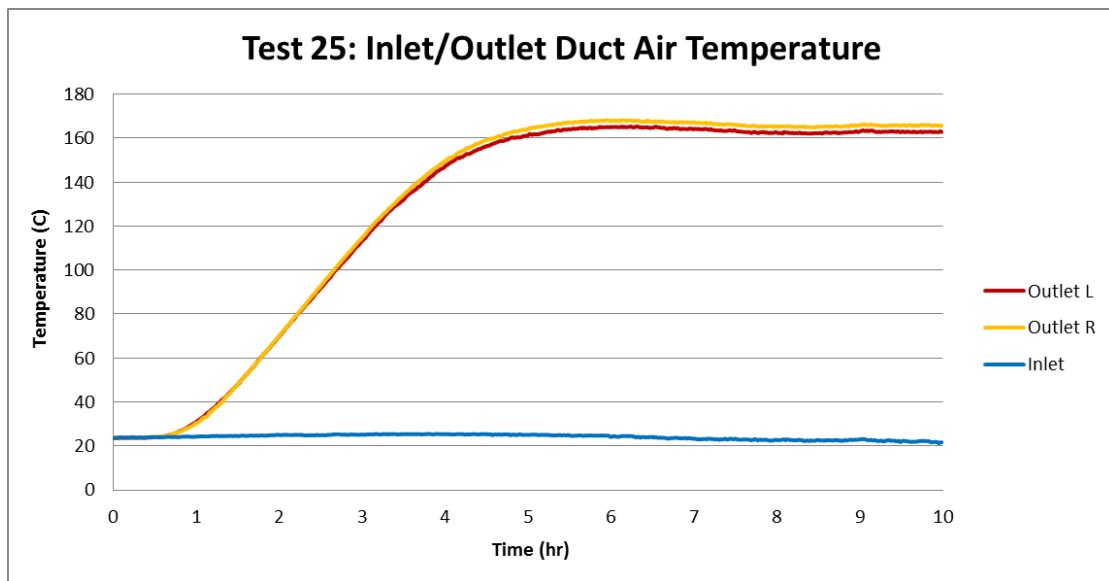


Figure 60 - Inlet/outlet duct air temperatures for Test 25 (Uncertainty:  $\pm 0.7^{\circ}\text{C}$ ).

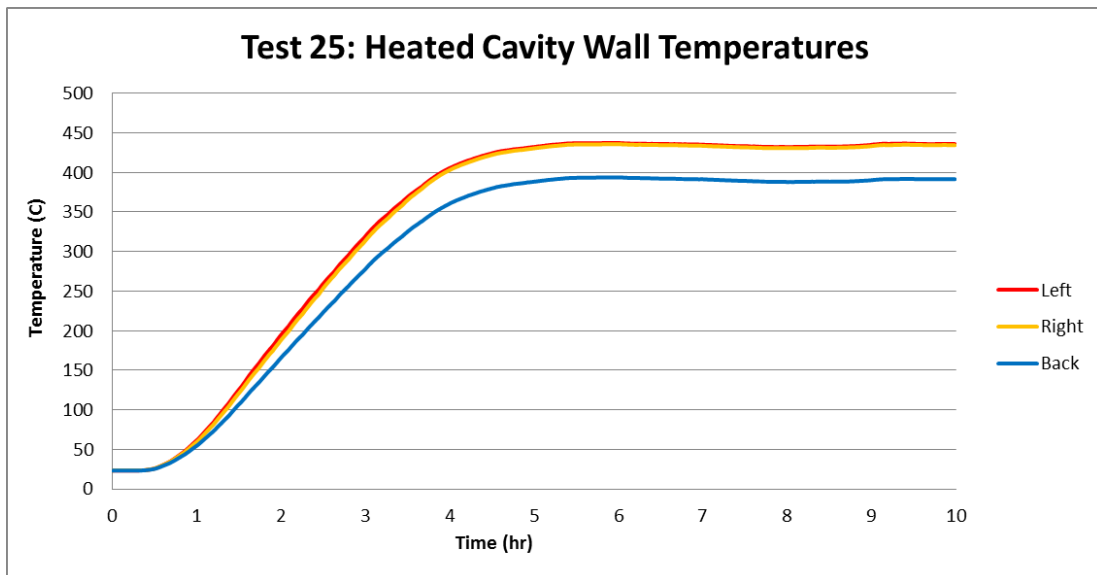


Figure 61 - Heated cavity wall temperatures for Test 25 (Uncertainty:  $\pm 0.7^{\circ}\text{C}$ ).

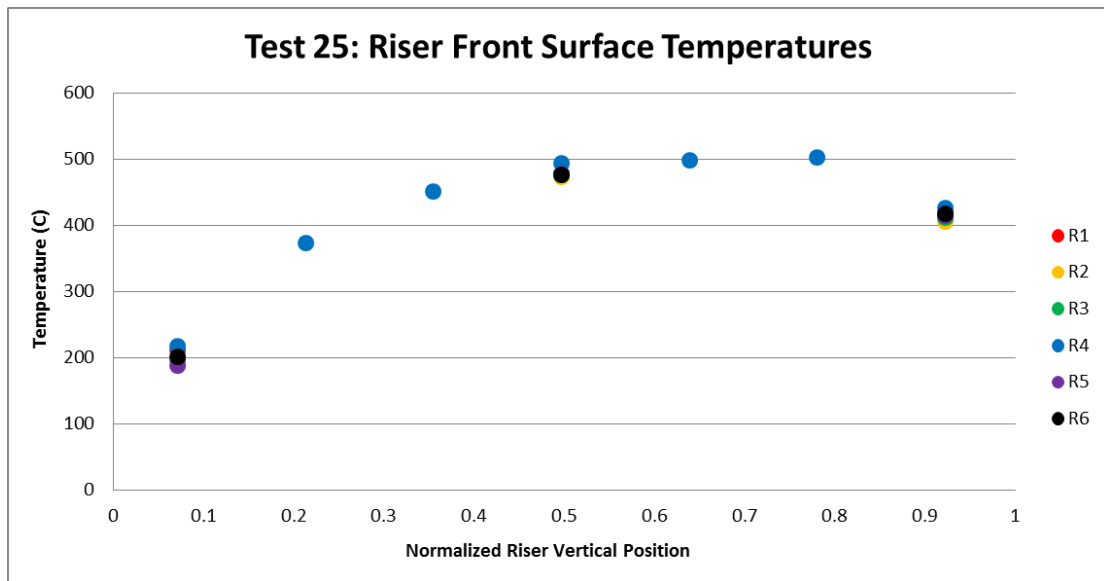


Figure 62 - Riser front surface temperatures for Test 25 (Uncertainty:  $\pm 2.2^{\circ}\text{C}$ ).

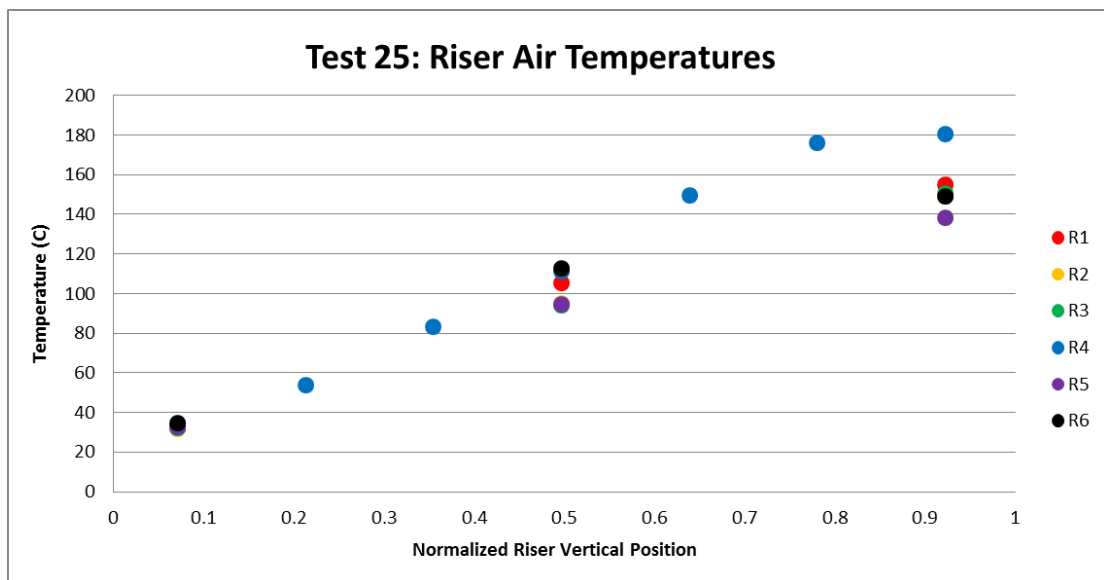


Figure 63 - Riser air temperatures for Test 25 (Uncertainty:  $\pm 0.7^{\circ}\text{C}$ ).

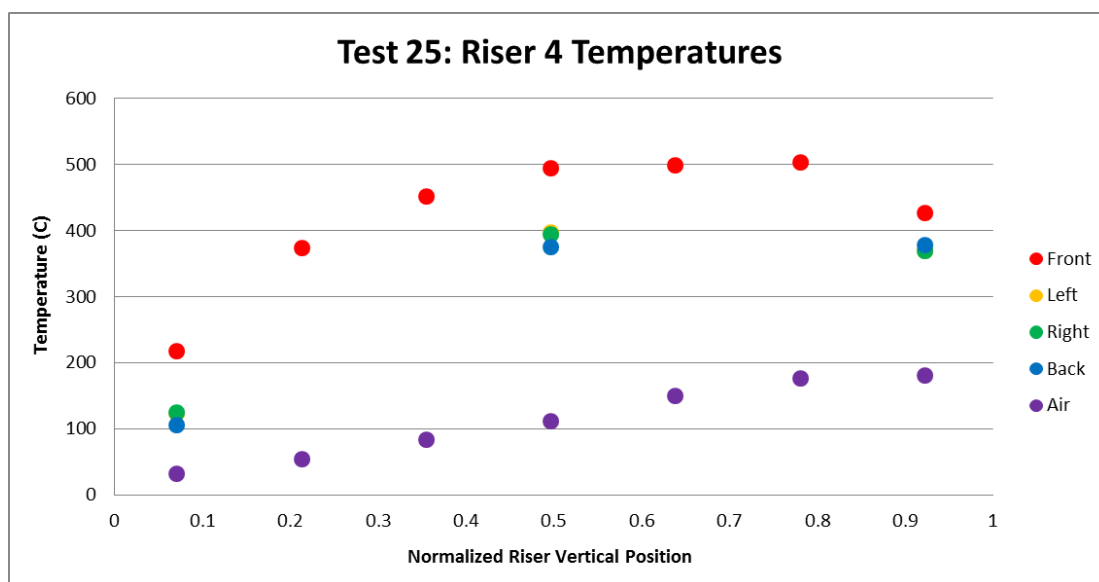


Figure 64 - Riser 4 temperatures for Test 25 (Uncertainty:  $\pm 2.2^{\circ}\text{C}$  for Front, Others  $\pm 0.7^{\circ}\text{C}$ ).

## 5.2 Asymmetric Power Shaping

The steady-state behavior with asymmetric power shaping was investigated to observe the thermal hydraulic behavior and to calculate the heat removal performance of the air RCCS. The two power levels for the heaters were 9.91 kW and 18.99 kW and were distributed equally into heater zones 1 and 2 (see Figure 65). Heater zones 3 and 4 were turned off.

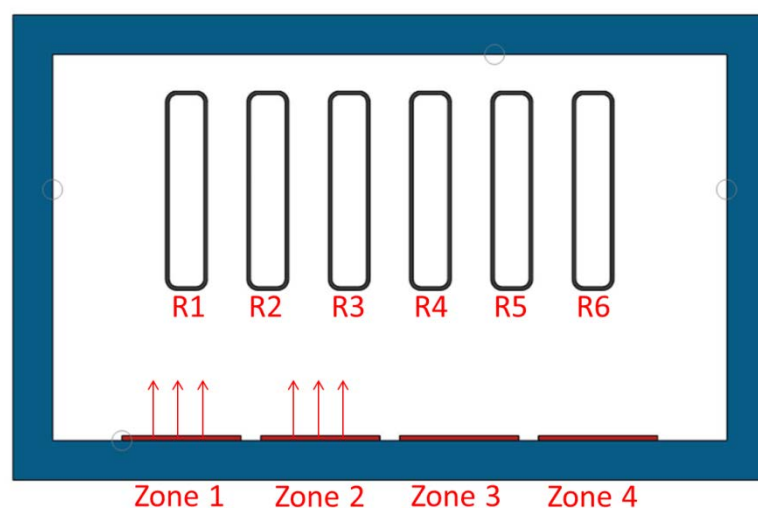


Figure 65 – Asymmetric power schematic.

### 5.2.1 Asymmetric Power at 9.91 kW

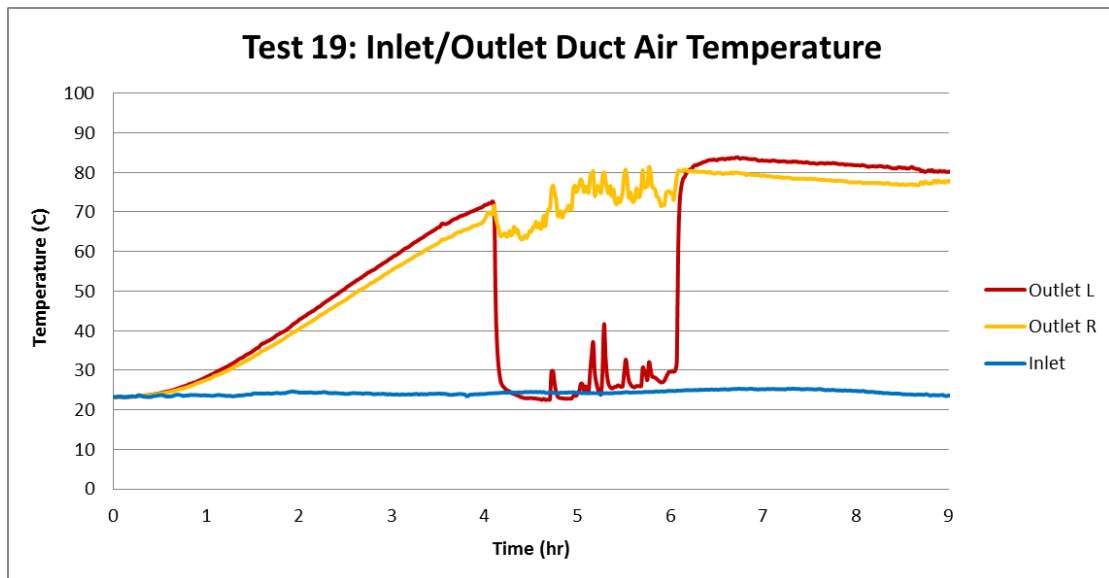
Test 19 was run with a heater input of 9.91 kW that was equally distributed to heater zones 1 and 2. The power delivered to the heaters was gradually increased with a ramp up time duration of 3 hours and 20 minutes. The experiment was run for 9 hours and thermal equilibrium was reached. Table 18 lists the parameters calculated for Test 19. An additional test, Test 21, was run under similar conditions and is documented in Section 5.3.3.

Table 18 - Test 19 parameters.

Parameter	Test 19
$\Delta T$ ( $^{\circ}\text{C}$ )	55.16
$\dot{m}_{total}$ (kg/s)	0.13
$\dot{m}_{total}c_p\Delta T$ (kW)	7.52

The time history for the inlet and outlet duct temperatures for Test 19 can be seen in Figure 66. A sharp drop in temperature can be observed which is believed to be caused by a flow reversal in one of the exhaust ducts. After two hours, the desired flow pattern is restored without any human intervention in Test 19.

The heated cavity wall for both tests can be seen in Figure 67. Time averaging was done between the seventh and ninth hour to observe trends for all risers at thermal equilibrium. The front surface temperatures at steady-state for Test 19 can be seen in Figure 68. The riser air temperatures at steady-state can be seen in Figure 69. Riser 4 temperature trends can be seen in Figure 70.

Figure 66 - Inlet/outlet duct air temperatures for Test 19 (Uncertainty:  $\pm 0.7^{\circ}\text{C}$ ).

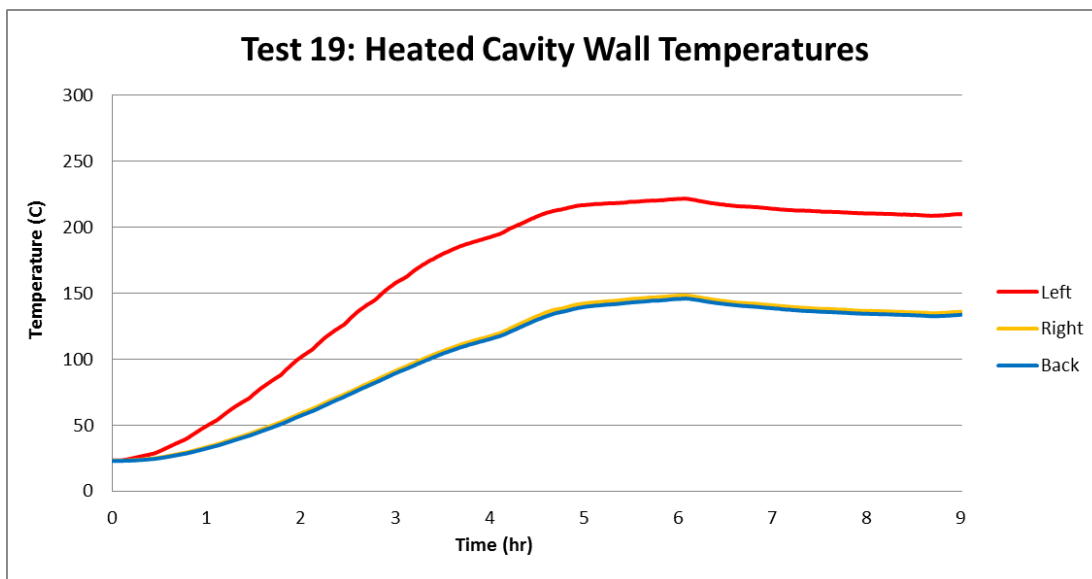


Figure 67 - Heated cavity wall temperatures for Test 19 (Uncertainty:  $\pm 0.7^{\circ}\text{C}$ ).

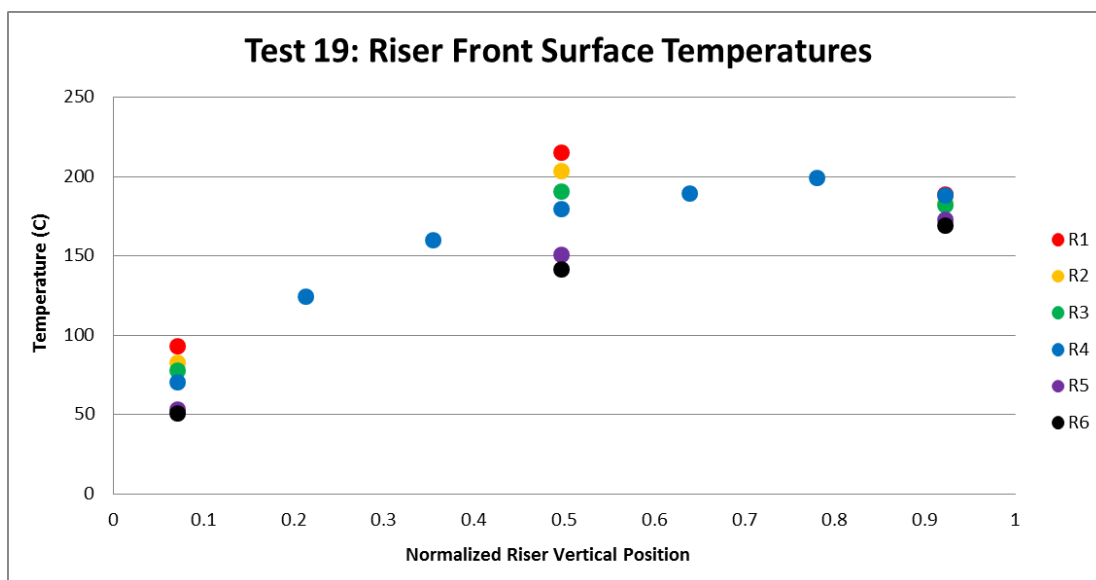


Figure 68 - Riser front surface temperatures for Test 19 (Uncertainty:  $\pm 0.7^{\circ}\text{C}$ ).

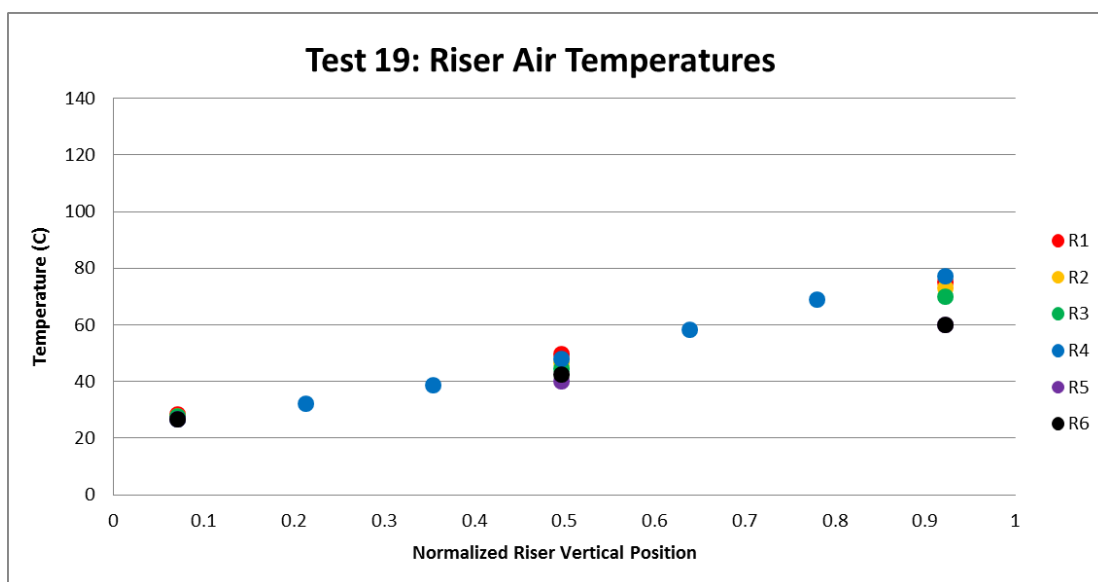


Figure 69 - Riser air temperatures for Test 19 (Uncertainty:  $\pm 0.7^{\circ}\text{C}$ ).

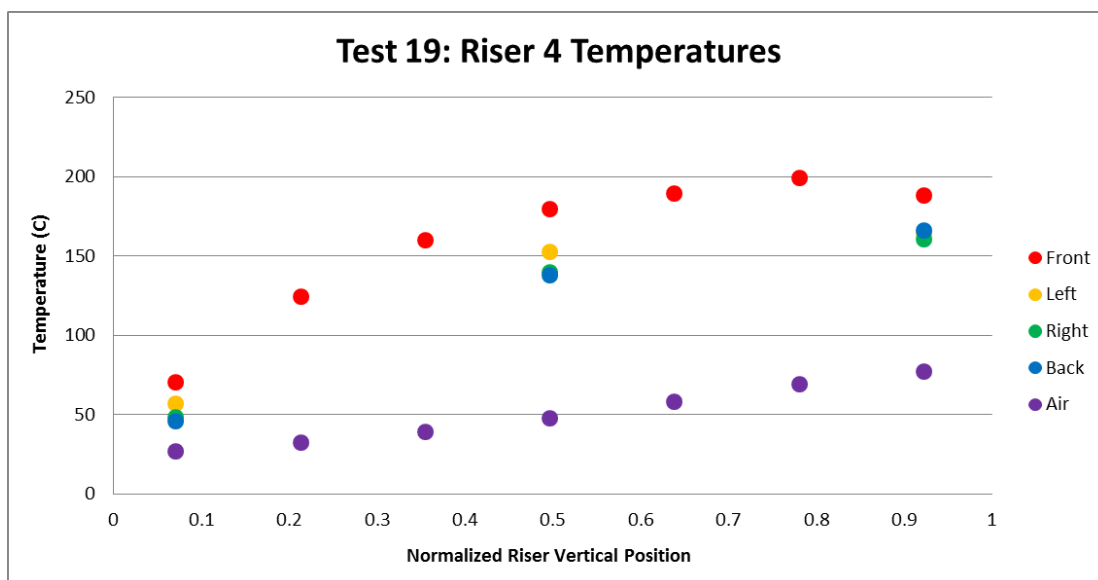


Figure 70 - Riser 4 temperatures for Test 19 (Uncertainty:  $\pm 2.2^{\circ}\text{C}$  for Front, Others  $\pm 0.7^{\circ}\text{C}$ ).

## 5.2.2 Asymmetric Power at 18.99 kW

Test 29 was run with a heater input of 18.99 kW that was equally distributed to heater zones 1 and 2. The power delivered to the heaters was gradually increased with a ramp up time duration of 3 hours and 20 minutes. The experiment was run for 10 hours and thermal equilibrium was reached. Table 18 lists the parameters calculated for Test 29. An additional test, Test 27, was run under similar conditions and is documented in Section 5.3.4.

Table 19 – Test 29 parameters.

Parameter	Test 29
$\Delta T$ ( $^{\circ}\text{C}$ )	85.38
$\dot{m}_{total}$ (kg/s)	0.15
$\dot{m}_{total}c_p\Delta T$ (kW)	12.97

The time history for the inlet and outlet duct temperatures for Test 29 can be seen in Figure 71. Test 29 experienced difficulty in establishing the desired flow path which could be due to a flow reversal in one of the exhaust ducts. Eventually, the desired flow pattern was established without any human intervention.

The heated cavity wall temperatures can be seen in Figure 72. Time averaging was done between the eighth and tenth hour for Test 29 to observe trends for all risers at thermal equilibrium. The front surface temperatures at steady-state for Test 29 can be seen in Figure 73. The riser air temperatures at steady-state can be seen in Figure 74. Riser 4 temperature trends can be seen in Figure 75.

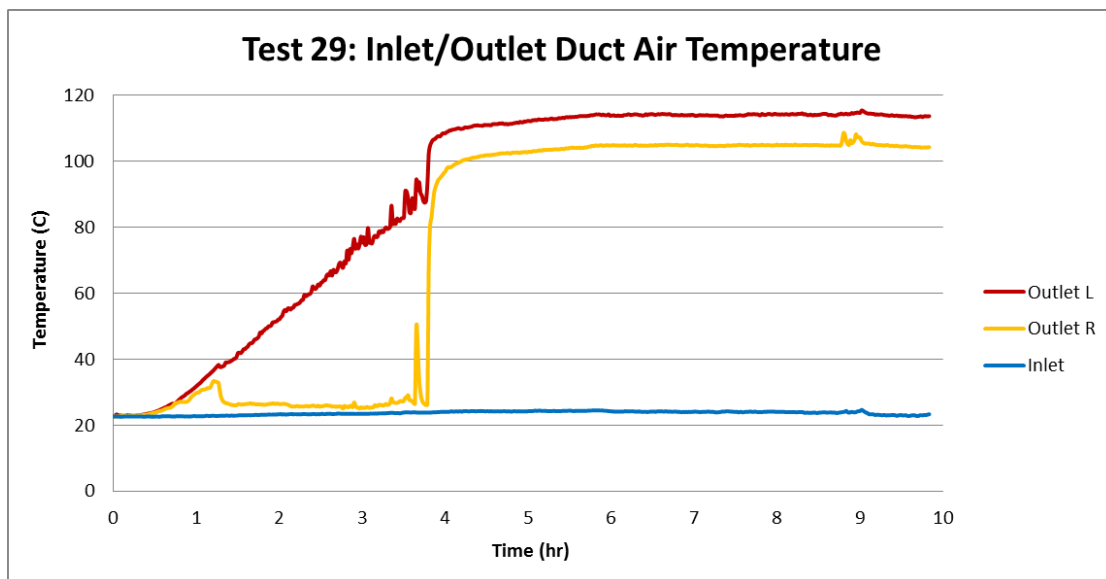


Figure 71 - Inlet/outlet duct air temperatures for Test 29 (Uncertainty:  $\pm 0.7^{\circ}\text{C}$ ).

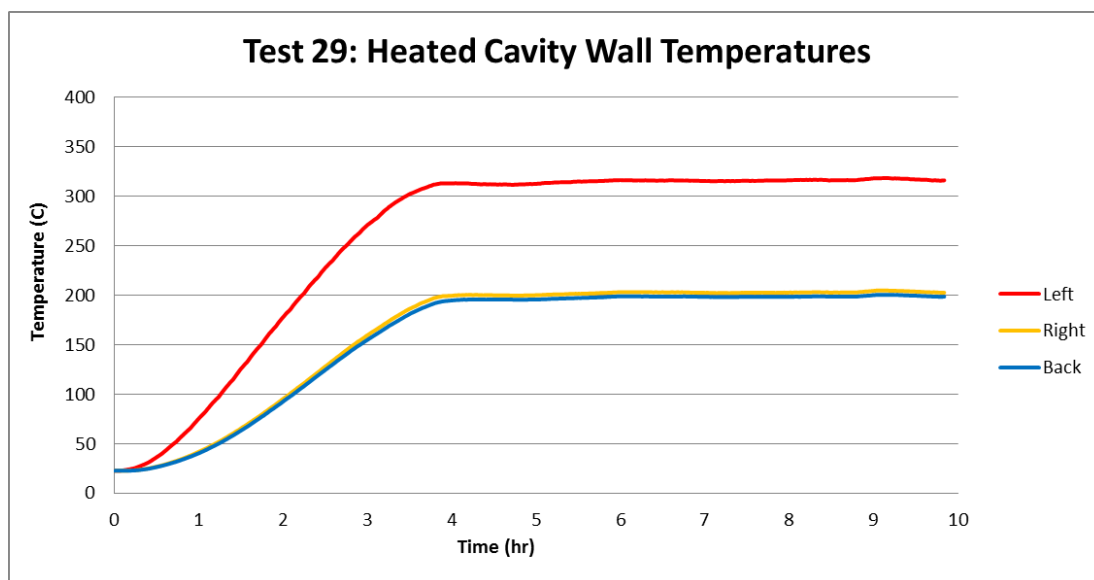


Figure 72 - Heated cavity wall temperatures for Test 29.

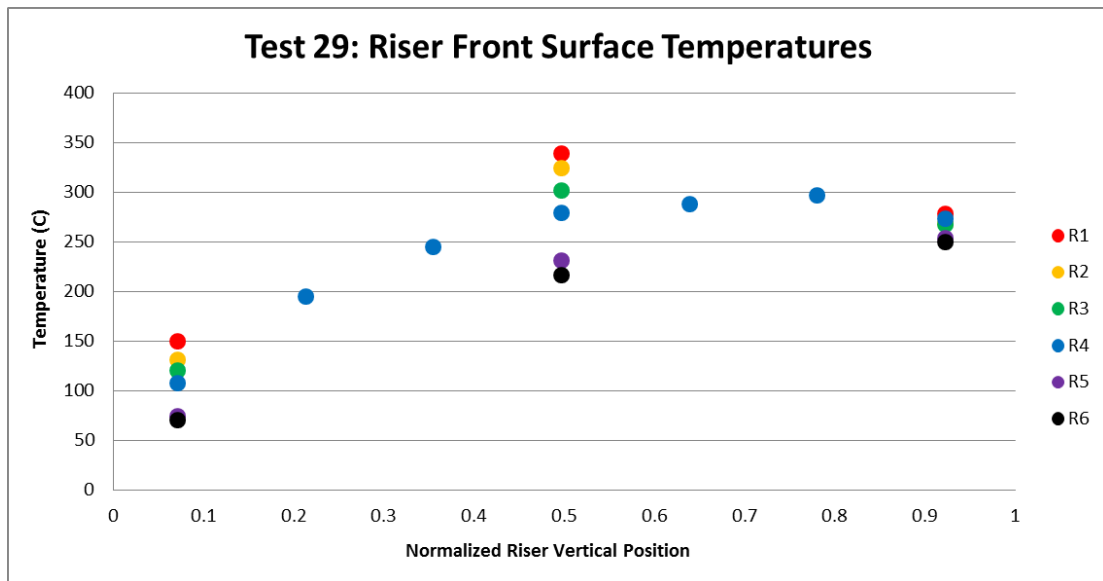


Figure 73 - Riser front surface temperatures for Test 29 (Uncertainty:  $\pm 0.7^{\circ}\text{C}$ ).

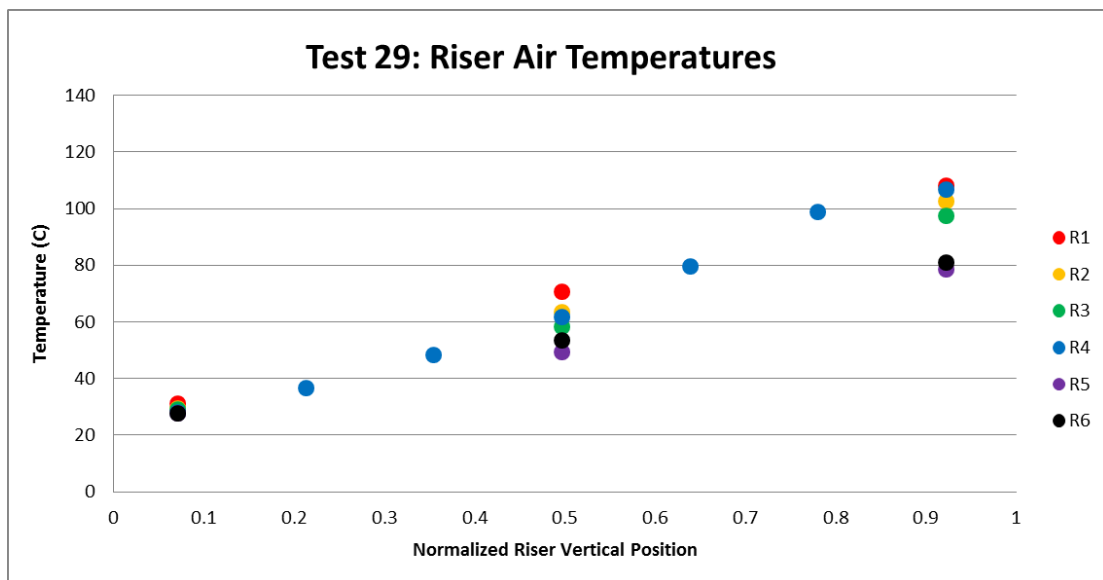


Figure 74 - Riser air temperatures for Test 29 (Uncertainty:  $\pm 0.7^{\circ}\text{C}$ ).

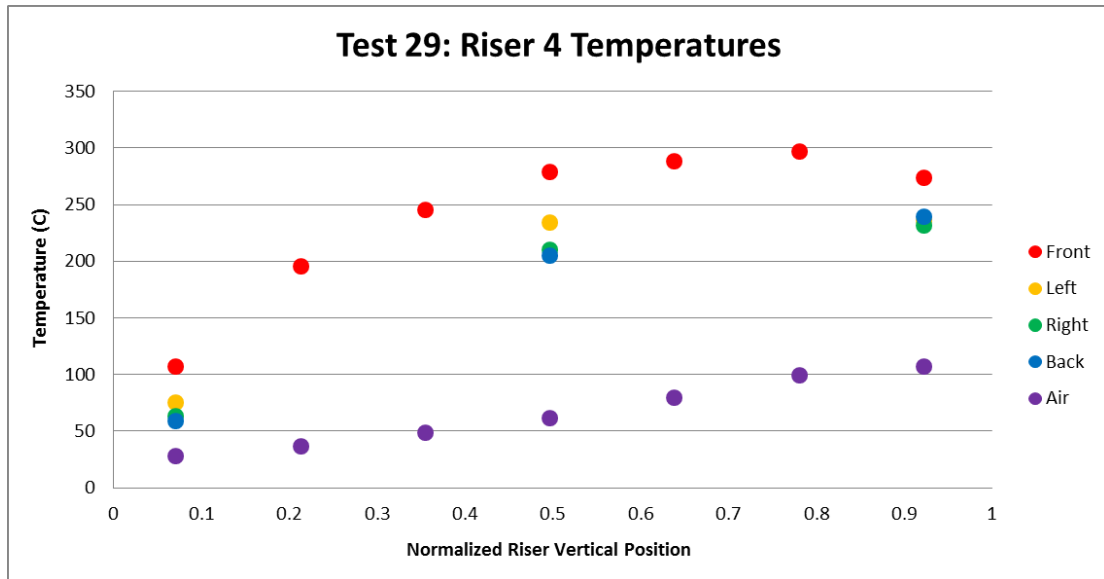


Figure 75 - Riser 4 temperatures for Test 29 (Uncertainty:  $\pm 2.2^{\circ}\text{C}$  for Front, Others  $\pm 0.7^{\circ}\text{C}$ ).

## 5.3 Natural Circulation Repeatability

Additional tests were run to check the repeatability of the results for natural circulation experiments. Flow instabilities were observed in which one of the exhausts ducts experienced a flow reversal. The occurrence of these instabilities and their impact on results gathered should be considered. Table 20 indicates that instabilities were predominantly observed at tests involving lower powers and asymmetric power profile shaping. Flow reversals were never observed for constant heat flux testing at 37.97 kW.

Table 20 – Observed flow instabilities.

Case	Power	Test	Instability Observed
Constant Heat Flux	19.82 kW	15	No
		17	Yes
	<b>37.97 kW</b>	<b>23</b>	<b>No</b>
		<b>25</b>	<b>No</b>
Asymmetric Power	9.91 kW	19	Yes
		21	Yes
	18.99 kW	27	Yes
		29	Yes

### 5.3.1 Constant Heat Flux at 19.82 kW

Both tests (Test 15 and Test 17) run under constant heat flux conditions at 19.82 kW showed repeatable results at steady state. Table 21 lists parameters calculated for each test and their deviation. Figure 49 shows the outlet duct air temperatures for Test 15 and Test 17. Test 15 did not experience a flow reversal in the exhaust ducts while Test 17 did experience instability. The average riser front surface temperatures for both tests can be seen in Figure 50. Figure 51 shows the average riser air temperatures for Test 15 and Test 17.

Table 21 - Test 15 and 17 parameters.

Parameter	Test 15	Test 17	Deviation
$\Delta T$ ( $^{\circ}\text{C}$ )	90.28	90.38	0.11 %
$\dot{m}_{total}$ (kg/s)	0.16	0.15	6.25 %
$\dot{m}_{total}c_p\Delta T$ (kW)	14.39	13.90	3.41 %

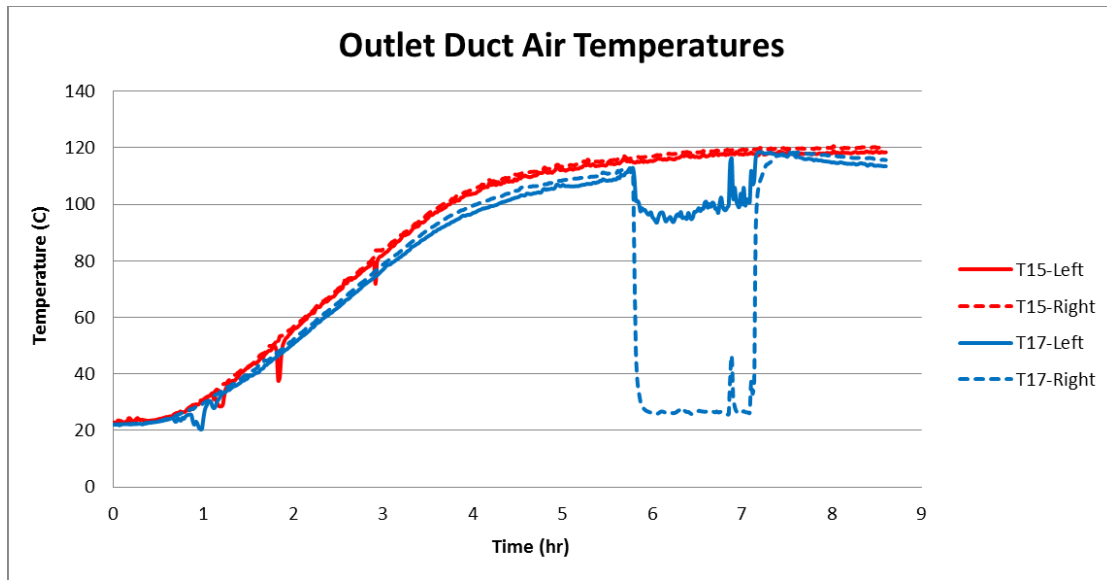


Figure 76 – Outlet duct air temperatures for Test 15 and Test 17.

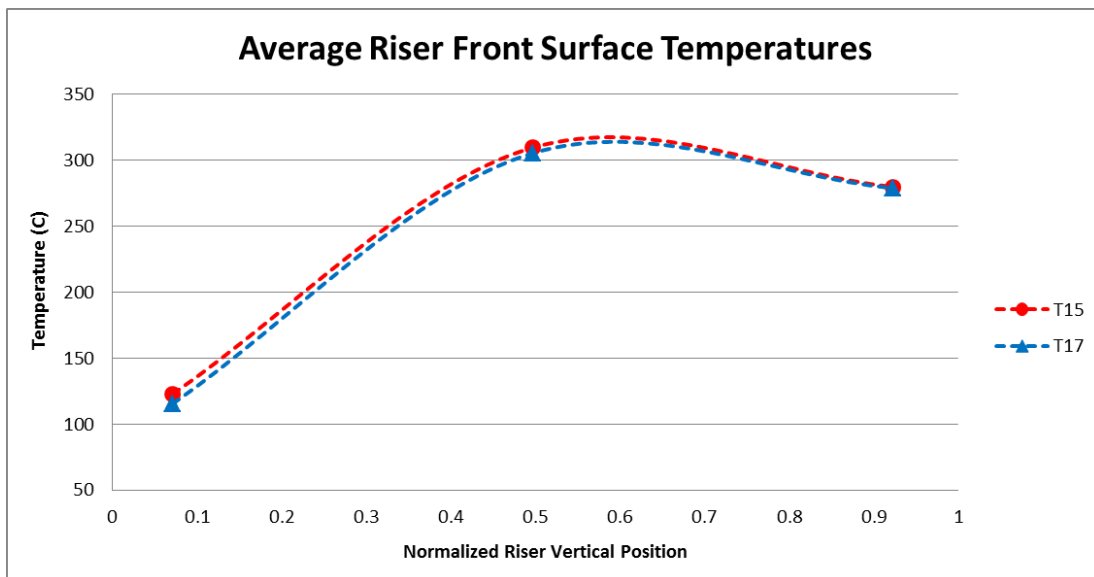


Figure 77 – Average riser front surface temperatures for Test 15 and Test 17.

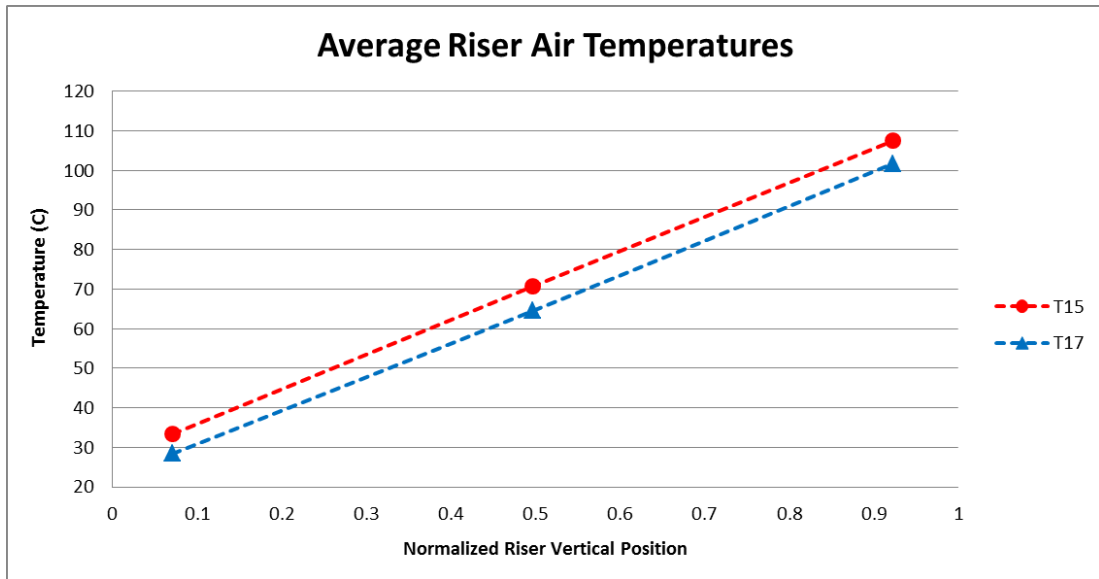


Figure 78 – Average riser air temperatures for Test 15 and Test 17.

### 5.3.2 Constant Heat Flux at 37.97 kW

Both tests (Test 23 and Test 25) run under constant heat flux conditions at 37.97 kW showed repeatable results at steady state. Table 22 lists parameters calculated for each test and their deviation. Figure 79 shows the outlet duct air temperatures for Test 23 and Test 25. Neither test experiences instabilities. The average riser front surface temperatures for both tests can be seen in Figure 80. Figure 81 shows the average riser air temperatures for Test 23 and Test 25.

Table 22 - Test 23 and 25 parameters.

Parameter	Test 23	Test 25	Deviation
$\Delta T$ ( $^{\circ}\text{C}$ )	141.63	141.71	0.06 %
$\dot{m}_{total}$ (kg/s)	0.18	0.18	-
$\dot{m}_{total}c_p\Delta T$ (kW)	25.60	25.43	0.66 %

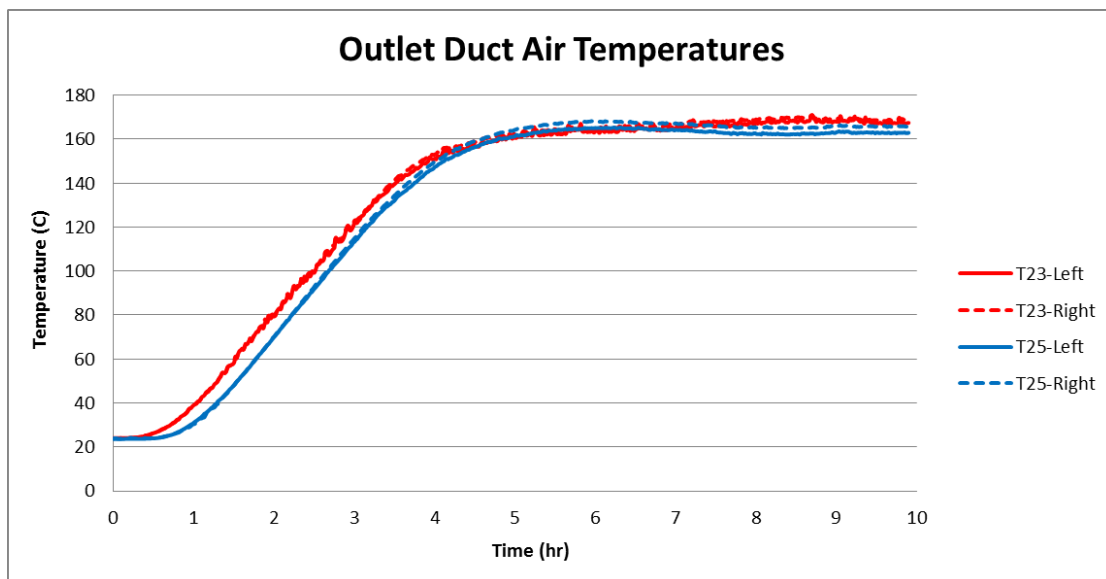


Figure 79 – Outlet duct air temperatures for Test 23 and Test 25.

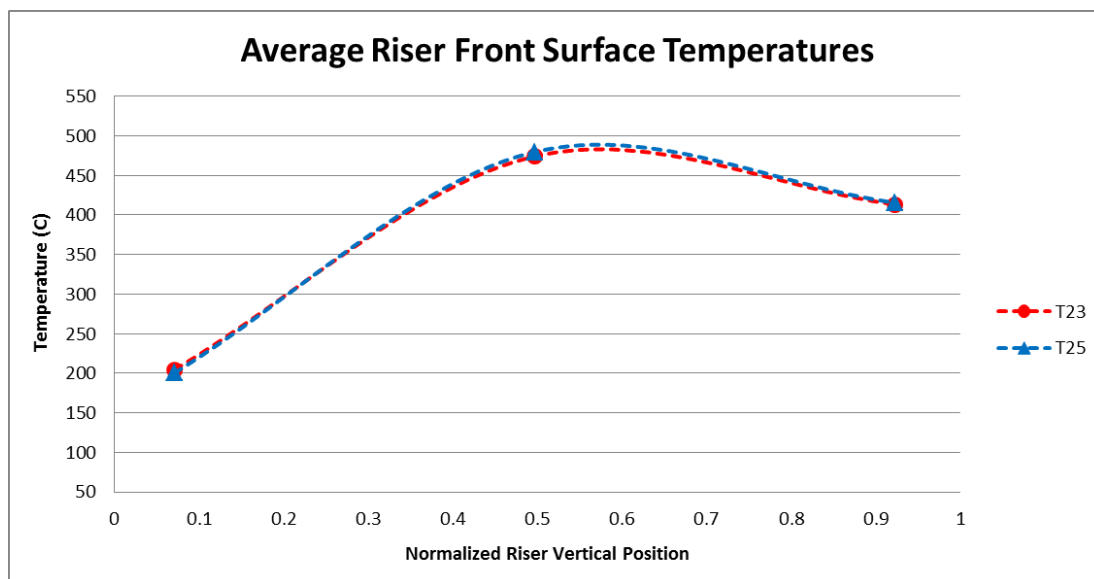


Figure 80 – Average riser front surface temperatures for Test 23 and Test 25.

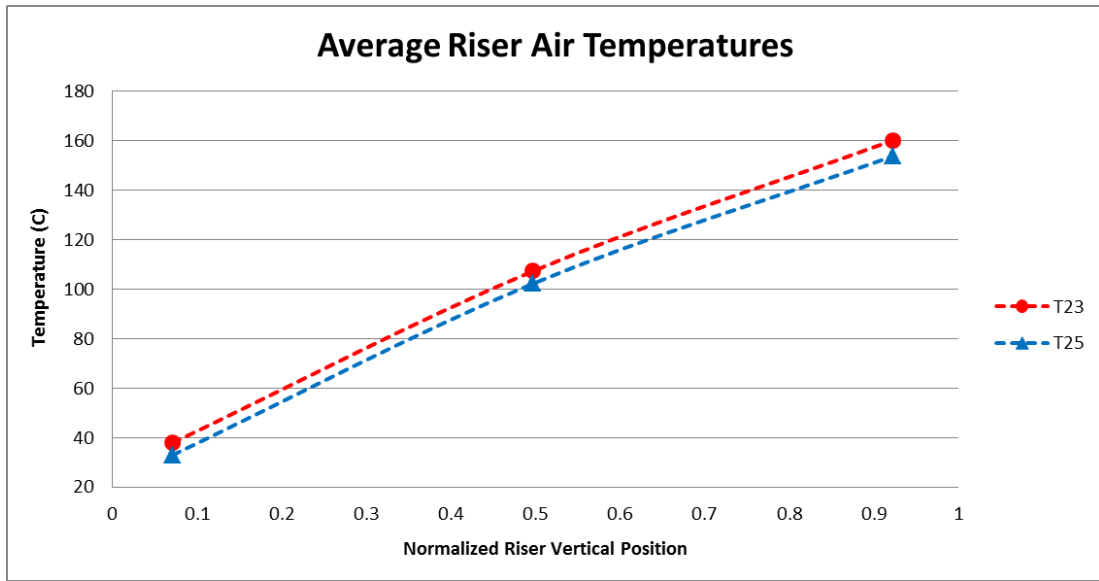


Figure 81 – Average riser air temperatures for Test 23 and Test 25.

### 5.3.3 Asymmetric Power at 9.91 kW

Test 19 and Test 21 were run under an asymmetric power profile shaping at 9.91 kW. Table 23 lists parameters calculated for each test and their deviation. Figure 82 shows the outlet duct air temperatures for Test 19 and Test 21. Both tests experienced instabilities. One flow reversal in the exhaust duct occurred in Test 19. Test 21 experienced multiple flow reversals in both exhaust ducts. The average front surface riser temperatures for both tests can be seen in Figure 83. Figure 84 shows the average riser air temperatures for Test 19 and Test 21.

Table 23 - Test 19 and 21 parameters.

Parameter	Test 19	Test 21	Deviation
$\Delta T$ ( $^{\circ}\text{C}$ )	55.16	62.18	11.29 %
$\dot{m}_{total}$ (kg/s)	0.13	0.12	7.69 %
$\dot{m}_{total}c_p\Delta T$ (kW)	7.52	7.49	0.40 %

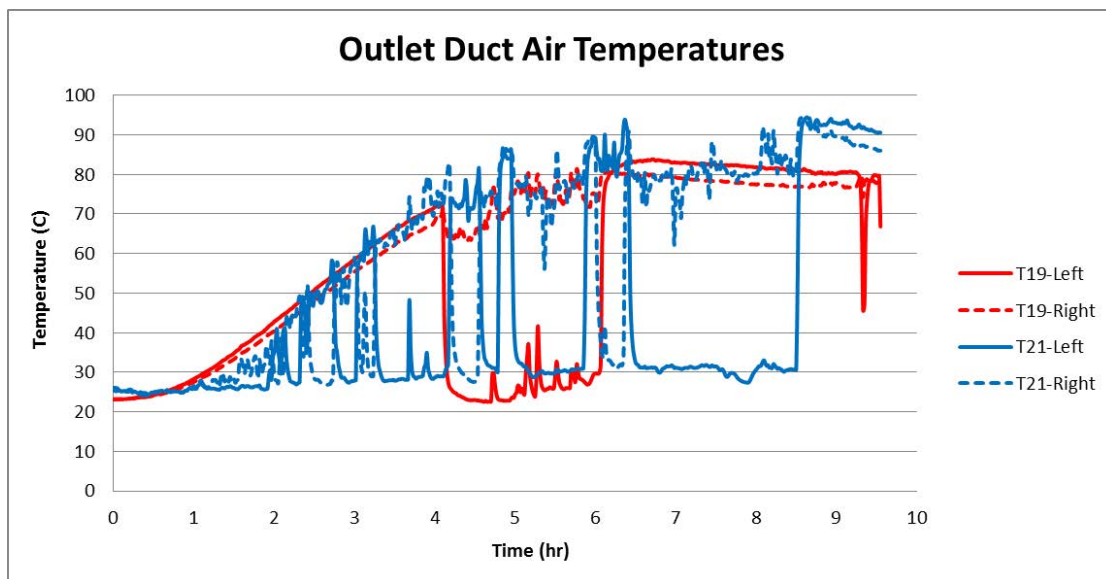


Figure 82 – Outlet duct air temperatures for Test 19 and Test 21.

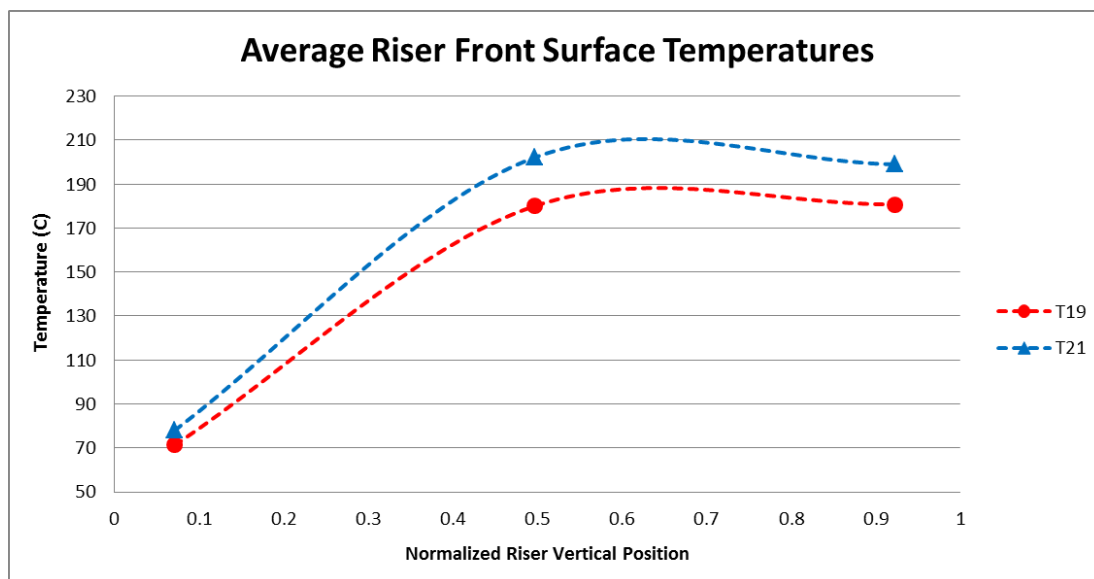


Figure 83 – Average riser front surface temperatures for Test 19 and Test 21.

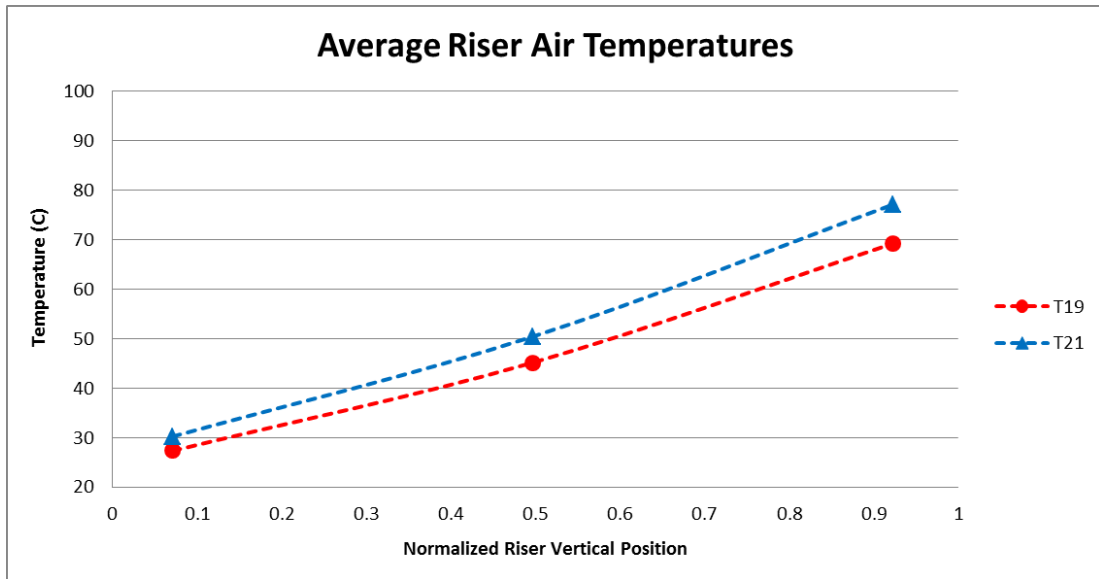


Figure 84 – Average riser air temperatures for Test 19 and Test 21.

### 5.3.4 Asymmetric Power at 18.99 kW

Test 27 and Test 29 were run under an asymmetric power profile shaping at 18.99 kW. Table 24 lists parameters calculated for each test and their deviation. Figure 85 shows the outlet duct air temperatures for Test 27 and Test 29. Both tests experienced instabilities. Test 27 experienced multiple flow reversals in one of the exhaust ducts. Test 29 experienced difficulty in establishing the desired flow path due air flowing from the environment into one of the exhaust ducts. The average front surface riser temperatures for both tests can be seen in Figure 86. Figure 87 shows the average riser air temperatures for Test 27 and Test 29.

Table 24 - Test 27 and 29 parameters.

Parameter	Test 27	Test 29	Deviation
$\Delta T$ ( $^{\circ}\text{C}$ )	82.08	85.38	3.87 %
$\dot{m}_{total}$ (kg/s)	0.16	0.15	6.25 %
$\dot{m}_{total} c_p \Delta T$ (kW)	13.58	12.97	4.49 %

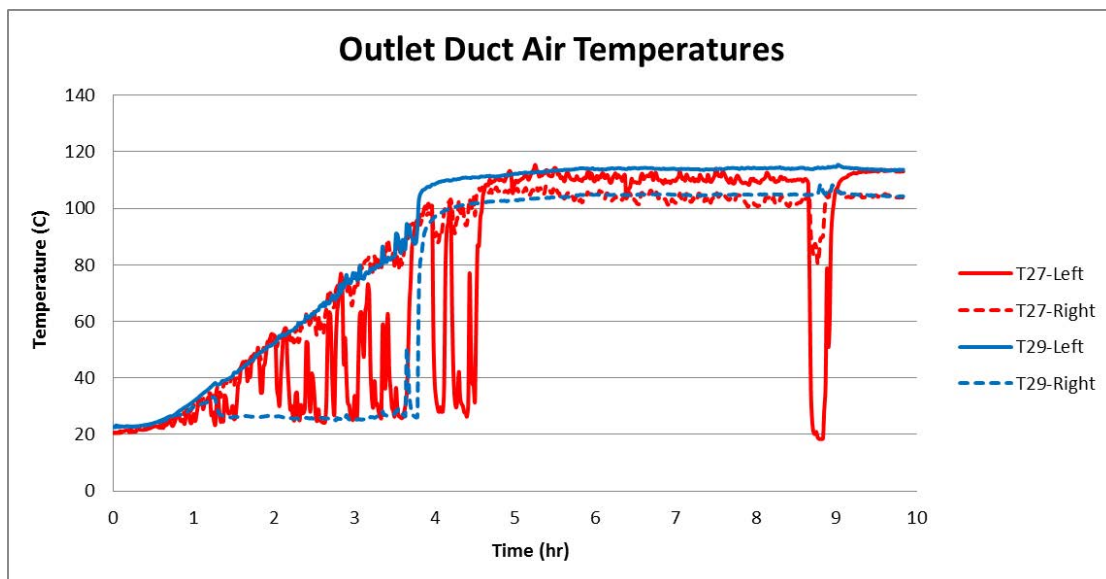


Figure 85 – Outlet duct air temperatures for Test 27 and Test 29.

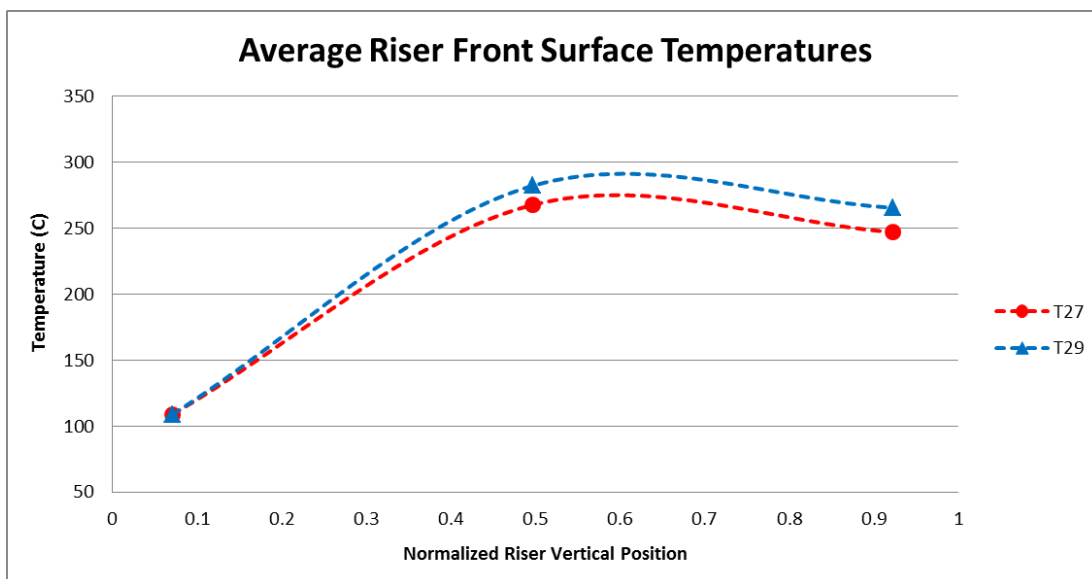


Figure 86 – Average riser front surface temperatures for Test 27 and Test 29.

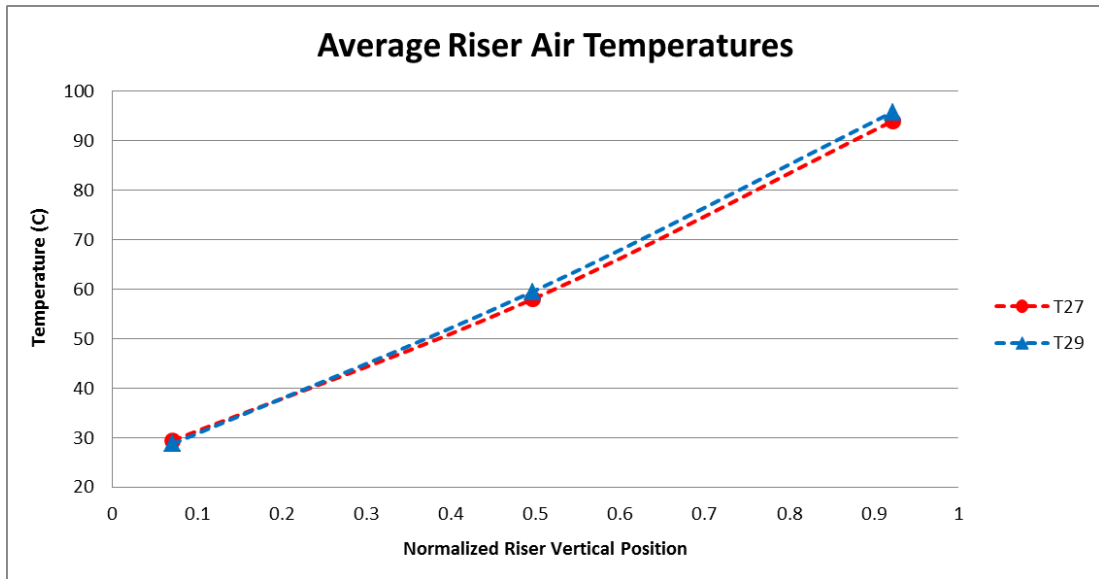


Figure 87 – Average riser air temperatures for Test 27 and Test 29.

## 5.4 Flow Instabilities

The environment outside the silo could potentially contribute to the flow reversals in the exhaust ducts. The flow reversals could also be potentially attributed to the nature of air natural circulation loops in which the driving forces are very small and a well-defined flow path cannot be established at lower powers. For the quarter-scale air cooled RCCS facility, these two scenarios are coupled due to the exhaust ducts being exposed to the outside environment instead of a controlled environment. Data collected from the weather station mounted on the silo exterior will be presented for two tests in which instabilities were observed. This data suggests that when there is a change in wind direction, the flow in one of the exhaust ducts stagnates which results in a pressure increase at the exit of the exhaust duct. The pressure at the exit of the exhaust duct rises to a pressure higher than the one inside the exhaust duct and the flow reversal occurs. Future testing is suggested to better understand these flow instabilities which should incorporate additional instrumentation in the exhaust ducts.

### 5.4.1 Test 19

Test 19 was run with an asymmetric power profile at 9.91 kW (see Section 5.2.1 for more details). Test 19 commenced at 11:00 a.m. on June 23<sup>rd</sup>, 2014 and ran for a total of nine hours. Figure 88 shows the exhaust duct temperatures for Test 19 and the time history is divided into three sections: A (ramp-up), B (flow reversal), and C (restored flow path). The flow reversal occurred between the fourth and sixth hour of the test. Figure 89 shows the outside wind speed and direction. During the flow reversal observed, the wind speed falls

from 3 to 1.5 miles per hour and the wind direction changes from southwest to southeast. Figure 90 shows the outside temperature and barometric pressure. During the flow reversal observed, the outside temperature slightly increased from 73 to 81 °F (22.78 to 27.22 °C). The barometric pressure slightly decreased from 29.80 to 29.78 inches of mercury (100.90 to 100.84 kPa).

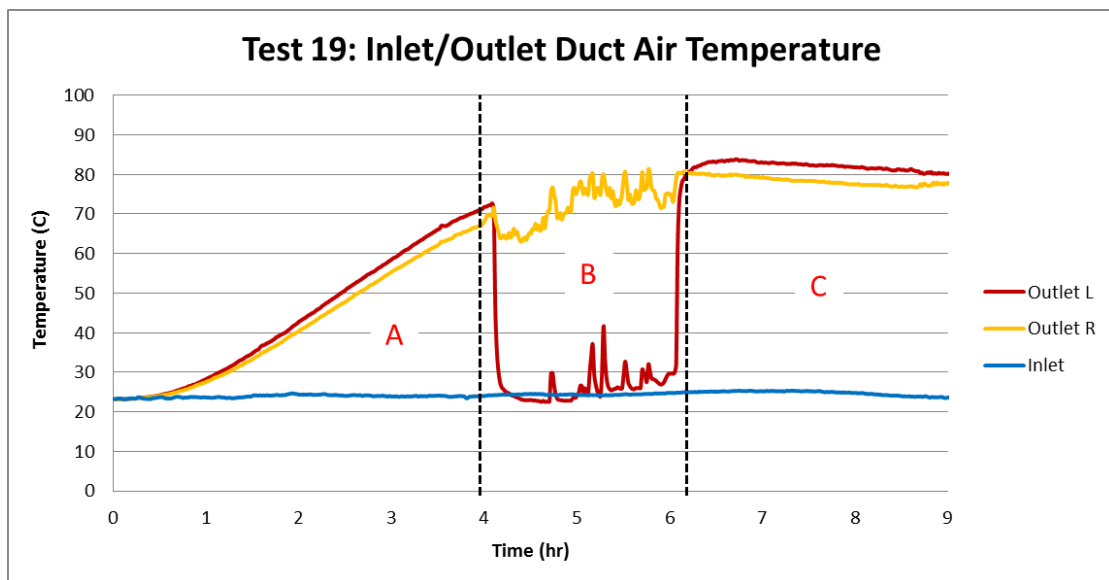


Figure 88 – Inlet and outlet duct air temperatures for Test 19.

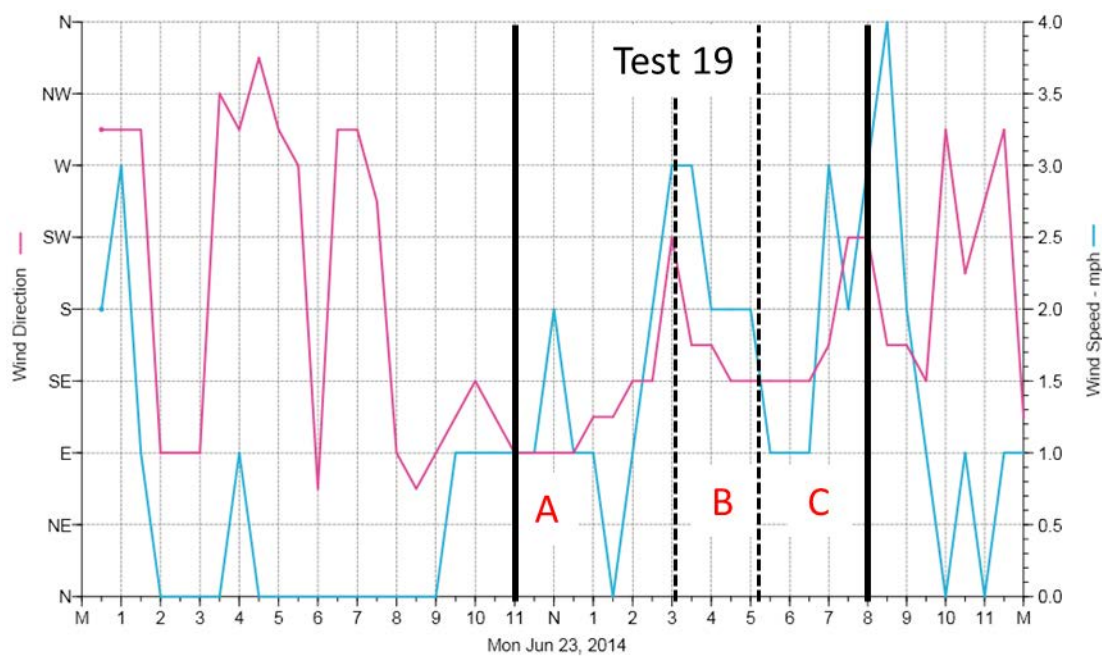


Figure 89 – Outside wind speed and direction for Test 19.

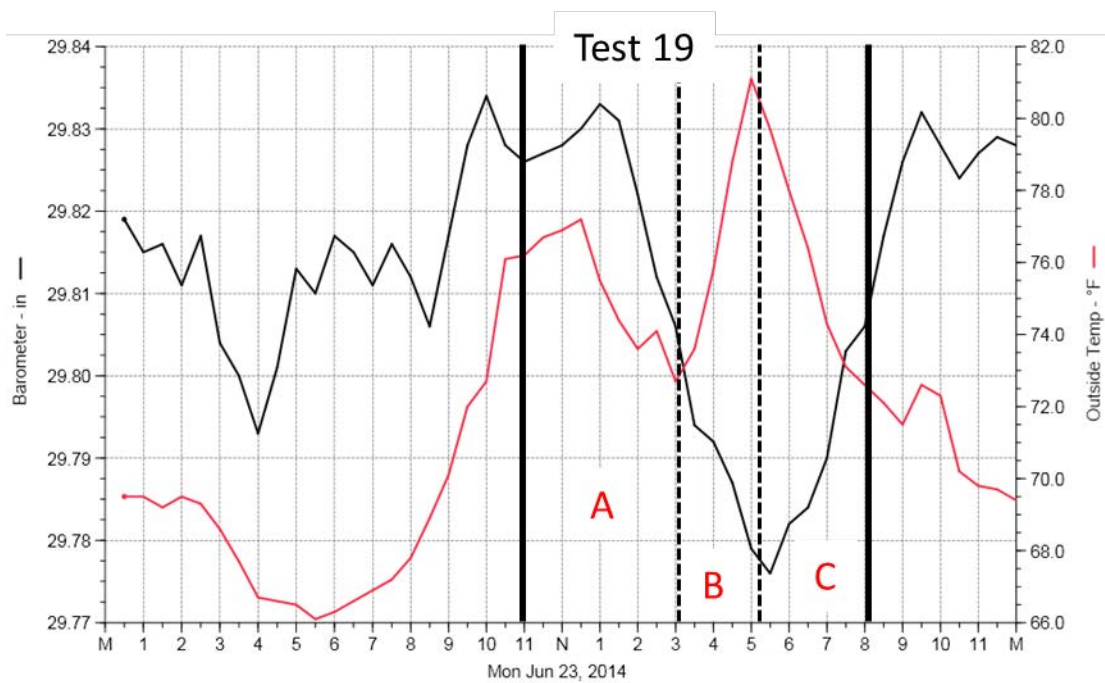


Figure 90 – Outside temperature and barometric pressure for Test 19.

## 5.4.2 Test 27

Test 27 was run with an asymmetric power profile at 18.99 kW (see Section 5.3.4 for more details). Test 27 commenced at 9:30 a.m. on July 1<sup>st</sup>, 2014 and ran for a total of ten hours. Figure 91 shows the exhaust duct temperatures for Test 27 and the time history is divided into four sections: A (ramp-up with flow reversal), B (desired flow path established), C (flow reversal), and D (restored flow path). A flow reversal occurred shortly before the ninth hour of the test. Figure 92 shows the outside wind speed and direction. Figure 93 shows the outside temperature and barometric pressure. These parameters varied slightly during the flow reversal at the time history division labeled C.

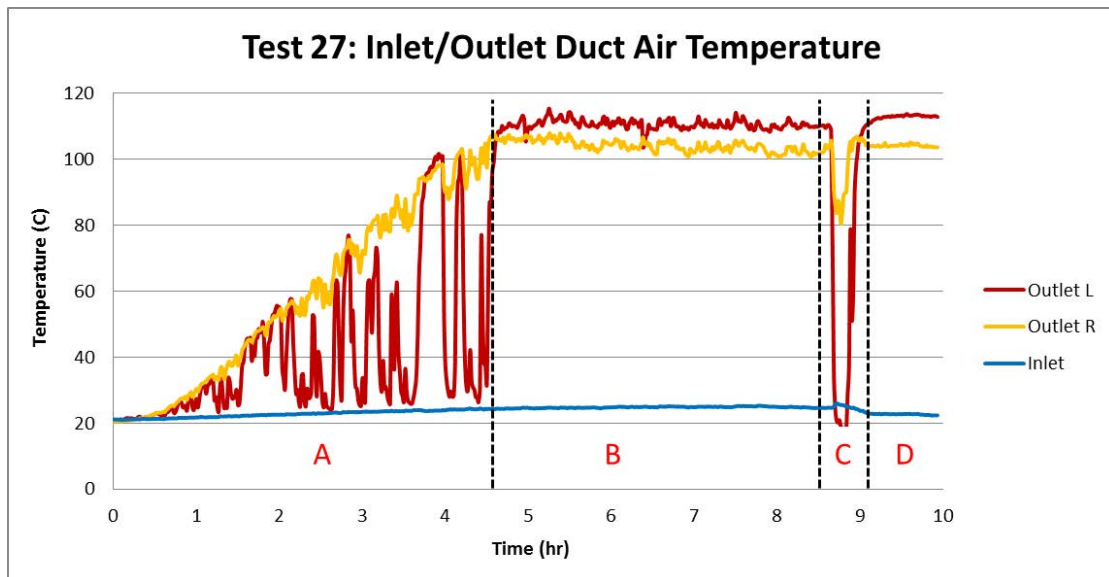


Figure 91 – Inlet and outlet duct air temperatures for Test 27.

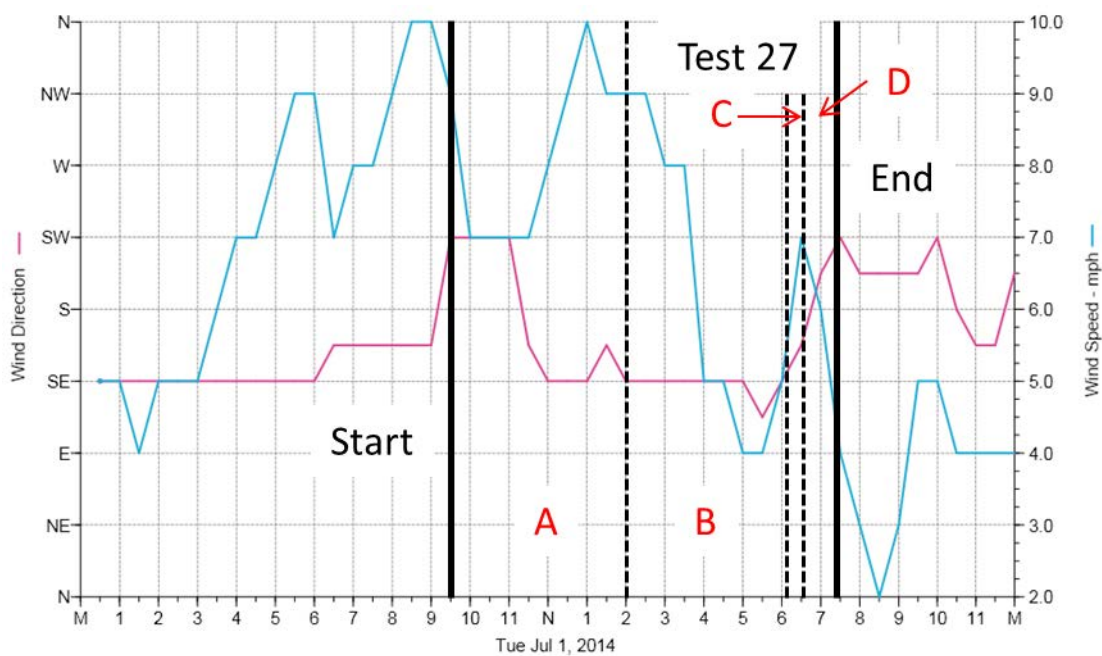


Figure 92 – Outside wind speed and direction for Test 27.

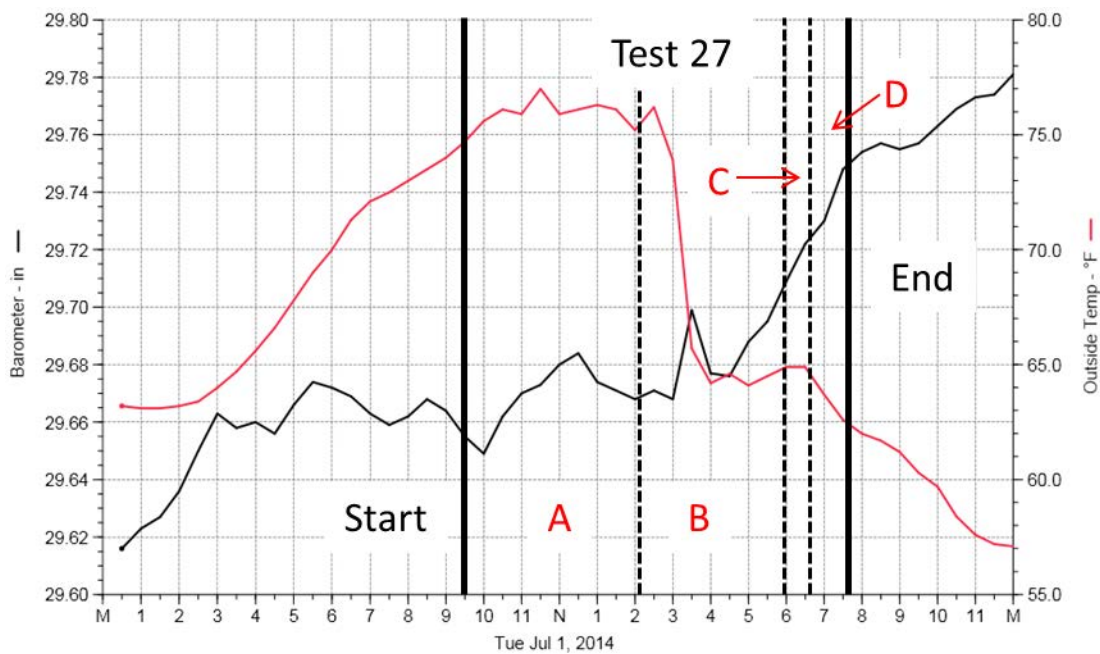


Figure 93 – Outside temperature and barometric pressure for Test 27.

## Chapter 6

# Conclusion and Recommendations

A scaled air-cooled Reactor Cavity Cooling System (RCCS) facility was successfully designed, constructed, and an initial test series completed. The RCCS facility was based on a scaling analysis developed by Argonne National lab with collaboration from researchers at UW-Madison. A series of scoping tests qualified the facility, as well as the associated test equipment and its instrumentation. Subsequently, a series of forced circulation tests and natural circulation tests were conducted with the facility, in which the thermal hydraulic phenomena and instabilities were observed and analyzed. The scoping tests that qualified the facility are not the major focus of this work. The forced circulation experiments and natural circulation experiments are the major focus of this work. The major independent variables for the dozen forced circulation and natural circulation experiments are the heater total power and the heater symmetry

## 6.1 Conclusion

Certain parameters across these experiments can be considered to show overall trends for the quarter-scale air-cooled RCCS. Table 25 lists the experimental results for the twelve experiments considered. Three different types of experiments were carried out. Forced flow testing was done with an inline duct fan placed at the inlet duct piping before entering the lower plenum. Constant heat flux testing was a natural circulation test in which the fan was removed from the facility. In order to achieve a constant heat flux across the test section, the

heater power was equally split to the four heater zones. Asymmetric power profile testing was also a natural circulation test in which the inline duct fan was not used. Two heater zones received power while the remaining two heater zones were turned off. This was done to accomplish a skew in the heating profile. The following parameters are listed in the table: total mass flow ( $\dot{m}_{total}$ ), system differential temperature ( $\Delta T$ ), energy balance for the air in the scaled RCCS facility ( $\dot{m}_{total}c_p\Delta T$ ), and whether instabilities were present. Forced flow testing produced very repeatable data due to the inlet duct fan providing a constant inlet flow. Overall, the natural circulation experiments showed good consistency at the highest heat power in which testing was done (37.97 kW). At lower powers, the natural circulation behavior of the scaled RCCS had slightly greater variability. Instabilities were observed in the scaled facility where flow reversals occurred in the exhaust ducts. Table 25 lists whether or not instability occurred for each experiment.

Table 25 – Scaled RCCS experimental results.

Test	Case	Power (kW)	$\dot{m}_{total}$ (kg/s)	$\Delta T$ ( $^{\circ}\text{C}$ )	$\dot{m}_{total}c_p\Delta T$ (kW)	Instability Observed
14	Forced Flow	19.82	0.38	41.50	15.76	No
16			0.39	41.13	15.93	No
15	Constant Flux	19.82	0.16	90.28	14.39	No
17			0.15	90.38	13.90	Yes
19	Asymmetric	9.91	0.13	55.16	7.52	Yes
21			0.12	62.18	7.49	Yes
18	Forced Flow	37.97	0.38	76.12	29.35	No
20			0.39	75.08	29.38	No
23	Constant Flux	37.97	0.18	141.63	25.60	No
25			0.18	141.71	25.43	No
27	Asymmetric	18.99	0.16	82.08	13.58	Yes
29			0.15	85.38	12.97	Yes

Figure 55 presents the flow rates observed at various powers. The differential temperatures of the scaled RCCS for various powers were linear across all natural circulation tests and can be

seen in Figure 96. The differential temperature of the facility was defined as the average temperature of the exhaust ducts minus the inlet duct temperature.

The scaled RCCS facility did experience instabilities. Flow reversals were observed in the exhaust ducts. Figure 98 shows the number of flow reversals observed for the natural circulation tests. Flow reversals were more likely to occur at lower powers and asymmetric power profile shaping.

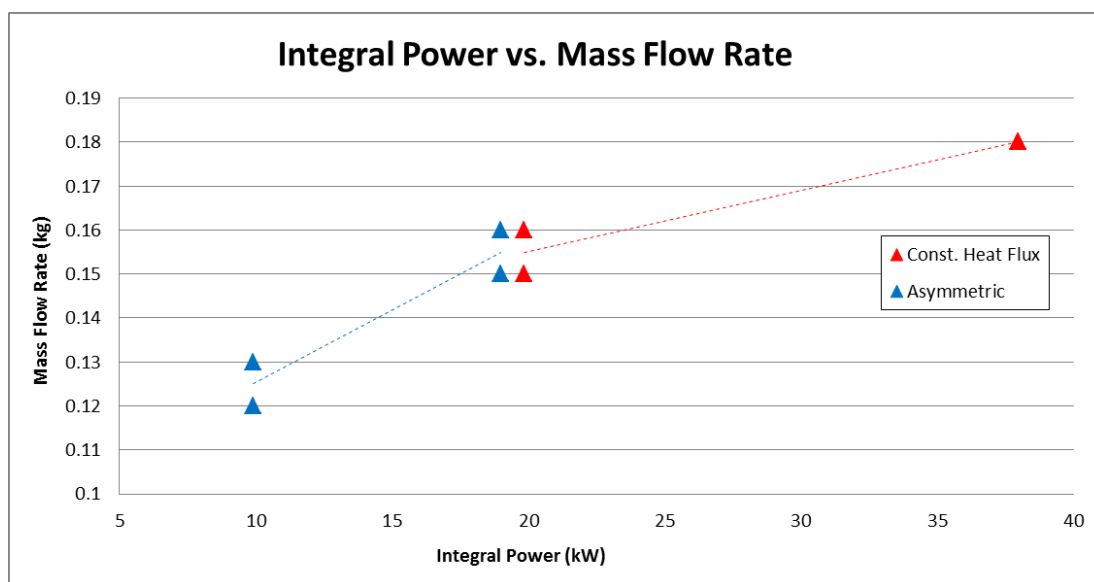


Figure 94 – Integral power vs. mass flow rate.

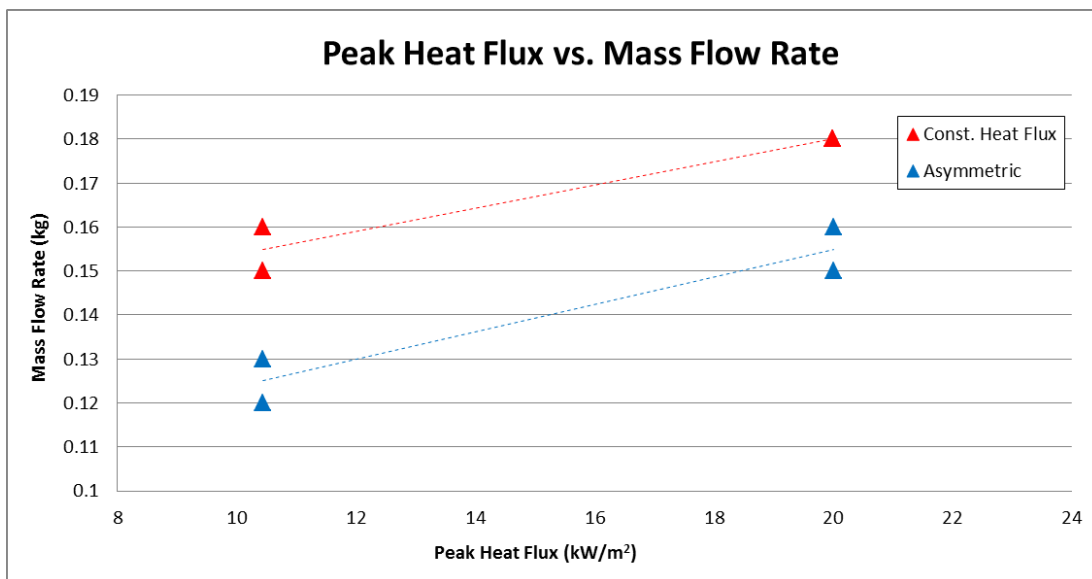


Figure 95 – Peak heat flux vs. mass flow rate (Areas: 18,987 cm<sup>2</sup> for Const. Heat Flux, 9,493.5 cm<sup>2</sup> for Asymmetric).

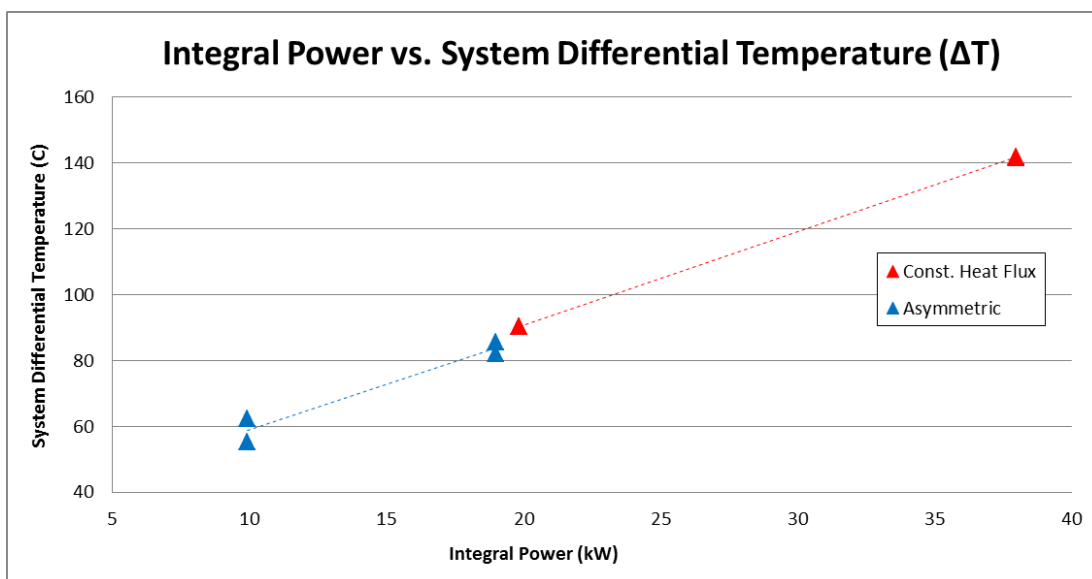


Figure 96 – Integral power vs. system differential temperature.

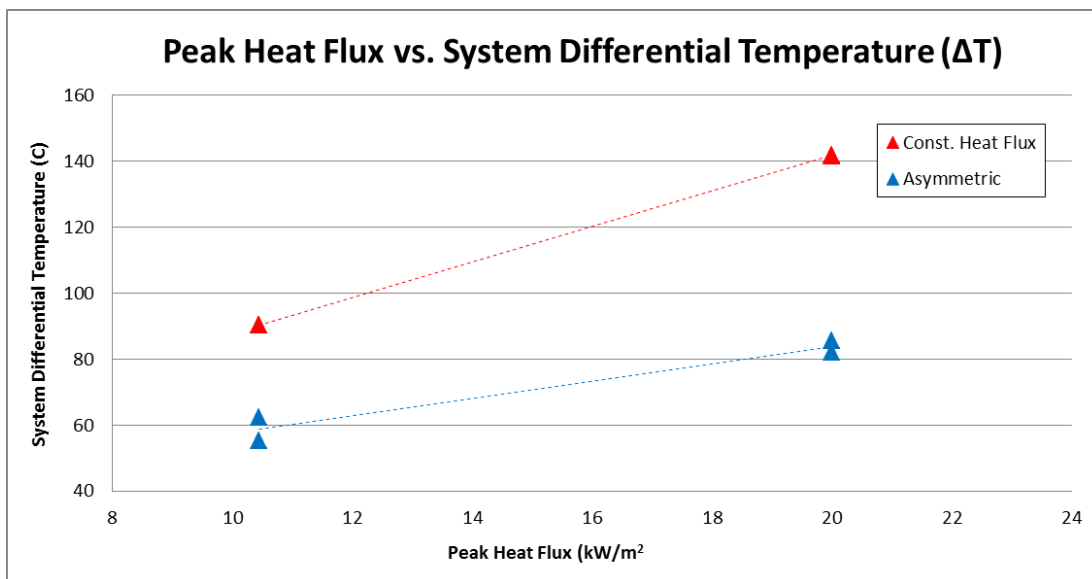


Figure 97 – Peak heat flux vs. system differential temperature (Areas:  $18,987 \text{ cm}^2$  for Const. Heat Flux,  $9,493.5 \text{ cm}^2$  for Asymmetric).

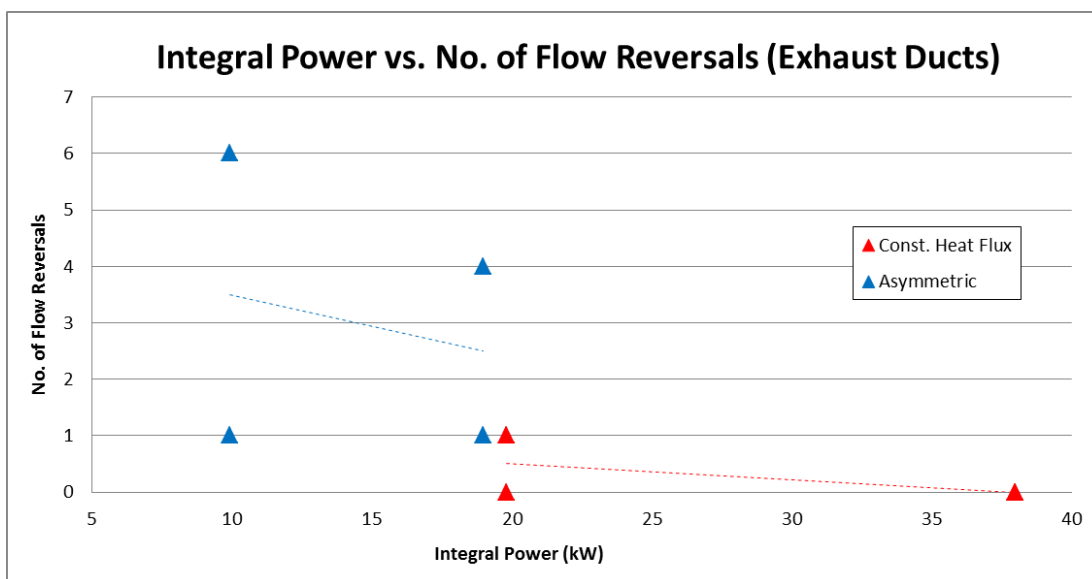


Figure 98 – Integral power vs. number of flow reversals.

## 6.2 Future Work

The scaled air-cooled RCCS at UW-Madison was completed in early 2014. A variety of experiments were run at different power levels and power shaping. Suggestions for future work related to this facility are made based on the results and observations gathered.

1. Exhaust Duct Modifications
2. Riser Duct Instrumentation
3. Upper Plenum Investigation

### 6.2.1 Exhaust Duct Modifications

The section of the exhaust ducts inside the silo is insulated with Pyrogel and Kaowool thermal insulation. The section of the exhausts ducts outside of the silo should be insulated which could help improve the natural circulation flow by minimizing heat losses. Fiberglass pipe insulation that is weather proof is recommended. Additional instrumentation (thermocouples and differential pressure sensors) should be added along the entire length of the exhaust ducts. The additional instrumentation would be of great value to better understand the flow instabilities in the exhaust ducts. A recommendation for the temperature measurements is to use a wireless thermocouple transmitter to avoid having to install thermocouple extension wire outside the silo.

## 6.2.2 Riser Duct Instrumentation

Placing differential pressure sensors in each one of the risers is suggested. Differential pressure data would be helpful in investigating local phenomena within each riser. In certain testing scenarios, Riser 4 experienced air temperatures higher than those in the other five risers. Current instrumentation did not provide a reasonable explanation as to why this is occurring.

## 6.2.1 Upper Plenum Investigation

A section of the experiment that was not instrumented heavily was the upper plenum. The flow patterns inside the upper plenum are crucial to ensure optimal performance and to prevent stratification of the flow. Recent work has been started in which a fiber optic cable has been placed inside of the upper plenum by graduate student Casey Tompkins. The fiber optic can provide planar temperature measurements with high resolution. Particle image velocimetry (PIV) should also be considered to visualize the flow inside the upper plenum.

# Bibliography

- [1] Cengel, Y.A, Cimbala, J.M., 2006. Fluid Mechanics, Second Edition. McGraw-Hill, New York.
- [2] HTGR-86-024, 1992. Preliminary Safety Information Document for the Standard MHTGR HTGR-86-024, Volume 1, Amendment 13. US Department of Energy.
- [3] Lisowski, D., Albiston, S., Scherrer, R., Haskin, T., Tokuhiko, A., Corradini, M., 2011. Experimental Studies of NGNP Reactor Cavity Cooling System with Water, Proc. of ICAPP 2011, Nice, France, Paper 11116.
- [4] Lisowski, D., Muci, M., Anderson, M., Corradini, M., 2013. Design Considerations for a Scaled Reactor Cavity Cooling System with Air for the VHTR, Proc. of NURETH 15, Pisa, Italy. May 12-15, 2013. NURETH.
- [5] Lisowski, D., 2013b. Thermal Hydraulic Analysis of an Experimental Reactor Cavity Cooling System with Water: Performance and Stability. University of Wisconsin-Madison.
- [6] Lomperski, S., Pointer, W.D., Tzanos, C.P., Wei, T.Y.C., Kraus, A.R., 2011. Air-Cooled Option RCCS Studies and NSTF Preparation, ANL-GenIV-179, Argonne National Laboratory.
- [7] Pope, M.A., Lee, J.I., Hejzlar, P., Driscoll, M.J., 2009. Thermal hydraulic challenges of Gas Cooled Fast Reactor with passive safety features. Nuclear Engineering and Design 239, 840-854.
- [8] Turner, J.S., 1966. Jets and Plumes with Negative or Reversing Buoyancy, J. Fluid Mech. 26, 779-792.
- [9] Tzanos, C.P., Farmer, M., 2006. Feasibility Study for Use of the Natural Convection Shutdown Heat Removal Test Facility NSTF for Initial VHTR Water-Cooled RCCS Shutdown, ANL-GenIV-079, Nuclear Engineering Division, Argonne National Laboratory.

## Appendix A: Facility Photographs



Figure 99 – Support structure being lifted into silo.



Figure 100 – Support structure lowered into silo.

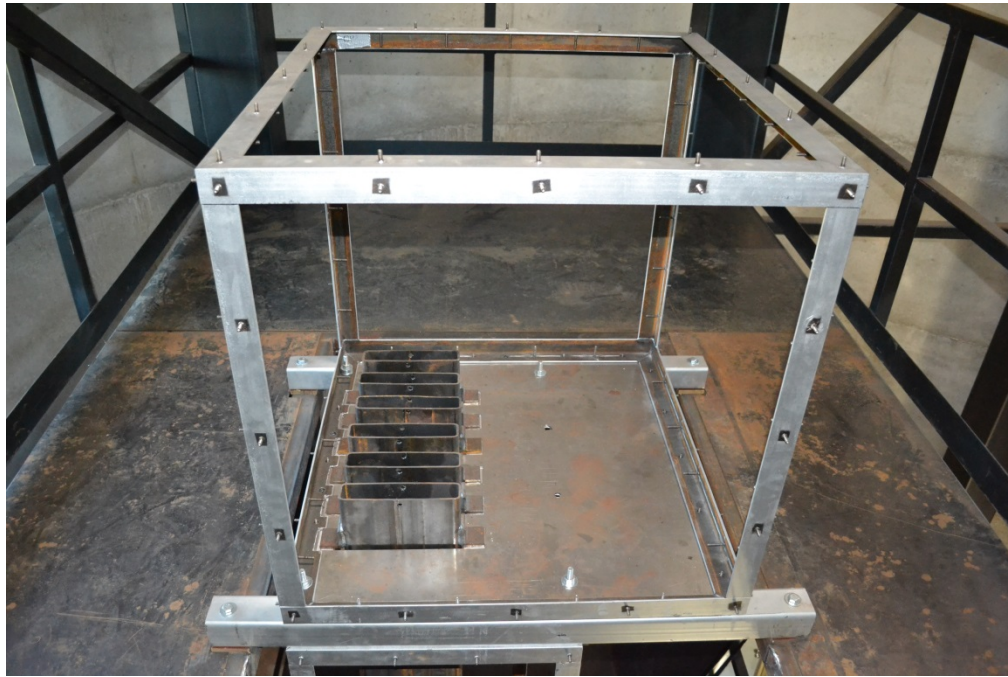


Figure 101 – Outlet plenum without insulation panels.



Figure 102 – Inlet Plenum and heated cavity without insulation panels.



Figure 103 – Heater frames.



Figure 104 – Assembled heater module.



Figure 105 – Heater module exterior.



Figure 106 – Insulation inside heated cavity.



Figure 107 – Finished riser ducts (Riser 4 missing in photo).



Figure 108 – Painted riser ducts inserted into cavity.



Figure 109 – Riser ducts inside heated cavity.



Figure 110 – Heater modules installed.



Figure 111 – Completed inlet plenum.



Figure 112 – Inlet duct piping.

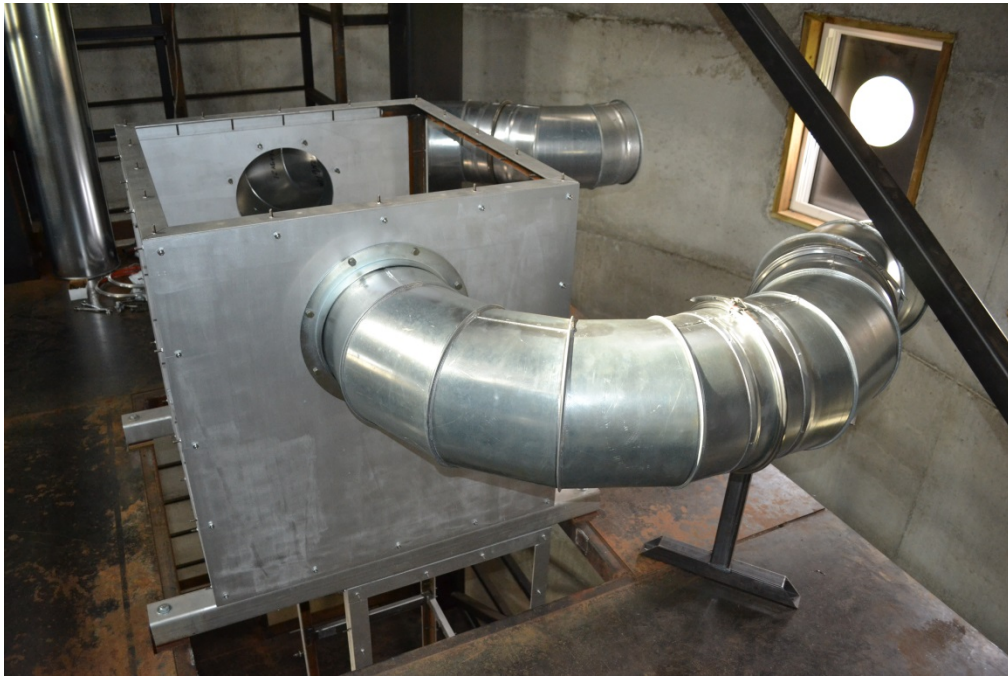


Figure 113 – Initial exhaust duct installation.



Figure 114 – Exhaust duct installation inside silo.

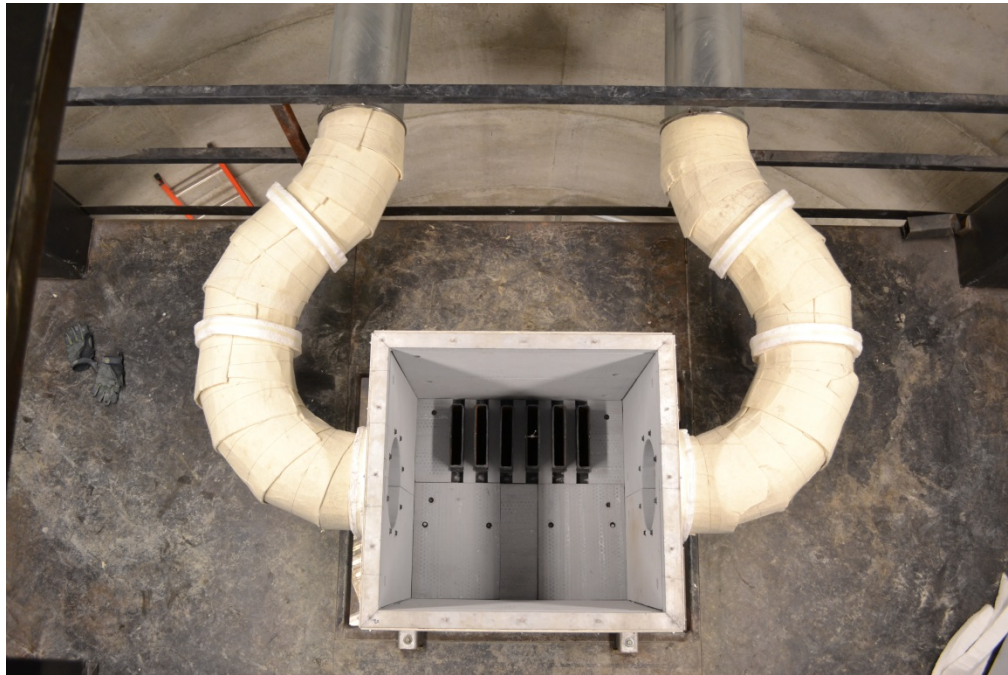


Figure 115 – Outlet plenum insulation.



Figure 116 – Exhaust ducts insulation.



Figure 117 – Exhaust ducts outside silo.



Figure 118 – Close-up of exhaust ducts.



Figure 119 – Electrical box housing data acquisition and controllers.

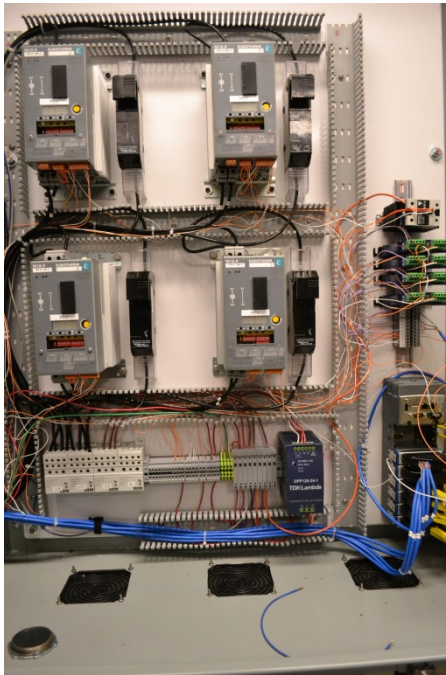


Figure 120 – Data acquisition and controllers.



Figure 121 – Transformer outside silo.



Figure 122 – Electrical line from Stoughton facility to silo.

## Appendix B: Engineering Drawings

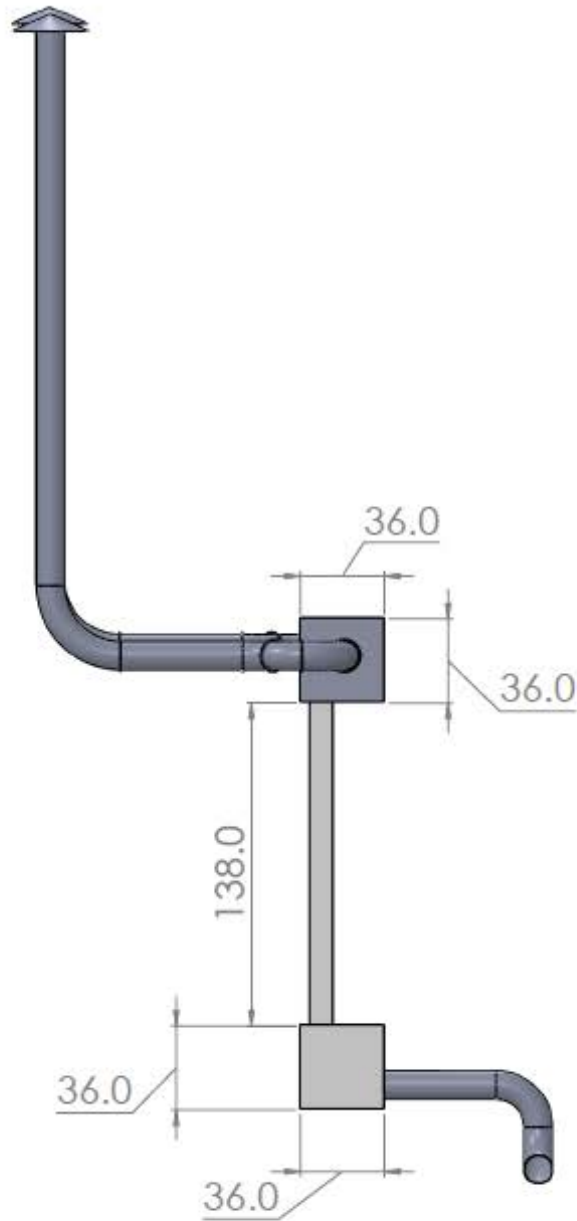


Figure 123 – Overall dimensions for quarter-scale air RCCS (in inches).

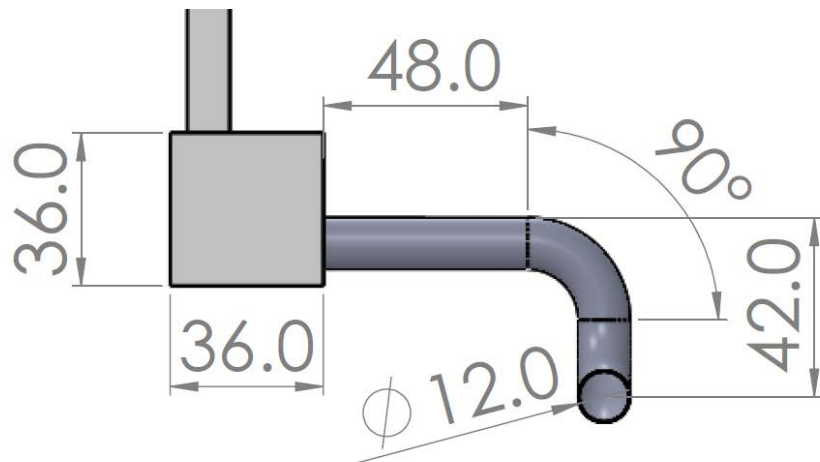


Figure 124 – Side view dimensions of inlet duct (in inches).

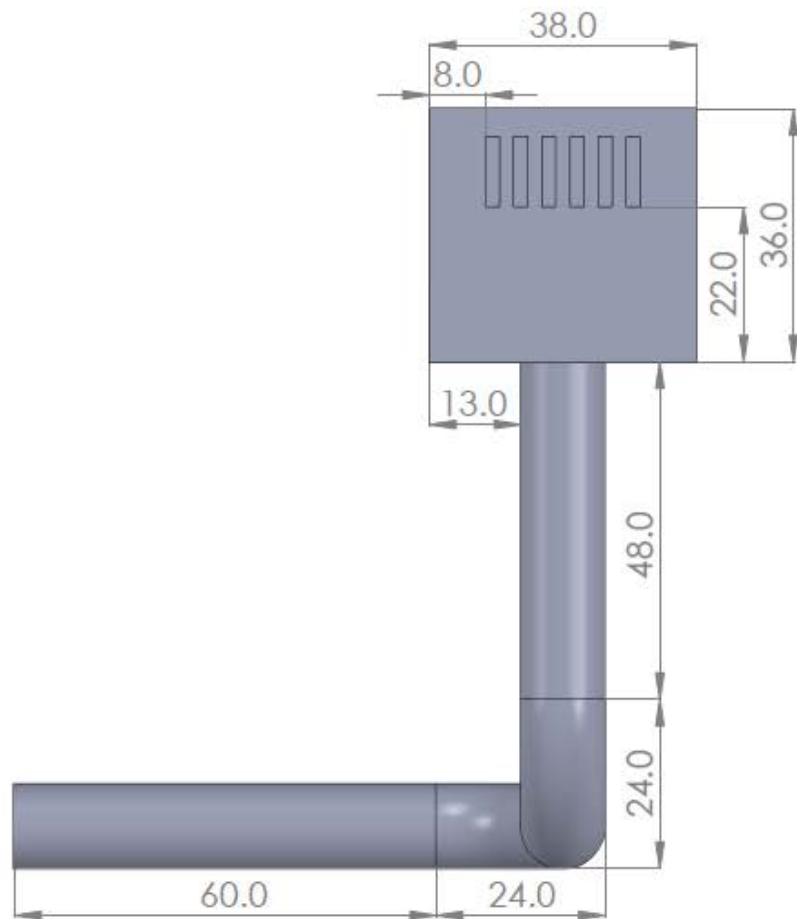


Figure 125 – Top view dimensions of inlet duct (in inches).

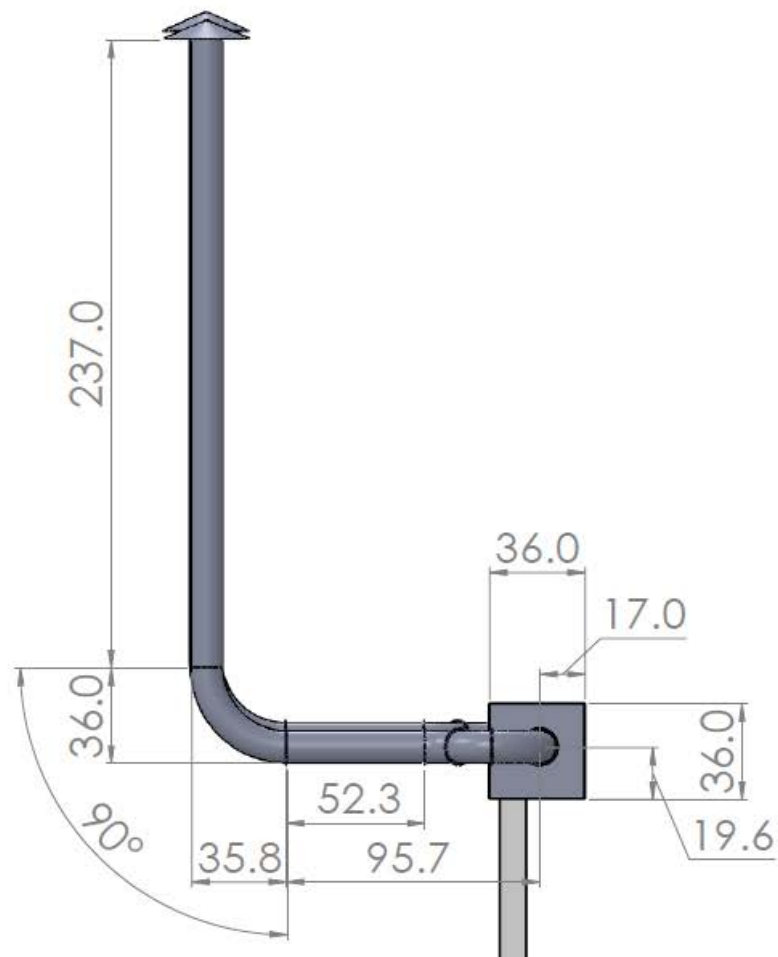


Figure 126 – Side view dimensions of exhaust duct (in inches).

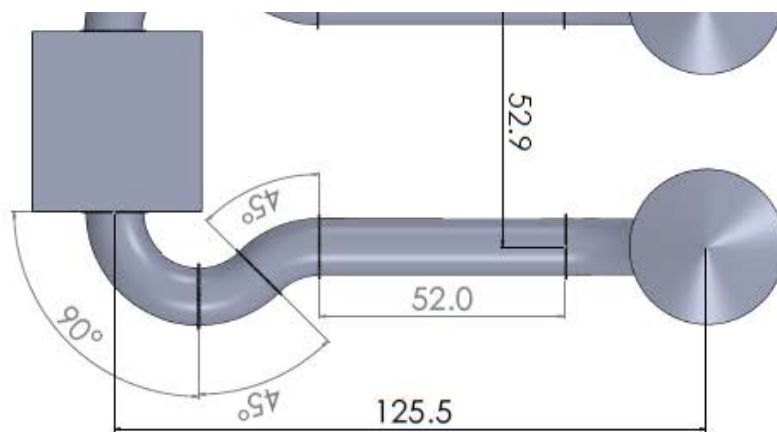


Figure 127 – Top view dimensions of exhaust duct (in inches).

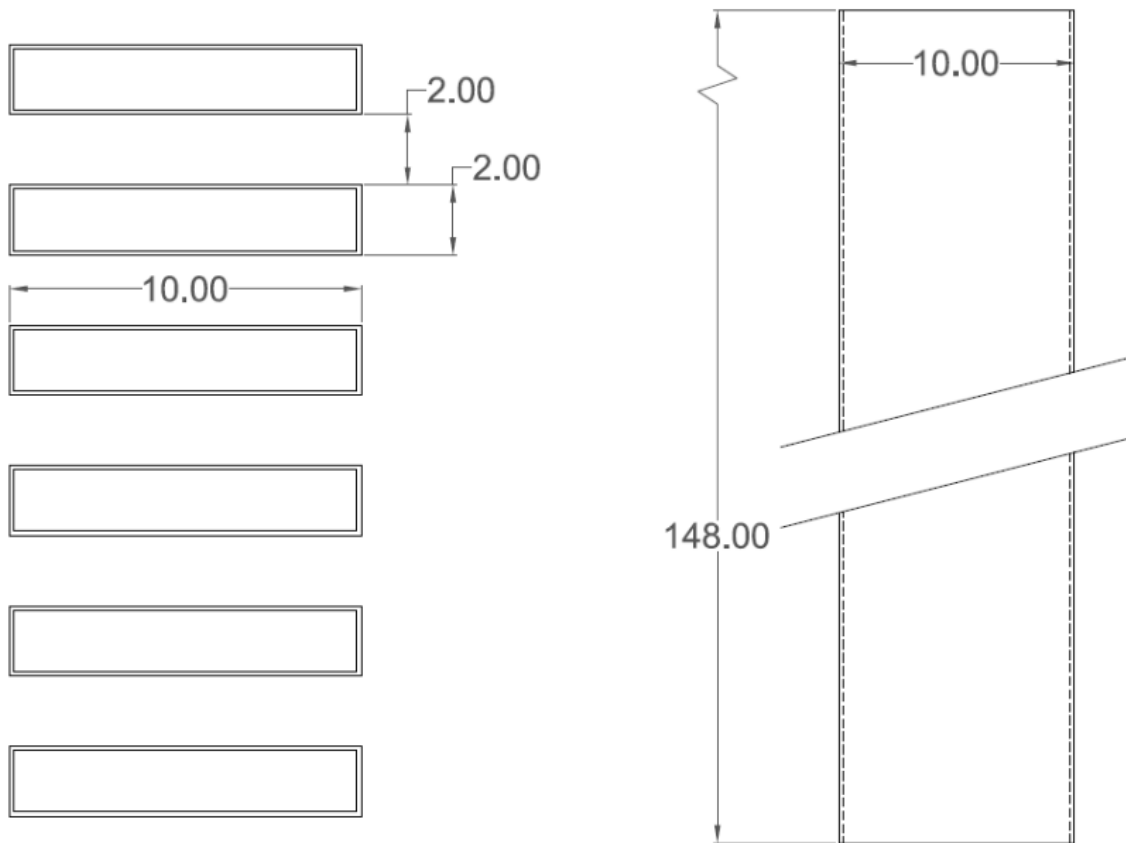


Figure 128 – Nominal riser duct dimensions (in inches).

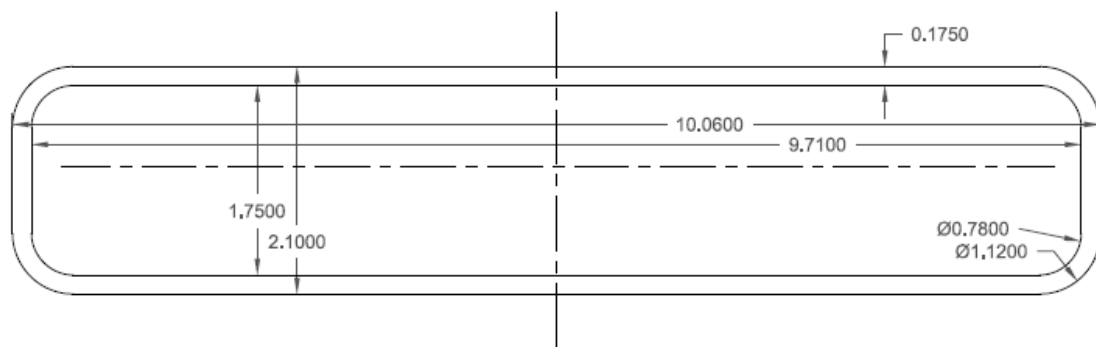


Figure 129 – Riser duct cross section (in inches).

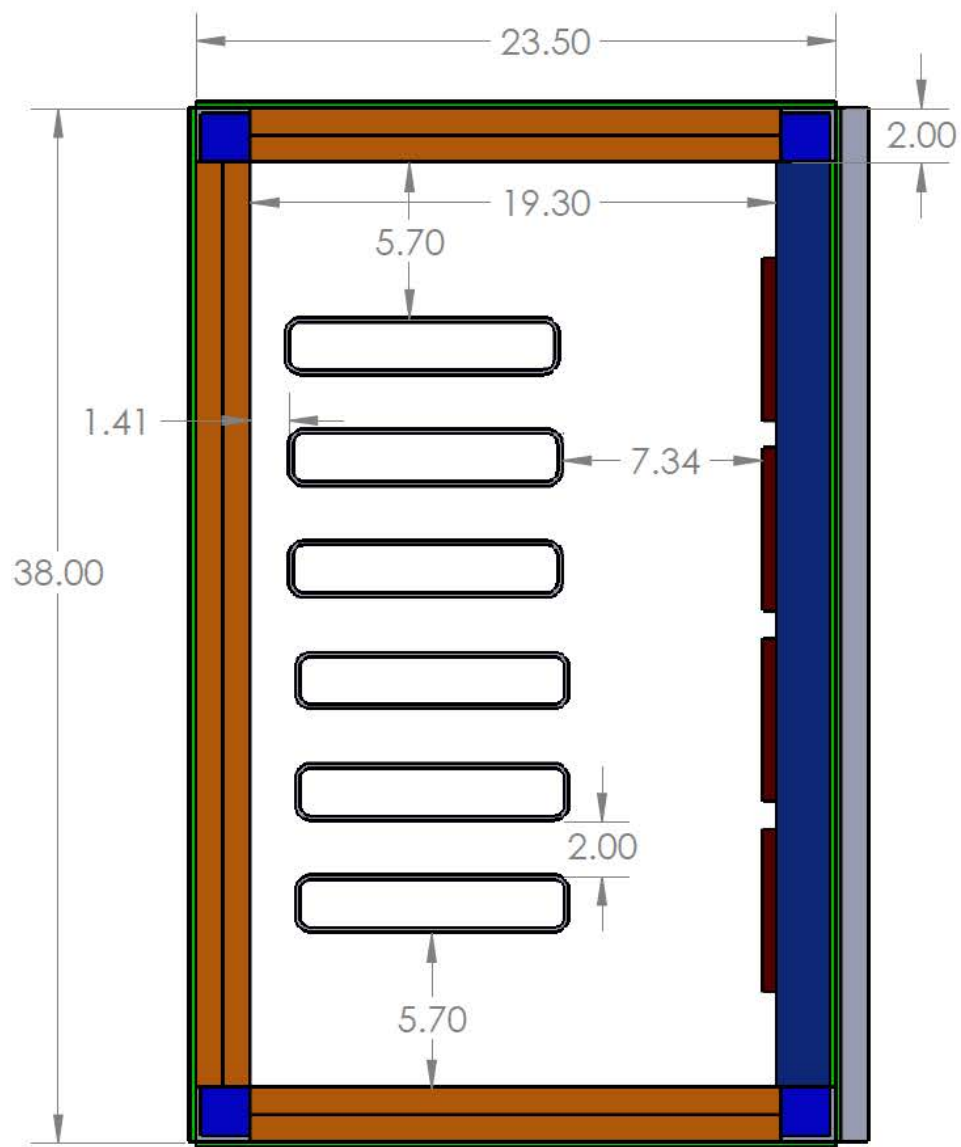


Figure 130 – Heated cavity dimensions (in inches).

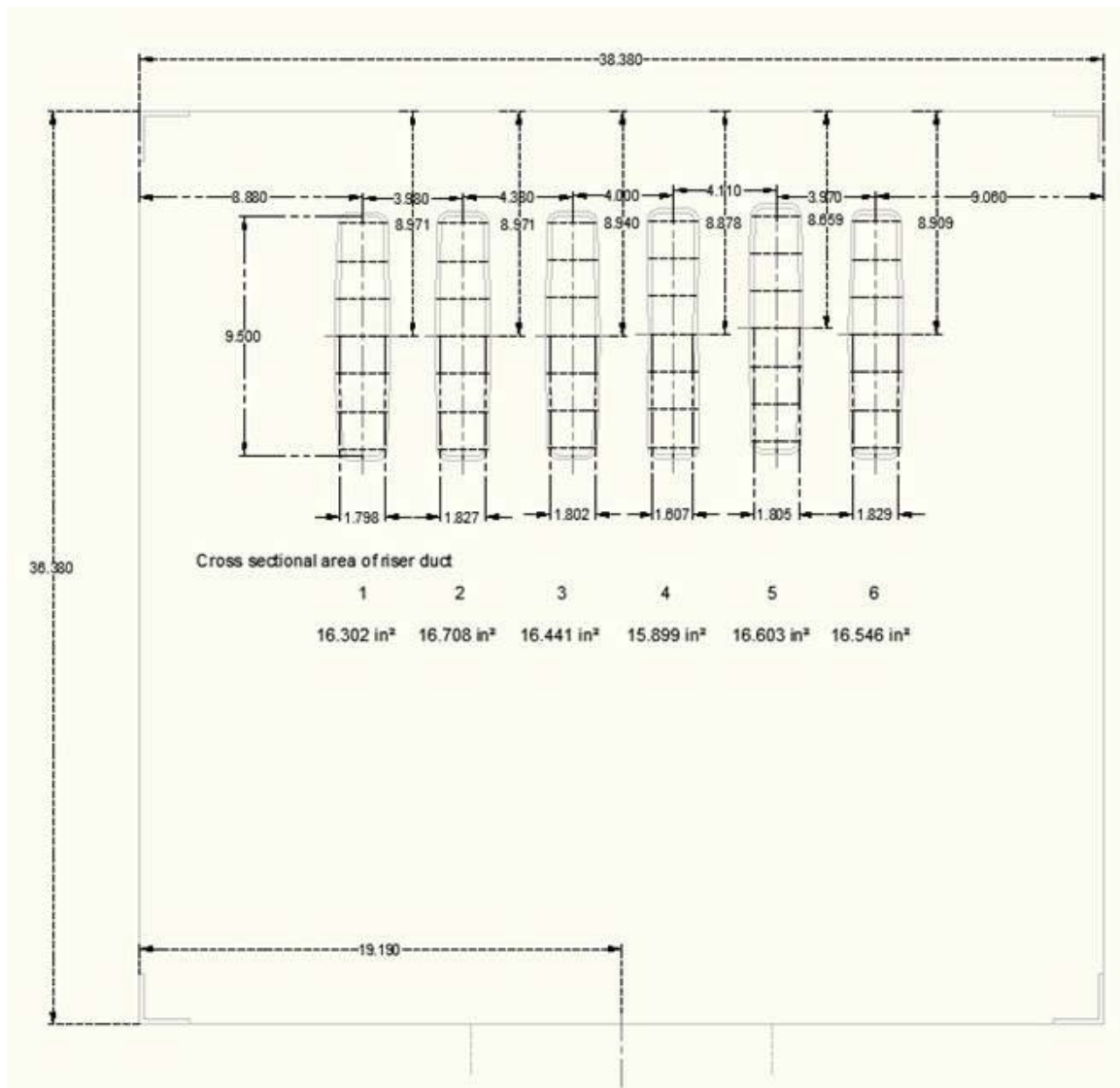


Figure 131 – As-built cross sectional area of inlet plenum (in inches).

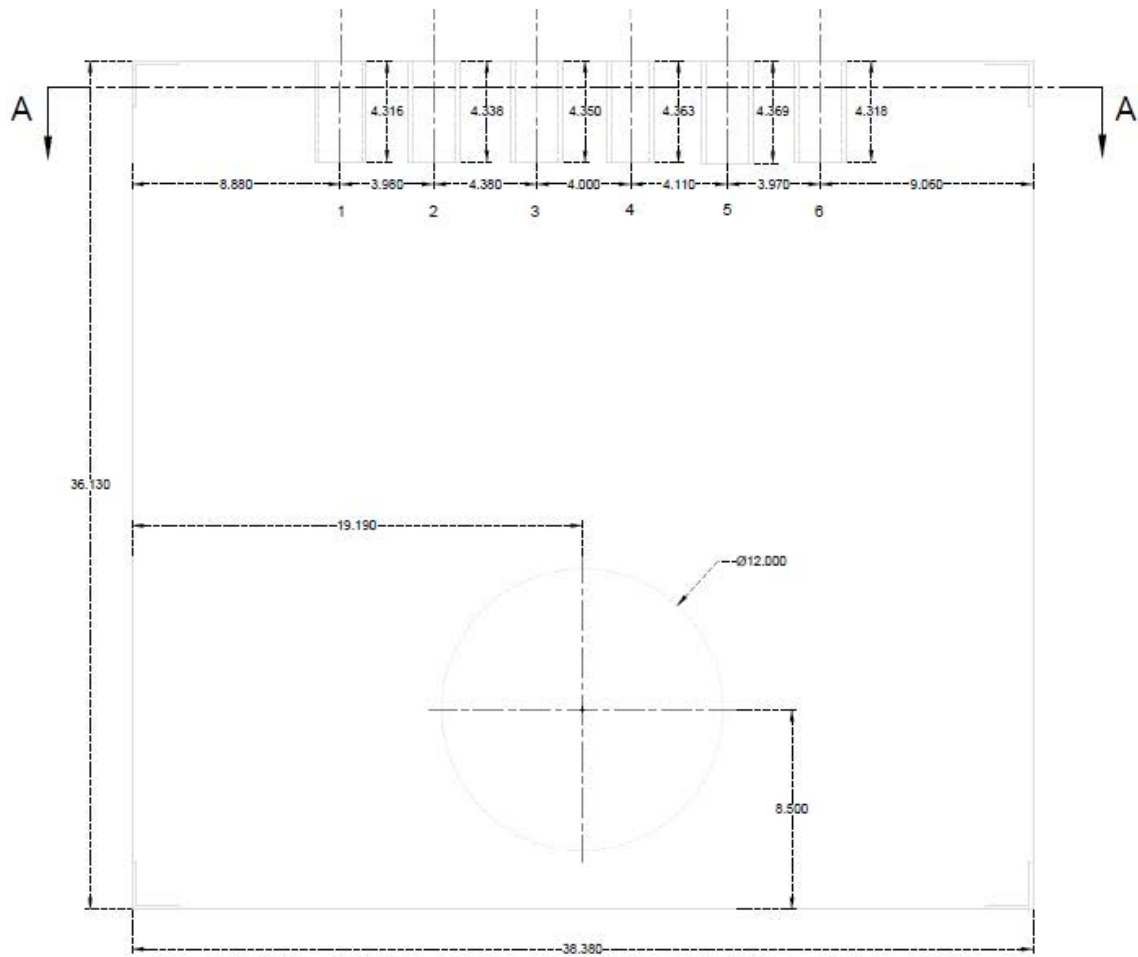


Figure 132 – As-built dimensions of inlet plenum (front view; in inches).

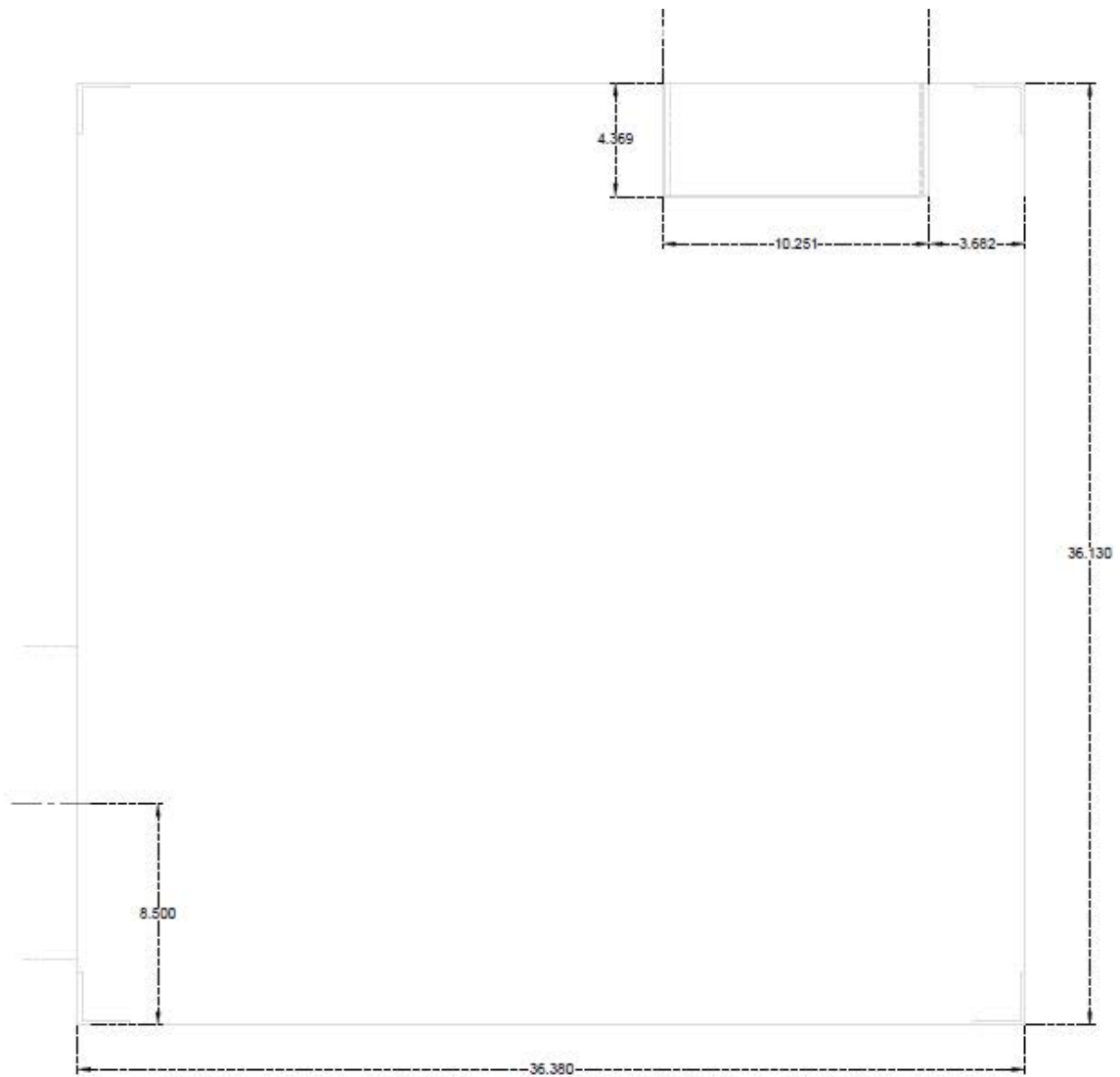


Figure 133 – As-built dimensions of inlet plenum (side view; in inches).

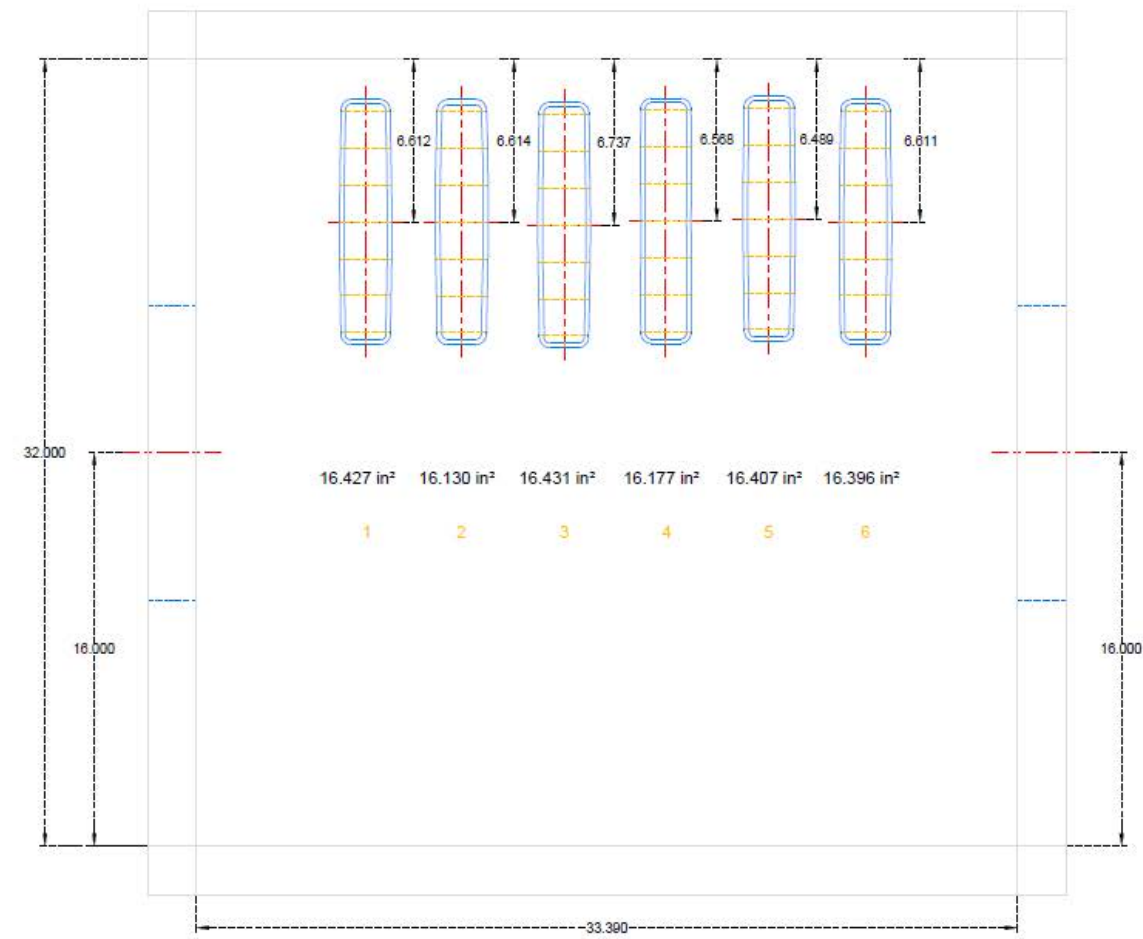


Figure 134 – As-built cross sectional area of outlet plenum (in inches).

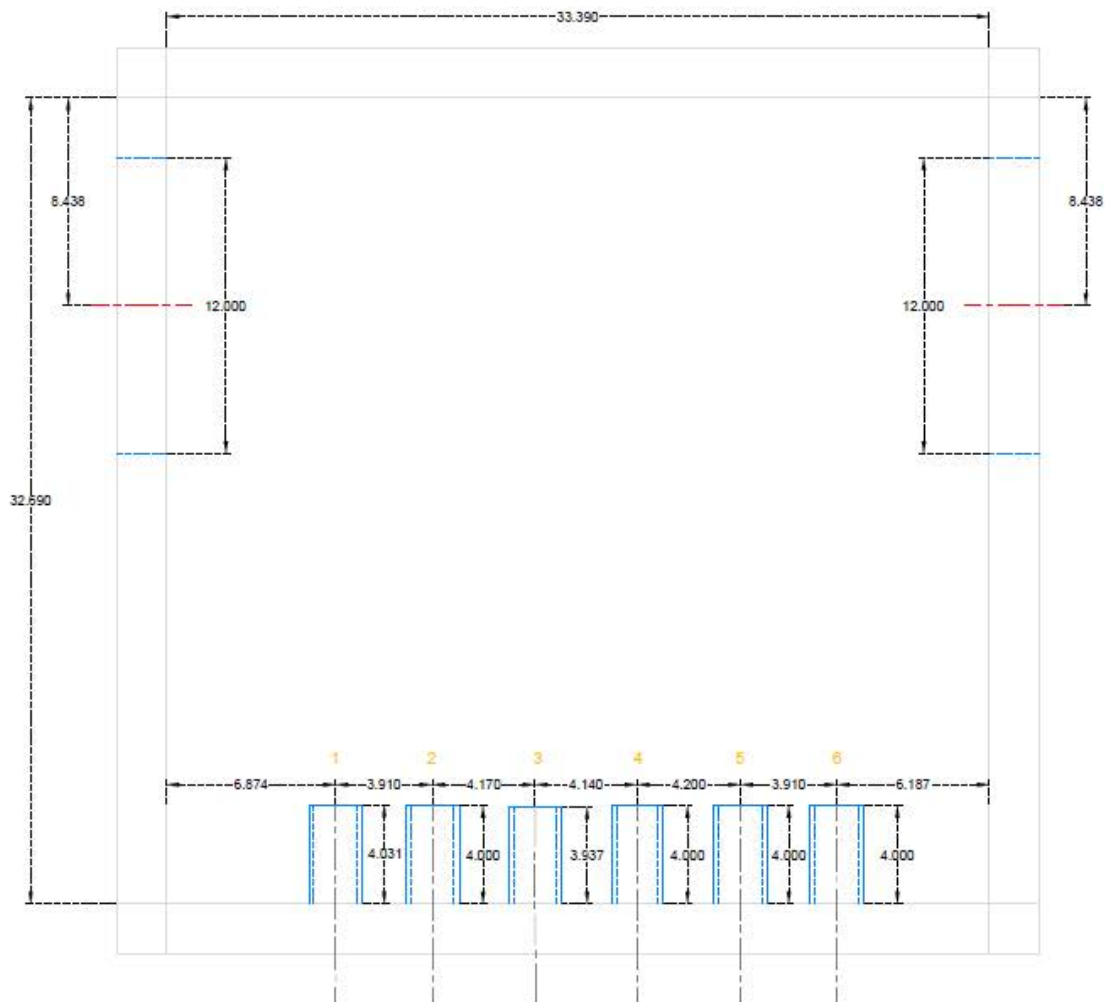


Figure 135 – As-built dimensions of outlet plenum (front view; in inches).

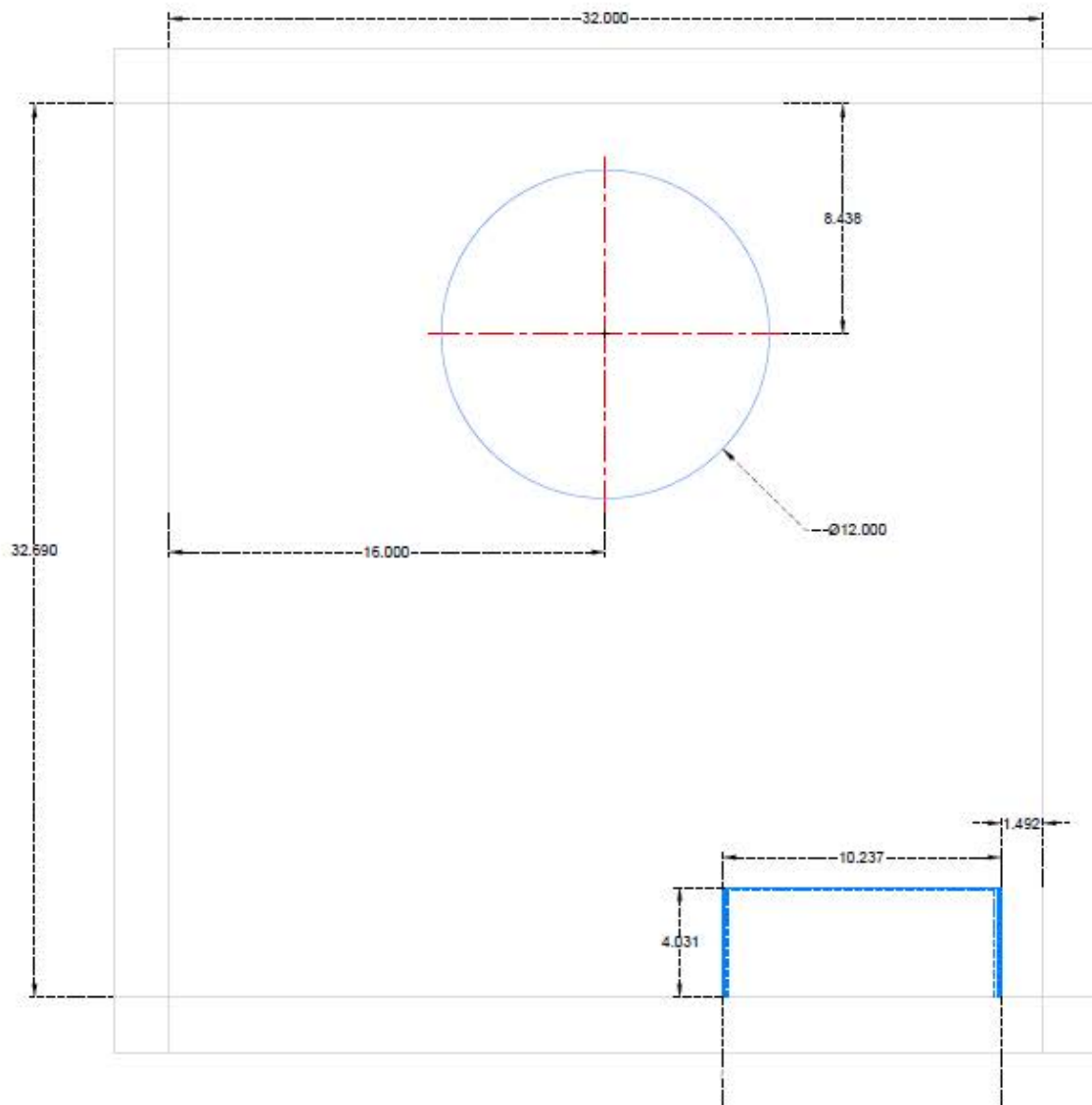


Figure 136 – As-built dimensions of outlet plenum (side view; in inches).

## Appendix C: Velocity Transducers in Risers

A discussion of the velocity transducers at the entry of the riser ducts and the inlet pipe is presented.

Data collected for Test 23 will be used. Test 23 was a natural circulation test with 37.97 kW input to the four heating zones. The velocity data presented was collected at the center point of the cross

sectional area of the riser ducts and inlet pipe. Figure 137 shows the inlet pipe velocity time history.

Figure 138 shows the riser duct velocity time histories. Table 26 lists the velocities for the various components which were averaged from the sixth to the tenth hour of the test.

Table 26 – Average velocities for Test 23.

Component	Avg. Velocity (m/s)
Inlet Pipe	1.92
Riser 1	3.05
Riser 2	2.97
Riser 3	3.09
Riser 4	2.98
Riser 5	3.02
Riser 6	3.23

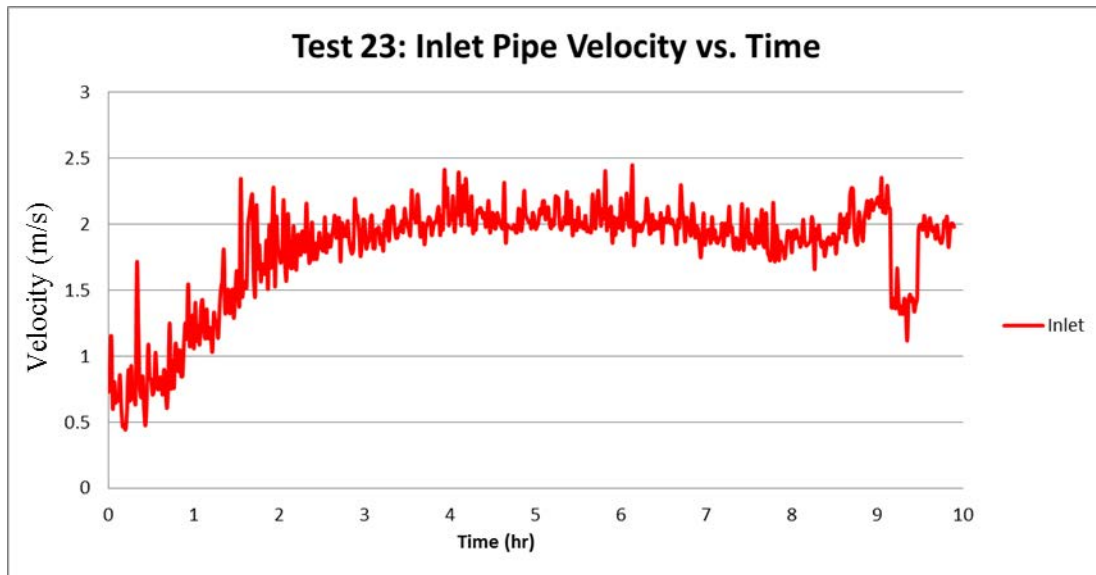


Figure 137 – Inlet pipe velocity vs. time for Test 23.

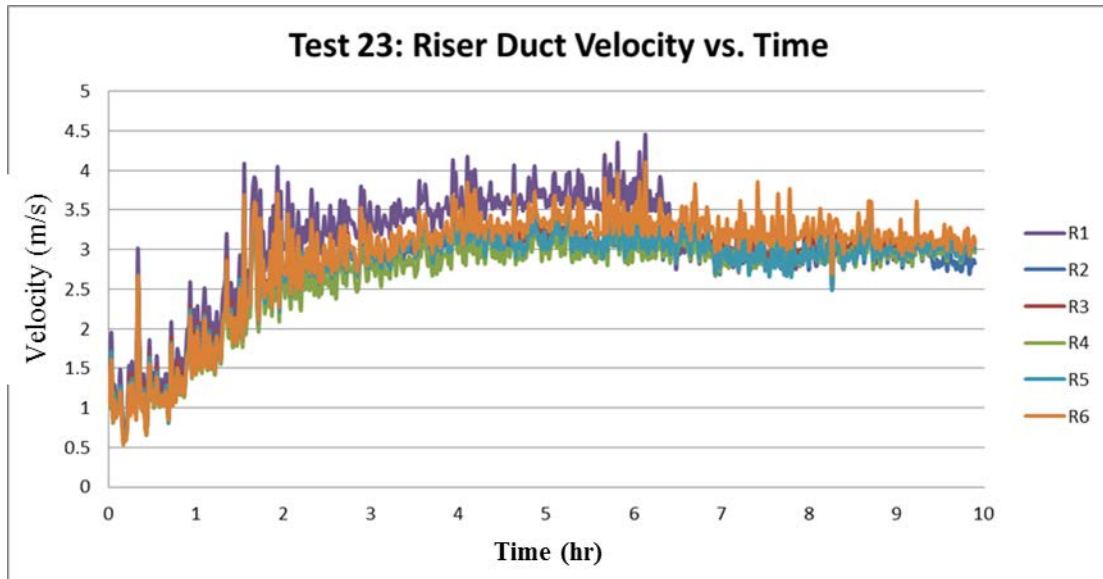


Figure 138 – Riser duct velocity vs. time for Test 23.

The inlet pipe velocity profile is known as it was measured. This resulted in a calculated mass flow of 0.18 kg/s. However, the velocity profile at the inlet of the riser ducts was not measured and is not known. For comparison purposes, the velocity profile at the riser duct measurement locations is assumed to be constant (as measured in the center) across the entire cross sectional area. This is not realistic and most likely would be an upper bound. The sum of the calculated riser duct yields 0.28 kg/s. The velocity profile at the riser ducts needs to be experimentally measured. Hence, the velocity data collected at the entry of the riser ducts were not used for any analysis in the thesis.

Table 27 – Mass flow rates for Test 23.

<b>Component</b>	<b>Mass Flow (kg/s)</b>
Inlet Pipe	0.18
Riser 1	0.047
Riser 2	0.045
Riser 3	0.047
Riser 4	0.046
Riser 5	0.046
Riser 6	0.050

## Appendix D: Heat Loss Calculation

A detailed analysis of parasitic heat losses is presented for Test 18. The integral heater power for the test is 37.97 kW with a constant heat flux profile. The heat losses were estimated for the following components of the scaled experiment: heated cavity, outlet plenum, and the section of the exhaust ducts inside the silo. Table 28 lists the parasitic heat losses for each component. The heated cavity is responsible for the majority of the heat loss (94.05 %).

Table 28 – Parasitic heat losses for Test 18.

<b>Component</b>	<b>Heat Loss</b>	<b>Percentage</b>
Heated Cavity	6.01 kW	94.05 %
Outlet Plenum	0.20 kW	3.13 %
Exhaust Ducts	0.18 kW	2.82 %
<b>Total</b>	<b>6.39 kW</b>	<b>100 %</b>

The heat loss through a panel can be calculated with the following equation:

$$\dot{Q}_{loss} = kA(T_{probe} - T_{infrared})/d$$

The equation can be modified to:

$$\dot{Q}_{loss} = (T_{probe} - T_{infrared})/R$$

where R is the thermal resistance calculated for the combined insulation layers for each component. The R value must be calculated for each panel because it is dependent the surface area, insulation material properties, and thickness of the insulation.

## Appendix E: Alternate Heat Loss Calculation

An alternate method for calculating heat losses was done for comparison purposes. 2 experiments were chosen (Test 19 and Test 23) in which the heat loss calculations were performed again with the new method. The heat loss coming from each panel cab calculated by:

$$\dot{Q}_{loss} = h_{conv}A(T_{infrared} - T_{atm})$$

The natural convection heat transfer coefficient can be calculated by:

$$h_{conv} = Nu(k)/L$$

The Nusselt number can be calculated by:

$$Nu = 0.1Ra^{1/3} = 0.1(GrPr)^{1/3}$$

Table 29 lists the parasitic heat losses calculated with the presented in this Appendix and the one presented in Chapter 4. The new calculation using natural convection results in lower estimated heat losses compared to the method presented in Chapter 4 where conduction equations are used.

Table 29 – Parasitic heat losses for new calculation method.

<b>Experiment</b>	<b>Heat Loss</b>	<b>Prior Method</b>
Test 19	2.03 kW	2.16 kW
Test 23	5.21 kW	8.15 kW

## Appendix F: Flow Profiles

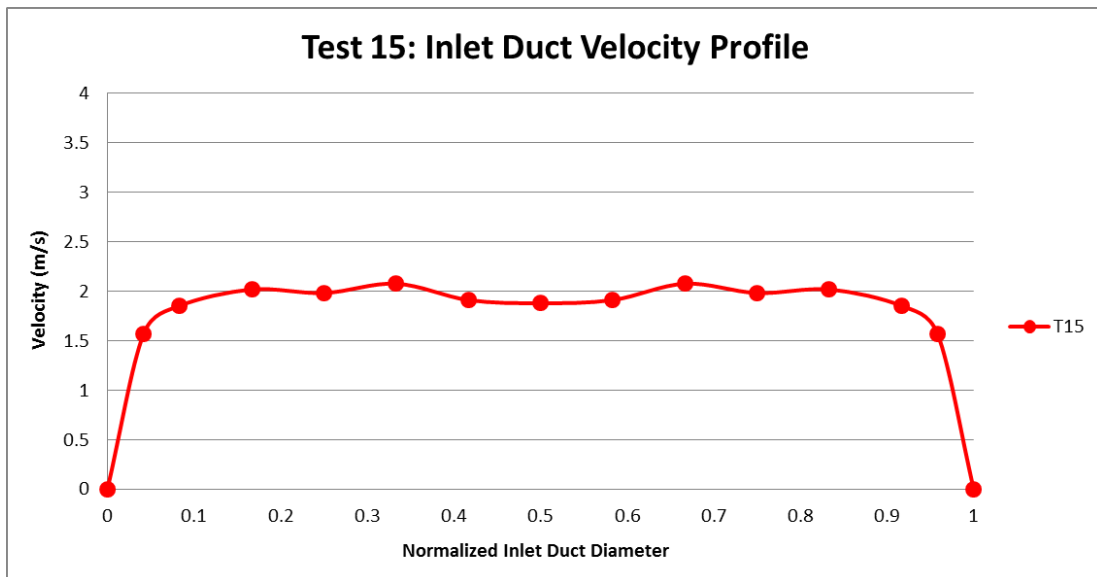


Figure 139 - Inlet duct velocity profile for Test 15.

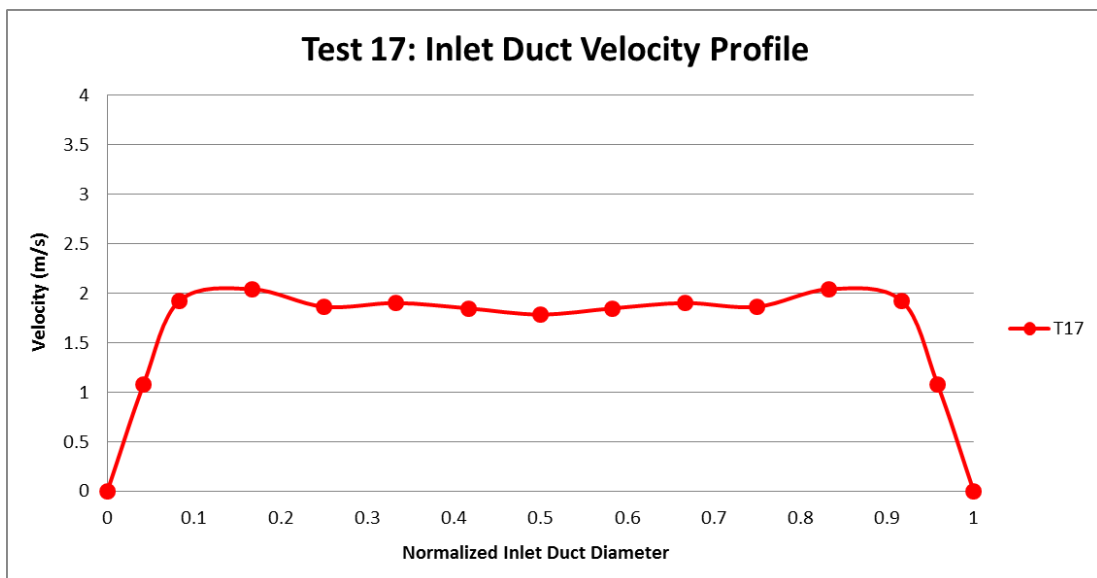


Figure 140 - Inlet duct velocity profile for Test 17.

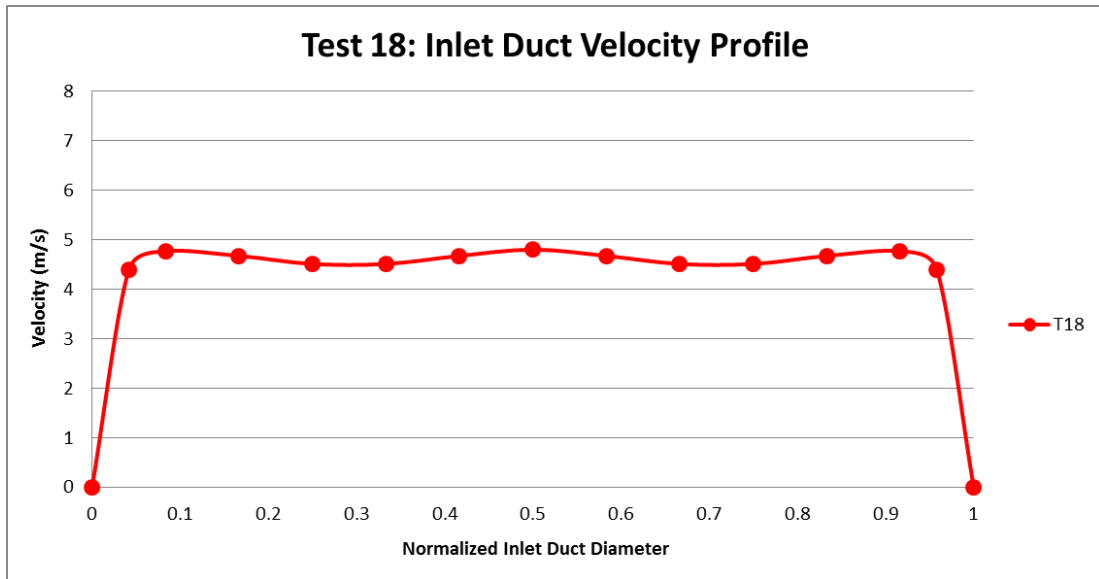


Figure 141 - Inlet duct velocity profile for Test 18.

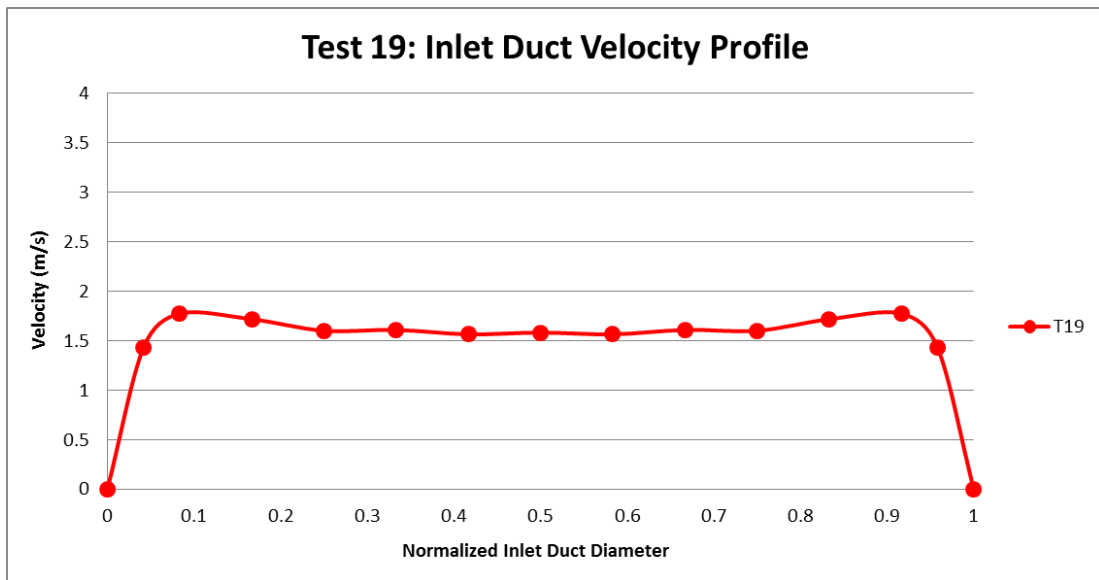


Figure 142 - Inlet duct velocity profile for Test 19.

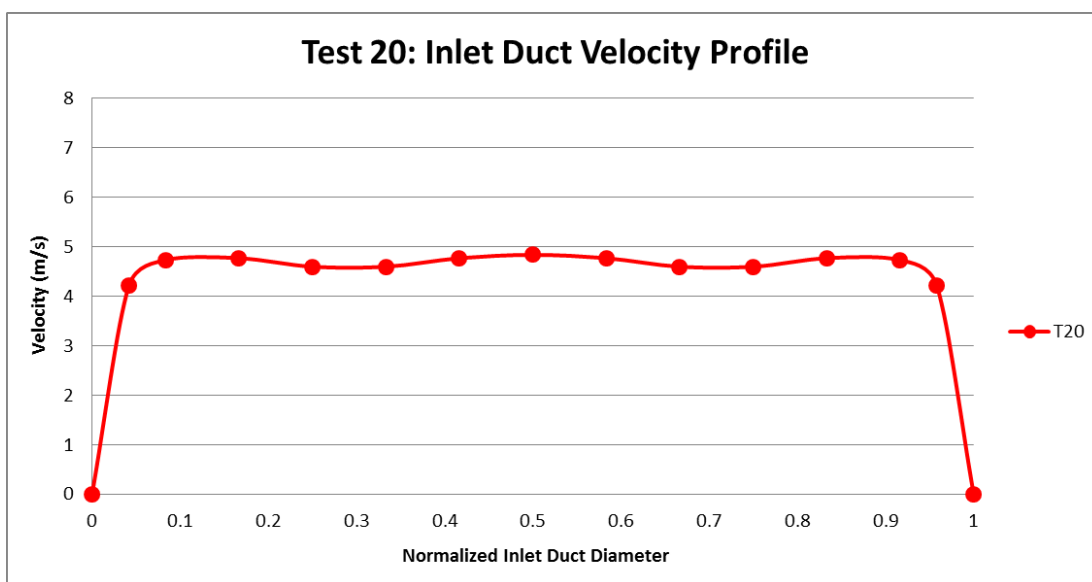


Figure 143 - Inlet duct velocity profile for Test 20.

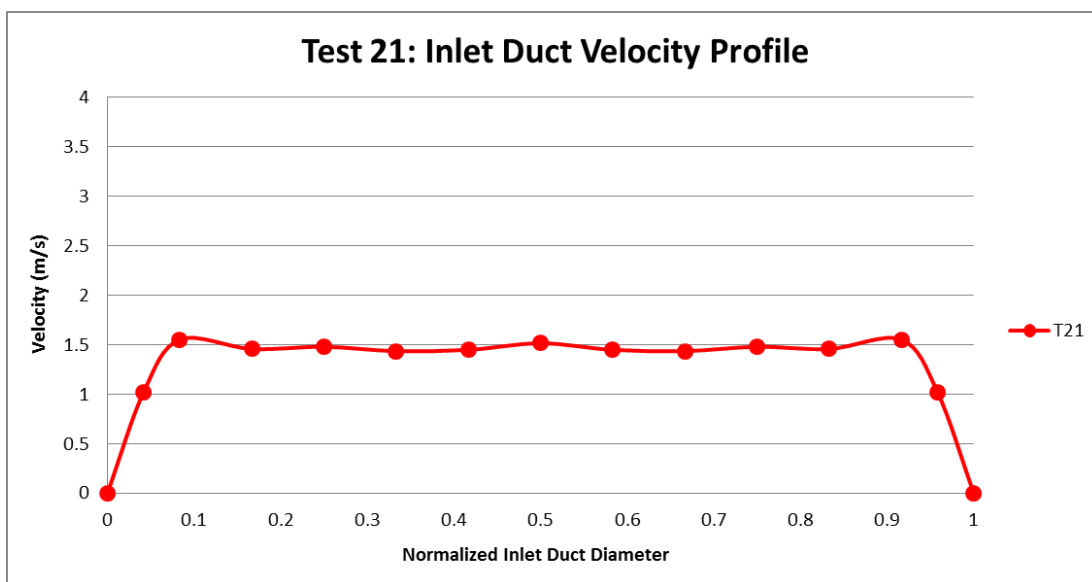


Figure 144 - Inlet duct velocity profile for Test 21.

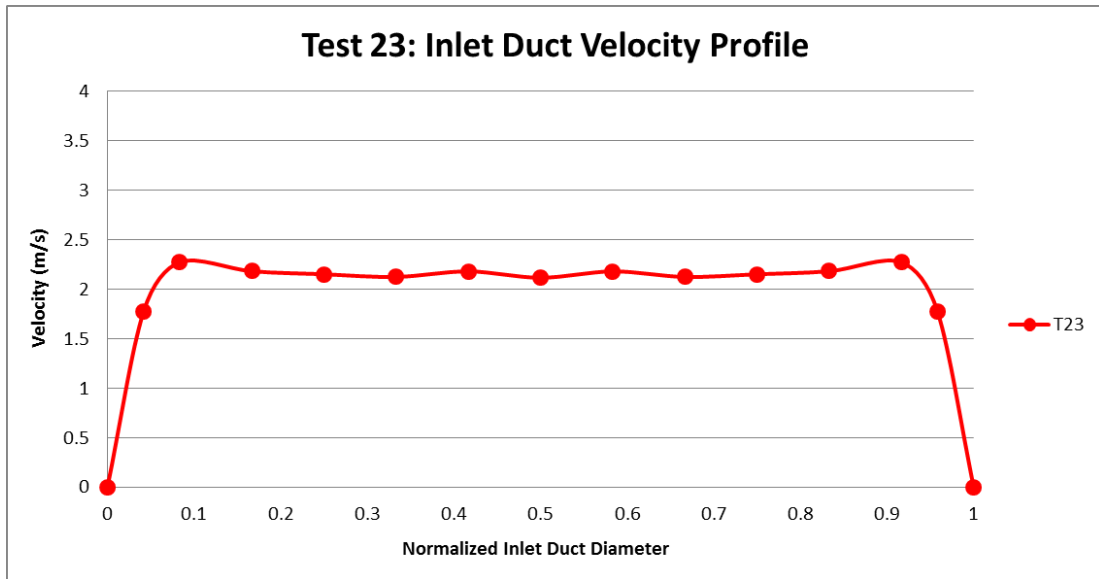


Figure 145 - Inlet duct velocity profile for Test 23.

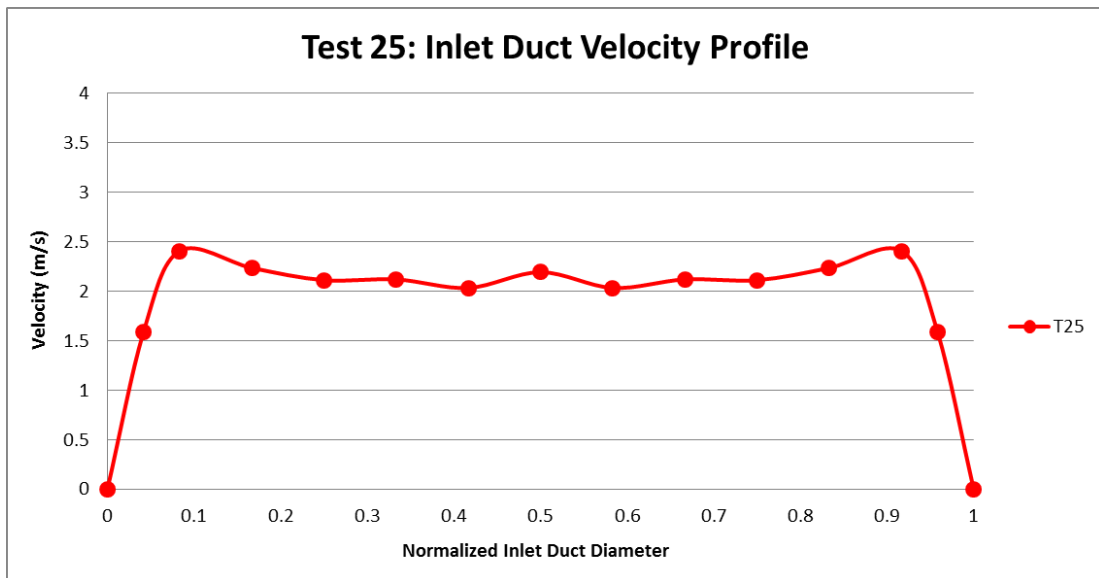


Figure 146 - Inlet duct velocity profile for Test 25.

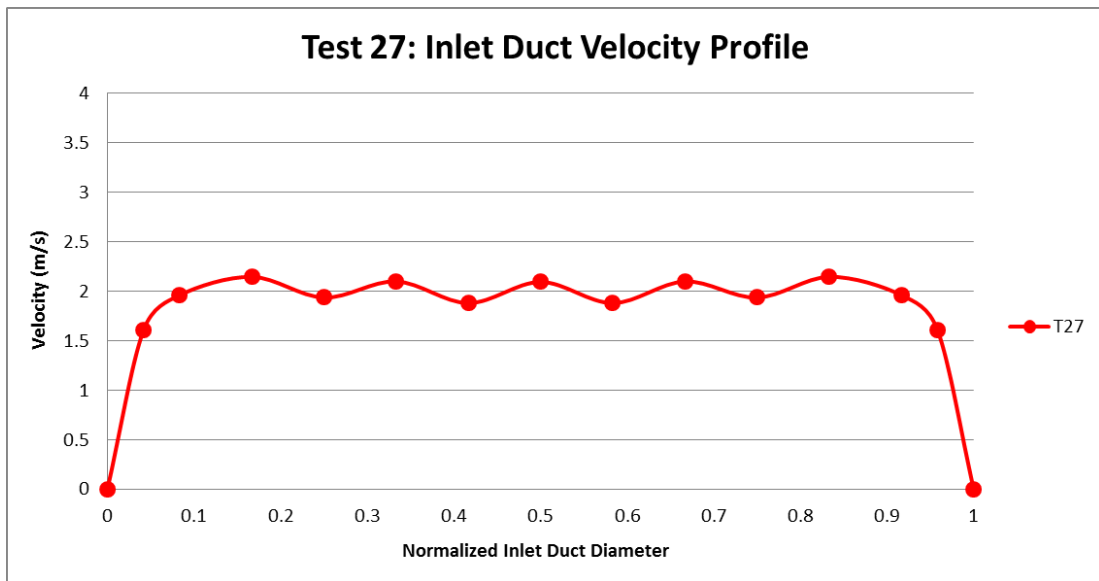


Figure 147 - Inlet duct velocity profile for Test 27.

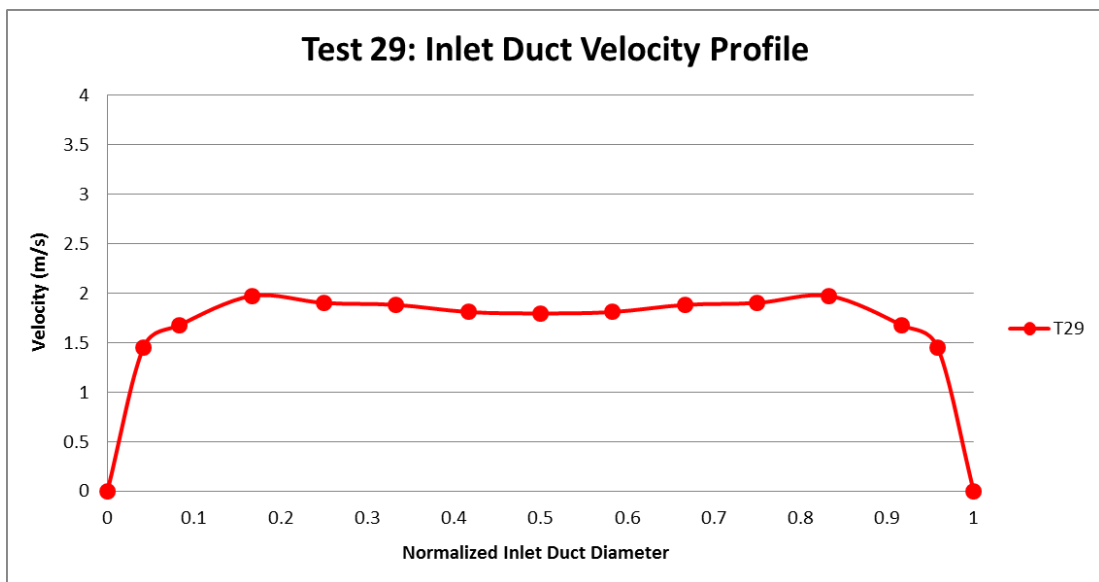


Figure 148 - Inlet duct velocity profile for Test 29.

## Appendix G: Time Variation of Inlet Piping Velocity Measurement

In order to obtain the velocity profiles for the inlet piping, a procedure must be followed. During ramp-up the velocity transducer is placed in the center of the cross sectional area. After thermal equilibrium is reached, the velocity probe must be physically moved across the inlet piping to obtain the velocity profile. The probe was scanned in the upper-half of the inlet duct and symmetry was assumed across the axis. Table 30 lists the velocities across the normalized inlet duct diameter. The probe was placed for five minutes at each location from 0 to 0.5 normalized diameter. Symmetry was then assumed from 0.5 to 1 normalized diameter.

Table 30 – Velocity at normalized inlet duct diameter.

<b>Normalized Inlet Duct Diameter</b>	<b>Velocity (m/s)</b>
0.000	0
0.042	1.43
0.083	1.77
0.167	1.72
0.250	1.60
0.333	1.61
0.417	1.56
0.500	1.58
0.583	1.56
0.667	1.61
0.750	1.60
0.833	1.72
0.917	1.77
0.958	1.43
1.000	0

## Appendix H: Forced Flow Tests 16 and 20

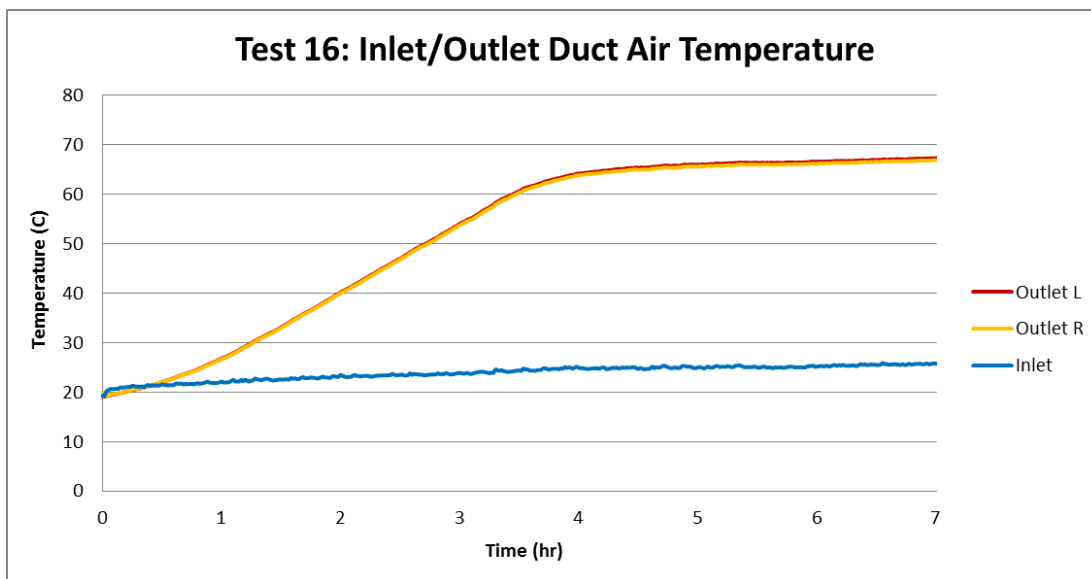


Figure 149 - Inlet/outlet duct air temperatures for Test 16 (Uncertainty:  $\pm 0.7^{\circ}\text{C}$ ).

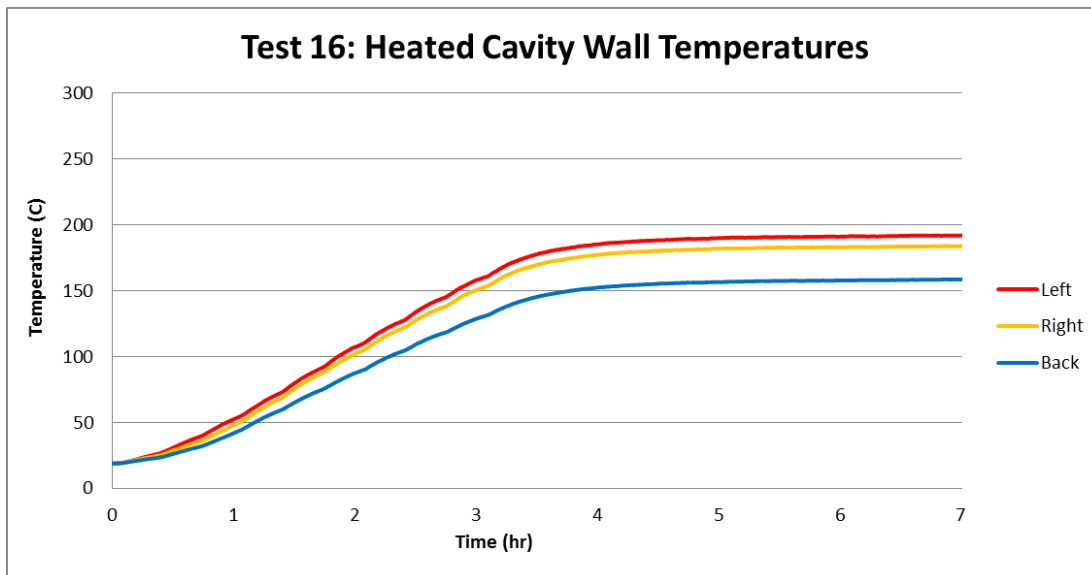


Figure 150 - Heated cavity wall temperatures for Test 16 (Uncertainty:  $\pm 0.7^{\circ}\text{C}$ ).

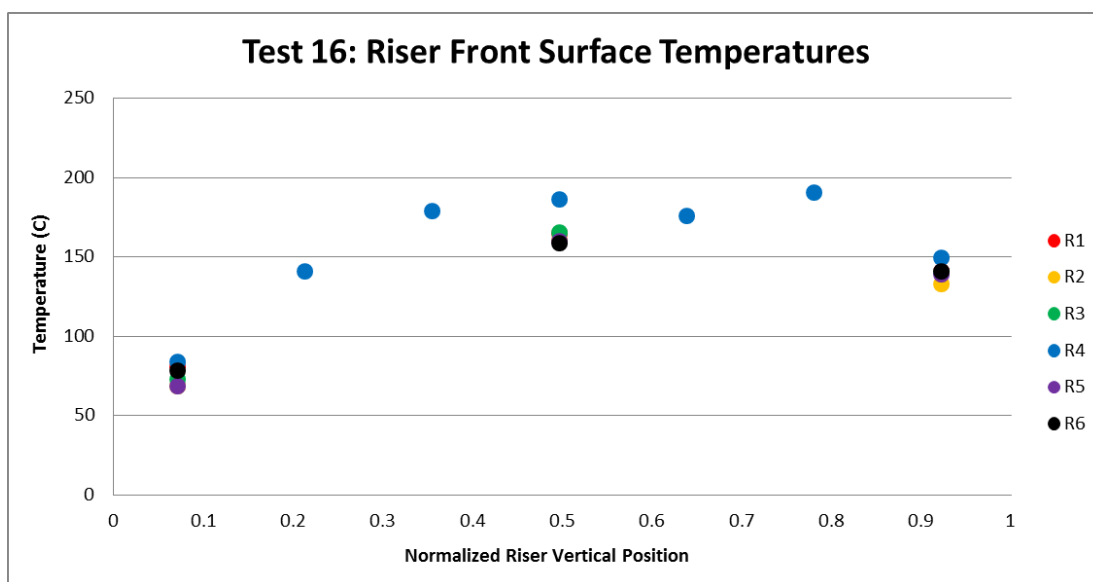


Figure 151 - Riser front surface temperatures for Test 16 (Uncertainty:  $\pm 2.2^{\circ}\text{C}$ ).

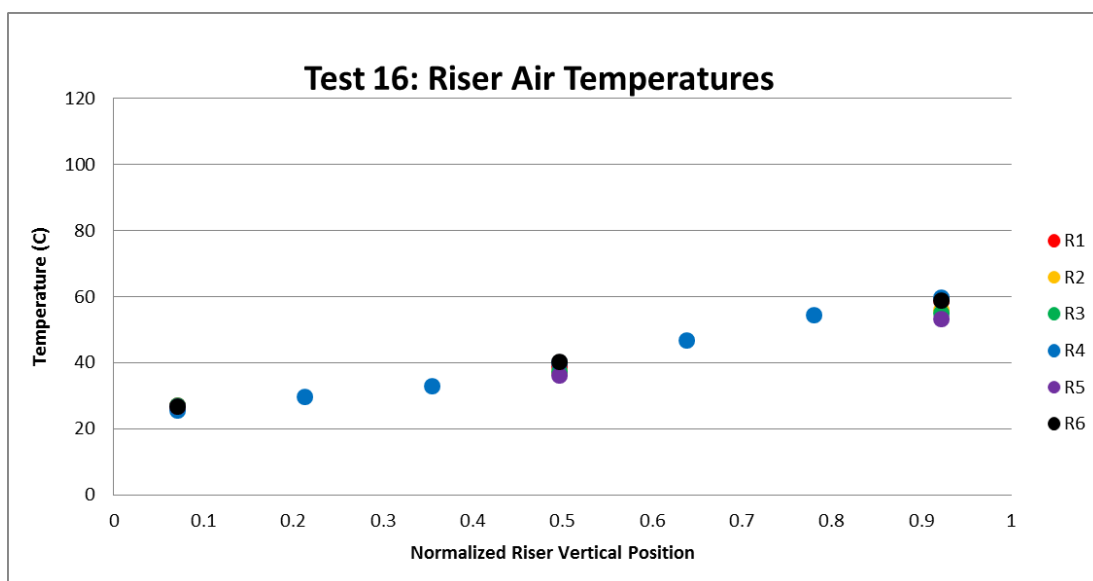


Figure 152 - Riser air temperatures for Test 16 (Uncertainty:  $\pm 0.7^{\circ}\text{C}$ ).

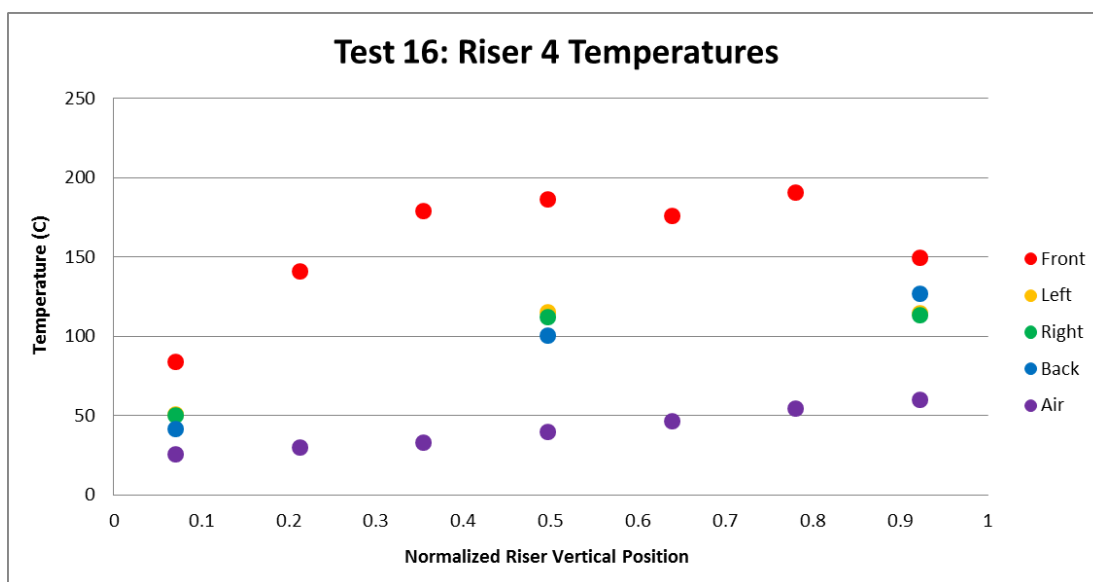


Figure 153 - Riser 4 temperatures for Test 16 (Uncertainty:  $\pm 2.2^{\circ}\text{C}$  for Front, Others  $\pm 0.7^{\circ}\text{C}$ ).

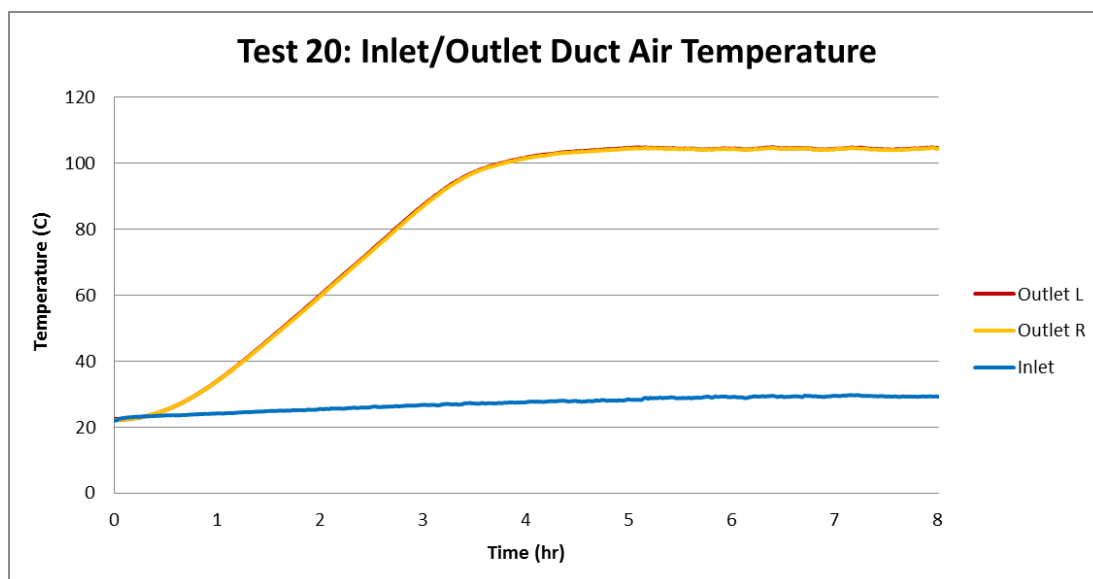


Figure 154 - Inlet/outlet duct air temperatures for Test 20 (Uncertainty:  $\pm 0.7^{\circ}\text{C}$ ).

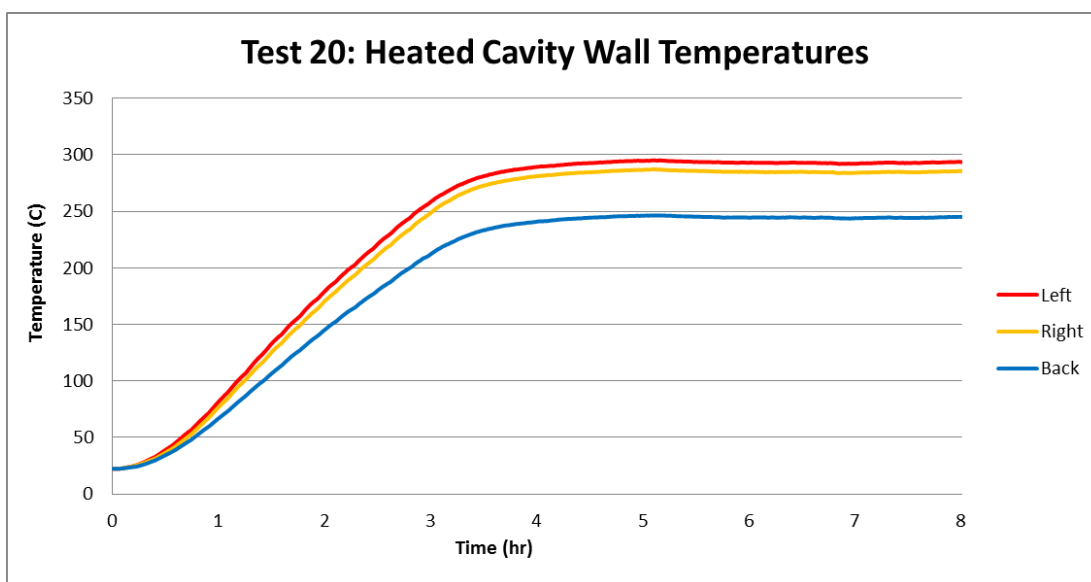


Figure 155 - Heated cavity wall temperatures for Test 20 (Uncertainty:  $\pm 0.7^{\circ}\text{C}$ ).

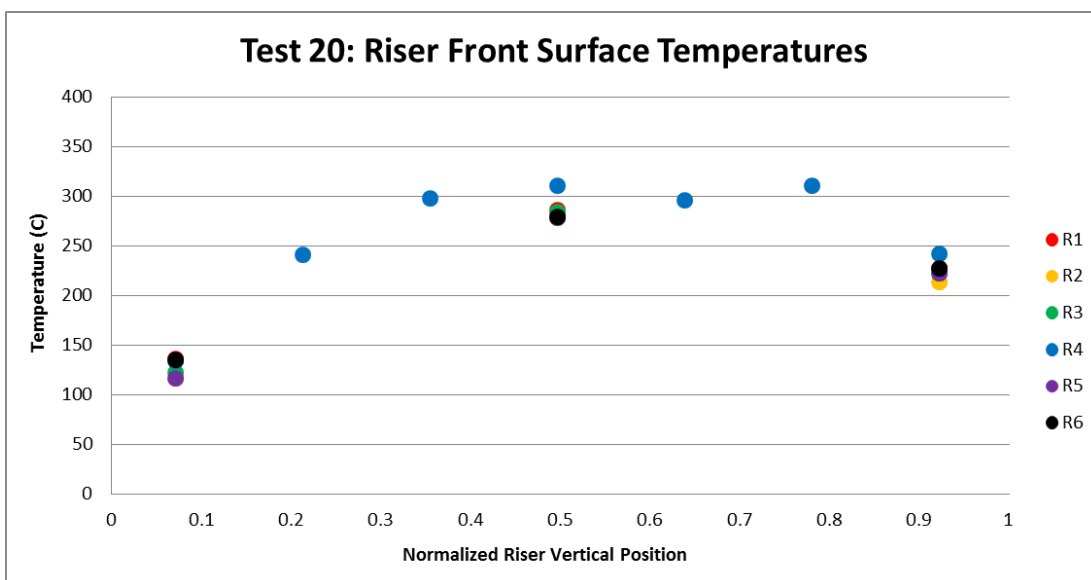


Figure 156 - Riser front surface temperatures for Test 20 (Uncertainty:  $\pm 2.2^{\circ}\text{C}$ ).

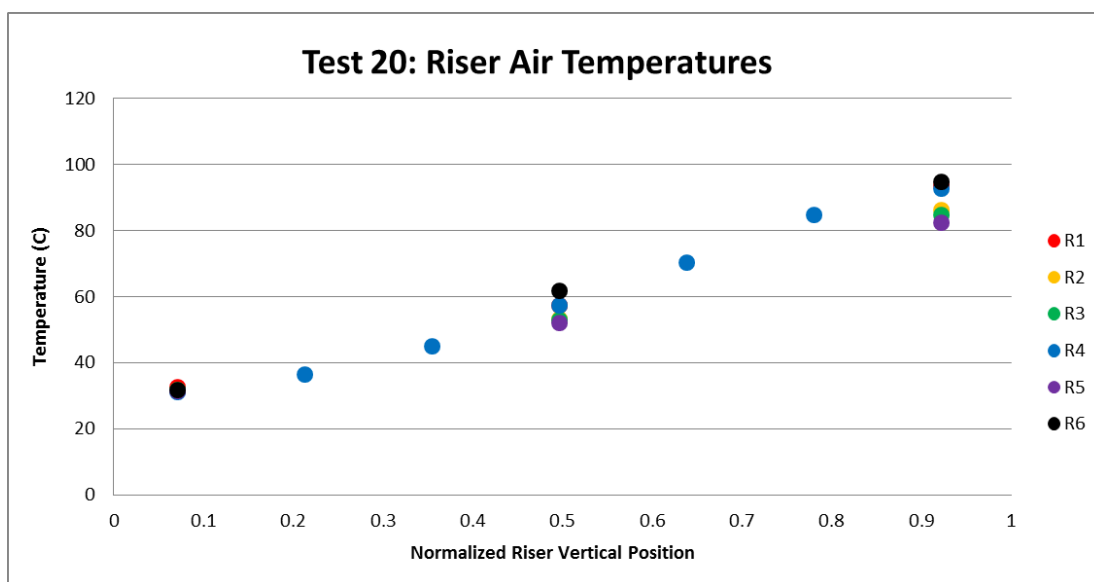


Figure 157 - Riser air temperatures for Test 20 (Uncertainty:  $\pm 0.7^{\circ}\text{C}$ ).

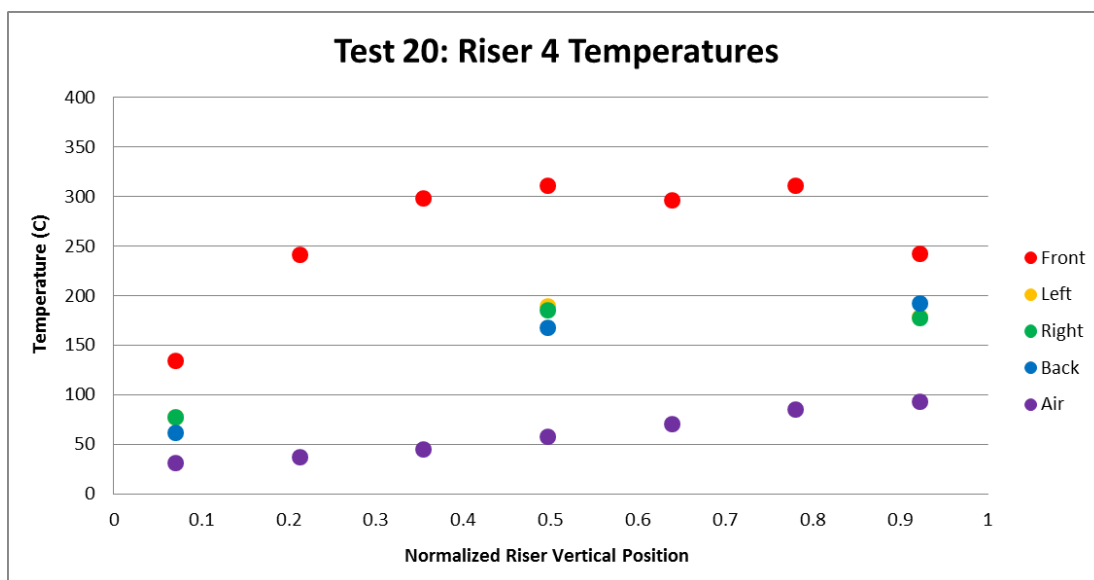
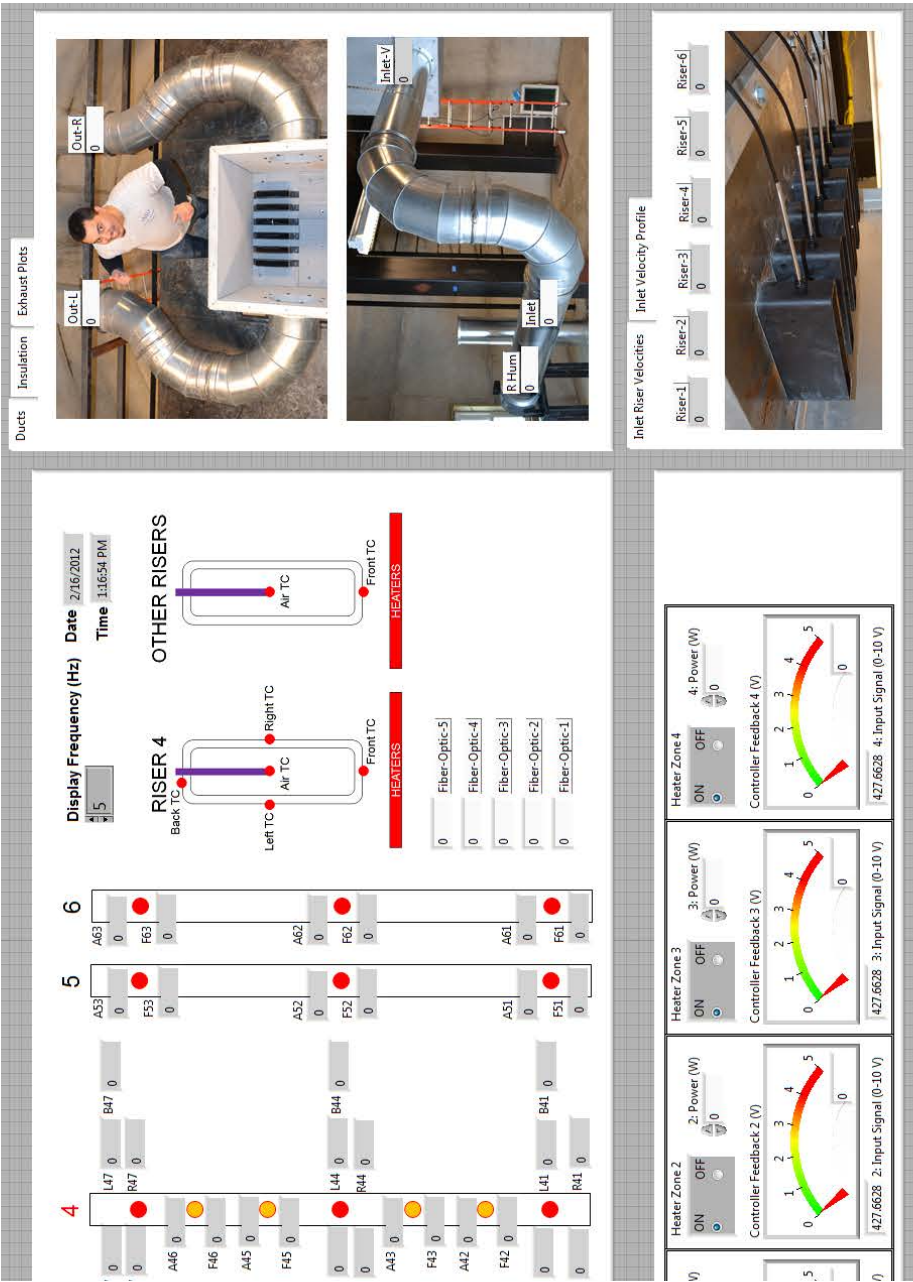


Figure 158 - Riser 4 temperatures for Test 20 (Uncertainty:  $\pm 2.2^{\circ}\text{C}$  for Front, Others  $\pm 0.7^{\circ}\text{C}$ ).

# Appendix I: LabVIEW Screen Shot



## Appendix J: Operational Manual

The following procedure was used to operate the LabVIEW program developed for the experiment. University of Wisconsin-Madison lab safety policies should be followed at all times. Extreme care should be taken when working in the quarter-scale air cooled RCCS facility at UW-Madison. The following hazards need to be considered in the facility: electrical hazards, fire hazards, and falling hazards.



- 1) Ensure that all electrical switches are turned off. Perform a walk-through of the silo facility and inspect all wiring and instrumentation. Add or remove the inlet duct fan depending if the test to be run is forced flow or natural circulation.
- 2) Open the LabVIEW program at the computer inside the Stoughton facility. The title of the program is Air-RCCS-Rio-RT.
- 3) Before running the program, click on the “DAQ” tab and type in the name for the data file. Set the frequency at which data will be recorded. It is suggested to record a sample every minute.
- 4) Start the program and inspect all temperature displays. All of the temperatures should read close to one another and be at ambient temperature.
- 5) Pull out the red safety switch on the control box containing the controllers and the data acquisition system on the second floor of the facility (Reference: Ground floor is considered the 1<sup>st</sup> floor). Turn on the 240V AC power inside the silo and exercise extreme caution. No one should enter the facility while it is power is active.
- 6) If the fan is being used, click on the “Fan” tab and enter a voltage from 0 to 10 V to control the fan. It is suggested to run the fan at 5V to run at 50% power.
- 7) To control the heater zones, click on the “Heaters” tab. There are four sets of controls for each of the four heater zones. The dial button on the top left of the control should be turned on during the duration of the test for all heater zones. There is a “Power (W)” input where the electrical power provided to heater zone via the controller can be changed. The control of the heaters is manual and there are no automated ramp-up or ramp-down features. The suggested interval rate at which power is increased or decreased

is 500 W (0.5 kW) every ten minutes. Ramping at faster intervals could damage the heater zones. The power inputs should be entered as Watts.

- 8) Once the desired power level is reached for all heating zones, a time interval needs to be established to allow the test to reach steady-state conditions and record experimental data. The time interval varied from six to ten hours depending on the power levels being used.
- 9) After recording sufficient data at steady-state, click on the “DAQ” tab and click on the only button available to stop data acquisition.
- 10) Commence the ramp-down by lowering the power input similarly as described in Step 7. In order to aid cooling the experiment, the inlet fan may be used for a natural circulation test (refer to Step 6).
- 11) After the ramp-down has been completed, click on the “Fan” tab and select the radio button “Off” or manually lower the voltage input to the fan. Turn off the 240V AC power to the facility and press in the red safety switch on the control box containing the controllers and the data acquisition system on the second floor of the facility (Reference: Ground floor is considered the 1<sup>st</sup> floor).

**Thermal-Hydraulic Analysis of an Experimental  
Reactor Cavity Cooling System with Air  
NEUP Final Report Part II: Tests and Modeling**

---

**PART I: Experiments**

**M. Corradini (UW PI), M.Anderson, M.Muci**  
Department of Engineering Physics, UW-Madison  
[Corradini@engr.wisc.edu](mailto:Corradini@engr.wisc.edu)

**PART II: Separate Effects Tests and Modeling**

**Y.Hassan\*, A.Dominguez\*, A.Tokuhiro\*\*, K.Hamman\*\***

\*Texas A&M University, \*\*University of Idaho

October 15, 2014

## **Abstract**

Computational fluid dynamics (CFD) scoping studies of the University of Wisconsin ¼-scale air reactor cavity cooling system were performed using STAR-CCM+ commercial CFD software. An initial CFD model of the outlet plenum was developed to explore the fluid behavior in the upper plenum, followed by an ‘integrated model’ of the three major components: inlet plenum, heated ducts, and outlet plenum. The computational overhead requirements of the integrated model, coupled with simulation convergence problems and availability of experimental data prompted the abandoning of the integrated model in favor of modeling one major component and sub-component, specifically the inlet plenum and heated duct #4. As part of this final analysis, CFD results were compared to experimental data using a calibration process, in which the duct wall heat flux boundary conditions were changed until the duct core flow CFD temperature profile approximated the experimental data. The results of this study identified optimal CFD simulation settings and the need for additional experimental data in order to evaluate the capabilities and limitations of a predictive simulation of the air reactor cavity cooling system.

## **Table of Contents**

A. INTRODUCTION.....	4
B. LITERATURE REVIEW .....	7
C. COMPUTATIONAL TOOLS.....	8
CFD Software .....	8
Hardware .....	9
D. CFD SCOPING STUDIES.....	9
Outlet Plenum Analysis (Scoping Study #1) .....	12
Symmetric Integrated Model (Scoping Study #2) .....	15
Full Integrated Model (Scoping Study #3).....	16
Inlet Plenum Analysis (Scoping Study #4) .....	16
Symmetric Heated Duct #4 Analysis (Scoping Study #5) .....	17
E. VERIFICATION AND VALIDATION.....	20
F. CONCLUSIONS AND RECOMMENDATIONS .....	20
G. REFERENCES .....	22
H. APPENDICES.....	24
Appendix A: Mesh Settings and Metrics .....	24
Appendix B: Simulation Settings and Boundary Conditions.....	25

## A. INTRODUCTION

The air reactor cavity cooling system (RCCS) is a safety related decay heat removal passive cooling system undergoing research and development in support of the new generation nuclear power plants, specifically the very high temperature gas reactor. The RCCS acts as a heat removal medium during normal operating conditions to maintain appropriate temperatures for the reactor cavity concrete, therefore; it is always available to remove decay heat during accident conditions [DOE 1992].

University of Wisconsin (UW) designed, built, and conducted initial testing of a  $\frac{1}{4}$ -scale air RCCS. The UW design was based on the  $\frac{1}{2}$ -scale Argonne National Laboratory Natural Convection Shutdown Heat Removal Test Facility (NSTF), which was based on the General Atomics (GA) RCCS conceptual design [Lomperski et al. 2010, Lomperski et al. 2011]. The UW experimental facility represents a 9.5 degree sector of the GA conceptual design. It includes three major components: inlet plenum, six riser ducts, and an outlet plenum [Muci 2014b].

The UW facility is capable of operating in either forced circulation or natural circulation. In forced circulation, a variable speed fan provides the motive force to move air into the inlet plenum where mixing of the air occurs prior to entering the riser ducts. Upon entering the risers, the air is heated by a bank of 32 heaters capable of generating a power of 40 kW. The heaters, located within the heated cavity, cover approximately 80% of the height of the ducts. The purpose of the heaters is to simulate the radiative and convective heat transfer from the reactor to the ducts. The air flow enters the outlet plenum where mixing occurs before the hot air exits the outlet plenum through two exhaust pipes; the hot air is discharged to the atmosphere via two chimneys [Muci 2014b]. The CFD geometry of the air RCCS is shown in Figure 1.

One of the most popular turbulence models used for the analysis of a wide variety of industrial problems is the K-Epsilon ( $k-\epsilon$ ) turbulence model [Pope 2001, Wilcox 2000, CD-adapco 2013]. The turbulence model consists of two transport equations: turbulent kinetic energy ( $k$ ) and turbulent dissipation rate ( $\epsilon$ ). Therefore, a 3-D simulation requires that a total of seven transport equations (mass, momentum, energy, and turbulence) are solved by the

commercial CFD software. Noteworthy is that a turbulent kinetic energy and turbulent dissipation rate can be related to turbulent intensity ( $I$ ) using Equation (1) through Equation (3), where  $L$  represents length scale,  $D_h$  represents hydraulic diameter,  $v$  represents local velocity, and  $C_\mu$  equals 0.09 [Cd-adapco 2009]. Turbulence intensity can be derived from experimentally measured data, so turbulent intensity along with an estimated turbulence length scale, are used as boundary conditions for the two transport equations. If turbulence intensity ( $I$ ) experimental data is not available, typically thumb rules are used. For example one thumb rule states: “[For] Flow in not-so-complex devices like large pipes, ventilation flows etc. or low speed flows (low Reynolds number). Typically the turbulence intensity is between 1% and 5%.” [CD-adapco 2014]

$$k \approx \frac{3}{2}(Iv)^2 \quad \text{Equation (1)}$$

$$\varepsilon \approx \frac{C_\mu^{3/4} k^{3/2}}{L} \quad \text{Equation (2)}$$

$$L \approx \frac{D_h}{10} \quad \text{Equation (3)}$$

STAR-CCM+ provides users with two options for a numerical solver: segregated and coupled. The segregated solver solves the transport equations in an ‘uncoupled’ fashion. For example, using a SIMPLE-type algorithm, each transport equation is solved independently; although, the linking of the momentum and mass continuity transport equations is accomplished using a predictor-corrector approach. The coupled solver solves the mass and momentum transport equations in a ‘coupled’ fashion. Each solver has advantages and disadvantages. For example, the coupled solver requires more memory; but it produces more accurate results for compressible flows and high Rayleigh number natural convection flows [STAR-CCM+ 2013].

One of the most difficult and time consuming steps of the modeling and simulation process is verifying that the mathematical equations are solved right (e.g., correct syntax, mesh

refinement analyses), comparing the numerical results with experimental data and/or DNS results, establishing the relative error of the results, and finally demonstrating that an appropriate level of software quality (e.g., version control, code documentation) was maintained. Typically referred to as 'Verification, Validation, and Uncertainty Quantification' (VV&UQ) and Code Quality Assurance (QA), these steps are mandatory for safety-related calculations (i.e., nuclear reactor safety); yet, it is important that non-safety-related calculations (e.g., fundamental research) should have some degree of rigor established - on par with the risk associated with the use of incorrect results [Oberkampf and Roy 2010]. This short-duration study was focused on CFD scoping studies. Consequently, a formal V&V methodology was not followed, although several components of a typical V&V methodology such as residual convergence, energy conservation, and comparison of numerical results with experimental data were employed.

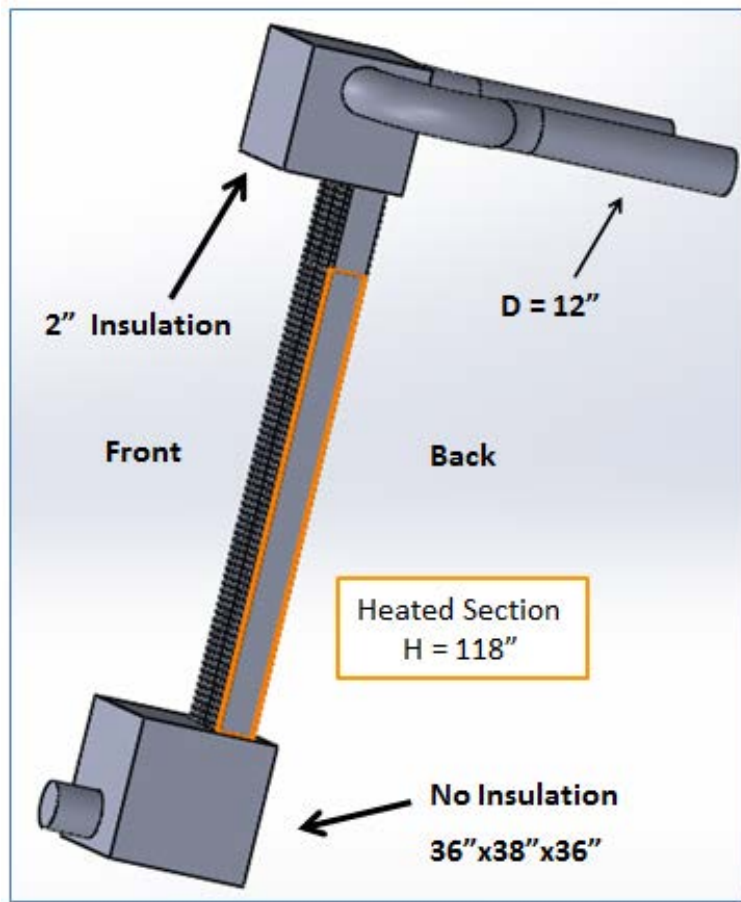


Figure 1 Air RCCS CFD Geometry (Analyses #4 and #5)

## **B. LITERATURE REVIEW**

Several CFD simulations of the RCCS and scaled models of the RCCS have been performed, primarily by Argonne National Laboratory (ANL) where the Natural Convection Shutdown Heat Removal Test Facility (NSTF) is located. One of the purposes of this facility is to generate experimental data for code validation.

In 2005, ANL published a CFD analysis report characterizing the applicability of the NSTF for the simulation of the VHTR RCCS. Two CFD simulations were performed to prove that the NSTF, originally built to provide experimental support for the design and analysis of the PRISM reactor vessel auxiliary cooling system, can be used to produce thermal-hydraulic flows that would replicate those of the full-scale RCCS. Few details were provided about the CFD simulation parameters (e.g., mesh generation information, boundary layer resolution, and numerical solver type), other than noting that the commercial CFD software STAR-CD and the standard high-Re K-Epsilon model were used [Tzanos 2005].

In 2010, ANL published a second report which focused on the analysis of the GA air RCCS design in support of scaling studies and instrumentation support [Lomperski et al. 2010]. The report includes CFD studies of the full-scale GA RCCS and the NSTF ‘experiment-scale’ simplified RCCS model. This study concluded that the NSTF design reproduces the major flow features of the anticipated RCCS design. STAR-CCM+ commercial CFD software was used for the studies.

In 2011, a follow-on to the second ANL report was published [Lomperski et al. 2011]. The primary objective of this study (and supporting CFD analyses) was the evaluation of experimental scaling relationships, which were to be used in modifying the existing NSTF into a scaled ‘experiment model’ of the GA RCCS. “In summary, the scaling evaluation updated the basis that the air-cooled RCCS can be simulated at the ANL NSTF facility at a prototypic scale in the lateral direction and about half scale in the vertical direction.” Additional CFD studies, including sensitivity analyses and analyses to support instrument placement, were performed. Several CFD design simulations were performed as part of this study; four promising designs were presented. CFD simulation settings were similar to those reported in the 2010 study; additionally, insight into the mesh settings was provided. For example, information on mesh refinement studies suggest that 3 prism layers were used with the two-layer all  $y^+$  K-Epsilon

turbulence model; more than 15 million computational elements with local refinement in the riser ducts were used.

In 2012 a conference paper was published summarizing the results of simulating NSTF natural circulation operation, using the commercial CFD code STAR-CCM+ [Dave et al. 2012]. In 2013, a follow-up conference paper to the 2012 paper was published identifying difficulties in obtaining good convergence [Hu and Pointer 2013]. Improved convergence was obtained by shifting from the segregated solver, which is a SIMPLE-type algorithm, to the coupled solver. Additionally, the mesh was refined resulting in greater than 20 million elements. Furthermore, based on a review of the figures presented in the paper, it appears that the number of prism layers was increased from three to five layers.

In 2013, a third conference paper was published summarizing the results of simulating the ‘experiment-1/4 scale’ RCCS using the commercial CFD code FLUENT [Lisowski et al. 2013]. The CFD simulation was used to assist in determining the placement of six riser ducts within the heated cavity in addition to providing confidence that adequate mixing will take place in the outlet plenum. Due to space limitations, a 6 riser duct heated assembly was constructed instead of a twelve riser duct assembly, which would have been consistent with the ANL ‘experiment-1/2 scale’ RCCS. The symmetry model consisted of 2.2 million tetrahedral computational elements. The following simulation settings were used: SIMPLE pressure-velocity coupling scheme, SST k- $\epsilon$  turbulence model<sup>1</sup>, body force weighted pressure method, and 2<sup>nd</sup> order spatial discretization.

## **C. COMPUTATIONAL TOOLS**

### **CFD Software**

The commercial CFD software STAR-CCM+ was used to generate the three-dimensional RANS velocity and temperature fields for this study [CD-adapco 2013]. STAR-CCM+ uses a cell-centered finite volume discretization technique and an unstructured mesh generator. Two generalized solvers are available, coupled and segregated. SolidWorks was used to generate the solid model geometry, which was imported into STAR-CCM+ [Dassault Systemes 2013].

---

<sup>1</sup> Due to a type-o in the paper, the most likely turbulence model used is SST k- $\omega$ .

## Hardware

A ZaReason 'Fortis Extreme 2' workstation with an AMD FX-8350 8-core processor and Linux Ubuntu 12.04 LTS operating system (Linux) was used to develop the CFD models. Small models were developed and run on this Linux box, but larger CFD models were run on the University of Idaho Big-STEM (HP DL 980G7) high performance computer. Big-STEM is comprised of 80 cores of the Intel Xeon E5-2680 2.40 Ghz processors and 4 Tb of RAM with a Red-Hat 6.5 operating system (Linux); 64 processors were allocated for this work.

## D. CFD SCOPING STUDIES

The preliminary design phase of the University of Wisconsin (UW) RCCS experimental facility used the commercial CFD code FLUENT to guide the design. During the final year of the project, several RCCS CFD scoping studies using the commercial code STAR-CCM+ were performed by University of Idaho in an effort to evaluate optimal mesh and simulation settings; comparison of the experimental data with the CFD results was performed as well. The realizable two-layer K-epsilon ( $k-\epsilon$ ) turbulence model in conjunction with the all  $y^+$  wall treatment was used for all simulations. A summary of the key mesh settings and simulation parameters are presented in Table 1 and Table 2. Hamman and Tokuhito provide additional details related to the scoping studies in project summary presentation [Hamman and Tokuhito 2014].

The information presented in this report briefly describes the scoping studies, which included five CFD analyses. One of the goals of the study was to focus on resolving the boundary layer in order to obtain as accurate a solution as possible, especially in the heated duct region. Initially the scoping studies, primarily Analysis #2, were guided by the FLUENT study performed by Lisowski et al. (2013), SolidWorks geometry provided by Muci (2013), and monthly project progress reports; as much as practical, simulation settings similar to those used in the FLUENT study were selected for the STAR-CCM+ simulations. For example, the

Lisowski study used the FLUENT's SIMPLE solver, while the STAR-CCM+ segregated solver was employed.<sup>2</sup>

Based on the importance of resolving the boundary layer, 10 prism layers were used for some of the initial analyses. The number of prism layers was increased in later analyses; the number of prism layers ranged from 20 to 21. Noteworthy is that STAR-CCM+ user documentation suggests that at least 15 cells should be used to resolve the boundary layer for heat transfer simulations, and the  $y^+$  values should remain less than 3 [CD-adapco 2013]. The general requirement in the FLUENT user guide is to ensure that at least 10 cells are used to resolve the shear layer (viscous boundary layer) [ANSYS 2012].<sup>3</sup>

Due to the limited computational resources initially available (i.e., 8-core Linux box), early simulations used only 10 prism layers; Table 3 presents computational information. As more computational resources became available (i.e., Big-STEM), the number of prism layers was increased. Consequently (and unexpectedly), residual convergence problems arose. Noteworthy is that accuracy problems, associated with energy conservation in the heat transfer simulations, were present; but they went unidentified for a period of time.

An additional literature search, conducted late in the project, revealed that analysts at Argonne National Laboratory identified a problem associated with energy conservation in previous simulations that utilized the segregated solver; but, they did not experience residual convergence problems [Hu and Pointer 2013]. The energy conservation problems were resolved by utilizing the coupled solver.

Based on the information learned from the Hu and Pointer study, Analysis #5 of this study utilized the coupled solver, which resolved accuracy related to energy conservation; but the residual convergence problems remained (e.g., plenums and Duct #4). Eventually, it was determined, through additional numerical experimentation that running the transient (instead of the steady-state) solver improved residual convergence for the inlet and outlet plenum simulations. Residual convergence issues associated with heated Duct #4 were resolved by

---

<sup>2</sup> The STAR-CCM+ segregated solver is based on the SIMPLE algorithm [CD-adapco 2013].

<sup>3</sup> "Generally speaking, it is more important to ensure that the boundary layer is covered with sufficient cells, then to achieve a certain  $y^+$  criterion. However, for simulations with high accuracy demands on the wall boundary layer (especially for heat transfer predictions) near wall meshes with  $y^+ \sim 1$  are recommended." [ANSYS 2012]

using a ramping function to gradually increase boundary conditions (velocity, heat flux, and turbulence parameters) to their desired values; ramping in conjunction with the steady-state coupled solver resulted in satisfactory convergence and energy conservation performance.

Table 1 – Key Mesh Parameters

	Component	Mesh Type	Boundary Layer Thickness	No. Prism Layers	No. Elements	Wall Y+ (heated)	Wall Y+ (other)	Wall Y+ (duct walls)
Analysis #1 (high velocity)	Outlet Plenum	Prism/Polyhedral	2.5 mm	10	690,920	N/A	0.31	5.00
	Outlet Plenum (Sym)	Prism/Polyhedral	2.5 mm	10	366,428	N/A	0.29	4.95
Analysis #1 (low velocity)	Outlet Plenum	Prism/Polyhedral	2.5 mm	10	690,920	N/A	0.06	1.00
	Outlet Plenum (Sym)	Prism/Polyhedral	2.5 mm	10	366,428	N/A	0.06	0.92
Analysis #2	Full RCCS (Sym)	Prism/Polyhedral	2.5 mm/0.35 mm	10	3,853,442	0.03	0.21	0.67
Analysis #3	Full RCCS	Prism/Polyhedral	3.0 mm	20	9,004,257	0.06	0.09	19.80
Analysis #4	Inlet Plenum	Prism/Polyhedral	3.5 mm	21	2,740,704	N/A	0.06	9.75
Analysis #5	Inlet Plenum	Prism/Polyhedral	3.5 mm	21	2,740,704	N/A	0.03	46.70
	Duct #4 (Sym)	Prism/Trimmer	3.0 mm	20	986,624	0.07	N/A	N/A

Table 2 – Key Simulation Parameters

	Component	Temporal Analysis Type	Numerical Solver	Inlet Boundary Conditions					
				Velocity (m/s)	Tke (J/kg)	Tdr ( $m^2/s^3$ )	Turb Intensity	Turb Length Scale	Temperature (C)
Analysis #1 (High)	Outlet Plenum	Steady	Segregated	See Table	See Table	See Table	N/A	N/A	See Table
	Outlet Plenum (Sym)	Steady	Segregated	See Table	See Table	See Table	N/A	N/A	See Table
Analysis #1 (Low)	Outlet Plenum	Steady	Segregated	See Table	See Table	See Table	N/A	N/A	See Table
	Outlet Plenum (Sym)	Steady	Segregated	See Table	See Table	See Table	N/A	N/A	See Table
Analysis #2	Full RCCS (Sym)	Steady	Segregated	(pressure = 0)	6.00E-04	7.92E-05	N/A	N/A	25.0
Analysis #3	Full RCCS	Transient	Segregated	5	3.75E-03	1.24E-03	N/A	N/A	15.9
Analysis #4	Inlet Plenum	Steady	Segregated	5	3.80E-03	1.00E-03	N/A	N/A	16.0
Analysis #5	Inlet Plenum	Transient	Coupled	4.788	N/A	N/A	2%	0.03048	17.2
	Duct #4 (Sym)	Steady	Coupled	0.52, -0.6974, 5.41	5.4964	1.08E+02	N/A	N/A	18.4

Table 3 – Computational Overhead Data

	Component	Computational Time (sec)	Computational Time (hrs)	Processors	Simulation Time (sec)
Analysis #1 (High)	Outlet Plenum	12,302	3.4	8 / Aries	N/A
	Outlet Plenum (Sym)	6,510	1.8	8 / Aries	N/A
Analysis #1 (Low)	Outlet Plenum	12,442	3.5	8 / Aries	N/A
	Outlet Plenum (Sym)	6,748	1.9	8 / Aries	N/A
Analysis #2	Full RCCS (Sym)	181,043	50.3	8 / Aries	N/A
Analysis #3	Full RCCS	1,076,906	299.1	64 / Big-STEM	1.86
Analysis #4	Inlet Plenum	7,294	2.0	24 / Big-STEM	N/A
Analysis #5	Inlet Plenum	273,095	75.9	48 / Big-STEM	1.00
	Duct #4 (Sym)	297,448	82.6	48 / Big-STEM	N/A

## Outlet Plenum Analysis (Scoping Study #1)

Two models, a full model and a symmetric model, were developed as part of Scoping Study #1 (outlet plenum study). Figures 2 through 5 present the full model geometry and results; the left exhaust pipe purposely is hidden in Figure 2. Due to the brevity of this report, the symmetric model results are not presented; detailed results can be found in the project summary presentation by Hamman and Tokuhiko (2014).

The initial scoping studies focused on CFD simulations of the outlet plenum, at inlet plenum velocities of approximately 0.5 m/s and 5.0 m/s; Table 4 presents the boundary conditions used for this analysis. As the construction of the UW RCCS progressed, it was realized that the RCCS experiment would not be instrumented to collect experimental data to establish CFD boundary conditions at the inlets of the 'outlet plenum.' Therefore, efforts were directed to modeling the majority of the RCCS components (e.g., lower plenum, heated ducts, and outlet plenum) since sufficient experimental data at the inlet of the 'inlet plenum' was expected to be available.

Similar to the studies by Argonne National Laboratory, the results of this analysis indicate that large vortex structures develop in the outlet plenum. Also, complex flow structures develop near the bottom wall of the outlet plenum. These complex flow structures are presented in Figures 4 and 5. Noteworthy is that the penetration of the heated ducts into the outlet plenum contribute to the complex flow patterns near the bottom of the outlet plenum. (Similar complexities were predicted in the lower plenum by follow-on CFD simulations.) Figure 3 presents the residuals for the full model; although not presented in this report, the residuals for the symmetric model decreased to less than  $1 \times 10^{-2}$ . In short, depending on whether the geometry is full or symmetric, residual convergence problems may be present. Although it is not conclusive, the convergence problem in Figure 3 may be the result of imposing two outlet pressure boundary conditions (one for each exhaust) on the full model; the symmetric model only requires one outlet pressure boundary condition.

Table - 4 Outlet Plenum Boundary Conditions

Duct #	Low Velocity Simulation			High Velocity Simulation			Temperature	
	$v$ (m/s)	$k$ (J/kg)	$\epsilon$ (J/kg-s)	$v$ (m/s)	$k$ (J/kg)	$\epsilon$ (J/kg-s)	T (F)	T ('C)
1	0.40	2.40E-05	2.56E-06	4.0	2.40E-03	2.56E-03	150.0	65.6
2	0.45	3.04E-05	3.65E-06	4.5	3.04E-03	3.65E-03	160.0	71.1
3	0.50	3.75E-05	5.01E-06	5.0	3.75E-03	5.01E-03	170.0	76.7
4	0.50	3.75E-05	5.01E-06	5.0	3.75E-03	5.01E-03	170.0	76.7
5	0.45	3.04E-05	3.65E-06	4.5	3.04E-03	3.65E-03	160.0	71.1
6	0.40	2.40E-05	2.56E-06	4.0	2.40E-03	2.56E-03	150.0	65.6

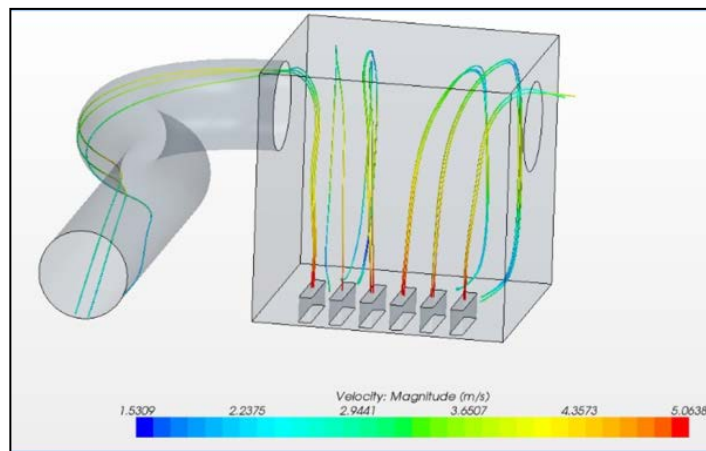


Figure 2 CFD Analysis #1 – Streamlines

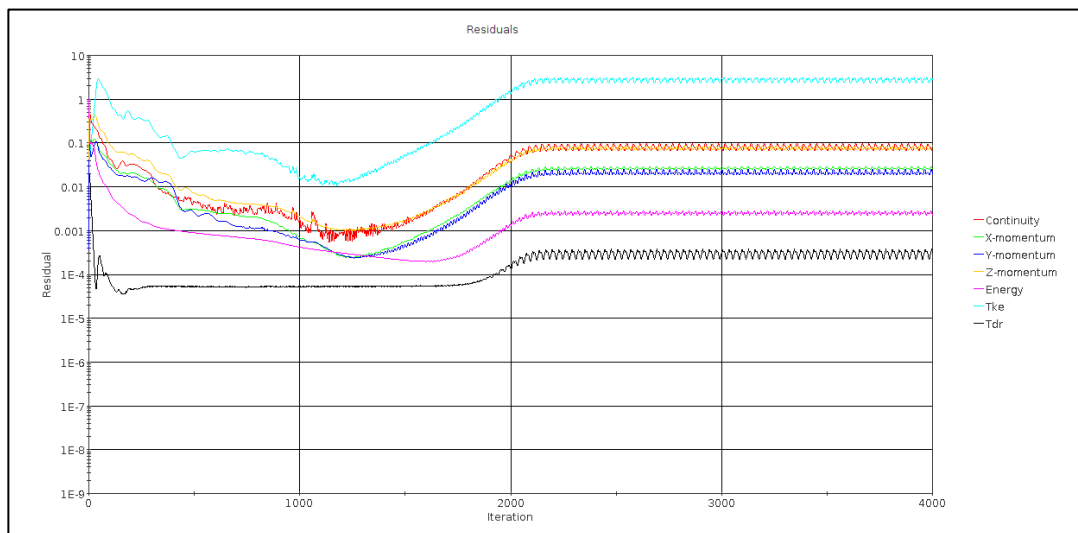


Figure 3 CFD Analysis #1 – Residuals (Full Model)

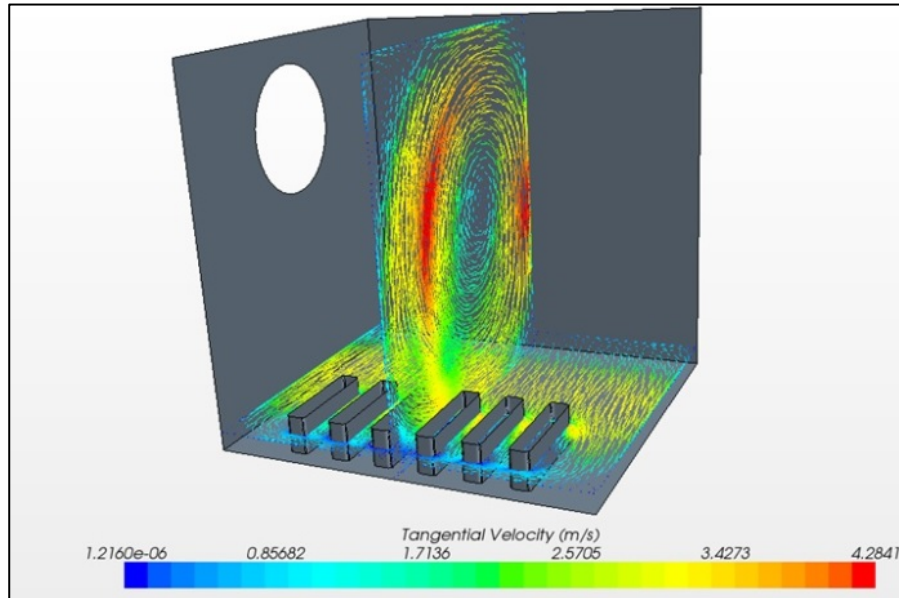


Figure 4 CFD Analysis #1 – Vector Velocity Plot

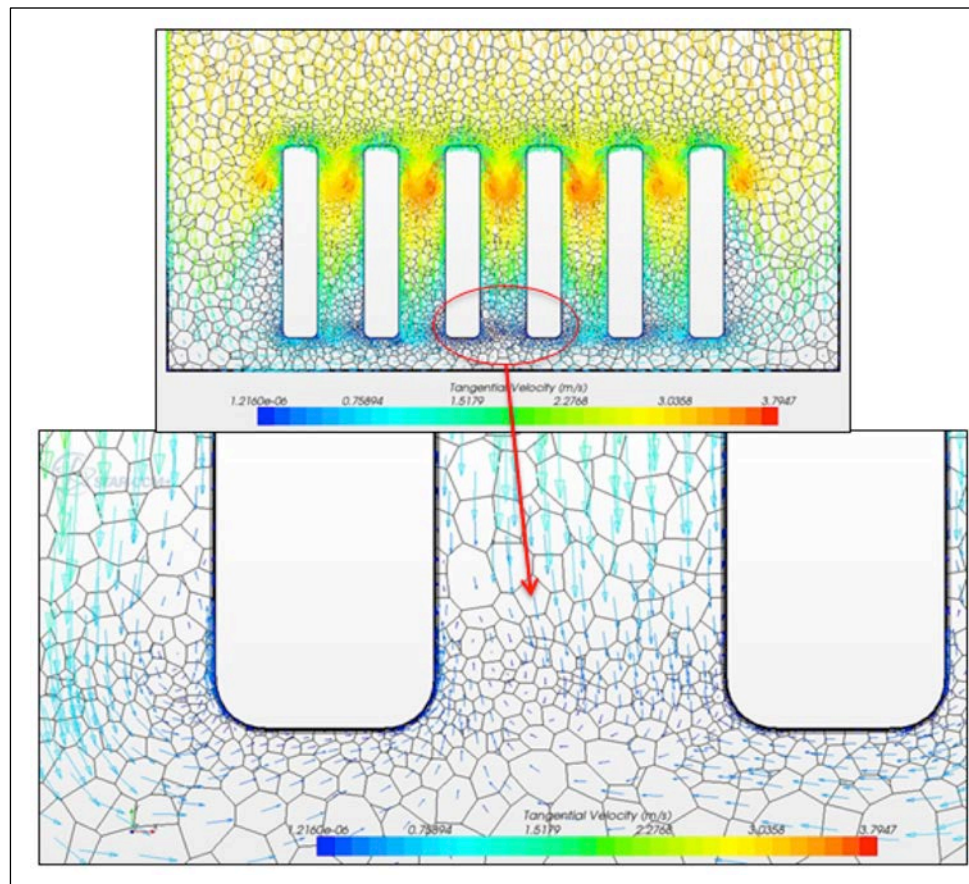


Figure 5 CFD Analysis #1 – 1.7" above bottom wall

## Symmetric Integrated Model (Scoping Study #2)

A 3-D simulation, using a symmetric geometry model of the air RCCS was performed in an effort to reproduce the results of Lisowski et al. (2013); the commercial CFD code FLUENT was used for that study. The CFD results are presented in Figure 6. The simulation was performed in three steps. First, adiabatic flow conditions were established using an inlet velocity of 1 m/s, followed by the application of a cosine shaped heat flux with a peak flux of  $1.68 \text{ kW/m}^2$ ; a total power of 9.91 kW was applied. Finally, natural circulation boundary conditions were established, and the simulation was run for 7000 iterations, where the energy residual flattened and all other residuals were reduced to less than  $1 \times 10^{-4}$ . Consistent with the results presented by Lisowski et al. (2013), a 2.36 m/s outlet velocity at the duct was predicted by STAR-CCM+. A boundary layer thickness of 0.35 mm was used for the heated duct walls; the remaining walls were 2.5 mm. The simulation time was 33 hours on the 8 core workstation.

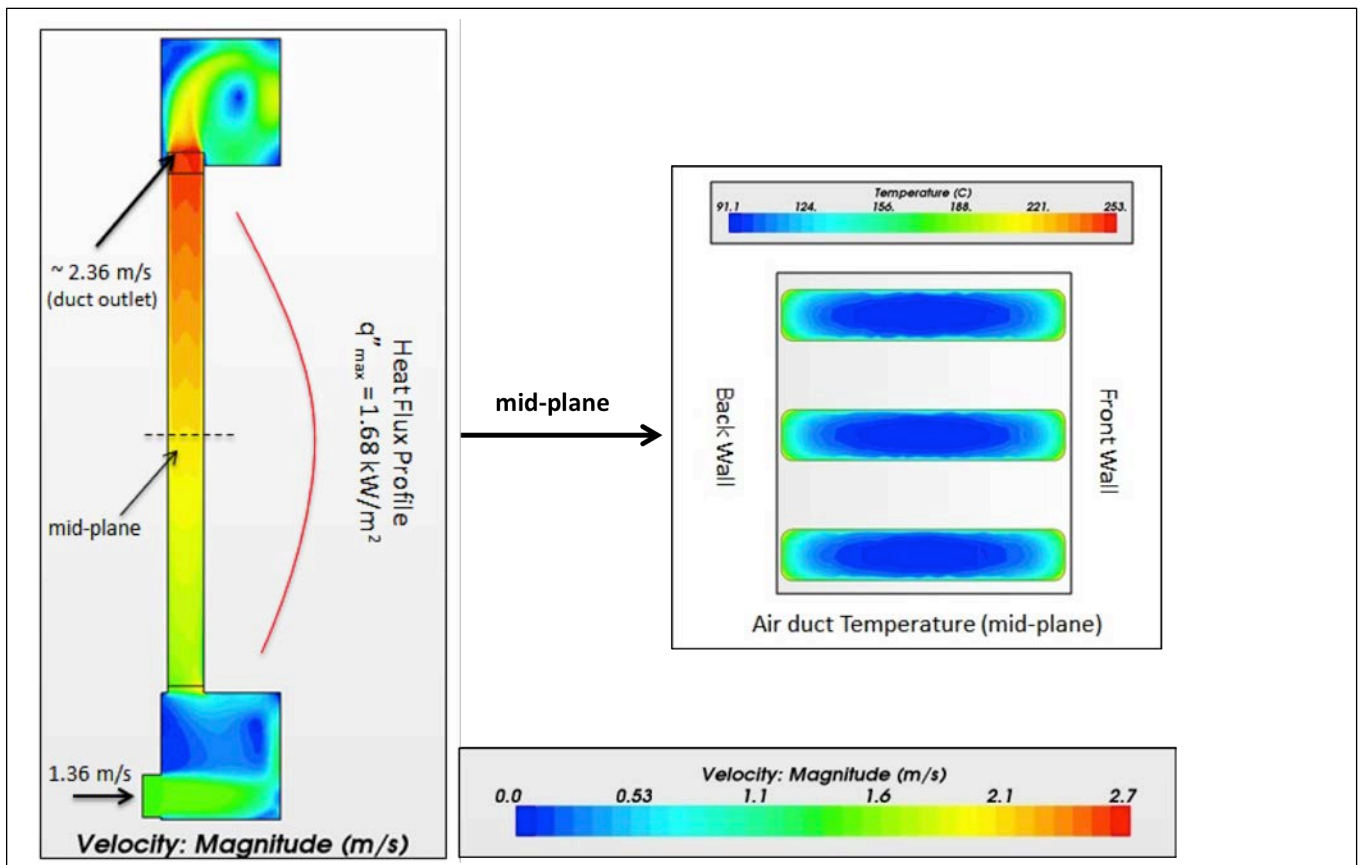


Figure 6 CFD Analysis #2 - Contour Plots

### Full Integrated Model (Scoping Study #3)

A third scoping study was performed as part of this study. The purpose of this study was to evaluate the challenges associated with simulating a full 3-D model. Additionally, the intent was to compare forced circulation simulation results with experimental data prior to moving on to a more advanced natural circulation simulation.

Although, a symmetric model reduces the computational overhead; a full model simulation is important in the understanding of abnormal operating conditions (e.g., plugged duct, corrosion buildup in ducts). Unfortunately, the computational overhead coupled with problems associated with residual convergence and energy conservation resulted in abandoning this simulation. Noteworthy is that shifting from the steady-state segregated solver to the transient segregated solver improved residual convergence; but inaccuracies in energy conservation remained. Unfortunately, a transient simulation is computationally expensive. For example, the simulation run time was 299 hours on 64 processors.

### Inlet Plenum Analysis (Scoping Study #4)

A fourth scoping study was performed as part of this study. The purpose of this analysis was to provide “qualitative” vector-velocity data of the inlet plenum to assist experimentalists with evaluating the uncertainty of heated duct velocity transducers [Muci 2014b]. While preparing for this study, an error was found in the CFD geometry; therefore, the dimensions of the CFD model were checked. A comparison of the CFD geometry with the “nominal” as-built experimental geometry revealed three errors in the CFD geometry. Specifically, the location of the inlet pipe to the inlet plenum was incorrect; the penetration depth into the inlet plenum was incorrect, and inlet plenum dimensions were increased since unlike the outlet plenum, the inlet plenum did not have any insulation. The CFD geometry was updated (Figure 1), and additional solver testing was performed. Figure 7 presents a vector-velocity plot showing the complex flow structures. Residual convergence problems were observed. Additional results from this analysis are presented in a project summary by Hamman and Tokuhiko [2014].

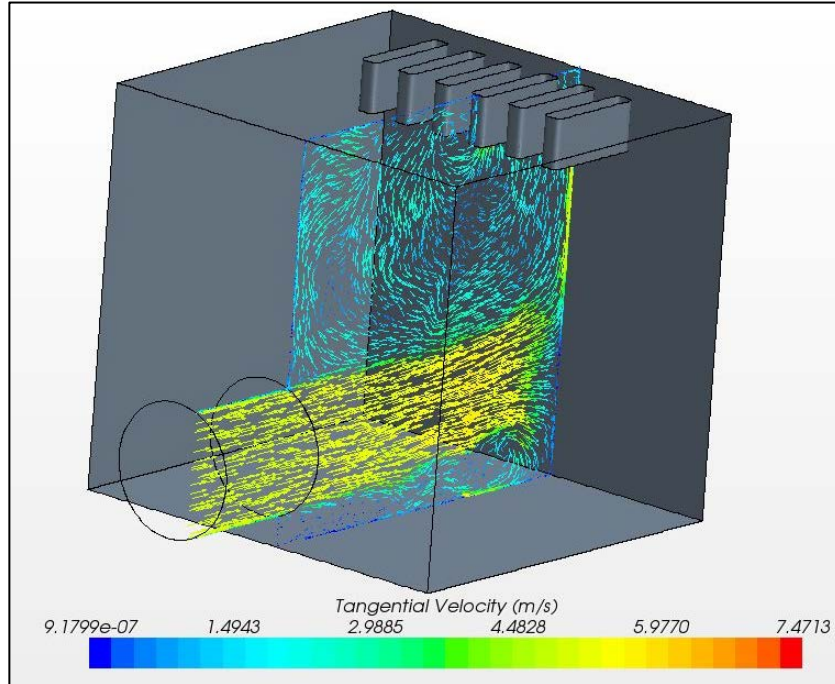


Figure 7 CFD Analysis #4 - Vector Velocity Plot (Duct #4 Plane)

#### Symmetric Heated Duct #4 Analysis (Scoping Study #5)

A fifth scoping study was performed as part of this study. The purpose of this analysis was to compare the CFD results with experimental data [Muci 2014a]. Based on the information learned in previous analyses, it was decided to abandon the full 3-D integrated modeling approach and independently model the inlet plenum and heated duct #4. In preparation for this final scoping study, an additional literature survey was performed. Two conference papers and several ANL technical papers were located, which provided insight into the problem size (i.e. mesh size), CFD solver settings, and convergence problems experienced by other analysts [Tzanos 2005, Lomperski et al. 2010, Lomperski et al. 2011, Dave et al. 2012, Hu and Pointer 2013]. A review of the additional literature suggests that three to five prism layers were used, yet it is not clear from the reports why the number prism layers were limited to five.

The boundary conditions used at the inlet to the heated duct were obtained from the results of a simulation performed of the inlet plenum. This was necessary since insufficient

experimental data was collected at the duct inlets in order to establish CFD inlet boundary conditions. For example, turbulence intensity and temperature were not measured. Additionally, the accuracy of the velocity measurements at the duct inlets was called into question. For example, the 'qualitative' CFD analysis (i.e., Analysis #4) showed that the velocity vectors were not normal to the velocity transducers [Muci 2014b].

The CFD settings for the lower plenum were similar to the settings used in previous simulations except that the transient coupled solver was used; these solver settings resulted in improved residual convergence for the lower plenum. An inlet velocity of 4.8 m/s and a temperature of 17.2 C were imposed on the inlet along with an assumed turbulence intensity of 2% and a turbulence length scale of one-tenth the inlet pipe diameter (0.03048 m); outflow boundary conditions were imposed on all ducts [CD-adapco 2009].

Duct #4 was modeled using simulation settings similar to those used for the inlet plenum except that the steady state coupled solver was used and the mesh type was changed from a polyhedral to a hexahedral to improve mesh metric results. The steady state solver, as opposed to the transient solver, was selected because to reduce computational time. Reduced computational time was critical, especially considering that numerous calibration simulations had to be performed. The surface average outlet values of the inlet plenum simulation were imposed as inlet conditions to duct #4. The boundary conditions applied at the inlet are specified in Table 9 located in the appendix. The boundary conditions at the duct sides were determined through a calibration process where heat flux values were guessed and successive simulations were ran until the core flow temperature CFD profile approximated the experimental values. The duct temperature profile for the final simulation is presented in Figure 8 and the residuals are presented in Figure 9. Additional results are presented by Hamman and Tokuhiko (2014).

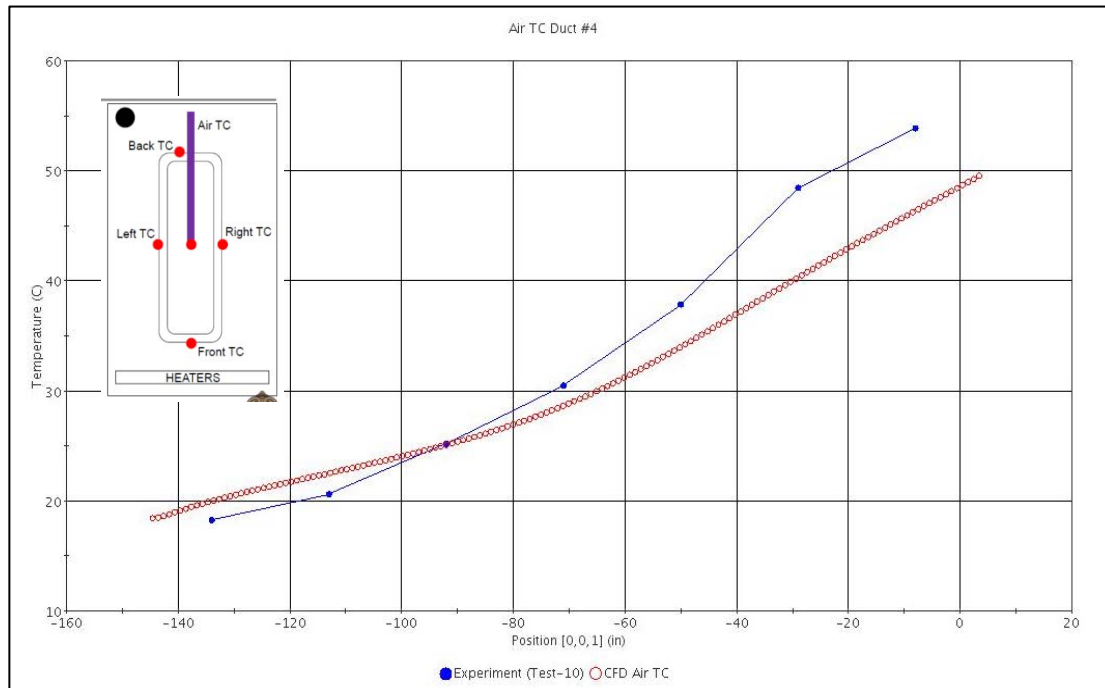


Figure 8 CFD Analysis #5 - Calibration Results (Air TC Location)

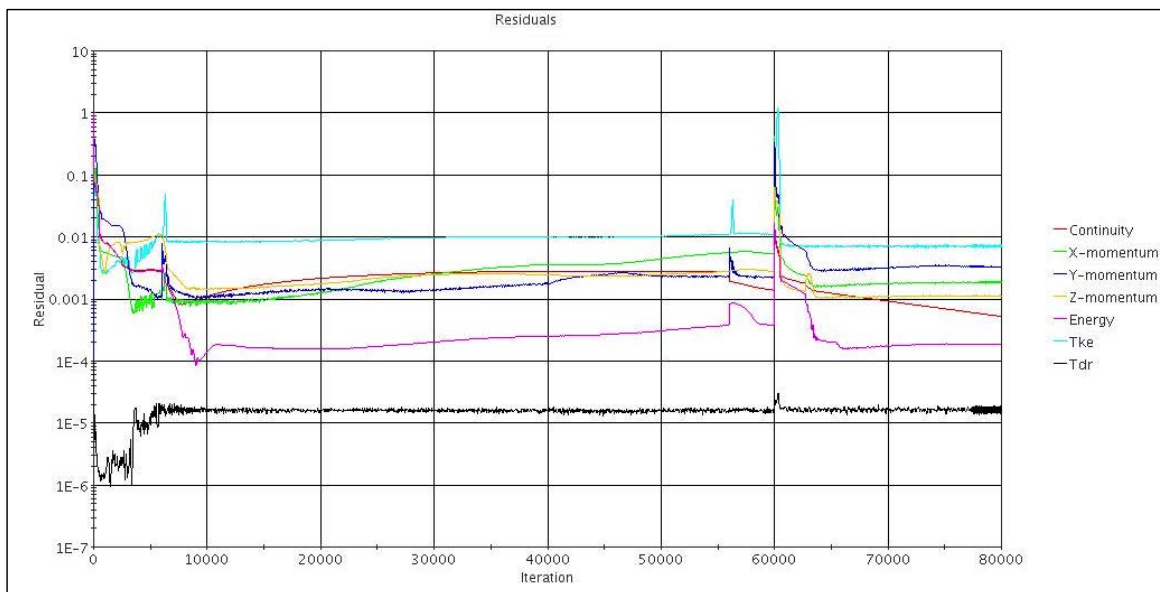


Figure 9 CFD Analysis #5 - Residuals

## **E. VERIFICATION AND VALIDATION**

Consistent with good engineering practice, the expected use of the results, and available project funds, a verification and validation methodology (V&V), for example a methodology similar to that presented by the NPARC Alliance, should be followed when comparing CFD results to experimental data. An informal V&V process was followed. This process included limited mesh refinement studies, primarily due to the complications that arose during this study (e.g., convergence problems and code calibration requirements), an iterative convergence study, and verification of consistency study (i.e., mass and energy conservation) [NPARC Alliance 2008, Oberkampf and Roy 2010].

## **F. CONCLUSIONS AND RECOMMENDATIONS**

Upon completion of this scoping study, the following is concluded:

1. CFD Modeling of the RCCS is complex.
2. The RCCS models require a significant amount of computational overhead, requiring the use of high performance computing.
3. To improve solution accuracy, especially in environments of high heat flux, sufficient prism layers should be used to resolve the velocity and thermal boundary layer.
4. The CFD model is sensitive to boundary layer resolution (i.e., number of prism layers)
5. The STAR-CCM+ ‘transient coupled’ solver should be used in models with a large number of prism layers and heat transfer present.
6. Computational overhead can be reduced by modeling the major components of the RCCS individually.

Based on the CFD scoping studies presented in this report, the following recommendations are provided in order to collect sufficient experimental information to support CFD code boundary conditions and validation:

1. The UW air RCCS experimental facility should be equipped with the appropriate instrumentation to collect turbulent data in order to compute turbulence intensity at key locations, for example upstream of the inlet plenum and at the inlets to the heated ducts.
2. The UW RCCS experimental facility should be equipped with the appropriate instrumentation in the heated duct to measure heat flux, over the length of each duct on each of the RCCS duct sides.
3. Consideration should be given to conducting a validation experiment, including storing the experimental data in a repository, so that experimental data could be available to other researchers for CFD modeling purposes.

## G. REFERENCES

ANSYS Inc., 2012. ANSYS-FLUENT Theory Guide, Release 14.5. Canonsburg, Pennsylvania.

CD-adapco, 2009. STAR-CCM+ Version 4.0x Foundation Training. New York.

CD-adapco, 2013. STAR-CCM+ User Guide, Version 8.04. New York.

CD-adapco, 2014. The Steve Portal Technical Article 3716.  
[https://cd-adapco.secure.force.com/index/Site\\_Login](https://cd-adapco.secure.force.com/index/Site_Login) (accessed 10.11.2014).

Dassault Systemes SolidWorks Corporation, 2013. SolidWorks 2013. Waltham, Massachusetts.

Dave, A., Hu, R., Manera, A., Merzari, E., and Pointer, W. D., 2012. CFD Simulation of NSTF. Transaction of American Nuclear Society, Vol. 106 pp. 1323-1326.

Department of Energy (DOE), 1992. Preliminary Safety Information Document for the Standard MHTGR, Volume 1. DOE Report HTGR-86-024 (Document # HTGR-86024 Rev. 13), September 9, 1992.

Hamman, K. D. and Tokuhiko, A., 2014. Air RCCS CFD Models Project Summary, University of Idaho presentation. October 15, 2014.

Hu, R. and Pointer W. D., 2013. CFD Analyses of Natural Circulation in the Air-Cooled Reactor Cavity Cooling System. M&C 2013, 5-9 May 2013, Sun Valley, Idaho.

Lisowski, D. D., Muci, M. A., Anderson, M. H. and Corradini, M. L., 2013. Design Considerations for a Scaled Reactor Cavity Cooling System with Air for the VHTR. 15<sup>th</sup> International Topical Meeting on Nuclear Reactor Thermal-Hydraulic NURETH-15, 12-17 May 2013, Pisa, Italy.

Lomperski, S., Pointer, W. D., Tzanos, C. P., Wei, T. Y. C., Crooks, C. M., and Rodriguez, O. A., 2010. RCCS Studies and NSTF Preparation Air-Cooled Option. Argonne National Laboratory report, ANL-GenIV-142.

Lomperski, S., Pointer, W. D., Tzanos, C. P., Wei, T. Y. C., and Krauss, A. R., 2011. Generation IV Nuclear Energy System Initiative. Air-Cooled Option RCCS Studies and NSTF Preparation. Argonne National Laboratory report, ANL-GenIV-179.

Muci, M. A., 2013. "RCCS PROJECT – CAD SOLID MODELS." E-mail communications with K.D. Hamman providing SolidWorks models for air RCCS (nominal geometry) on August 28, 2013.

Muci, M. A., 2014a. "Forced Circulation Experimental Data." E-mail communications with K.D. Hamman related to Test-10 experimental data on May 27, 2014.

Muci, M. A., 2014b. Thermal Hydraulic Analysis of an Experimental Reactor Cavity Cooling System with Air. Master Thesis, University of Wisconsin.

National Program for Applications-Oriented Research in CFD (NPARC Alliance,) 2008. Overview of CFD Verification and Validation.

[www.grc.nasa.gov/WWW/wind/valid/tutorial/overview.html](http://www.grc.nasa.gov/WWW/wind/valid/tutorial/overview.html) (accessed 7.11.2014).

Oberkampf, W.L . and Roy, C.J., 2010. Verification and Validation in Scientific Computing. Cambridge University Press, New York.

Pope, S.B., 2001. Turbulent Flows. Cambridge University Press, Cambridge.

Tzanos, C. P., 2005. CFD Analysis for the Applicability of the Natural Convection Shutdown Heat Removal Test Facility (NSTF) for the Simulation of the VHTR RCCS. Argonne National Laboratory report, ANL-GenIV-55.

Wilcox, David C., 2000. Turbulence Modeling for CFD. DCW Industries, Inc., La Cañada California.

## H. APPENDICES

### Appendix A: Mesh Settings and Metrics

Table 5 – Mesh Parameters

	Component	Mesh Type	Boundary Layer Thickness	No. Prism Layers	No. Elements	Wall Y+ (heated)	Wall Y+ (other)	Wall Y+ (duct walls)
<b>Analysis #1 (high velocity)</b>	Outlet Plenum	Prism/Polyhedral	2.5 mm	10	690,920	N/A	0.31	5.00
	Outlet Plenum (Sym)	Prism/Polyhedral	2.5 mm	10	366,428	N/A	0.29	4.95
<b>Analysis #1 (low velocity)</b>	Outlet Plenum	Prism/Polyhedral	2.5 mm	10	690,920	N/A	0.06	1.00
	Outlet Plenum (Sym)	Prism/Polyhedral	2.5 mm	10	366,428	N/A	0.06	0.92
<b>Analysis #2</b>	Full RCCS (Sym)	Prism/Polyhedral	2.5 mm/0.35 mm	10	3,853,442	0.03	0.21	0.67
<b>Analysis #3</b>	Full RCCS	Prism/Polyhedral	3.0 mm	20	9,004,257	0.06	0.09	19.80
<b>Analysis #4</b>	Inlet Plenum	Prism/Polyhedral	3.5 mm	21	2,740,704	N/A	0.06	9.75
<b>Analysis #5</b>	Inlet Plenum	Prism/Polyhedral	3.5 mm	21	2,740,704	N/A	0.03	46.70
	Duct #4 (Sym)	Prism/Trimmer	3.0 mm	20	986,624	0.07	N/A	N/A

Table 6 – Mesh Metrics

	Face Validity	Face Validity	Volume Change	Volume Change	Volume Change	Volume Change	Volume Change
	1.00	0.95 to 1.00	1 to 10 <sup>-1</sup>	10 <sup>-2</sup> to 10 <sup>-1</sup>	10 <sup>-3</sup> to 10 <sup>-2</sup>	10 <sup>-4</sup> to 10 <sup>-3</sup>	10 <sup>-5</sup> to 10 <sup>-4</sup>
<b>Analysis #1 (High)</b>	100%	0%	96.126%	3.557%	0.317%	0.00%	0.00%
	100%	0%	96.099%	3.575%	0.326%	0.00%	0.00%
<b>Analysis #1 (Low)</b>	100%	0%	96.126%	3.557%	0.317%	0.00%	0.00%
	100%	0%	96.099%	3.575%	0.326%	0.00%	0.00%
<b>Analysis #2</b>	~ 100%	(7 elements)	93.207%	6.763%	0.030%	0.00%	0.00%
<b>Analysis #3</b>	~ 100%	(9 elements)	99.451%	0.457%	0.075%	0.017%	0.00%
<b>Analysis #4</b>	100%	0%	99.549%	0.253%	0.140%	0.057%	0.00%
<b>Analysis #5 (LP)</b>	100%	0%	99.549%	0.253%	0.140%	0.057%	0.00%
<b>Analysis #5 (Duct)</b>	100%	0%	100%	0%	0%	0%	0%

## Appendix B: Simulation Settings and Boundary Conditions

Table 7 – Simulation Settings (1)

		Temporal	Numerical	Under-Relaxation Factor					Courant
	Component	Analysis Type	Solver	Velocity	Pressure	Energy	k-ε Turb.	k-ε Viscosity	
Analysis #1 (High)	Outlet Plenum	Steady	Segregated	0.7	0.3	0.9	0.8	1.0	N/A
	Outlet Plenum (Sym)	Steady	Segregated	0.7	0.3	0.9	0.8	1.0	N/A
Analysis #1 (Low)	Outlet Plenum	Steady	Segregated	0.7	0.3	0.9	0.8	1.0	N/A
	Outlet Plenum (Sym)	Steady	Segregated	0.7	0.3	0.9	0.8	1.0	N/A
Analysis #2	Full RCCS (Sym)	Steady	Segregated	0.7	0.3	0.9	0.8	1.0	N/A
Analysis #3	Full RCCS	Transient	Segregated	0.8	0.2	0.9	0.8	1.0	N/A
Analysis #4	Inlet Plenum	Steady	Segregated	0.3	0.7	0.9	0.01	0.1	N/A
Analysis #5	Inlet Plenum	Transient	Coupled	N/A	N/A	N/A	0.8	1.0	5.0
	Duct #4 (Sym)	Steady	Coupled	N/A	N/A	N/A	N/A	N/A	5.0

Table 8 – Simulation Settings (2)

	Component	Flow Type	Ideal	Turbulence	Wall
		(Circulation)	Gas (Air)	Model	Treatment
Analysis #1 (High)	Outlet Plenum	Forced	X	Realizable K-Epsilon (two layer)	All Y <sup>+</sup> (two layer)
	Outlet Plenum (Sym)	Forced	X	Realizable K-Epsilon (two layer)	All Y <sup>+</sup> (two layer)
Analysis #1 (Low)	Outlet Plenum	Forced	X	Realizable K-Epsilon (two layer)	All Y <sup>+</sup> (two layer)
	Outlet Plenum (Sym)	Forced	X	Realizable K-Epsilon (two layer)	All Y <sup>+</sup> (two layer)
Analysis #2	Full RCCS (Sym)	Natural	X	Realizable K-Epsilon (two layer)	All Y <sup>+</sup> (two layer)
Analysis #3	Full RCCS	Forced	X	Realizable K-Epsilon (two layer)	All Y <sup>+</sup> (two layer)
Analysis #4	Inlet Plenum	Forced	X	Realizable K-Epsilon (two layer)	All Y <sup>+</sup> (two layer)
Analysis #5	Inlet Plenum	Forced	X	Realizable K-Epsilon (two layer)	All Y <sup>+</sup> (two layer)
	Duct #4 (Sym)	Forced	X	Realizable K-Epsilon (two layer)	All Y <sup>+</sup> (two layer)

Table 9 – Inlet Boundary Conditions

	Component	Inlet Boundary Conditions					
		Velocity (m/s)	Tke (J/kg)	Tdr (m <sup>2</sup> /s <sup>3</sup> )	Turb Intensity	Turb Length Scale	Temperature ( C )
Analysis #1 (High)	Outlet Plenum	See Table	See Table	See Table	N/A	N/A	See Table
	Outlet Plenum (Sym)	See Table	See Table	See Table	N/A	N/A	See Table
Analysis #1 (Low)	Outlet Plenum	See Table	See Table	See Table	N/A	N/A	See Table
	Outlet Plenum (Sym)	See Table	See Table	See Table	N/A	N/A	See Table
Analysis #2	Full RCCS (Sym)	(pressure = 0)	6.00E-04	7.92E-05	N/A	N/A	25.0
Analysis #3	Full RCCS	5	3.75E-03	1.24E-03	N/A	N/A	15.9
Analysis #4	Inlet Plenum	5	3.80E-03	1.00E-03	N/A	N/A	16.0
Analysis #5	Inlet Plenum	4.788	N/A	N/A	2%	0.03048	17.2
	Duct #4 (Sym)	0.52, -0.6974, 5.41	5.4964	1.08E+02	N/A	N/A	18.4

Table 10 – Heat Transfer Boundary Conditions

		Heat Transfer	Total		
		F/B/L/R	Heat Transfer	Outlet	Ramp
	Component	(W/m <sup>2</sup> )	(kW)	Boundary Cond.	Parameters
<b>Analysis #1 (High)</b>	Outlet Plenum	No	N/A	pressure = 0	No
	Outlet Plenum (Sym)	No	N/A	pressure = 0	No
<b>Analysis #1 (Low)</b>	Outlet Plenum	No	N/A	pressure = 0	No
	Outlet Plenum (Sym)	No	N/A	pressure = 0	No
<b>Analysis #2</b>	Full RCCS (Sym)	1678*cosine[ f(z) ] {all faces}	9.785	pressure = 0	No
<b>Analysis #3</b>	Full RCCS	145.7/0/441.8/441.8	4.365	pressure = 0	No
<b>Analysis #4</b>	Inlet Plenum	No	N/A	flow-split	No
<b>Analysis #5</b>	Inlet Plenum	No	N/A	pressure = 0	No
	Duct #4 (Sym)	2239.9/1318.7/1686.8/NA	1.435	pressure = 0	Yes